Approche structurale et étude de la conduction ionique de verres a base de thioarsenite de lithium et de verres a formateur mixte, thioborate et thioarsenite de lithium

Do-Young Seung

n° d'ordre : 1297

THESE

PRESENTEE A

L'UNIVERSITE BORDEAUX I

ECOLE DOCTORALE DES SCIENCES CHIMIQUES

par M. Do-Young SEUNG

POUR OBTENIR LE GRADE DE

DOCTEUR

SPECIALITE : CHIMIE DU SOLIDE, SCIENCES DES MATERIAUX

Titre : *Approche structurale et étude de la conduction ionique de verres à base de thioarsenite de lithium et de verres à formateur mixte, thioborate et thioarsenite de lithium.*

Soutenue le : 11 Juillet 1995

Après avis de : M. J. H. CHOY Rapporteurs
Mme D. GONBEAU

Devant la commission d'examen formée de :

MM.	J. ETOURNEAU	Professeur	Président
	J. H. CHOY	Professeur	Examinateurs
	H. GASPAROUX	Professeur	
Mme	D. GONBEAU	Directeur de Recherche au CNRS	
MM.	A. LEVASSEUR	Professeur	
	T.S. PARK	Directeur du Centre de Recherche SAMSUNG	
Melle	A. PRADEL	Chargée de Recherche au CNRS	

-1995-

REMERCIEMENTS

Ce travail a été réalisé au sein du Groupe Ionique du Solide, interface entre l'Institut de Chimie de la Matière Condensée de Bordeaux, que dirige Monsieur J. ETOURNEAU, et l'Ecole Nationale Supérieure de Chimie et de Physique de Bordeaux, dirigée par Monsieur H. GASPAROUX. Je les remercie de m'avoir accueilli et de participer au jury de ma thèse.

Monsieur J.H. CHOY, Professeur de l'Université Nationale de Séoul me fait l'honneur d'être rapporteur et de participer à mon jury de thèse. Je lui exprime toute ma reconnaissance et je le remercie pour les longues discussions que nous avons eues au sujet des mesures de spectroscopie d'absorption X.

Madame D. GONBEAU, Directeur de recherche CNRS au Laboratoire de Physicochimie Moléculaire de l'Université de Pau et des Pays de l'Adour, a bien voulu mobiliser son temps et ses compétences pour être rapporteur et membre du jury. C'est dans ce laboratoire qu'ont été réalisées les mesures de spectroscopie de photoélectrons X. Qu'elle et toute son équipe soient assurées de ma sincère reconnaissance.

Mes plus vifs remerciements vont également à Mademoiselle A. PRADEL, de l'Université de Montpellier, et à Monsieur T.S. PARK, Directeur du Centre de Recherche SAMSUNG (Samsung Advanced Institute of Technology), qui ont bien voulu participer à ce jury.

Monsieur A. LEVASSEUR, Professeur à l'Ecole Nationale Supérieure de Chimie et de Physique de Bordeaux, a dirigé mes recherches. Il m'a fait bénéficier jour après jour de sa grande expérience et de ses compétences, avec toujours beaucoup de disponibilité et de gentillesse.

Je remercie également Monsieur M. MENETRIER, Ingénieur de Recherche au CNRS. Je lui exprime toute ma reconnaissance pour le soutien constant qu'il m'a apporté et pour l'aide précieuse qu'il m'a fournie lors de l'élaboration de ce mémoire.

Je remercie également Monsieur C. DELMAS, co-responsable de l'équipe "Ionique du Solide", pour ses conseils amicaux.

Qu'il me soit permis d'exprimer toute ma reconnaissance à ceux qui ont participé à la réalisation de ce travail : Messieurs M. INGRAM et J.A. DUFFY, Professeurs à l'Université d'Aberdeen, pour les conseils qu'ils m'ont prodigués dans le domaine des études de basicité optique ; Messieurs M. COUZI et J.C. LASSEGUES, du Laboratoire de Spectroscopie Moléculaire et Cristalline, n'ont pas compté leur temps pour les mesures de spectroscopie Raman et Infrarouge, et pour les nombreuses discussions que nous avons eues sur ce sujet.

Monsieur P. GRAVEREAU m'a initié à la détermination structurale sur monocristaux et L. TRUT a passé beaucoup de temps à m'expliquer les subtilités du goniomètre quatre-cercles ainsi que les techniques Weissemberg et Burger.

Je remercie également beaucoup Messieurs G. LE FLEM et F. ADAMIER pour les mesures d'indice de réfraction.

Mes remerciements vont également à Madame G. PFISTER-GUILLOUZO, Directeur du Laboratoire de Physicochimie Moléculaire de l'Université de Pau et des Pays de l'Adour, qui m'a accueilli dans son laboratoire pour les mesures XPS et a participé aux discussions et interprétations des résultats obtenus. Je remercie très vivement Monsieur L. BENOIST, qui a réalisé en grande partie les mesures XPS et qui a participé aux discussions.

Je tiens aussi à remercier tous les chercheurs et techniciens du laboratoire qui ont contribué à ce travail, et en particulier L. RABARDEL, J. VILLOT, S. GOMA, C. DENAGE et H. DUJARRIC ; je remercie aussi J. PONTI et M. MALLACE pour leur disponibilité et leur gentillesse lors de la réalisation de ce mémoire.

Une très grande part de mes remerciements va à Shin-Tae SEUNG, mon épouse, et Joon-Sung SEUNG, mon fils. Je leur suis très reconnaissant de la patience dont ils ont fait preuve !

Enfin, je ne saurais oublier de remercier tous mes collègues du laboratoire :
A. AATIQ, F. CAPITAINE, L. DEMOURGUES, K.S. HAN, M. HESS, H. MOUDDEN, J.P. PERES, A. ROUGIER, M.C.R. SHASTRY, et P. VINATIER.

Mes remerciements s'adressent également à la Région Aquitaine pour l'aide matérielle qu'elle a apporté à ce travail.

Contents

INTRODUCTION

D'une manière générale, les matériaux amorphes ont des propriétés tout à fait remarquables. Il n'est pas inutile de rappeler les deux principales : ils sont isotropes et leurs propriétés varient continûment avec leur composition.

La compréhension des propriétés physiques et chimiques de ces matériaux passe par la connaissance de leur structure ; mais l'absence de toute périodicité réticulaire est une difficulté importante et seul le recoupement des résultats obtenus par l'utilisation de techniques susceptibles d'atteindre l'ordre local va permettre d'avoir une idée de la structure de ces matériaux.

Pour cela, il est nécessaire d'apporter des réponses ou des éléments de réponses aux questions suivantes :

- Quel est l'ordre à courte distance (quel est l'environnement de chaque atome, sa coordination, la longueur et l'angle des liaisons,...) ;
- Quelle est l'évolution de cet ordre à courte distance avec la composition ;
- Quel est l'ordre à moyenne distance (enchaînement des polyèdres de coordination,...) ;
- Le matériau est-il parfaitement homogène (y-a-t-il séparation de phase) ?

Cette liste n'est, bien sûr, pas exhaustive, mais, des réponses que l'on pourra apporter à ces questions, dépendra, comme nous l'avons mentionné, la connaissance que l'on aura de ces matériaux.

Le Groupe Ionique du Solide étudie depuis une vingtaine d'années des matériaux amorphes conducteurs ioniques.

Après toute une série d'études sur des verres à base d'oxydes-borates de lithium en particulier-, les travaux se sont poursuivis sur des verres à base de thioborates de lithium. C'était, en fait, la reprise de travaux initiés dans les années 60 par P. HAGENMULLER, F. CHOPIN, A. HARDY et B. DARRIET sur les systèmes B_2S_3-Li_2S et B_2S_3- Na_2S (1-4).

L'étude de la conductivité ionique de ces verres binaires a montré qu'ils étaient 1000 fois plus conducteurs que leurs homologues oxygénés (5,6).

Ces travaux ont ensuite été étendus à des verres ternaires B_2S_3-Li_2S-LiI (7-9). Dans ce dernier cas, la conduction ionique est de l'ordre de 10^{-3} Ω^{-1} cm^{-1} à température ambiante, ce qui les place parmi les meilleurs conducteurs ioniques du lithium connus jusqu'à présent (10,11).

Des travaux plus récents ont, par ailleurs, montré que des verres comportant deux formateurs associés à un modificateur ont une conductivité supérieure à ce qu'elle est lorsqu'un seul de ces formateurs est associé au modificateur. Cet effet, appelé "formateur mixte", peut être expliqué par deux modèles suivant que les matériaux amorphes sont homogènes ou hétérogènes. Dans le premier cas, il s'agit d'une extension de la théorie des électrolytes faibles (12), qui considère que le verre est constitué d'un mélange endothermique de compositions limites qui, pour des raisons cinétiques, ne subiraient pas de séparation de phases. De tels mélanges provoquent une augmentation de l'activité thermodynamique des composés limites et donc de leur conductivité. Dans le deuxième cas, le matériau est constitué de deux phases amorphes à l'interface desquelles se trouveraient de très nombreux défauts, qui permettraient, suivant la composition du mélange, d'avoir une conductivité beaucoup plus élevée que l'un ou l'autre des matériaux de départ (13-15).

Quel que soit le type de matériaux, le mélange de deux formateurs avec un modificateur semble conduire à une augmentation de la conductivité. Ce phénomène, extrêmement intéressant, permettait d'espérer d'un thioborate de lithium vitreux dont la conductivité est très élevée et en l'associant à un autre verre tout aussi performant, d'obtenir un nouveau matériau comportant une conductivité tout à fait exceptionnelle.

Des études préliminaires faites dans notre laboratoire avaient montré que les verres à base d'arsenite de lithium avaient une conductivité voisine de celle des thioborates de lithium amorphes (16, 17).

Le but du travail présenté dans ce mémoire est de développer l'étude d'une nouvelle famille de verres à base d'arsénites de lithium, puis d'associer certains de ceux-ci à des thioborates de lithium afin d'étudier le phénomène de formateur mixte.

Après une première partie présentant des généralités sur l'état vitreux, ainsi que les techniques expérimentales, une seconde partie du travail présenté dans ce mémoire sera consacrée à l'étude des verres obtenus dans les systèmes As_2S_3-Li_2S et As_2S_3-Li_2S-LiI.

L'approche structurale de ces verres sera effectuée par des techniques susceptibles d'atteindre l'ordre local (spectroscopies IR et Raman, RMN, XPS, XAS,...). Elle sera complétée par une comparaison cristal-verre de même composition. (Li_3AsS_3 sera comparé au verre binaire 0.75 Li_2S-0.25 As_2S_3). Un autre type de monocristal a pu être isolé, $LiAsS_2$ et sa structure déterminée. Il n'existe malheureusement pas de verre de composition correspondante.

La conduction ionique des verres à base d'arsénites de lithium sera étudiée en fonction de leur composition.

Une autre partie sera consacrée à l'étude du système ternaire Li_2S-B_2S_3-As_2S_3 qui comporte deux sulfures formateurs B_2S_3 et As_2S_3.

Enfin, une dernière partie sera consacrée à la basicité optique de ces verres.

Bibliographie

1) P. Hagenmuller et F. Chopin, C.R. Acad. Sci., **255** (1962) 2259
2) P. Hagenmuller et F. Chopin, C.R. Acad. Sci., **256** (1963) 5578
3) F. Chopin et A. Hardy, C.R. Acad. Sci., **261** (1965) 142
4) B. Darriet, D.E.S. (Sciences Physiques), Univ. de Bordeaux I (1965)
5) A. Levasseur, R. olazcuaga, M. Kbala, M. Zahir et P. Hagenmuller, C.R. Acad. Sci. **293** (1981) 563
6) S. Susman, L. Boehm, K.J. Volin et C.J. Delbecq, Solid State Ionics, **5** (1981) 667
7) H. Wada, M. Ménétrier, A. Levasseur et P. Hagenmuller, Mat. Res. Bull, **18** (1983) 189
8) W. Burckhardt, M. Makyta, A. Levasseur et P. Hagenmuller, Mat. Res. Bull, **19** (1984) 1083
9) M. Makyta, A. Levasseur et P. Hagenmuller, Mat. Res. bull, **19** (1984) 1361
10) M. Ménétrier, A. Hojjaji, C. Estournès et A. Levasseur, Solid State Ionics, 48 (1991) 325

Chapter I. Preparation and characterization methods of glasses and single crystals

I.1 Preliminary

I.1.1 Definition of glassy state

There has been up until now no satisfactory definition of a glass. As briefly discussed in the general introduction, the definition of a glass has various aspects, but we will adopt the definition of glass proposed by the A.S.T.M. (American Society for Testing Materials); *glass is an inorganic product of fusion which has cooled to a rigid condition without crystallising (absence of X-ray diffraction pattern).* We will consider in this work this definition as the more appropriate. *This definition excludes certain organic substances such as glucose or glycerol which can be supercooled to a rigid condition without crystallising, and which in this form possess many of the characteristics of glasses. The foregoing definition would also exclude amorphous substances prepared by methods other than melt cooling, for example, by vacuum evaporation techniques (some of these materials have structures and properties that closely resemble those of glasses as defined above and therefore it may be thought artificial to exclude them from the general definition of the vitreous state).*

If a melt of a pure substance is cooled, it is generally observed that there is a definite freezing point at which solidification occurs due to the formation of crystals. However, it is sometimes possible to continue the cooling of a liquid below its freezing point without encountering crystal formation. In this case the liquid is said to be supercooled. A supercooled liquid represents a metastable state since its free energy is higher than that of the corresponding

crystal but the structure of the supercooled liquid has a lower free energy than any immediately neighbouring structure. The relationship between the glassy state and the "normal" solid and liquid states can be understood on the basis of what happens during the cooling of melts. For a substance which crystallises, it is observed that there is a closely defined temperature at which solidification and a discontinuous volume change occurs. In addition heat is evolved when solidification takes place. For a substance which can be cooled to the glassy state on the other hand, no discontinuous volume change is observed and there is no exothermic effect corresponding to the change from the liquid to the solid state. Instead, the viscosity of the melt increases progressively as the temperature falls and eventually the viscosity attains values which are so high that for all practical purposes the substance behaves as a rigid solid. A material is considered as a solid when its viscosity is higher than 10^{13} Poises (1). Thus the glassy state can be thought of as a continuum of the liquid state and is distinguished from the normal liquid state by a high magnitude of viscosity.

Additionally, if the substance shows a structural relaxation, it could be considered as a glass. Structural relaxation is defined by the existence of a well defined temperature interval, the glass transition region, where, due to the onset of long range atomic and molecular motion, mechanical and thermodynamic properties become time dependent. The onset of molecular motion itself results in a dramatic increase in heat capacity, which can be detected by differential scanning calorimetry (DSC). The glass transition temperature Tg can be defined as the onset point associated with the heat capacity change.

I.1.2 Condition of glass formation

Since oxide based glasses have been extensively studied for some time, all the examples given will be from this family of glasses.

To form a glass, one needs substances like a glass former, glass modifier and possibly a dopant. Glass formers or network formers are so called because of their ability to build up

continuous three dimensional random networks. By itself, a network modifying substance is one which is incapable of building up a continuous network and the effect of such a substance is usually to weaken the glass network. An intermediate material is one which although, not usually capable of forming a glass, can take part in the glass network.

Zachariasen (2) developed the random network theory of glass structure and proposed certain conditions for glass formation. For an oxide M_xO_y to form a glass, it was proposed that;

1) an oxygen atom must not be linked to more than two M atoms,

2) the number of oxygen atoms surrounding M must be small,

3) the oxygen polyhedra must share corners only and not edges or faces,

4) the polyhedra must be linked in a three-dimensional network.

For example, the oxides M_2O and MO cannot meet the conditions proposed by Zachariasen. The oxide M_2O_3 can do so if the oxygens form triangles around each M atom and the oxides MO_2 and M_2O_5 can do so if the oxygens form tetrahedra around each M atom.

Other correlations of glass forming tendency of oxides have been made by Stanworth (3) who derived the following criteria;

1) the cation valence must be three or greater,

2) the tendency to glass formation increases with decreasing cation size,

3) the electronegativity should be between about 1.5 and 2.1 on Pauling's scale.

I.1.3 Bonding criteria

The criteria for glass formation and for characterizing the role of oxides in the glass structures discussed so far have essentially been geometrical in nature and have emphasised the role of ionic radius. It is clear, however, that the nature of the bonding between the cations and oxygens plays a critical role. Those oxides that form highly covalent bonds to oxygen are more likely to assume the role of network formers than oxides in which the bonding is predominantly ionic. One measure of the power of a cation to attract electrons, and therefore its ability to

form covalent bonds, is the ionic field strength given by $F = Z/r^2$, where Z is the valency and r the ionic radius. The following Table I.1 represents the ionic field strength of cations present in glasses.

The concept of field strength represents a simplified point of view since it considers the ions and atoms to behave as rigid spheres. This is not strictly true because large ions of low charge and non-noble gas ions are deformable. Nevertheless, the field strength concept is a useful aid to understanding the role of various ions in glass structure.

Using the criteria of Stanworth (3) leads to various groups of oxides:

1) Strong glass formers; Si, Ge, As, P and B.

2) Intermediate glass formers which form glasses only by splat cooling; Sb, V, W, Mo and Te.

3) Non glass forming oxides whose formation is only possible on oxidsed surfaces of their metals; Al, Ga, Ti, Ta, Nb and Bi.

4) Other oxides that do not form glasses.

Some oxides such as tin and chromium do not fit into this scheme.

Ion	Ionic radius (Å)	Field strength (Z/r^2)	Structural role in glass
B^{3+}	0.20	75.0	Network forming ions
P^{5+}	0.34	43.2	
Si^{4+}	0.41	23.8	
As^{5+}	0.47	22.6	
Ge^{4+}	0.53	14.2	
Be^{2+}	0.31	20.8	Intermediate ions
Al^{3+}	0.50	12.0	
Ti^{4+}	0.68	8.7	
Zr^{4+}	0.80	6.3	
Mg^{2+}	0.65	4.7	Network modifying ions
Li^{+}	0.60	2.78	
Ca^{2+}	0.99	2.04	
Na^{+}	0.95	1.11	
Ba^{2+}	1.35	1.10	
K^{+}	1.33	0.57	

Table I.1 Ionic field strength of cations present in glass (4).

I.1.4 Formation of sulphide glasses

The previous generalities given for oxide based glasses can be extended partly to sulphide-based glasses.

A new class of sulphide-based glasses, were developed in the early eighties (5,6). These glasses are formed by rapid quenching of melts consisting of a network-forming compound such as B_2S_3, SiS_2, GeS_2 or P_2S_5, a network modifier and a doping salt. The starting materials used for the preparation and the glass obtained are sensitive to moisture, therefore all the preparation process had to be carried out in a dry argon atmosphere. The glass forming ability for these sulphide glasses, summarised by Ravaine (7), is shown in Table I.2.

Conventional glass former	SiS_2, GeS_2, B_2S_3, P_2S_5, ...
Unconventional glass former	As_2S_3, Ga_2S_3, La_2S_3, Sb_2S_5,...
Network modifier	Ag_2S, Li_2S, Na_2S,...
Doping salt	LiI, LiBr, ...

Table I.2 Classification of compositions according to the glass forming ability (7).

I.2 Structural order in amorphous solids

Before discussing the conceptual framework for describing the variation of structural units, some definitions of structural order are presented.

I.2.1 Short-range order (SRO)

SRO is usually described in terms of well defined local coordinated polyhedra in covalent materials. If the limit for SRO is set to the third nearest neighbour distance (generally of the order of 5 to 6 Å), then the element of SRO will be ;

1) two particle correlations or bond lengths,

2) three particle correlation or bond angles,

3) four particle correlations or dihedral angles,

4) the local site symmetry.

That is, the parameters are the number (N_j) of nearest neighbour (j) around atom of type (i), the nearest-neighbour bond length r_{ij}, the bond angle subtended at atom i, θ_i, and the corresponding quantities when atom j is regarded as the origin, N_i and θ_j are sufficient to describe topological SRO (8). These SRO parameters are illustrated in Fig. I.1.

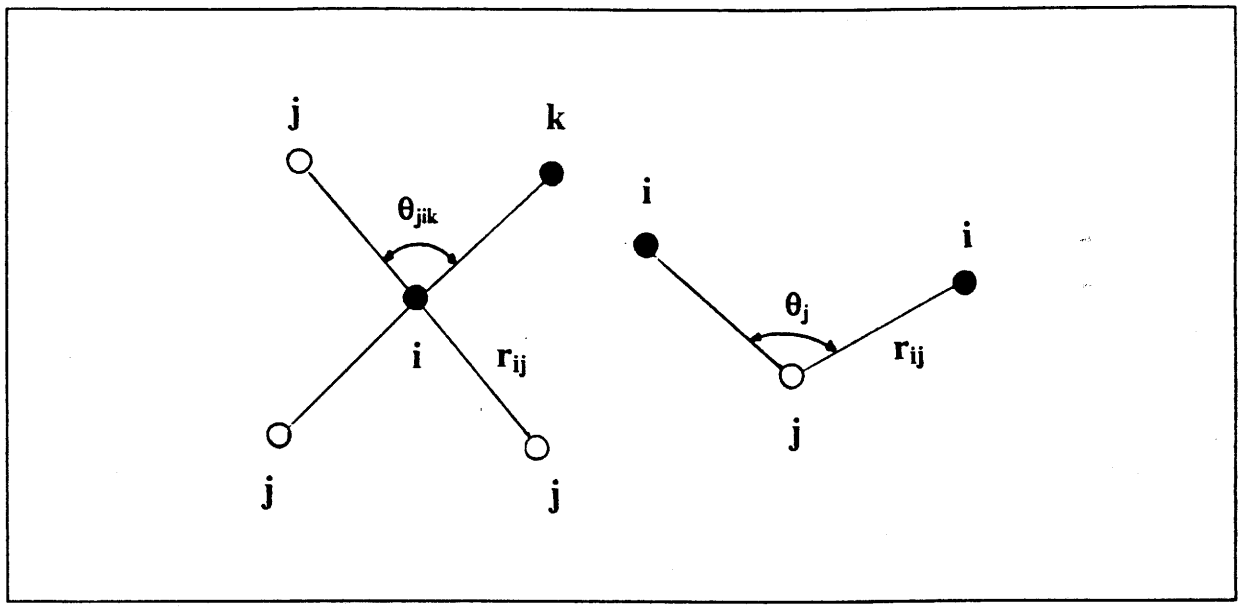

Fig. I.1 Schematic representation of the parameters describing SRO in covalent amorphous solid (8).

I.2.2 Medium-range order (MRO)

In the definition of MRO, there is a degree of arbitrariness. Following the precise description of MRO, it can be defined as a part of correlations extending to larger number of atoms, up to about 10. It could also be regarded simply as the next highest level of structural organisation beyond SRO, on a distance scale of 5~20 Å. Hence, MRO exists when there are correlations extending to five or more atoms, which means that pairs of dihedral angles that are "phase locked" present the most elementary MRO unit.

In general, structures of this sort do not have a well-defined spectroscopic signature and therefore cannot be readily observed.

I.2.3 Long-range order (LRO)

LRO is defined by crystalline translational symmetry, i.e., only materials that have at least microcrystallinity, observable via X-ray or electron diffraction will be defined as having LRO.

I.3 Review of structural modelling of glasses

From a conceptual point of view the description of glass structure can be divided into several models, i.e. *crystallite* (9), *random network* (2) and *paracrystalline* (10). These fundamental approaches have emerged depending on the nature of the chemical systems involved .

I.3.1 Continuous random network model

The structure of single component covalent glass-formers, such as SiO_2, has traditionally been described in terms of the *continuous random network theory* (2) in which structural units similar to those in the corresponding crystalline material are linked together randomly to form a continuous three-dimensional network, as illustrated schematically in two dimensions in Fig. I.2. This model treats the structure of a covalently bonded amorphous material as a giant macromolecule in which perfect connectivity is maintained (except for the surface of the model), with all the atoms retaining their normal valence. In this case, the structures can be regarded as perfect since bonding defects such as dangling bonds or voids are excluded.

In three dimensions, disorder is introduced into such a structure through torsional rotations about A-X bonds and a distribution of A-X-A bond angles, any distortion of the structural units (AX_3 triangles in Fig. I.2) usually being comparable to that in the crystal. Zachariasen's criteria for glass formation (cf. I.1.2) suggest that glass formation in such systems is favoured by structural units (A_{xn}) with a relatively small coordination number ($n_{A(X)}$)

of X around A, which share corners rather than edges or faces. In addition the formation of a three dimensional network requires at least 3 corners of each unit to be shared. In multicomponent systems the individual constituents may be classified as network formers or network modifiers as described in I.1.3 and I.1.4, the addition of a further network former to a single component glass will result in a mixed network of two different structural units. The traditional view of a network modifier, on the other hand, is that it leads to the formation of negatively charged non-bridging X atoms; the network modifying cations occupying nearby holes in the resulting network. If the local environments of modifiers are to be incorporated in a complementary way with network formers, the overall structure will necessarily comprise two-interlacing sublattices as network regions constructed from network formers and inter-network regions made up of modifiers (11,12).

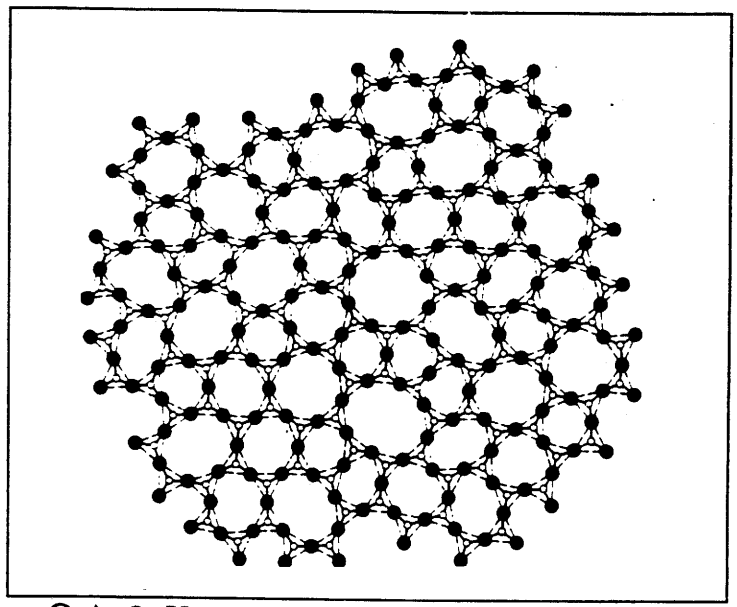

O:A; ●: X

Fig. I.2 Schematic two-dimensional representation of an A_2X_3 random network.

Modern X-ray or electron diffractions and EXAFS evidence (11) suggests that the network modifying cations adapt their local environment to create their own desired coordination polyhedron as found in related crystalline materials. This alteration of the local

network modifying cation environment does not necessarily imply the introduction of regions of crystalline order (crystallite), but is simply the consequence of radius ratio effects. Fig. I.3 illustrates a model in 2 dimensions for a glass of approximate composition M_2O_3-G_2O_3 (13). The M ions are glass modifying cations and G ions are glass forming cations. Both modifier and former have been allotted 3-fold coordination for convenience. There are two types of oxygen present: one coordinated to two G's (bridging) and the other coordinated to two M's and one G (non-bridging). This schematic representation is a typical example of the ***modified random network*** (MRN) model and which is partly ionic and partly covalent in nature. In the proportions chosen the structure is characterised by percolation channels and comprises of peninsulas and islands of network interspersed by channels and lakes of modifier. Whether the modified regions in a MRN extend to percolation channels will depend on the composition via the volume fraction of modifier.

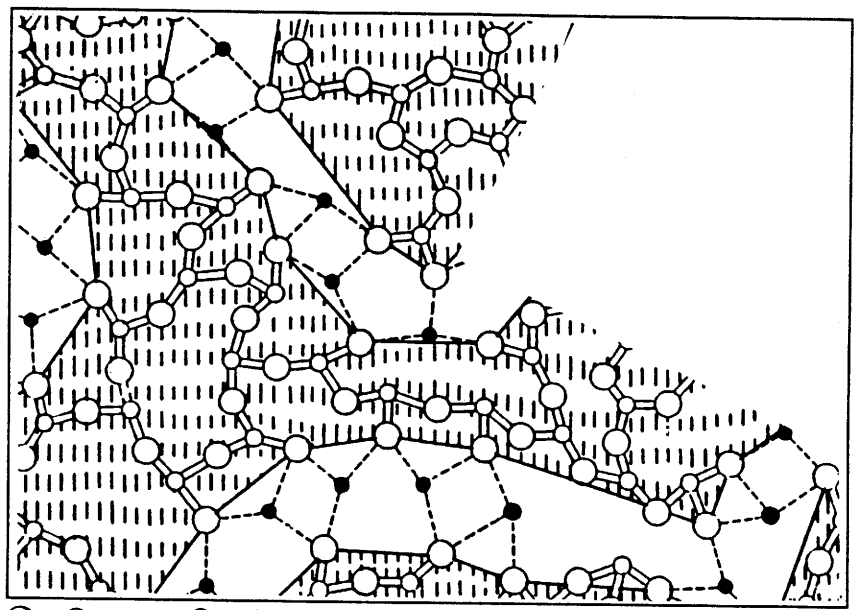

Fig.I.3 A modified random network (MRN) for a 2 dimensional oxide glass. The nominal composition is M_2O_3-G_2O_3, where M's are modifying cations and G's are network forming cations. Covalent bonds are shown by the solid lines and ionic bonds by the dotted lines. The unshaded regions are defined by the boundary which run through the G-O (non-bridging) bond. These highlight the percolation channels of M_2O_3 that run through the network (13).

I.3.2 Random close-packing model

Many amorphous metals are quenched from the liquid state and have predominantly non-directional bonding and it is natural to consider the structure as being that of a frozen liquid. In this regard, the random close packing model of single-sized hard spheres has been proposed by Bernal (14,15). In such structures, the important concepts are those of radius ratio, packing density and hole filling. These ideas are frequently used in discussions of metallic and ionic crystal structures, but are often neglected when considering the structures of the equivalent glasses. Characterisation of this model involves calculating the RDF (*radial distribution function*) and the packing fraction. The non-crystalline packing fraction, η_p, obtained for the physical model has been determined to be 0.61 (15) - 0.6366 (8). The random packing model of equisized spheres is dense in the sense that no internal voids exist which are large enough to accept a normal sized sphere. This does not, however, mean that there are no reasonably large voids present in the structure. The holes in this model can be broken down into a set of polyhedral holes found between molecules (Fig. I.4). This model is suitable for representing the structure of pure amorphous metals (Bi, Ga, etc.).

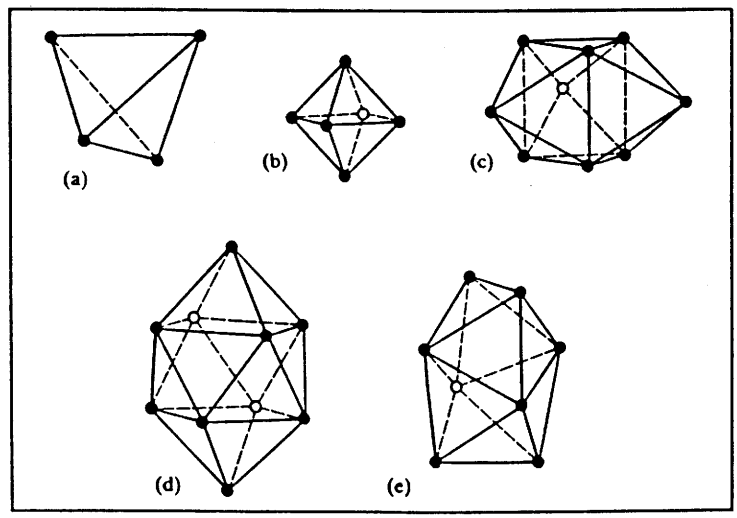

Fig.I.4 Forms of holes in ideal equidistant molecule model of a liquid; a: tetrahedron, b: octahedron, c: trigonal prism capped with three half octahedra, d: archimedean antiprism capped with two half octahedra, e: tetragonal dodecahedron (15).

A variation of the random close packing model, applicable to ionic systems, in particular halide glasses, is the ***locally ordered random packing model***. Brunner (16) has presented an unconventional view of crystalline close packing in which he argues that; given a finite volume, the close packed arrangement results from the requirement that the separation between neighbouring atoms/ions should be maximised. In this case, the spatial distribution of the centres is considered and assumptions of spherical shapes and mutual contact are in fact unnecessary. The mutual repulsion idea can clearly be extended to ionic glasses and to the ion cores in metallic systems; in the glass, crystalline close packing will be replaced by random close packing. Polk (17,18) has suggested a model for the transition metal-metalloid glasses in which metalloid atoms (M) are inserted into the larger Bernal holes in a random close packed array of transition metal atoms (T). If all such holes are filled, the composition is very close to the (T_4M) of the deep eutectic which occurs in many of these systems. Optimum glass formation occurs around this eutectic composition and Polk argues that the presence of the metalloid atoms in the holes stabilises the structure. The main objection to Polk's model is that the metalloid atoms are considered to be almost totally passive. This is in contradiction to that found in amorphous solids where the absence of a periodic structure means that an added atom/ion can very easily adapt to its immediate environment, in order to satisfy its own local bonding/radius ratio requirements. Subsequent work by Cargill (19) has shown that there is in fact insufficient void volume available to accept any but the very smallest type of metalloid atoms. Gaskell (20,21) discussed further that the metalloid coordination polyhedron in the corresponding crystalline T-M alloys is that of a trigonal prism and hence it is likely that metalloid atoms inserted initially into other types of Bernal holes would modify their environment accordingly.

I.3.3 Other structural models

The ***Random coil model*** was originally proposed for amorphous linear organic polymers. This model considers as a whole, that a three dimensional random chain of finite length is a globule floating in a supporting medium. Such an object has overall geometrical properties, for example a characteristic radius, which can be directly associated with measurable physical properties of macromolecules in diluted solution (22-24). This model can be considered simply as a special case of a random network model in which the local network dimensionality is two (in the absence of cross-links). Zallen discussed the random coil model in some detail, in particular its relationship to random walks (25).

The random network model for the structure of vitreous materials has under gone some challenges. The problem is to physically distinguish between this model and alternative hypotheses. The most clear evidence comes from X-ray and neutron diffraction. The general features of the radial distribution function arise quite naturally from a random network model. In the tetrahedral network, for example, the first and second coordination shells are identical in spacing and number to those in a perfect diamond lattice, but the rotation of tetrahedra about their common bond varies the distance to third neighbours. This provides a single physical explanation for the loss of the third peak in the RDF as one moves from crystalline to amorphous silicon. It is difficult, however, to prove conclusively that such features are inconsistent with hot solid or perturbed microcrystal disorder. This leads to an interpretation of observed radial distribution functions in glasses and liquids implicit in what is called the ***paracrystalline model*** (10). A slightly different interpretation attributed the apparent broadening of the peaks to diffraction effects from quasi-crystals, treating them as distinguishable objects of finite size L, describing the apparent decay of the correlation function, randomly distributed in the medium (26-30).

The historically old ***Crystallite model***, was first proposed by Lebedev (9). This model considered that a glass is constituted of an assembly of microcrystallites whose sizes are sufficiently small that no coherent diffraction occurs (i.e. no x-ray diffraction line appears). Meanwhile, a simple calculation of X-ray broadening shows that for silica the size of crystallite is less than about 8 Å.

I.4 Experimental methods for the characterisation of crystals and vitreous materials

1.4.1 Structural determination

The structure of Li_3AsS_3 and $LiAsS_2$ crystals were determined with the help of L. Trut and P. Gravereau.

For structural determinations the quality of the crystal is crucial. Crystal selection was carried out using an optical microscope equipped with a video camera installed in a dry argon filled glove box. Selected optimum sized crystals were introduced into a glass capillary and sealed under argon atmosphere. Absorption corrections were necessary because of the use of the glass capillary.

Calculations were performed on a IBM 3090-400 computer at the computing centre of Montpellier using SHELX 76 (31). Absorption correction was performed by an empirical algorithm (32) using ABSORB (33). Molecular graphics were obtained using CERIUS (34) on a Silicon Graphic system.

I.4.2 IR spectroscopy

IR spectroscopy measurements were performed with the help of J. C. Lassègues, at the Laboratoire de Spectroscopie Moléculaire et Cristalline (Université Bordeaux I).

Infrared spectroscopic studies in the mid-infrared and far-infrared regions provide valuable information in determining local structural arrangements (short-range order) of the glass matrix.

Mid-IR spectra were obtained using a Perkin-Elmer 930G model, in the range 200 - 1200 cm^{-1}. The spectral resolution was 4 cm^{-1}, and the samples were dispersed in KBr powder with the ratio of KBr to sample at 200:1 by weight. Samples measuring 13 mm in diameter were pelletised under 7 MPa.

The Far-IR spectra were obtained using a Fourier Transform interferometric vacuum spectrometer (Nicolet 20F). The source used was a Globar and the detector was a DTGS in the range 50 - 650 cm^{-1}, with a spectral resolution of 4 cm^{-1}. Samples were dispersed in polyethylene (PE) with the ratio of PE to sample at 50:1. The sample size was the same as above but the pelletising pressure was 4 MPa. All the measurements were done under flowing dry nitrogen gas atmosphere to avoid water contamination from the atmosphere.

I.4.3 Raman spectroscopy

Raman spectroscopy measurements were done with the help of M. Couzi, Laboratoire de Spectroscopie Moléculaire et Crystalline. Raman spectra were recorded in right angle geometry using a Dilor Z24 monochromator. The excitation source was a Spectra Physics model 171 Ar ion laser with an emission line at 528.7 nm. The power source was 200 mW and detection was achieved using a Hamamatsu model R94302 cooled photomultiplier coupled with a photon counter, spectral resolution 1.8 cm^{-1}. To avoid moisture contamination, sealed quartz containers were used. No beam damage was observed at the surface of the sample.

The crystalline samples were mounted inside a glass capillary of 0.5 mm diameter because of their hygroscopic nature and the spectra was obtained using a Dilor OMARS 89 micro Raman spectrometer. The laser wavelength used to excite the phonons was 514.5 nm at ~50 mW.

I.4.4 ^{11}B NMR experiment

NMR experiments were been done in cooperation with M. Ménétrier. NMR spectra were obtained using a Bruker MSL 200 spectrometer, utilizing a "one pulse" sequence under the following conditions; pulse length; 2 μs, pre acquisition delay; 10 μs, recycling time; 30 seconds and 200 scans were usually accumulated to get a satisfactory signal to noise ratio.

The measurements were carried out on well ground glass powder which had been introduced into a silica tube and sealed under vacuum.

1.4.5 X-ray photoelectron spectroscopy (XPS)

This experiment was performed in cooperation with Mme. D. Gonbeau, Mme. G. Pfister-Guillouzo and L. Benoist in Laboratoire de Physico-Chimie Moléculaire, (Université de Pau et des pays de l'Adour).

The XPS analyses were performed with a SSI (Surface Science Instruments) Spectrometer, Model 301, using small area (diameter of irradiated area ; 300 μm) monochromatized Al-Kα radiation (hν = 1486.6 eV). The residual pressure inside the analysis chamber was about 10^{-10} torr.

The spectrometer was calibrated using the photoemission lines of Au ($Au4f_{7/2}$ = 83.9 eV) and Cu ($Cu2p_{3/2}$ = 932.5 eV) to maintain scale linearity, with a pass energy of 50 eV.

The sample was fixed on a specifically designed sample holder in a glove box under purified nitrogen, the sample was then fractured under high vacuum (about 10^{-10} torr) in the sample preparation chamber just before introduction into the analysis chamber. In this condition, the atomic percentage of oxygen was found between 6 and 10 % (for few samples, the oxygen percentage was found between 25 and 30 %; in this case, a high energy As3d peak was detected corresponding to an oxygen environment of an arsenic atom). During the X-ray radiation of the sample, the surface of the sample was showered using a flood gun to neutralise the surface charging effect. The reproducibility of measurement was checked by comparing

several different fractured surfaces of each sample. The calculation of binding energy scale was done with the C1s line (284.6 eV), found intrinsically in all samples. Obtained XPS spectra were analysed by a peak decomposition program in which a non linear background was assumed, and the fitting peaks were defined by a partly Gaussian (80%), partly Lorentzian (20%) function. The curve fits for the whole set of compounds have been obtained using fixed amplitude ratios, FWHM ratios and spin splits, the degrees of freedom have been limited for each doublet to chemical shift amplitude and FWHM.

1.4.6 XAS experiment and data analysis

EXAFS and XANES measurements were done in cooperation with Prof. J. H. Choi and Mr. D. K. Kim, the Dept. of Chemistry, Seoul National University. XAS spectra were measured in transmission mode on a BL 10B station at the Photon Factory, at the National Laboratory for High Energy Physics (PF-KEK) in Tsukuba, Japan, using synchrotron radiation at room temperature. The storage ring was operated at 2.5 GeV, with a ring current in the range 260 - 370 mA. A Si (3 1 1) channel-cut monochromator was used, and the intensities of incident and transmitted beam were measured with ionisation chambers filled with a mixture of nitrogen and argon gases. All samples were very sensitive to air, and therefore care was taken to ensure sample stability during measurements. Samples for XAS measurements were ground to fine powders in an argon-filled dry box, and uniformly packed into sealed tubes with kapton windows in order to obtain an optimum absorption jump ($\Delta\mu t < 1$), low enough to be free from the thickness and pin-hole effects. The energy scale was calibrated by monitoring the inflection point (E = 11867 eV) of the main absorption edge of the spectrum of v-As_2S_3 for each measurement.

The data analysis of the experimental spectra were performed by standard procedures as follows. The inherent background in the data was removed by fitting a polynomial to the pre-edge region, and extrapolating through the entire spectrum, from which it was subtracted.

The resulting spectra, $\mu(E)$, were normalised to an edge jump of unity by comparing the X-ray absorption near edge structure (XANES) directly with one another. The absorption spectrum for the isolated atom, $\chi_0(E)$, was approximated by a cubic spline. The extended X-ray absorption fine structure (EXAFS) function, $\chi(E)$, was obtained from $\chi(E) = \{\chi(E) - \chi_0(E)\}/\chi_0(E)$. Further analysis was performed in k space, where the photoelectron wavevector **k** is defined as $\mathbf{k} = [(2m/h^2)(E-E_0)]^{1/2}$, where m is the electron mass, h is the Planck's constant and E_0 is the threshold energy of photoelectron at $\mathbf{k} = 0$. The resulting EXAFS spectra were **k**-weighted and Fourier transformed in the range of ~3 $Å^{-1} < k <$ ~12 $Å^{-1}$ with a Hanning function to reduce the truncation effect. In order to determine the structural parameters of the As-S bond, a nonlinear least-squares curve fitting procedure was performed on the inverse Fourier transformation $\mathbf{k}^3\chi$ (k) of the first shell corresponding to the As-S bonding pair in the Fourier transform (FT). The EXAFS formula based on the single scattering theory and the plane-wave approximation can be expressed as follows:

$$\chi(E) = - S_0^2 \sum N_i F_i(k) \exp(-2\sigma_i^2 k^2) \exp\{(2R_i/\lambda(k) \} \sin\{2kR_i+\phi_i(k)\}/(kR_i^2)$$

The backscattering amplitude, $F_i(k)$, the total phase shift, ϕ_i (k), and the photoelectron mean free path, $\chi(k)$, have been theoretically calculated for all scattering paths including multiple scatterings by a curved wave ab initio EXAFS code FEFF 5 (35). In the course of nonlinear least-squares curve fitting between the experimental spectrum and theory, structural parameters such as the bond distance (R_i), the coordination number (N_i), the Debye-Waller factor (σ_i^2), and the threshold energy difference $\mu(E_0)$ were optimised as variables. The amplitude reduction factor (S_0^2) was set equal to 0.9 in the entire course of the fitting procedure. The reliability of the fit is determined by the F factor, $F = [\Sigma\{\chi(k)_{exp} - \chi(k)_{fit})k^3\}^2/(N-1)]^{1/2}$, where N is the number of data points.

1.4.7 Measurement of the glass transition temperature (Tg)

The glass transition temperature (Tg) was determined by Differential Scanning Calorimetry (DSC) using a heating rate of 5 °Cmin^{-1} on a Setaram DSC 92. The sample was sealed in a stainless steel crucible before placing in the DSC. Tg was determined as the onset point of the endothermal peak instead of using T_3, the medium temperature between T_1 and T_2 on the curve (Fig. I.5).

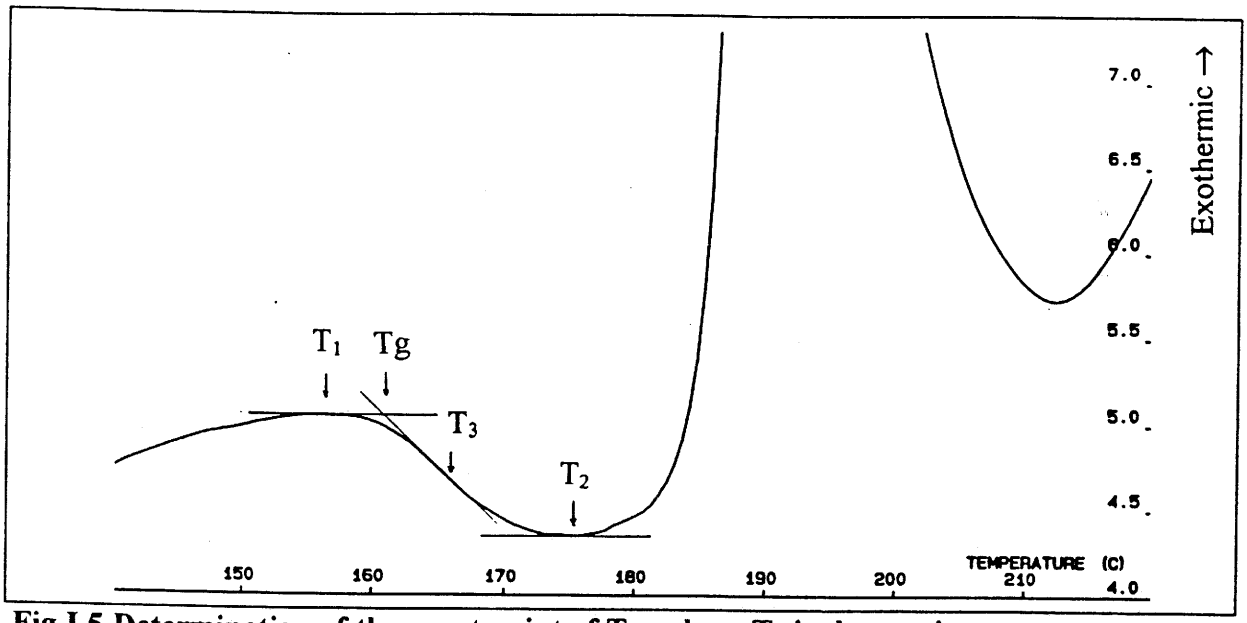

Fig.I.5 Determination of the onset point of Tg, where T_1 is the maximum temperature of the peak, and T_2 is the minimum temperature of the valley.

1.4.8 DC conductivity measurements

To determine the ionic conductivity of glasses, the complex impedance method developed by Bauerle (36) was used. The impedance spectra were represented as a variation of imaginary part versus the real part of impedance for each frequency. Conductivity measurements were performed on pellets pressed from well ground material. Two types of electrodes were used: TiS_2 and gold, as semi-blocking and blocking respectively (against mobile Li^+ ions). Hojjaji (37) showed that irrespective of electrode type used the measured

ionic conductivity had the same value. Therefore, TiS_2 electrodes were more generally utilised as they were more convenient to handle and use in a glove box.

The sample was connected in series with a reference resistor and an a.c. signal in the frequency range 1 Hz-95 KHz supplied by a Solartron 1174 frequency generator. The response analyser installed in the Solartron measures the complex ratio of potential across the sample (V_y) to that across the reference resistor (V_x) under the same current. Thus, at each frequency we obtain an imaginary and real part of the impedance (Z) of the sample. The measurement were made from room temperature to 70 °C with the glasses exhibiting Arrhenius behaviour $\sigma = \sigma_0 \exp(-Ea/kT)$ over the range studied.

1.4.9 Density measurement

Densities were determined by the usual Archimedes method using bromobenzene as the fluid. The measurement has been performed in collaboration with L. Rabadel and J. Villot.

1.4.10 Chemical analysis

Chemical analysis was carried out using an Inductively Coupled Plasma spectrometry (ICP) located at Service Central d'Analyse du CNRS (Vernaison). The results consistently revealed about a 5 wt.% of oxygen and a 2 wt.% of carbon contamination, which could not be avoided in the preparation of samples.

I.5 Preparation of glasses

Since materials used for the preparation of the glasses and the glasses themselves were sensitive to moisture the entire preparation process was performed in a dry argon atmosphere glove box containing less than 5ppm of H_2O.

I.5.1 As_2S_3 glass

As_2S_3 glass was prepared by a melt quenching method. The commercial amorphous As_2S_3 powder was introduced into a sealed silica tube and heated to 400 °C, the tube was then quenched into cold water. The glass thus obtained was dark red in colour. The chemical analysis of this glass is shown in Table I.3.

Atomic species	Theo. (at. %)	Exp.(at. % ± 0.5)
As	40	41
S	60	59

Table I.3 Chemical analysis obtained using Inductive Coupled Plasma spectrometry (ICP).

I.5.2 Li_2S-As_2S_3 binary glass

Vitreous carbon crucibles were systematically used because of the known reaction that occurs between boron, lithium sulphides and silica (which commences at 400 °C) (38). The obtained glasses were checked by X-ray diffraction (XRD).

The binary xLi_2S-$(1-x)As_2S_3$ ($0.67 \leq x \leq 0.75$) glass forming range has already been reported by Shastry et al. (39). The glass was prepared from commercially available Li_2S, As_2S_3 (amorphous) powders and the procedure was as follows. The weighed powder reactants were well mixed then transferred into a vitreous carbon crucible, itself placed into a silica tube. The ampoule was sealed under vacuum then heated at 650 °C for 18 h. The ampoule was then quenched into cold water. The products were generally partially opaque indicating either partial crystallisation or de-mixing. These were re-ground and re-melted in an amorphous carbon crucible, using a high frequency induction furnace attached to dry argon glove box, then quenched between two stainless steel blocks. Reddish brown coloured transparent glasses without a crystalline phase were obtained.

I.5.3 LiI-Li_2S-As_2S_3 ternary glass

The glasses obtained in the LiI-Li_2S-A_2S_3 system were prepared from commercial Li_2S, amorphous As_2S_3 and LiI powder. The preparation procedure is the same as described in I.5.2 These ternary yLiI-(1-y)[xLi_2S-(1-x)As_2S_3] glasses were formed in the range of x = 0.70 ($0 \leq y \leq 0.5$), and x = 0.75 ($0 \leq y \leq 0.5$), respectively (Fig. I.6). The colour of glass changed from transparent reddish brown to transparent orange like brown upon increasing the LiI content.

I.5.4 Li_2S-B_2S_3-As_2S_3 ternary glass

xLi_2S-(1-x)[(1-y)B_2S_3-yAs_2S_3] glasses were prepared from Li_2S, B (amorphous), S and As_2S_3 (amorphous). The well mixed reactants were introduced into a vitreous carbon crucible and transferred to a silica tube which was sealed under vacuum after evacuation for 4 h. The mixture was heated for 18 hours at between 700 - 750 °C, depending on the composition, then quenched in cold water. The composition y = 0 was heated to 750 °C; the remaining compositions being heated to 700 °C.

The substance obtained was opaque indicating de-mixing or partial crystallisation. These were re-melted in an open vitreous carbon crucible by means of a high frequency inductive furnace attached to a glove box, then quenched between two stainless steel blocks inside a glove box. The formation of the glass which was transparent and brownish in colour was critically affected by the quenching rate. As Fig.I.7 shows, this ternary system exhibits a very narrow glass forming domain. XRD revealed that for As_2S_3 contents greater than y = 0.3 (x = 0.67 and x = 0.70) and y = 0.1 (x = 0.75), crystalline phase corresponding to $LiAsS_2$ were always detected.

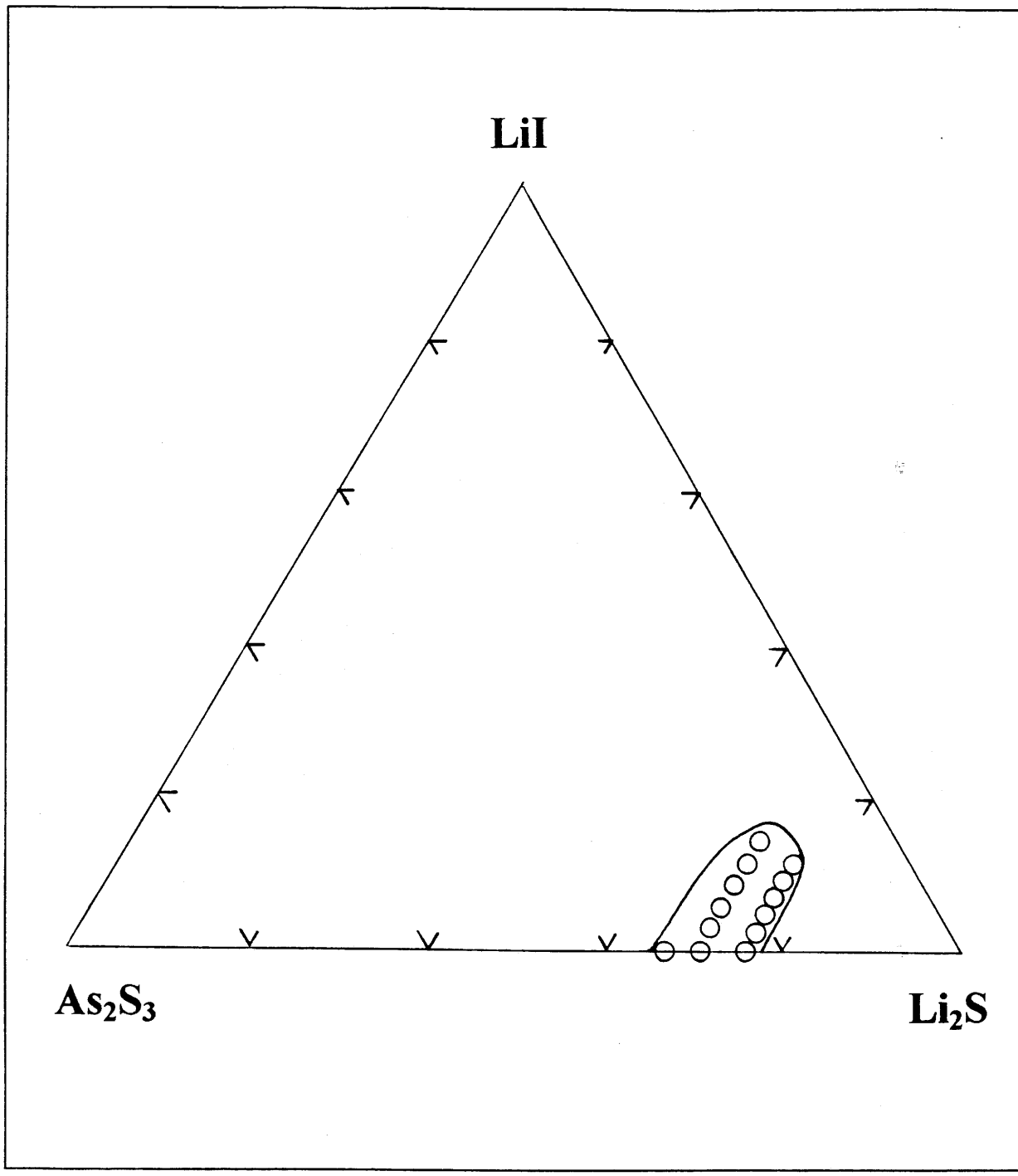

Fig. I.6 Glass forming region of yLiI-(1-y)[xLi$_2$S-(1-x)As$_2$S$_3$] ternary glass system.

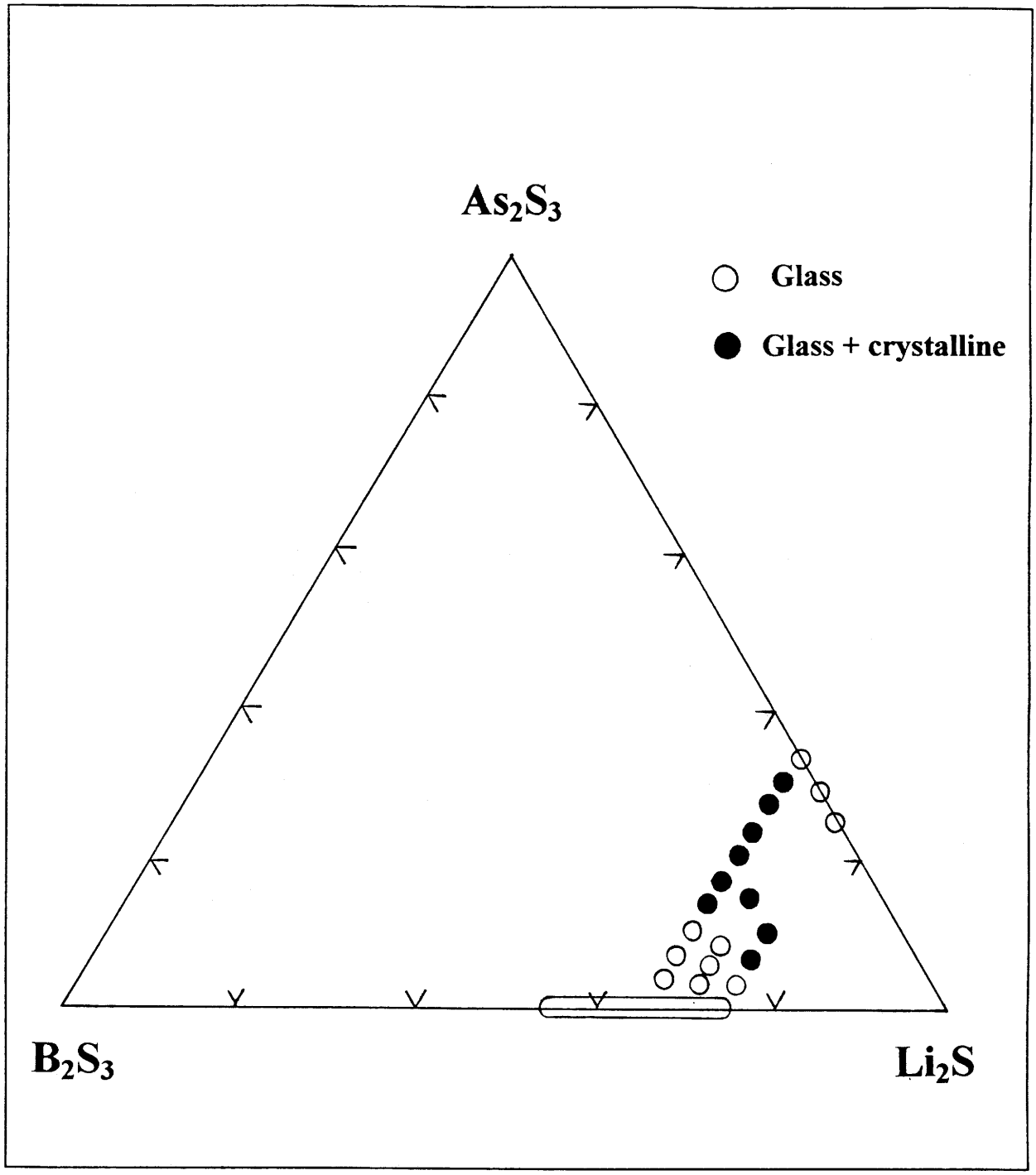

Fig. I.7 Glass forming region of xLi_2S-$(1-x)[(1-y)B_2S_3$-$yAs_2S_3]$ ternary glass system.

For both x = 0.67 and x = 0.70, amorphous compounds were obtained in the range $0 \leq y \leq 0.3$ but homogeneous glasses (i.e. exhibiting only one Tg) are present only in the range $0 \leq y \leq 0.3$ and $0 \leq y \leq 0.1$ respectively. The other compositions exhibit two glass transition temperatures (Fig. I.8). For x = 0.75 amorphous compound were obtained in the range $0 \leq y \leq 0.1$ but only y = 0 corresponds to a homogeneous glass.

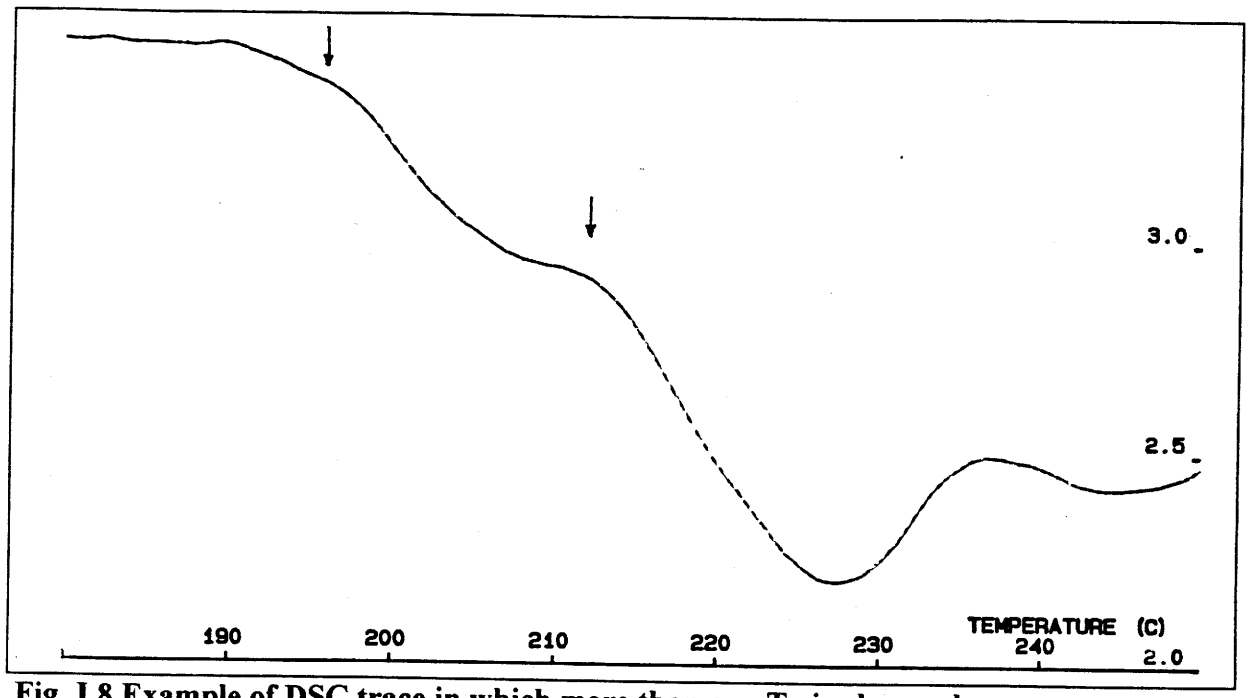

Fig. I.8 Example of DSC trace in which more than one Tg is observed.

I.5.5 Lead doped glass

Lead doped glasses were prepared for Li_2S-B_2S_3 and Li_2S-As_2S_3 binary based glasses. Such glasses were prepared from Li_2S, As_2S_3 (amorphous) and PbS or Li_2S, B, S and PbS, respectively. The method of glass preparation was the same as previously described. Glasses were consistently doped with 0.05 moles of PbS being added to 1 g of the host glass. This low concentration of PbS allows lead doping of glasses in the whole vitreous domain previously found in the two systems.

I.6 Preparation of single crystals

In order to compare the structure of a crystalline compound to the glasses having the same chemical composition, several crystal growths were attempted. Only crystals corresponding to $0.5Li_2S$-$0.5As_2S_3$ (i.e. $LiAsS_2$) and $0.75Li_2S$-$0.25As_2S_3$ (i.e. Li_3AsS_3) compositions respectively were prepared. Attempts to obtain $0.66Li_2S$-$0.34As_2S_3$ crystal (i.e. $Li_4As_2S_5$) always resulted in a polycrystalline mixture of $LiAsS_2$ and Li_3AsS_3.

I.6.1 Growing of $LiAsS_2$ single crystal

A Li_2S:As_2S_3 = 1:1 mole ratio mixture was introduced into a carbon crucible, itself placed in a silica tube sealed under vacuum. The tube was then heated to 650 °C and held at this temperature for 20 hours allowing complete chemical reaction. The assembly was then cooled slowly to room temperature at a rate of 0.6 $°Ch^{-1}$. This was then annealed at 240 °C for 7 days. The ampoule was opened inside a glove box, whereupon shiny gray metal coloured crystals inside a block of polycrystalline material was recovered. Chemical analysis showed that both the single crystalline phase and polycrystalline phase had the same $LiAsS_2$ composition.

I.6.2 Growing of Li_3AsS_3 single crystal

Starting from a mixture of Li_2S + As_2S_3 (3:1) the same procedure as described previously was repeated. It was possible to separate, after crushing, the two types of crystals from the polycrystalline block. One crystal type corresponding to $LiAsS_2$ was shining metallic gray and the other type, confirmed by XRD to be Li_3AsS_3, was green.

References

(1) H. Eckert, Progress in NMR Spectroscopy, **24** (1992), 159

(2) W. H. Zachariasen, J.Am. Ceram. Soc., **54** (1932), 3841

(3) R. H. Doremus, *Glass Science* (John Wiley & Sons, 1973)

(4) P. W. McMillan, *Glass Ceramics* (Academic Press, 2nd Ed., 1979)

(5) J. P. Malugani and G. Robert, Solid State Ionics, **1** (1980), 519

(6) H. Wada, M. Ménétrier, A. Levasseur, P. Hagenmuller, Mater. Res. Bull., **18** (1983), 189

(7) D. Ravaine, J. Non-Cryst. Solids, **73** (1985), 287

(8) S. R. Elliott, *Physics of Amorphous Materials*
(Longman Scientific & Technical, 2nd Ed., 1990)

(9) J. Zarzycki, *Les verres et l'état vitreaux* (Masson, 1982)

(10) R. Hosemann and S. N. Bacchi, *Direct Analysis of Diffraction by Matter*
(North Holland, Amsterdam, 1962)

(11) G. N. Greaves, A. Fontaine, P. Lagarde, D. Raoux and S. J. Gurman,
Nature, **293** (1981) 611

(12) G. N. Greaves, La Recherche, **137** (1982) 1184

(13) G. N. Greaves, J. Non-Cryst. Solids, **71** (1985) 203

(14) J. D. Bernal, Nature, **183** (1959) 141

(15) J. D. Bernal, Nature, **185** (1960) 68

(16) G. O. Brunner, Acta Crystallogr., **A27** (1971) 388

(17) D. E. Polk, Scr. Metall., **4** (1970) 117

(18) D. E. Polk, Acta Metallogr., **20** (1972) 485

(19) G. S. Cargill, *Solid State Physics*,
Vol 30, F. Seitz, D. Turnbull and H. Ehrenreich Ed (Academic, 1975)

(20) P. H. Gaskell, J. Non-Cryst. Solids, **32** (1979) 207

(21) P. H. Gaskell, J. Phys., **C12** (1979) 4337

(22) P. J. Flory, *Principles of Polymer Chemistry* (Ithaca, Cornell University Press, 1953)

(23) M. L. Huggins, *Physical Chemistry of High Polymers* (Wiley, New York 1958)

(24) G. C. Berry and E. F. Casassa, *Macromolecular Reviews* (4ed, 1970) 1

(25) R. Zallen, *The Physics of Amorphous Solids* (Wiley, 1983)

(26) R. Kaplow, S. L. Strong and B. L. Auerbach, Phys. Rev., **A138** (1965) 1336

(27) A. J. Leadbetter and A. C. Wright, J. Non-Cryst. Solids, **7** (1972) 23

(28) A. J. Leadbetter and A. C. Wright, J. Non-Cryst. Solids, **7** (1972) 37

(29) A. J. Leadbetter and A. C. Wright, J. Non-Cryst. Solids, **7** (1972) 141

(30) A. J. Leadbetter and A. C. Wright, J. Non-Cryst. Solids, **7** (1972) 156

(31) G. M. Sheldrick, *SHELX 76* (1976),

Program for Crystal Structure Determination, Univ. of Cambridge, England

(32) N. Walker and D. Stuart, Acta Cryst., **A39** (1983), 158

(33) F. Ugozzoli, Comput. Chem., **11** (1987), 109

(34) Molecular Simulation, *CERIUS* Version 3.1

(St. Johns Innovation Centre, Cambridge, England, 1993)

(35) J. J. Rehr, J. Mustre de Leon, S. I. Zabinsky and R. C. Albers, J. Am. Chem. Soc., **113** (1991); A. O'Day, J. J. Rehr, S. I. Zabinsky and G. E. Jr. Brown, J. Am. Chem. Soc., **116** (1994) 2938.

(36) J. E. Bauerle, J. Phys. Chem. Solids, **30** (1969) 2657

(37) A. Hojjaji, Ph. D. These, Univ. Bordeaux I, 1990

(38) H. U. Hunther, B. Krebs, H. Eckert and W. Muller-Warmuth,

Inog. Chem., **24** (1985), 1288

(39) M. C. R. Shastry, M. Ménétrier and A. Levasseur, Solid State Comm., **85** (1993), 887

Chapter II. Structure of As_2S_3 glasses

Introduction

Vitreous samples of arsenic sulphide can be easily prepared by cooling a melt of amorphous powder of commercially available As_2S_3. This simple method of preparation leads to vitreous As_2S_3 being extensively studied as the basis of simple sulphide glasses much as SiO_2 or B_2O_3 are for oxide glasses. The crystalline form of As_2S_3 is also well documented. Comparison of the amorphous and crystalline states of the same material has been, for sometime, the subject of many studies. As_2S_3 also exhibits a so called photo-darkening effect which results from a structural alteration. This colour change is of interest in the field of optical device research. The photo-darkening effect causes the annealed yellow As_2S_3 glass to change to a redder colour on illumination (photo-darkened state). Heating of the material to a temperature near its glass transition temperature causes it to return to the undarkened state. The reason for this effect is not clear, but is probably related to an intermediate-range order variation. There is no conclusive spectroscopic evidence that an intermediate-range order exists in As_2S_3 glass. There is, however, a general consensus on the existence of short-range order. This feature provides the essential framework for the understanding of the structure of As_2S_3 glass, and also the network modifying processes which occurs in binary or ternary glasses based on As_2S_3.

Before considering the effects of modifiers, doping salts and the influence of a second glass co-former, it is essential to establish the structure of crystalline As_2S_3 and to discuss the various published works pertaining to structure of vitreous As_2S_3.

In the following crystalline As_2S_3 will be denoted as c-As_2S_3 and vitreous As_2S_3 as v-As_2S_3.

II.1 Crystal structure of As_2S_3

The structure of orpiment (c-As_2S_3) is well known and the first structural determination was done by N. Morimoto (1). The structural data of this crystal are reported in Table II.1.

Mineral name	**Orpiment**
crystal system	Monoclinic
space group	$P2_1/n$, C^5_{2h} (No. 11)
cell parameters	
a	11.49 Å
b	9.59 Å
c	4.25 Å
β	90°27'
All atoms are placed in general position	(4e) ±(x, y, z; ½ - x, y +½, ½ - z)

Table II.1 Structural data for As_2S_3 single crystal (2,3).

Fig. II.1 shows the atomic arrangement for the data shown in ref. (2) using CERIUS (4) for the representation.

The structural feature of this crystal is that it has a layered character with spiral chains of S-As-S-As running parallel to the c-axis. The layers are arranged perpendicularly to the b-axis. Each layer contains twelve-membered rings of alternating As and S atoms. The average bond length within the layer is 2.24 Å, and the smallest interatomic separation between layers is 3.56 Å. The very weak inter-layer bonding (due to van der Waals interaction) facilitates inter-planar cleaving.

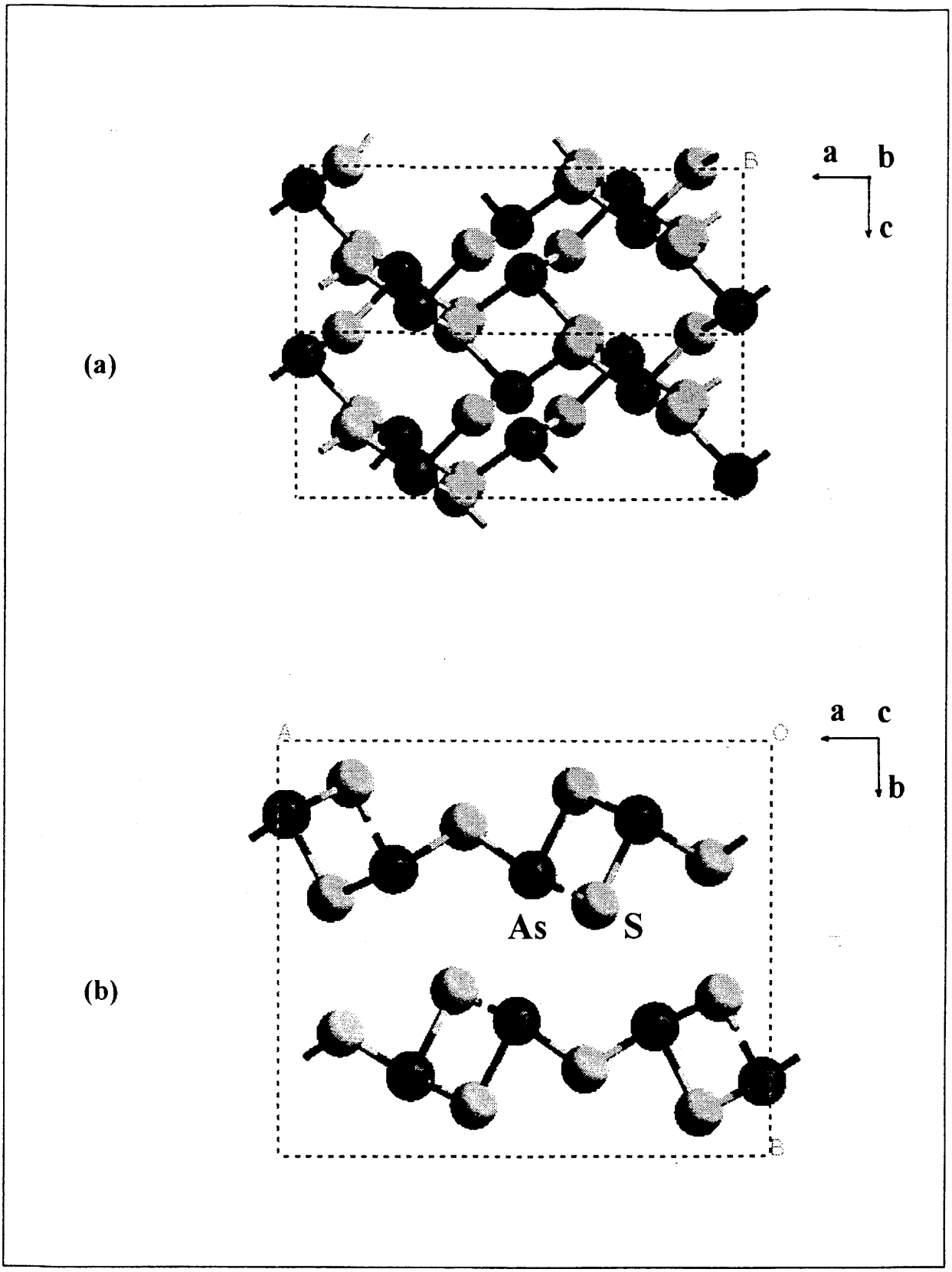

Fig. II.1 Crystal structure of As_2S_3 ; (a) a view along the b-axis, looking down on a single layer, (b) a view along the c-axis.

Within the tightly bound layer, each As atoms has threefold coordination and each S atom has two fold coordination. Each As atom is bonded to three S atoms forming strong covalent bonds in a triangular pyramidal arrangement with the As atom at the apex and the three S atoms forming the base. The AsS_3 pyramids are linked together by As-S-As bonds (5).

II. 2 Structural hypothesis of v-As_2S_3

II.2.1 Molecular model

Lucovsky and Martin (6,7) proposed a structural model for v-As_2S_3 and v-As_2Se_3 based on Raman and IR spectroscopic studies, in which they observed that certain vibrational modes still follow selection rules determining whether the modes are IR or Raman active. In this molecular model it was suggested that the glass consists of molecular components (the AsS_3 or $AsSe_3$ pyramids) which have bond-bending or bond stretching vibrational modes at frequencies corresponding to the spectral peaks. The definition of a 'molecule' is a AsS_3 with bridging S atoms. Additionally, the three S atoms which are bonded to the As, are each in turn bonded to one other As atom in a network configuration (Fig. II.2). Locally, the structure has some aspects of a two-dimensional polymer and reflects the short-range order of the layered crystal.

The bent As-S-As bond must be taken into account when considering the interaction between the AsS_3 'pyramidal molecules' and thus the normal vibrational modes of the real system can only be obtained by considering this coupled system. However, the intermolecular coupling is considered to be sufficiently weak and thus the molecule (AsS_3) and bridging chain (As-S-As) are treated independently. This model successfully fitted the observed frequencies and led to proposition that the glass structure could consist of such linked molecular units.

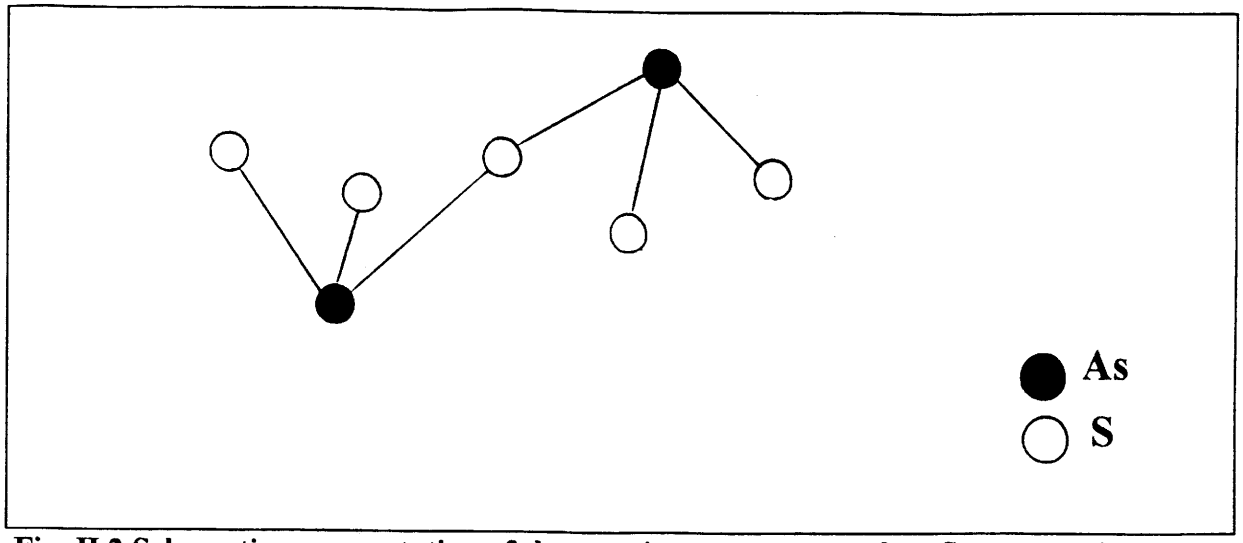

Fig. II.2 Schematic representation of the atomic arrangement of As_2S_3 network in the molecular model (6).

II.2.2 Planar-random network model

Bermudez (8) has extrapolated the layered character of both crystalline and glassy As_2S_3 by computer generating a two-dimensional A_2B_3 glass like disordered network having a Gaussian distribution of A-B-A bond angles. A part of the network is shown in Fig. II.3.

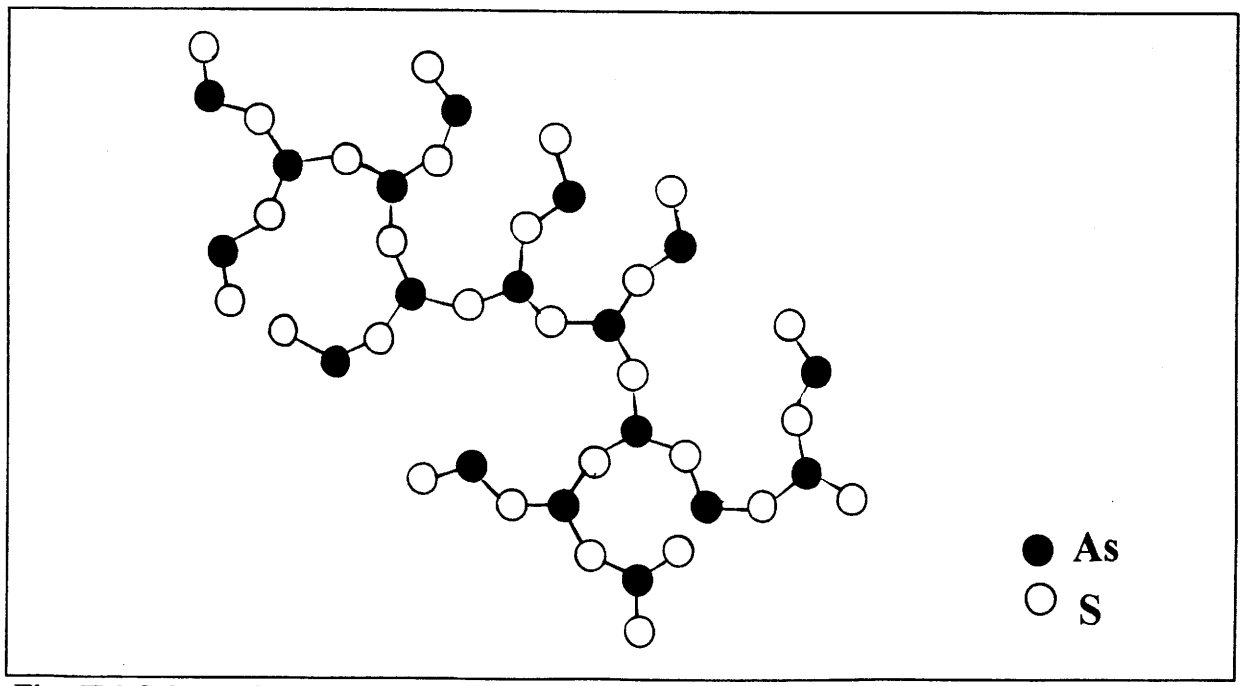

Fig. II.3 Schematic representation of the atomic arrangements in the planar random network model (8).

The equations of motion were derived, by deLaunay (9), for nearest-neighbour central and non-central interactions. Density of states spectra were calculated by applying the negative eigenvalue theorem (10) to the dynamic matrix. Eigenvectors for selected frequencies were computed by inverse iteration (11) after first calculating the exact eigenvalues by standard methods (11). Under appropriate choice of boundary conditions, the bonds in the computed densities of states adequately reproduce those in the experimental spectra both in number and position.

This network model has also been analysed in terms of the internal modes of vibration of the AsS_3 plane-trigonal unit where the 'As-S-As' are considered to move similarly to water molecules. However, the calculated density of states based on this model predicts the different vibrational modes to that found by Raman experiments (12). Data from Raman spectra of the planar random network model and molecular model are compared and summarised in Table II.2.

Planar random network model	**Molecular model**
●340 cm^{-1} antisymmetric As-S-As stretching vibration ●310 cm^{-1} stretching of the S-As-S bond in the AsS_3 triangular units	●344 cm^{-1} antisymmetric pyramidal deformation ●309 cm^{-1} symmetric pyramidal deformation

Table II.2 Comparison between planar random network model and molecular model (12).

As discussed previously in this chapter the existence of AsS_3 pyramidal units is widely acknowledged, and most descriptions of SRO or higher order structure are based on molecular models.

II.2.3 Higher order structure model

For higher ordered structure, the general consensus which existed for SRO no longer exists. Some comparative studies between crystal and glass by vibrational spectroscopy have suggested layered structural configurations such as -As-S-As-S-As- chains that link together and form planar structures (13). Another possibility from such spectroscopic results is an explanation based on bridged parallel chains which centre on 12-membered rings of alternating As and S atoms (14). The study of IRO (intermediate-range order) of v-As_2S_3 is principally a question of the degree of the order that is seen in the crystalline state such as; AsS_3 pyramids, pyramids linked into As-S-As-S-As chains, chains held together with bridging S atoms or alternate layers of bridged parallel chains which also exist in v-As_2S_3. The study of IRO which was defined in I.2.2 has some difficulties in terms of concept and experiment. The conceptional problem relates to the actual definition of IRO as discussed extensively several years ago (15-17). Second, the experimental determination of IRO in glass is difficult because of symmetry dependent experimental techniques and disorder broadening. These difficulties cause a problem in the theoretical modelling of a v-As_2S_3 structure.

The existing models on high order structure of v-As_2S_3 are the following:

1) Rechtin et al. (18) proposed a model of amorphous As_2S_3 containing 100 atoms. This model began with a random cluster (small well ordered units) of atoms which was then relaxed using a Monte-Carlo method so that it fits a given experimental radial distribution function. This model shows good agreement with the experimental radial distribution function, but is somewhat unrealistic in that it has a large number of internal dangling bonds which are known to be absent in the real material.

2) Fujiwara et al. (19) proposed a model which originates with a random close-packed structure of atoms which is relaxed using an atomic potential which involves bond length and

bond angles only. The results showed good agreement with the experimental radial distribution function, and the model presented evidence for two dimensional planar structures. However, this model also contains a large portion of internal dangling bonds.

3) Fowler and Elliott (20) created a model of v-As_2S_3 by a substitution method. They expected that this model could accurately simulate the X-ray diffraction without resorting to layers or bridged parallel chains, but concluded that these structures were unlikely in v-As_2S_3.

4) Pfeiffer et al. (21) used the relaxed 'stick-ball method' (hand made structure) to build several models and the models showed evidence for the existence of helical forms of intermediate-range order.

5) Brabec (22) used a computer model which considered the values of dihedral-angle distribution. Through a study of dihedral angle statistics, Brabec characterised the intermediate-range order in v-As_2S_3 in terms of small helical segments comprised of linked AsS_3 pyramids (Fig. II.4). Additionally, the evidence for the existence of six-membered rings that form the termination of two intersecting helical chains was highlighted.

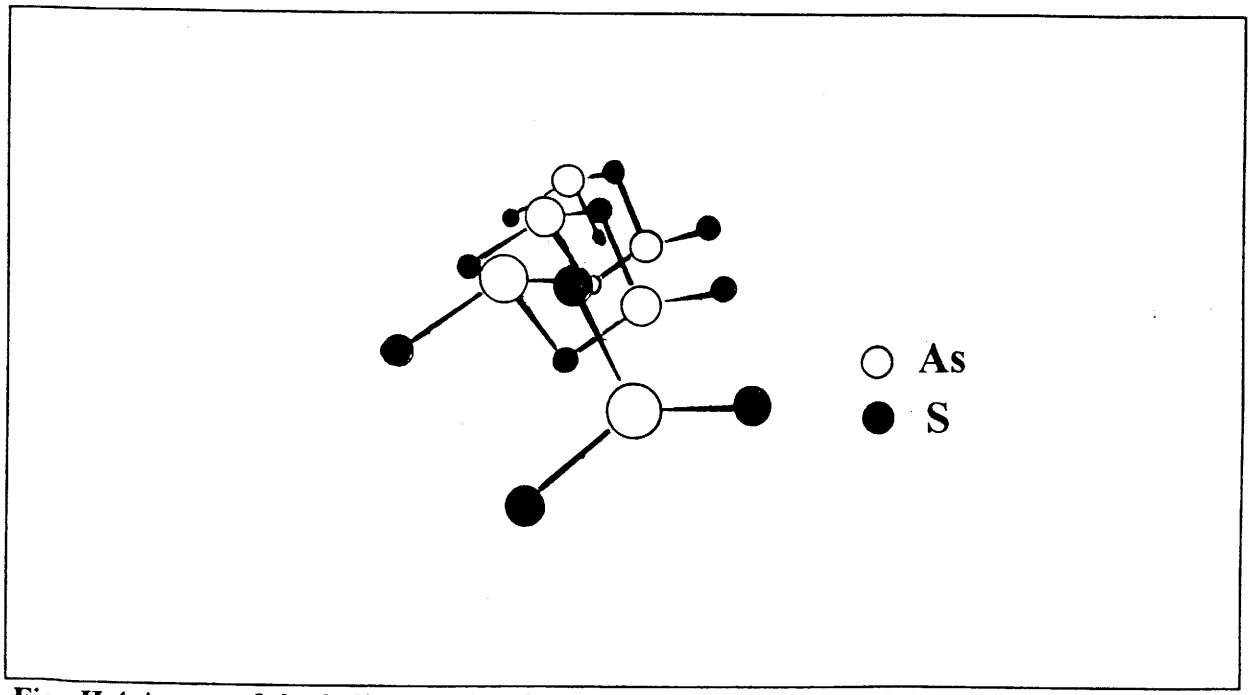

Fig. II.4 A part of the helical chain of v-As_2S_3.

II.3 Spectroscopic considerations of As_2S_3 glass

II.3.1 Raman spectroscopy

It is well accepted that in amorphous materials, all vibrational modes can contribute to the first order Raman scattering, whereas, in a crystal the constraint of **k** vector conservation allows only certain phonons near **k** = **0** to contribute, but as described previously, this fact is no longer applicable to v-As_2S_3.

As_2S_3 glasses have long been studied by IR and Raman spectroscopy; various aspects, such as comparing with crystalline As_2S_3 (5,13), compositional dependence (23), or cooling temperature dependence (24) have all been investigated. The vibrational mode in AsS_3 pyramidal units is illustrated in Fig. II.5 (25).

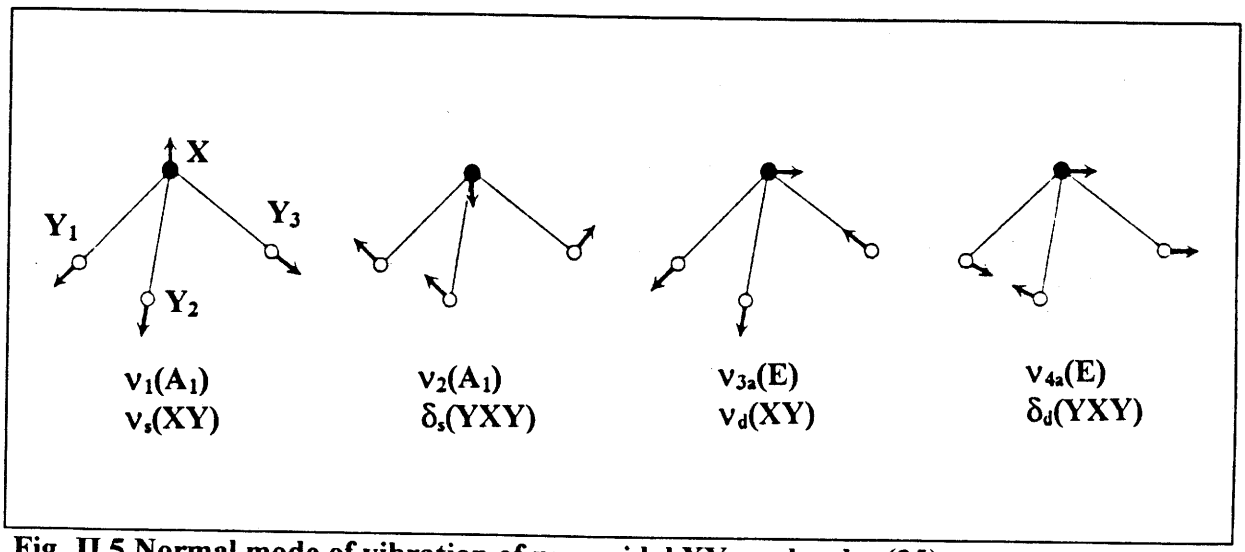

Fig. II.5 Normal mode of vibration of pyramidal XY_3 molecules (25).

As it was shown in II.2.1, by assigning vibrational modes, the intermolecular coupling is assumed to be sufficiently weak so that the 'molecule' (AsS_3) and the corresponding bridging chain (As-S-As) modes may be treated independently. Also, due to weak inter-molecular coupling, vibrational modes retain their inherent symmetry and are only observed in their respective spectra. That is, dominant IR (ν_3) and Raman (ν_1) modes occur at different

frequencies corresponding respectively to the antisymmetric and symmetric stretching modes of the pyramidal molecule.

Recently, Shastry et al. (26) assigned new water molecular like vibrational modes to pure v-As_2S_3 as collated in Table II.3 from Raman spectra (Fig. II.6) and the IR spectrum of v-As_2S_3 (cf. II.3.2).

Molecular species	Mode	Cal.(cm^{-1}) (5)	Rep.(cm^{-1}) (27)
AsS_3 pyramid	ν_1	344	355
	ν_2	162	160
	ν_3	310	310
	ν_4	133	120-150
As-S-As water molecule	ν_1'	218	230
	ν_2'	55	55
	ν_3'	438	400

Table II.3 Reported and calculated vibrational frequencies for As_2S_3 glass(IR & Raman).

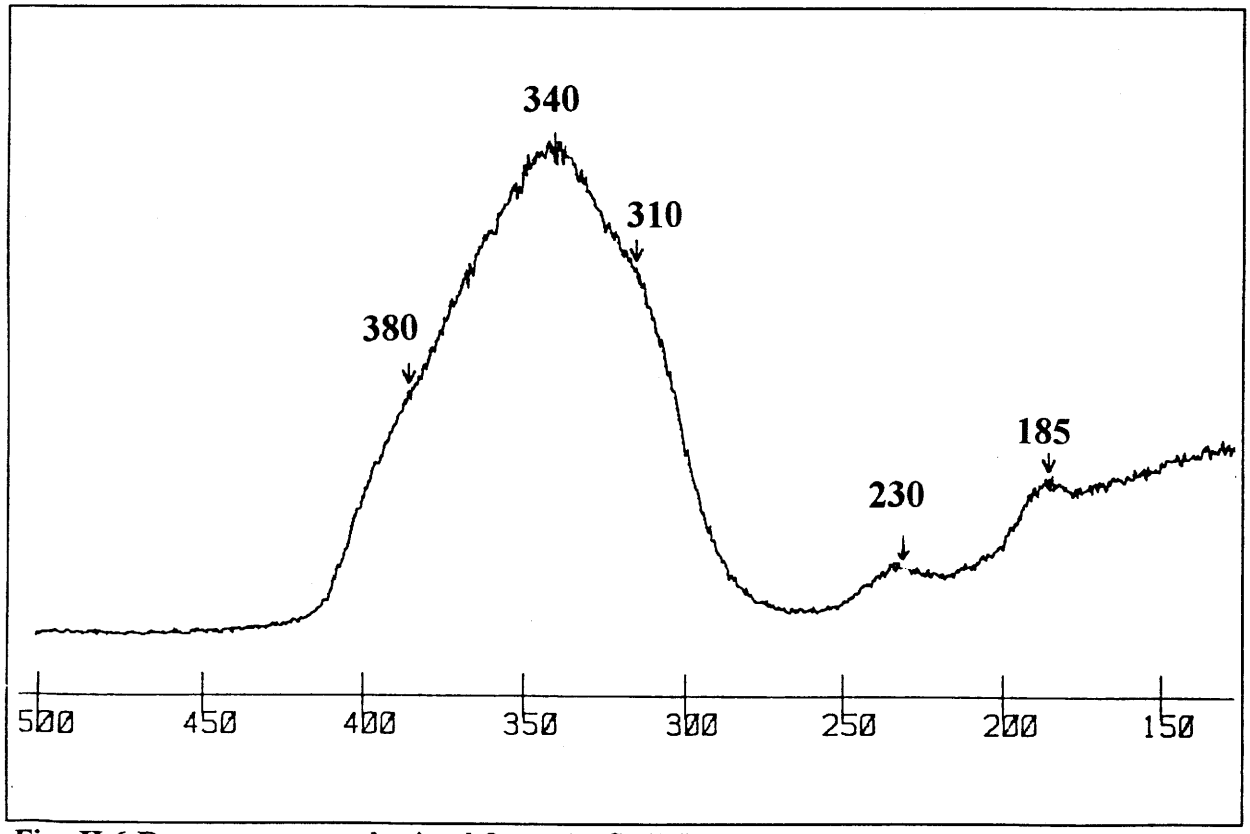

Fig. II.6 Raman spectra obtained for v-As_2S_3 (26).

The peak at 230 cm^{-1} could originate from As-As homopolar bonds as predicted by Tanaka (24) due to the loss of some sulphur during melting. This also affects XAS results as will be discussed later in II.3.3.

II.3.2 IR spectroscopy

The fact that the infrared spectra are influenced mainly by short-range order and are relatively insensitive to long-range order highlights the techniques adaptation to the study of glass. It is known that the As_2S_3 glass maintains short-range order units which exist in crystalline As_2S_3 as described previously. Fig. II.7 shows an IR spectrum comparing crystalline and glassy As_2S_3. The spectral feature of glass consists of a strong absorption at 310 cm^{-1} with weak shoulders at 350 cm^{-1} and 380 cm^{-1}. The origin of the 380 cm^{-1} vibration is not clear but it is recognised as originating from coupling of pyramidal units bridged by sulphur atoms. The strong absorption at 310 cm^{-1} originates from the ν_3 vibrational mode and the weak shoulder at 350 cm^{-1} is due to a ν_1 vibrational mode as described in the previous section.

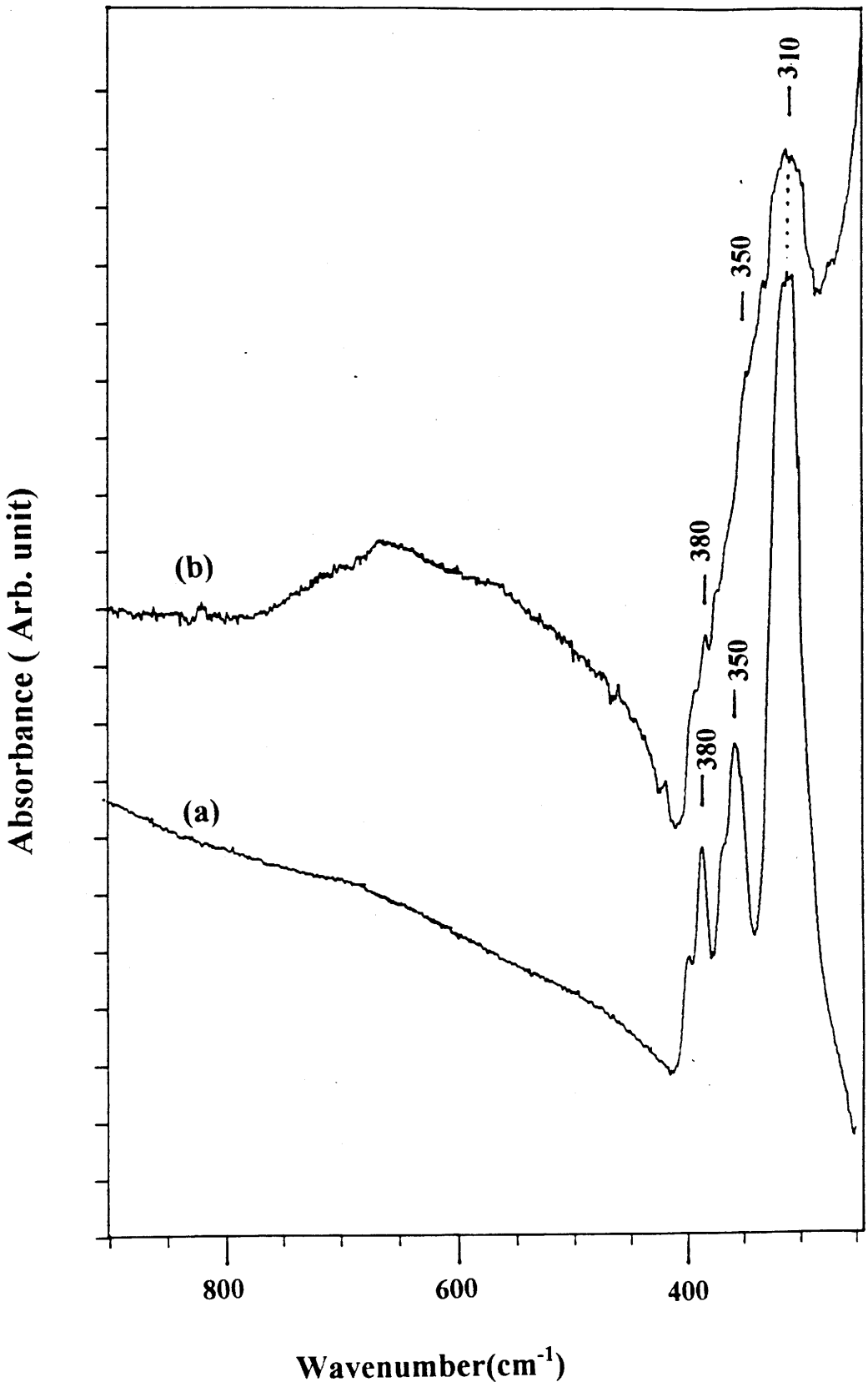

Fig. II.7 IR spectra obtained for (a) c-As_2S_3 and (b) v-As_2S_3.

II.3.3 XAS spectroscopy

Fig. II.8 shows the k^3-weighted $\chi(k)$ data for the v-As_2S_3 glass, and Fig. II.9 the Fourier transform taken over a k-range from 2.5 to 13 $Å^{-1}$. Curve fitting was done with one shell fitting, and these are compared with experimental curves. As shown in Fig. II.8, the fitting line matches the experimental data very well, except for a slight deviation at high k. The measured coordination number of As is 2.8, and the average As-S distance is 2.28 Å. The measured coordination number is lower than the one expected i.e. 3 (ideal case), and the distance is longer than 2.24 Å (5), but similar to those of an $As_{42}S_{58}$ stoichiometric sample (27). This result is proposed to be caused by the loss of sulphur during melting and the existence of homopolar As-As bonds. Table II.4 represents the comparison of radial distance As-S obtained from this work and other results.

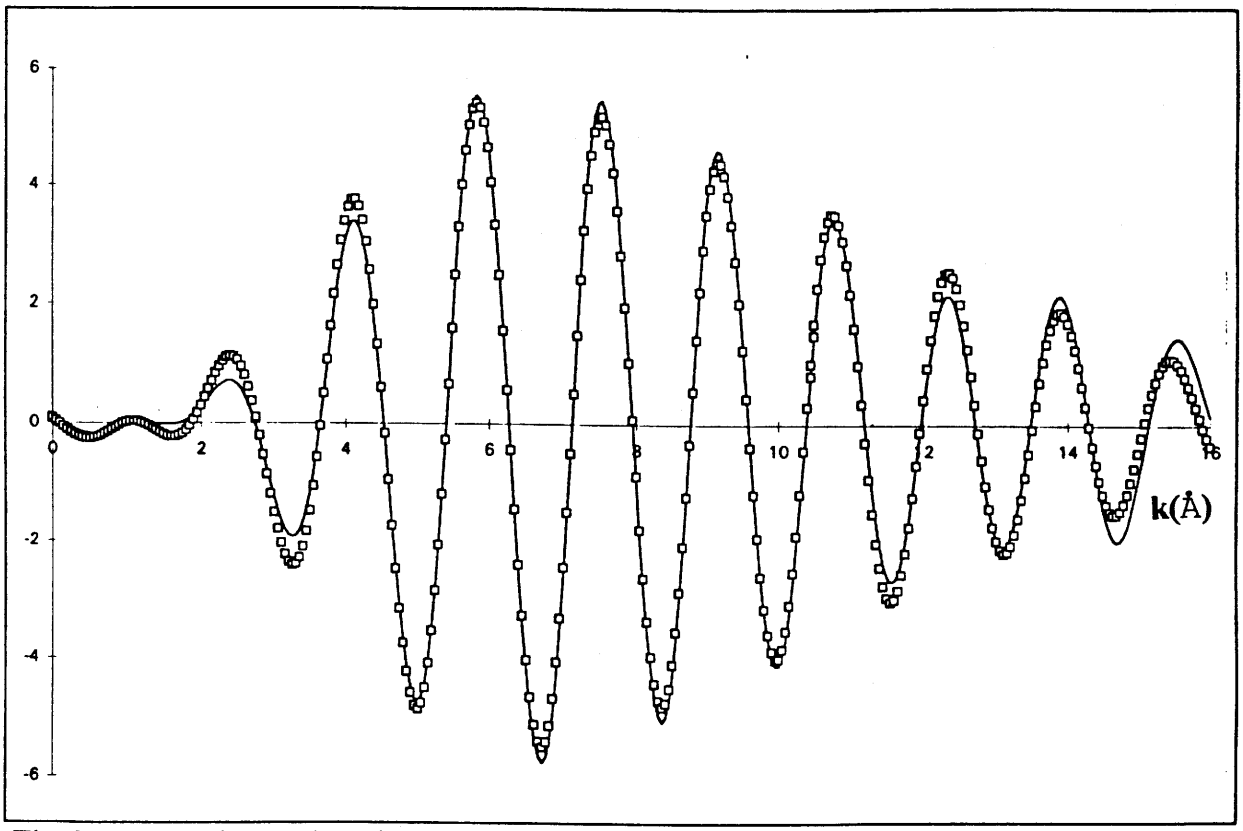

Fig. II.8 Experimental (solid line) and best fitted (white dotted line) As K-edge EXAFS spectra $k^3(\chi)$ for v-As_2S_3.

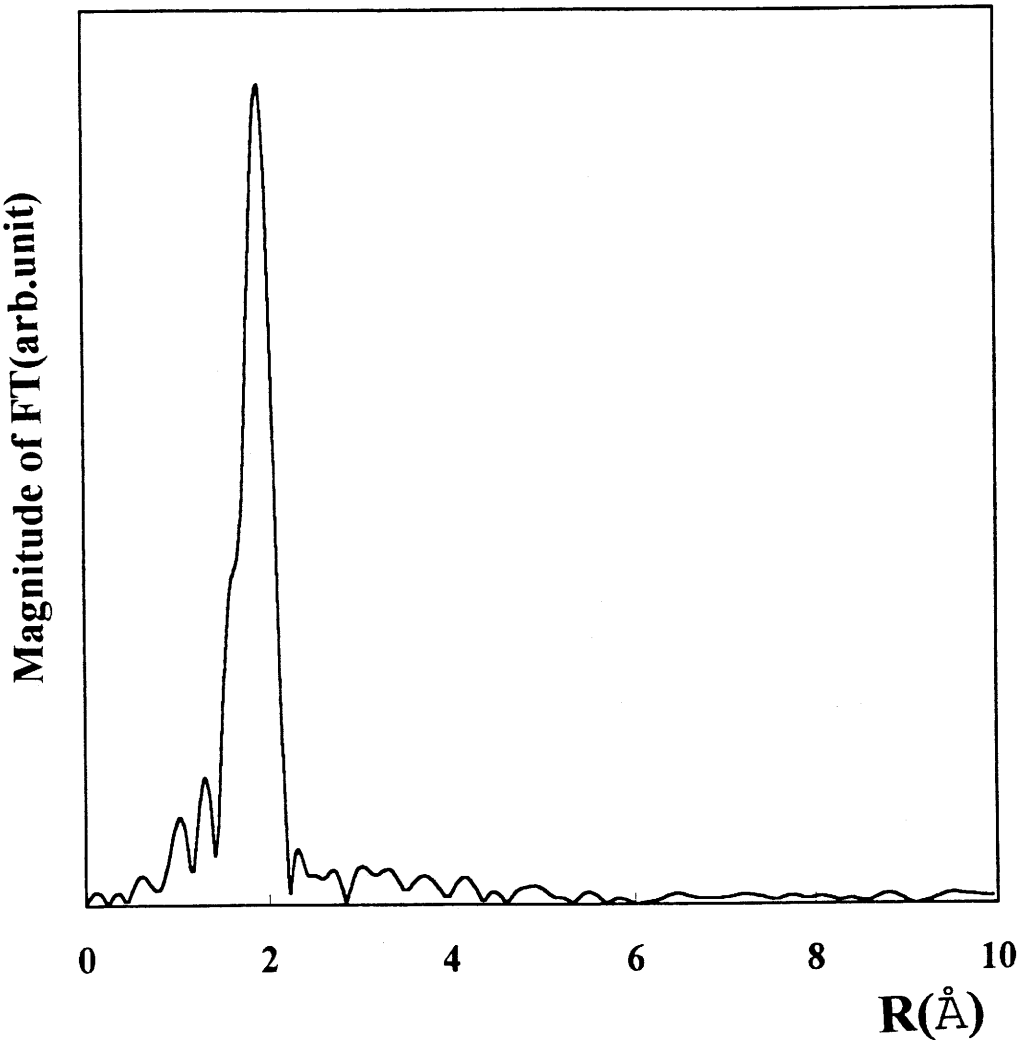

Fig. II.9 Magnitude of FTs in the range of ~2.5 Å^{-1} <k<~13 Å^{-1} $k^3\chi(k)$ for glassy As_2S_3.

R_{As-S}(Å)	Experimental method	Measured sample
2.25	EXAFS	bulk (28)
2.28	EXAFS	thin film (27)
2.28	Neutron diffraction	thin film (29)
2.28	EXAFS	bulk (this work)

Table II.4 Measured average radial distance As-S using several experimental methods.

Conclusion

Structural models of v-As_2S_3 have been reviewed in terms of structural orders. The comparison of these provides a profound understanding of the v-As_2S_3 structure and a base for understanding the structure for alkali modified binary glasses.

The vibrational spectroscopic features of v-As_2S_3 have been discussed on the basis of the molecular model proposed by Lucovsky and Martin. These show that the short-range order of crystalline As_2S_3 is well conserved in v-As_2S_3. The stoichiometry of v-As_2S_3 is slightly changed during melting due to loss of sulphur, and the existence of small amount of As-As homopolar bonding is suggested from the spectroscopic experimental results.

XAS investigation of v-As_2S_3 suggests the coordination number of As is 2.8 and the average As-S distance is 2.28Å. Comparison of such results shows a good agreement with other works on XAS and neutron diffraction.

The different interpretation of IR and Raman spectroscopic results illustrates the difficulty to propose a structure for an amorphous material.

References

(1) N. Morimoto, Mineral. J.(Sapporo), **1** (1954) 160

(2) R. G. Wyckoff, *Crystal structures*, **Vol. 2** (New York, Wiley 1957) 26

(3) JCPDS-ICDD, **27-28** (1988)

(4) Molecular Simulations, *CERIUS* Version 3.1

(St Johns Innovation Centre, Cambridge, England, 1993)

(5) R. Zallen, M. L. Slade and A. T. Ward, Phys. Rev, **B3** (1971) 4257

(6) G. Lucovsky, Phys. Rev., **B6** (1972) 1480

(7) G. Lucovsky and R. M. Martin, J. Non-Cryst. Solids, **8-10** (1972) 185

(8) V. M. Bermudez, J. Chem. Phys., **57** (1972) 2793

(9) J. deLaunay, Solid State Physics, ed. F. Seitz and D. Turnbull,

Vol. 2 (Academic, New York, 1956)

(10) P. Dean and M. D. Bacon, Proc. Roy. Soc. (London), **A283** (1965) 64

(11) J. H. Wilkinson, *The Algebraic Eigenvalue Problem* (Clarendon, Oxford, 1965)

(12) R. J. Kobliska and S. A. Solin, Phys. Rev., **B8** (1973) 756

(13) A.P. DeFonzo and J. Tauc, Phys. Rev., **B18** (1978) 6957

(14) J. C. Phillips, C. A. Beevers and S. E. B. Gould, Phys. Rev., **B21** (1980) 5724

(15) G. Lucovsky, J. Non-Cryst. Solids, **97-98** (1987) 155

(16) S. R. Elliott, J. Non-Cryst. Solids, **97-98** (1987) 159

(17) L. Cervinka, J. Non-Cryst. Solids, **97-98** (1987) 207

(18) M. O. Rechtin, A. L. Renninger and B. L. Averbach, J. Non-Cryst. Solids, **15** (1974) 74

(19) T. Fujiwara, S. Itoh and M. Okazaki, J. Non-Cryst. Solids, **45** (1981) 371

(20) T. G. Fowler and S. R. Elliott, J. Non-Cryst. Solids, **92** (1987) 31

(21) G. Pfeiffer, C. J. Brabec, S. R. Jefferys and M. A. Paesler, Phys. Rev., **B39** (1989) 12861

(22) C. J. Brabec, Phys. Rev., **B44** (1991) 13332

(23) A. T. Ward, J. Phys. Chem., **72** (1968) 4133

(24) K. Tanaka, Phys. Rev., **B36** (1987) 9746

(25) K. Nakamoto, *Infrared Spectra of Organic and Coordination Compounds* (John Wiley & Sons, 1963)

(26) M. C. R. Shastry, M. Couzi, A. Levasseur and M. Ménétrier, Phil. Mag., **B68** (1993) 551

(27) C. Y. Yang, M. A. Paesler and D. E. Sayers, Phys. Rev., **B36** (1987)980

(28) W. Zhou, M. A. Paesler and D. E. Sayers, Phys. Rev., **B46** (1992) 3817

(29) A. J. Leadbetter and A. J. Apling, J. Non-Cryst. Solids, **15** (1974) 250

Chapter III. Structural study of As_2S_3 based crystals

Introduction

Sulphide glasses with a high alkali content are studied because of their high ionic conductivities (~10^{-3} Ω^{-1} cm^{-1} at room temperature), and much research is devoted to studying the relationship between structure and ionic conductivity. Recently, lithium arsenic sulphide glasses, designated as xLi_2S-$(1-x)As_2S_3$, have been synthesized, giving homogeneous glasses for $0.67 \leq x \leq 0.75$ (1). In addition, no crystalline phase has been reported until now in the Li_2S-As_2S_3 system.

This chapter reports the preparation and structural determination of Li_3AsS_3 (corresponding to $x = 0.75$). It also includes a tentative structural determination of $LiAsS_2$ (corresponding to $x = 0.5$). The latter part of this chapter is devoted to a spectroscopic characterization of these phases to provide references in understanding the local structure of Li_2S-As_2S_3 binary glasses. The aim of this chapter, therefore, is to obtain structural information which could be used to obtain a better understanding of glasses which have the same chemical composition as their crystalline counterparts.

III.1 Crystal structure of Li_3AsS_3

The single crystal analysis was done with the help of P. Gravereau and L. Trut. The crystals obtained were green and irregular in size and shape (cf. I.6). The detailed structural parameters have been obtained in the $Pna2_1$ space group in the orthorhombic crystalline system. The chemical analysis performed on collected crystals results in ratios of S/As and Li/As close to 3.

III.1.1 Structure determination and refinement

Preliminary investigations of the crystals were made with Buerger and Weissenberg films and were consistent with orthorhombic symmetry. The systematic absence, (0 h l); $h + l \neq 2n$ and (h k 0); $h \neq 2n$, points to the space groups Pnma (No.62) or $Pn2_1a$ (No.33). The precise structure of Li_3AsS_3 was determined from intensity data collected with an Enraf-Nonius CAD4 four-circle auto-diffractometer using graphite monochromatized Mo-Kα radiation ($\lambda = 0.7107$ Å). The unit cell parameters of the single crystal were refined from the angular positions of 25 centred reflections. The intensities of 8921 reflections were measured in the range $-15 \leq h \leq 15$, $0 \leq k \leq 19$, and $-13 \leq l \leq 13$ with a $\theta/2\theta$ scan mode. The intensity data were corrected for Lorentz and polarization effects and equivalent reflections were averaged to provide a set of 802 independent reflections with $I > 3\sigma(I)$, where $\sigma(I)$ is the standard deviation in the intensity, with internal consistency factor $R_{int} = 10$ %. Trials with deconvolution of the Patterson function in the centrosymmetric Pnma space group did not succeed and led to the minimum residual index R of approximately 20 %. On the contrary, the treatment in the non-centrosymmetric $Pn2_1a$ space group provided an hypothesis for the arsenic atom site. The atomic sites of S and Li atoms appear with several successive Fourier difference functions.

The refinement of the structure was carried out by a full matrix least squares fit on F with isotropic thermal parameters for all atoms using the programme SHELX-76 (2). The intensities were weighted by a $w = 1/\sigma^2$ function. The refinement converged to $R \approx 6\%$, $R_w \approx 7\ \%$ (where R: residual index, R_w: weighted residual index). With this isotropic model, empirical absorption correction was done using the algorithm of Walker and Stuart (3) and the programme ABSORB (4). Such corrected values for the observed modules of the structure factors result in $R_{int} = 3.4\ \%$. The final calculation with 802 independent reflections and anisotropic thermal parameters for all atoms gave $R = 2.50\ \%$, $R_w = 2.52\ \%$. As the reference space group in International Tables (5) is $Pna2_1$ (and not $Pn2_1a$), cell parameters (Table III.1) and atomic parameters (Table III.2) are relative to the space group $Pna2_1$.

Crystal data	
Formula weight	191.931g
Crystal symmetry	Orthorhombic
Space group	$Pna2_1$ (No. 33)
Lattice parameters	
a	8.0522(3)Å
b	6.6323(5)Å
c	9.8146(2)Å
V	524.14(3)Å^3
Formula unit/cell, Z	4
Density(Calc.), Dx	2.417 g/cm^3
Radiation	Mo-Kα (λ = 0.7107 Å)

Table III.1 Li_3AsS_3 crystal data and detailed measurements and structure solution

Scan mode	$\theta/2\theta$
Scan width	$(1.00 + 0.35\ tg\theta)°$
Scan range	$0° < \theta < 45°$
Range of Miller indices	$-15 \leq h \leq 15$
	$0 \leq k \leq 19$
	$-13 \leq l \leq 13$
Temperature of measurement	293 K
Crystal size	irregular plate (350 × 100) μm^2
Crystal colour	greenish
Linear absorption coefficient	74.4 cm^{-1}
(single crystal only)	
Data collection	
Number of measured reflections	8921
Number of observed reflections	6533 [$I \geq 3\sigma(I)$]
Number of independent reflections	802 [$<F_o^2> \geq 3\sigma(<F_0^2>)$]
R_{int}	10 % (before absorption correction)
	3.4% (after absorption correction)
Refinement	
Weighting scheme	$w = 1/\sigma^2(F_0)$
R	2.50 %
R_w	2.52 %
Number of independent reflections	802 reflections
Number of refined parameters	63

Table III.1' Continued over Table III.1.

Species	Wyckoff position	Site symmetry	x	y	z	B_{eq}
Li(1)	4(a)	1	0.0678(14)	0.0496(16)	0.7790(12)	2.04(32)
Li(2)	4(a)	1	0.0766(13)	0.3548(15)	0.3114(11)	1.97(31)
Li(3)	4(a)	1	0.2489(15)	0.3855(16)	0.6100(11)	2.00(33)
S(1)	4(a)	1	0.0443(1)	0.1397(2)	0.5102(2)	1.10(3)
S(2)	4(a)	1	0.3150(2)	0.2195(4)	0.1865(2)	1.21(5)
S(3)	4(a)	1	0.3396(2)	0.2091(4)	0.8271(2)	1.14(4)
As	4(a)	1	0.2532(1)	0.4027(1)	0	0.982(12)

Table III.2-a Fractional atomic coordinates and equivalent isotropic displacement parameters(Å^2) in Pna2$_1$, $Beq = (8\pi^2/3)\sum_i\sum_j U_{ij}a_i^*a_j^*a_ia_j$.

Species	U_{11}	U_{22}	U_{33}	U_{23}	U_{13}	U_{12}
Li(1)	0.0268(52)	0.0227(50)	0.0281(50)	-0.0054(43)	0.0054(47)	-0.0010(41)
Li(2)	0.0241(48)	0.0230(46)	0.0279(54)	0.0030(43)	0.0047(45)	-0.0036(40)
Li(3)	0.0257(43)	0.0221(46)	0.0281(47)	-0.0046(41)	0.0005(51)	0.0016(49)
S(1)	0.0155(4)	0.0126(4)	0.0136(6)	0.0003(6)	0.0006(6)	0.0015(3)
S(2)	0.0187(6)	0.0150(8)	0.0121(6)	0.0007(6)	0.0012(5)	-0.0014(6)
S(3)	0.0177(6)	0.0127(7)	0.0131(6)	-0.0020(6)	-0.0010(5)	-0.0010(5)
As	0.0118(1)	0.0127(1)	0.0128(1)	-0.0009(4)	-0.0002(4)	0.0010(2)

Table III.2-b. Anisotropic thermal parameters of Li_3AsS_3 relative to the thermal factor, $T = \exp[-2\pi^2(h^2a^{*2}U_{11}+k^2b^{*2}U_{22}+l^2c^{*2}U_{33}+2hka^*b^*U_{12}+2klb^*c^*U_{23}+2lhc^*a^*U_{13})]$.

III.1.2 Structural description

Arsenic atoms together with sulphur atoms form the first coordination sphere, typically trigonal AsS_3 pyramids; these pyramids are interconnected by Li-ions, forming two LiS_4 tetrahedra and one LiS_3 pyramid. Li(2) and Li(3) atoms are four coordinated by sulphur atoms and Li(1) is three coordinated by sulphur atoms. Li(1) is at the top of a sulphur atoms based pyramid. All the $Li(2)S_4$ and $Li(3)S_4$ tetrahedra are linked together by their corners. The principal interatomic distances are listed in Table III.3. The average bond distance of As-S is 2.25 Å, which is similar to the value observed in orpiment (2.24 Å, (6)), Ag_3AsS_3 (2.25 Å, (7)), or Tl_3AsS_3 (2.25 Å, (8)). These As-S distances within the pyramids are longer than the As-S bond distance of c-$LiAsS_2$ (As-S; 2.21 Å). The distance of Li(1)-S, Li(2)-S and Li(3)-S are respectively 2.50 Å, 2.45 Å and 2.51 Å, which are similar to the distances found in c-Li_2S and c-Li_3BS_3 (9,10). In Fig. III.1, the structure of Li_3AsS_3 is presented by projection onto the (0 1 0) and (0 0 1) planes. Fig. III.2 shows a 3-dimensional view of the Li_3AsS_3 atomic arrangement. These images were obtained using CERIUS (11). Fig. III.3 shows the LiS_4 tetrahedra for two unit cells. The structure can be described as AsS_3 pyramids linked by two LiS_4 tetrahedra and one LiS_3 pyramid.

AsS_3 entities	
As-S(1^{i}) 2.267(2)	S(1^{i})-As-S(2) 100.3(1)
As-S(2) 2.253(2)	S(1^{i})-As-S(3^{ii}) 102.0(1)
As-S(3^{ii}) 2.239(2)	S(2)-As-S(3^{ii}) 103.8(1)
Li(1)S_3 pyramid	
Li(1)-S(2^{iii}) 2.551(11)	S(2^{iii})-Li(1)-S(3) 96.2(7)
Li(1)-S(3) 2.476(11)	S(2^{iii})-Li(1)-S(3^{iV}) 153.5(7)
Li(1)-S(3^{iV}) 2.482(11)	S(3)-Li(1)-S(3^{iV}) 110.0(7)
Li(2)S_4 tetrahedron	
Li(2)-S(1) 2.431(11)	S(1)-Li(2)-S(2) 105.7(4)
Li(2)-S(2) 2.448(11)	S(1)-Li(2)-S(2^{iv}) 100.9(4)
Li(2)-S(2^{iv}) 2.486(11)	S(1)-Li(2)-S(3^{i}) 122.8(4)
Li(2)-S(3^{i}) 2.450(11)	S(2)-Li(2)-S(2^{iv}) 110.2(4)
	S(2)-Li(2)-S(3^{i}) 99.6(4)
	S(2^{iv})-Li(2)-S(3^{i}) 117.0(4)
Li(3)S_4 tetrahedron	
Li(3)-S(1) 2.578(11)	S(1)-Li(3)-S(1^{V}) 114.5(4)
Li(3)-S(1^{V}) 2.516(11)	S(1)-Li(3)-S(2^{vi}) 112.2(4)
Li(3)-S(2^{vi}) 2.395(11)	S(1)-Li(3)-S(3) 91.4(4)
Li(3)-S(3) 2.538(11)	S(1^{V})-Li(3)-S(2^{vi}) 125.5(4)
	S(1^{V})-Li(3)-S(3) 102.5(4)
	S(2^{vi})-Li(3)-S(3) 103.0(4)

Symmetry codes; (i) -x+1/2, y+1/2, z-1/2 (ii) x, y, z-1 (iii) -x+1/2, y-1/2, z+1/2
(iv) x-1/2, -y+1/2, z (v) x+1/2, -y+1/2, z (vi) -x+1/2, y+1/2, z+1/2

Table III.3 Main interatomic distances(Å) and bond angles(°) in Li_3AsS_3.

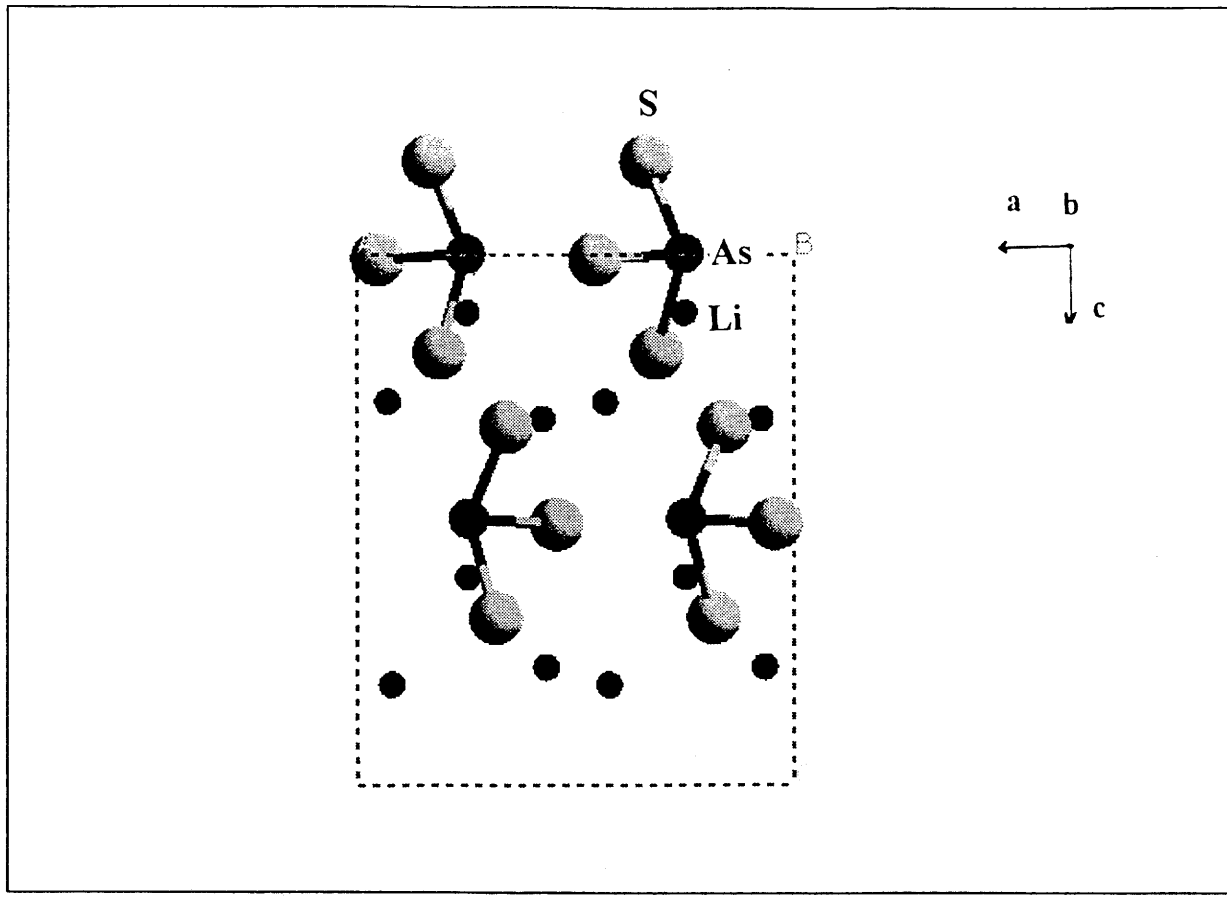

Fig. III.1-a) Atomic arrangement of c-Li_3AsS_3 viewed along b-axis.

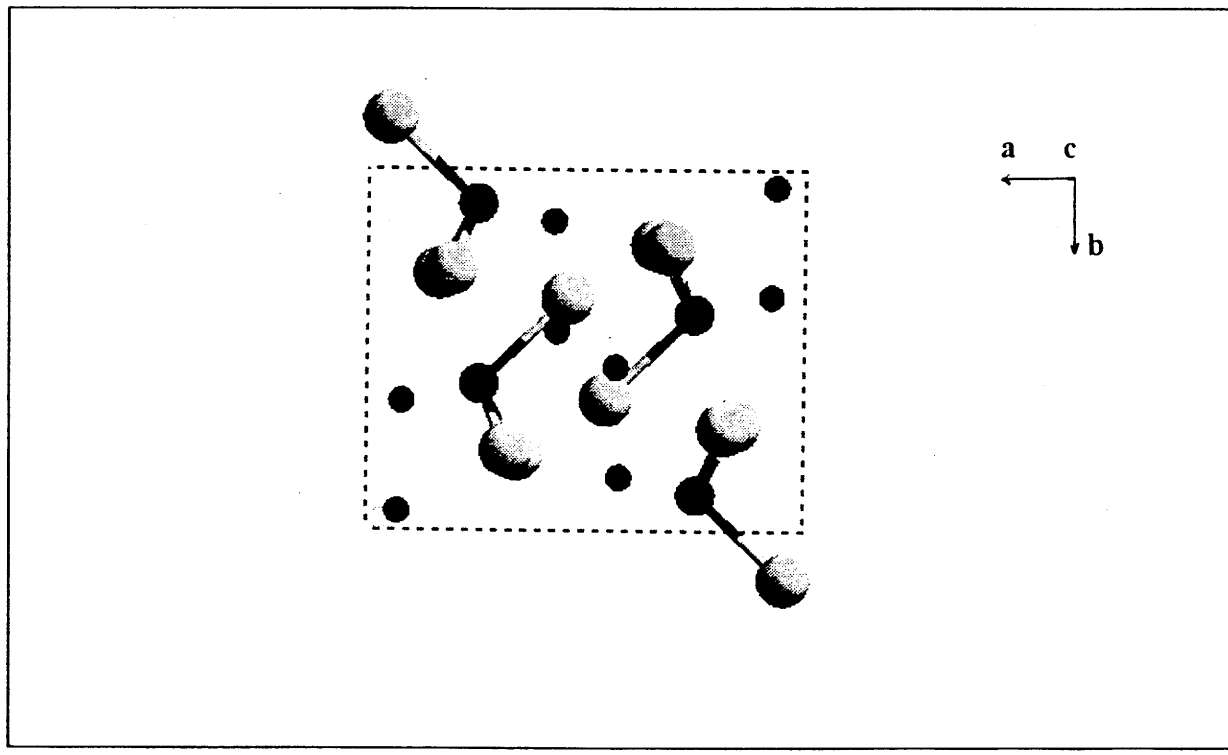

Fig. III.1-b) Atomic arrangement of c-Li_3AsS_3 viewed along c-axis.

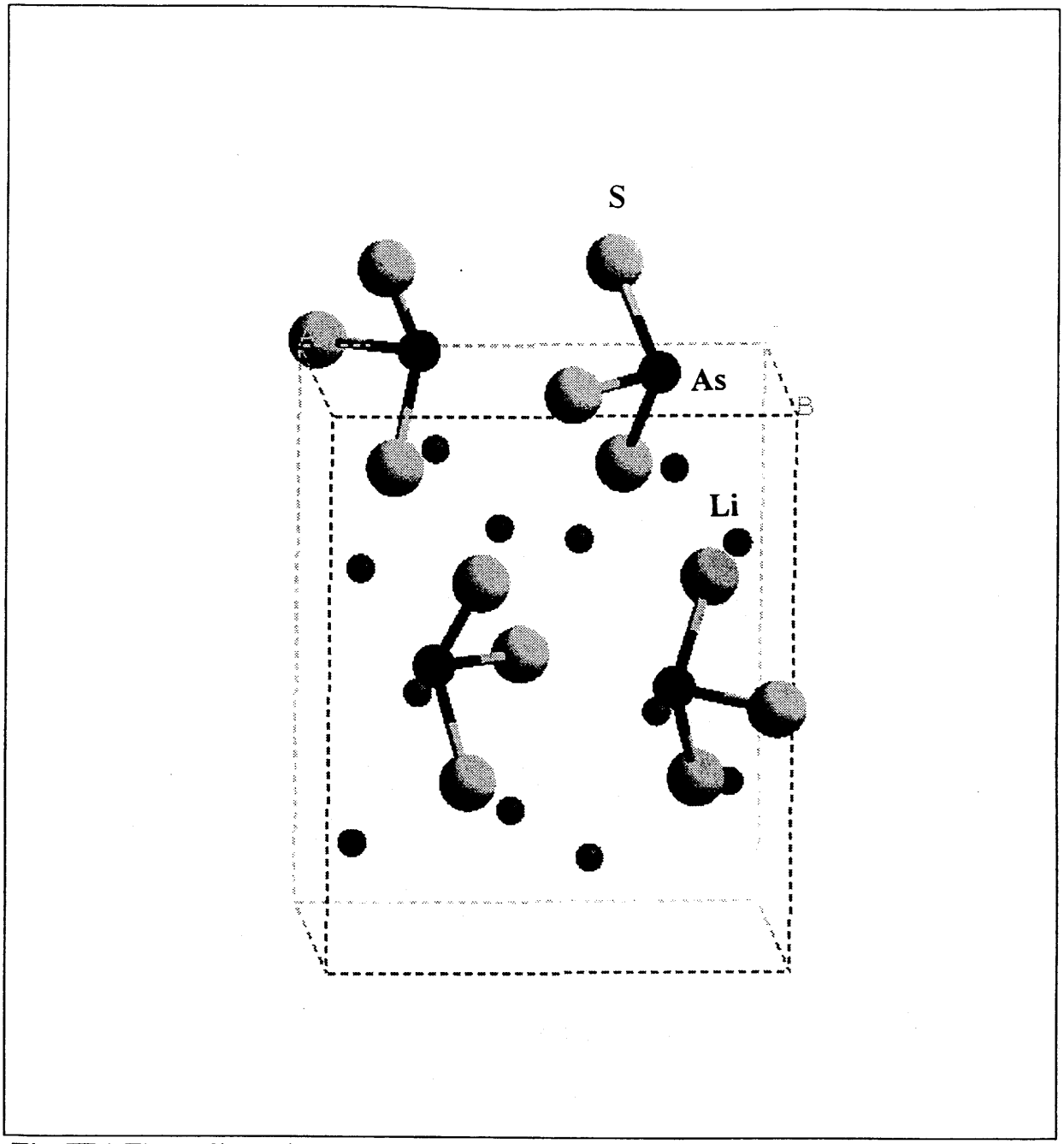

Fig. III.2 Three-dimensional view of c-Li_3AsS_3.

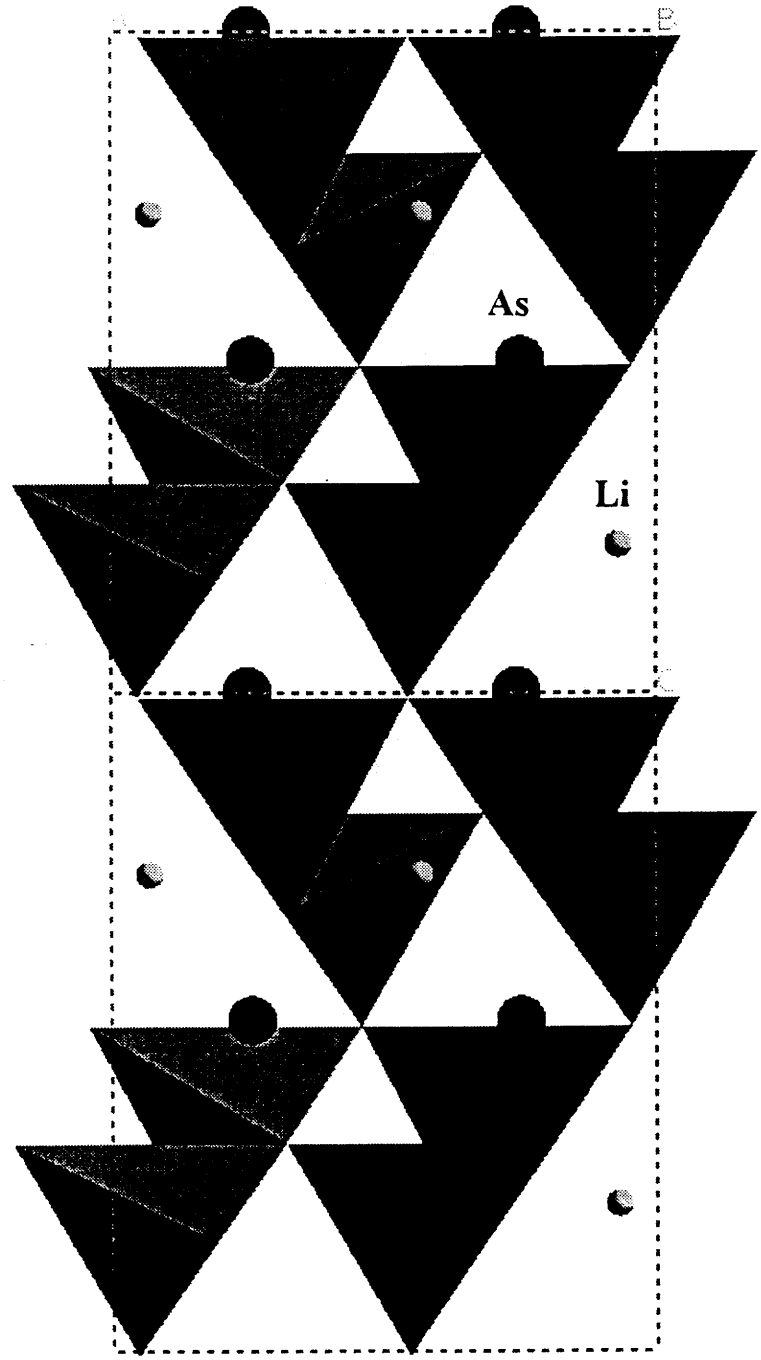

Fig. III.3 View of the arrangement of some of the Li polyhedra (Li(2), Li(3)).

III.2 Crystal structure of $LiAsS_2$

The crystals obtained were gray, irregular in size and plate shaped. The detailed structural parameters have been obtained in the Cc space group and the crystal symmetry is monoclinic. The chemical analysis carried out on collected crystals, results in a S/As ratio close to 2 and Li/As close to 1.

III.2.1 Structure determination and refinement

The preliminary investigations of the crystal were made with Buerger and Weissenberg films and were consistent with monoclinic symmetry. The extinction conditions lead to the space group Cc (No. 9).

The crystal structure of $LiAsS_2$ was determined by adopting the same methods as for Li_3AsS_3(cf. III.1). The unit cell parameters of the single crystal were refined from the angular position of 25 centred reflections. The intensities of 4581 reflections were collected in the range $-23 \leq h \leq 23$, $-10 \leq k \leq 6$ and $-10 \leq l \leq 10$ with a $\theta/2\theta$ scan mode. The intensity data were corrected for Lorentz and polarization effects and equivalent reflections were averaged to provide a set of 1181 unique reflections with $I > 3\sigma(I)$ with an internal consistency factor $R_{int} = 9.1$ %. The crystal data, detailed measurement and structure solution are listed in Table III.4. The refinement of the structure was carried out by full matrix least squares fit on F with isotropic thermal parameters for Li atoms and anisotropic thermal parameters for As and S atoms respectively using the programme SHELX-76 (2). The intensities were weighted by $w = 1/\sigma^2$. This refinement gives R = 10.1 % and $R_w = 13.2$ %. Empirical absorption correction was done using the same algorithm and programme as in III.1. These corrected values for the observed modules gives $R_{int} = 5.4$ %, but which also results in a negative electron density at Li sites, indicating the presence of more electronic density on average at these positions. Here, we have introduced an hypothesis that 8 % of As and Li atoms are transposed to each other sites

and the final calculations with 1181 independent reflections and anisotropic thermal parameters for all atoms lead to R = 10 %, R_w = 12.7 %. This result shows that the proposed structure is not a true reflection of the actual structure. It seems that more As has to be present in the Li sites. This error could be due to the hand made selection of the crystals which were analyzed. A small error in the chemical analysis could be at the origin of this reliability factor. The final atomic coordinates, obtained after applying our hypothesis, and equivalent isotropic displacements are listed in Table III.5-a) and anistropic thermal parameters are in Table III.5-b).

Crystal data	
Formula weight	188.847g
Crystal system	Monoclinic
Space group	Cc (No. 9)
Lattice parameters	
a	11.869 Å
b	5.382 Å
c	5.348 Å
β	113°36'
V	313.62 $Å^3$
Formula unit/cell, Z	4
Density(Calc.), Dx	2.448 g/cm^3
Radiation	Mo-Kα (λ = 0.7107 Å)
Scan mode	θ/2θ
Scan width	(1.5 + 0.35 tgθ)°
Scan range	0.1 < θ < 45°
Ranges of Miller indices	-23 ≤ h ≤ 23
	-10 ≤ k ≤ 6
	-10 ≤ l ≤ 10

Table III.4 $LiAsS_2$ crystal data and detailed measurements and structure solution.

Temperature of measurement	293 K
Crystal size	irregular plate
Data collection	
No. measured reflections	4581
No. observed reflections	3887 ($I > 3\sigma(I)$)
No. independent reflections	1181 [$<F_o^2> \geq 3\sigma(<F_o^2>)$]
R_{int}	9.1 % (before absorption correction)
	5.4 % (after absorption correction)
Refinement	
Weighting scheme	$w = 1/\sigma^2(F_o)$
R	10 %
R_w	12.7 %
No. unique observations	1181 reflections
No. refined parameters	37

Table III.4' Continued over Table III.4.

Species	Wyckoff position	Site symmetry	x	y	z	B_{eq}
As(1)	4(a)	1	0	0.2206(2)	0	0.90(3)
As(2)	4(a)	1	0.7591(10)	0.2067(21)	0.2376(20)	1.45(31)
S(1)	4(a)	1	0.9614(3)	0.1985(5)	0.3956(7)	1.38(8)
S(2)	4(a)	1	0.7976(3)	0.2416(8)	0.8423(8)	1.67(9)
Li(1)	4(a)	1	0.7591(10)	0.2067(21)	0.2376(20)	1.45(31)
Li(2)	4(a)	1	0	0.2206(2)	0	0.90(3)

Table III.5-a Fractional atomic coordinates and equivalent isotropic displacement parameters(Å^2) in Cc, $Beq = (8\pi^2/3)\Sigma_i\Sigma_j U_{ij} a_i^* a_j^* a_i a_j$.

Species	U_{11}	U_{22}	U_{33}	U_{23}	U_{13}	U_{12}
As(1)	0.0133(4)	0.0129(4)	0.0084(3)	-0.0011(5)	0.0048(2)	-0.0046(5)
As(2)	0.0206(48)	0.0242(56)	0.0111(38)	0.0024(28)	0.0071(29)	0.0154(30)
S(1)	0.0232(12)	0.0154(10)	0.0151(11)	0.0001(8)	0.0089(9)	-0.0005(8)
S(2)	0.0187(12)	0.0267(15)	0.0180(12)	0.0017(10)	0.0071(9)	-0.0011(9)
Li(1)	0.0206(48)	0.0242(56)	0.0111(38)	0.0024(28)	0.0071(29)	0.0154(30)
Li(2)	0.0133(4)	0.0129(4)	0.0084(3)	-0.0011(5)	0.0048(2)	-0.0046(5)

Table III.5-b. Anisotropic thermal parameters of $LiAsS_2$ relative to the thermal factor, $T = \exp[-2\pi^2(h^2 a^{*2}U_{11} + k^2 b^{*2}U_{22} + l^2 c^{*2}U_{33} + 2hka^*b^*U_{12} + 2klb^*c^*U_{23} + 2lhc^*a^*U_{13})]$.

III.2.2 Description of the structure

c-$LiAsS_2$ consists of AsS_3 pyramids coupled via S atoms; one of the three S atoms being non-bridging as presented in Fig. III.4. Arsenic atoms and bridging sulphur atoms form AsS_2 chains parallel to the c-axis.The major interatomic distances and bond angles are listed in Table III.6. The average As-S bond distance where the S is a bridging sulphur atom is 2.33 Å. The As-S bond distance with a non-bridging sulphur is 2.21 Å. This structure is comparable to that of $TlAsS_2$ (with bridging sulphurs, As-S; 2.31 Å and 2.34 Å, and non-bridging sulphurs, As-S; 2.17 Å (8,12)). Fig. III.5 shows the atomic arrangement of $LiAsS_2$ viewed along the b-axis. The unit cell contains 4 chemical units of $LiAsS_2$. The inter-chain distance is 3.3 Å. The bond angle of S-As-S in the pyramid is smaller than in $TlAsS_2$ (8,12) or $AgAsS_2$ (13) crystals. The easy cleaving character of this crystal probably originates from the weak interchain bonding character (Van der Waals bonding). A 3-dimensional view of this is shown in Fig. III.6. Lithium atoms appear to be three coordinated as in Li_3AsS_3, i.e. the lithium atom is at the top of a pyramid but really linked to the NBS.

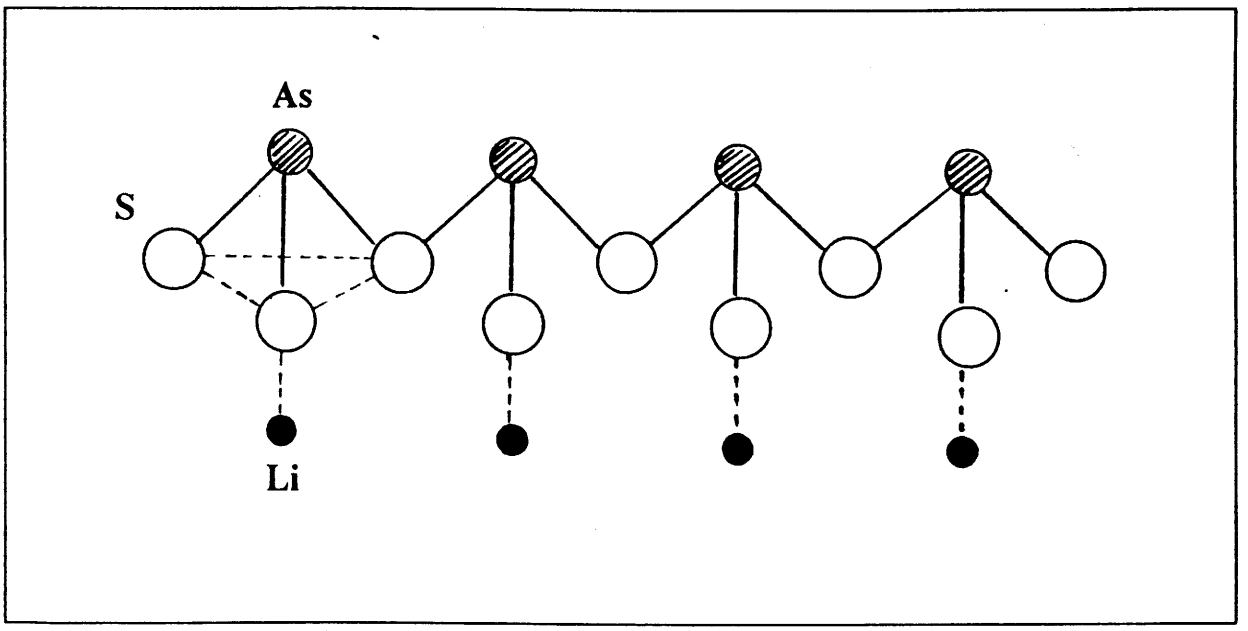

Fig. III.4 Expected molecular constitution in c-$LiAsS_2$.

As-S-As chain	
As(1)-S(1^{i}) 2.339	S(1^{i})-As-S(1^{ii}) 94.4317
As(1)-S(1^{ii}) 2.325	As(1)-S(1^{ii})-As(1^{iii}) 100.1339
As(1^{iii})-S(1^{ii}) 2.339	
Li-S-Li chain	
Li(1^{i})-S(2^{iv}) 2.341	Li(1^{i})-S(2^{iv})-Li(1^{v}) 92.3728
Li(1^{v})-S(2^{iv}) 2.478	S(2^{ii})-Li(1^{v})-S(2^{iv}) 101.3998
Li(1^{v})-S(2^{ii}) 2.341	
AsS_3 unit	
As(1)-S(1^{i}) 2.339	S(1^{i})-As(1)-S(1^{ii}) 94.4317
As(1)-S(1^{ii}) 2.325	S(1^{i})-As(1)-S(2^{iv}) 76.9799
As(1)-S(2^{iv}) 2.211	S(1^{ii})-As(1)-S(2^{iv}) 82.9439

*Symmetric codes; i) (x-1, y, z) ii) (x-1, -y, z-3/2) iii) (x, -y, z-1/2) iv) (x-1, y, z-1) v) (x-1, -y, z-1/2)

Table III.6.Main interatomic distances(Å) and bond angles(°) in crystalline $LiAsS_2$.

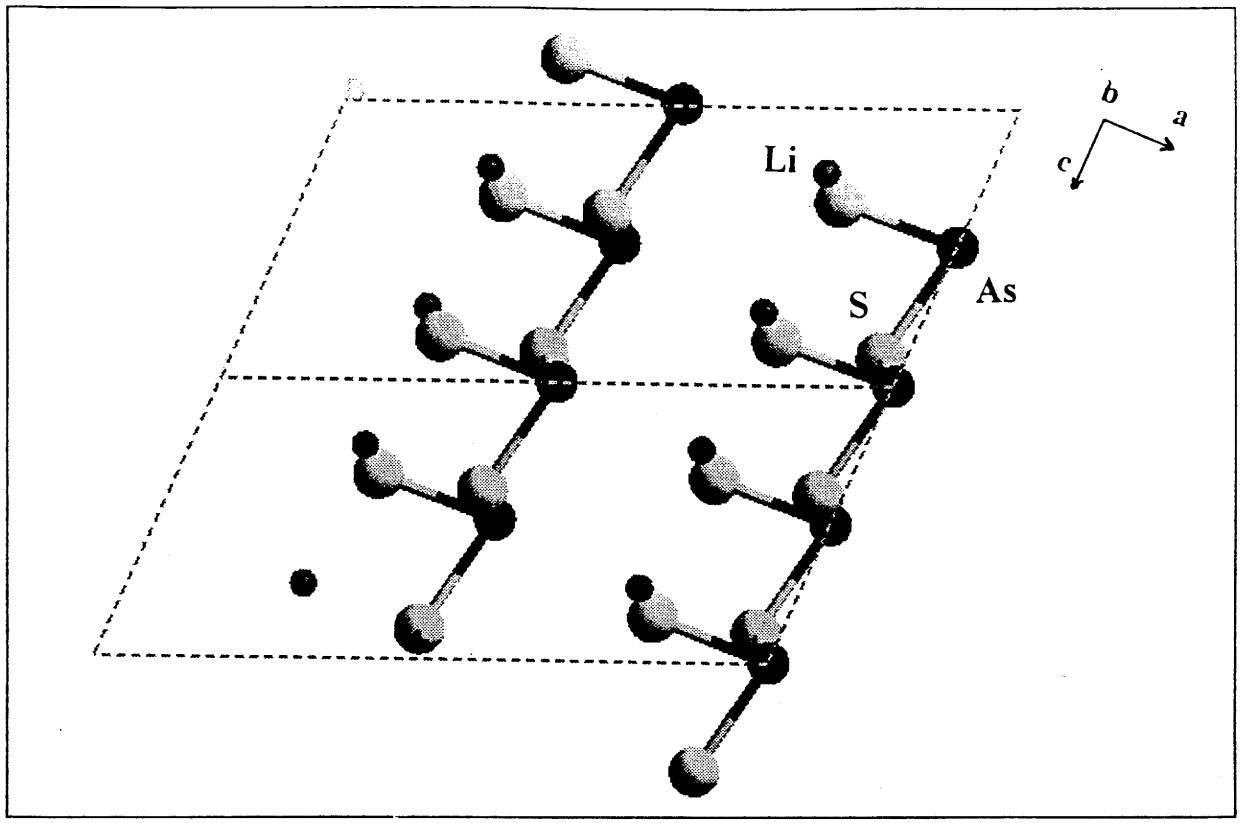

Fig.III.5 Atomic arrangement of c-$LiAsS_2$ viewed along b-axis.

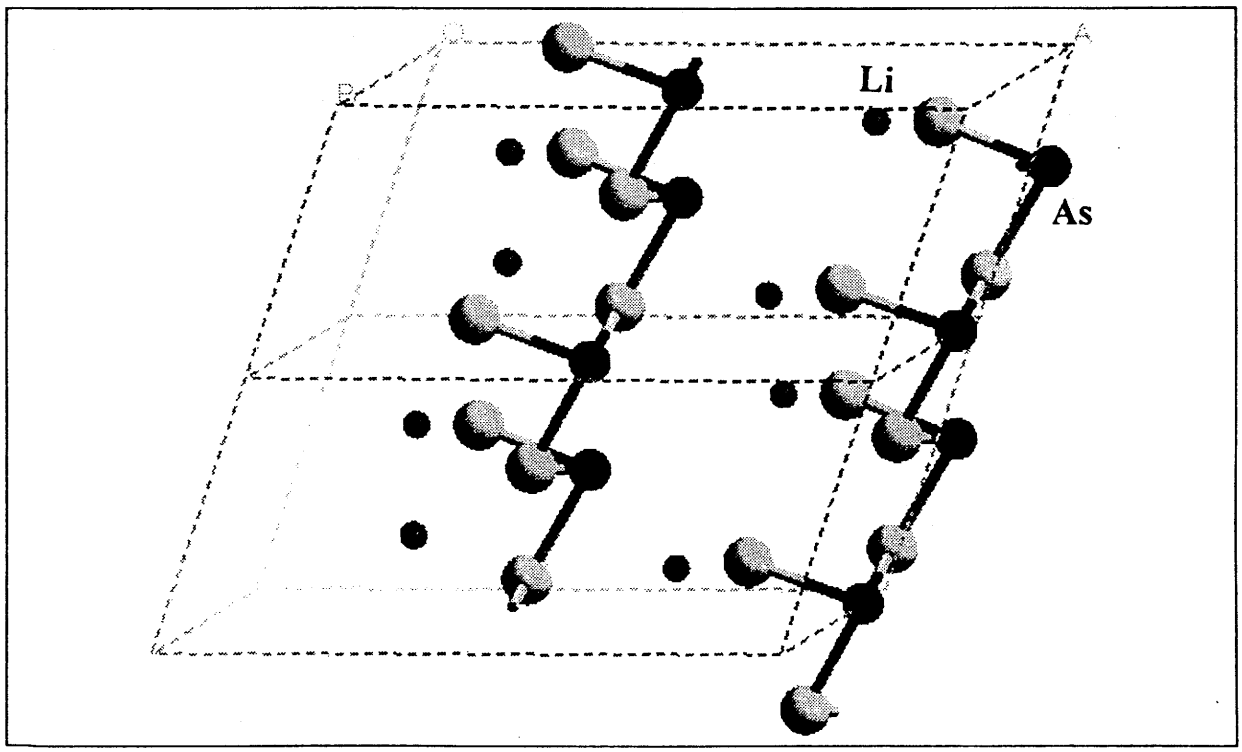

Fig.III.6 Three-dimensional view of c-$LiAsS_2$.

III.3 Spectroscopic study of crystals

III.3.1 X-ray photoelectron spectroscopy (XPS)

XPS is known as a useful method for obtaining information on the oxidation state and the local environment of an atom. Here, the differentiation in electronic state between bridging and non-bridging sulphur atoms in Li_2S-As_2S_3 based crystals was obtained by XPS.

This study was carried out with the help of Mme. D. Gonbeau, Mme. G. Pfister-Guillouzo and L. Benoist at the Laboratoire de Physico-Chimie Moléculaire - Université de Pau et des pays de l'Adour. The detailed experimental procedure was presented in chapter I. The binding energy (E_b) of the electron in the core energy level was obtained by $E_b = h\nu - E_k - \phi$, where $h\nu$ is the energy of the X-ray source used and E_k is the measured kinetic energy of the photoelectron ejected from a certain energy level, and ϕ represents a combination of the spectrometer work function (14).

Fig. III.7 represents XPS spectra for both (a) $LiAsS_2$ and (b) Li_3AsS_3 crystals. The curve fitting was done using a combination of Gaussian (80%) and Lorentzian (20%) line shapes.

$LiAsS_2$ crystal shows two S_{2p} doublets. In the previous section, III.2, this crystal structure was shown to contain two types of sulphur atoms; one a bridging sulphur in As-S-As chains and the other a non-bridging sulphur. The $As\text{-}S^-$ (NBS) involved in AsS_3 pyramidal units is noted to be shorter than the As-S (BS) associated with the chains.

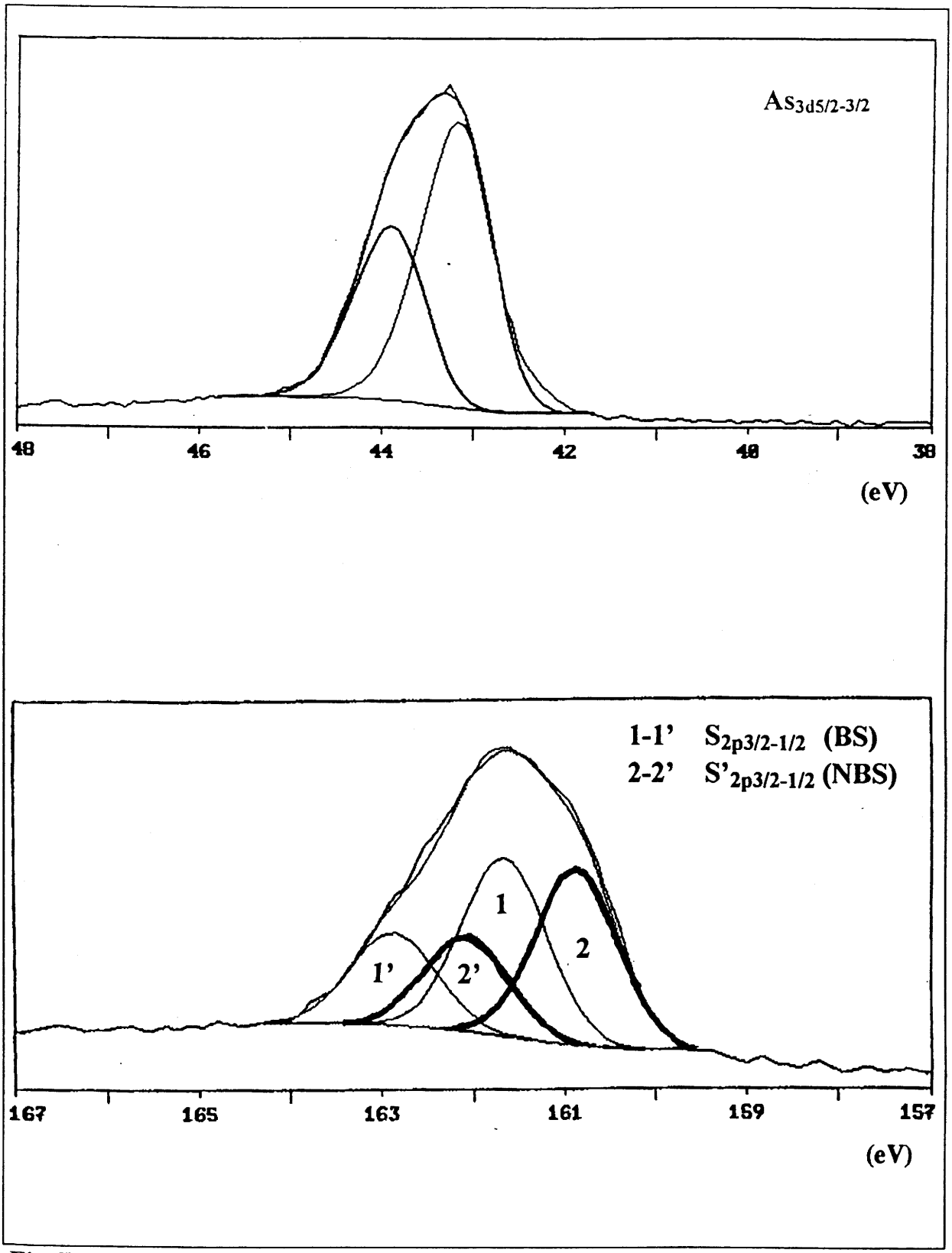

Fig. III.7-a) XPS spectra of As_{3d} and $S_{2p3/2-1/2}$ for c-$LiAsS_2$.

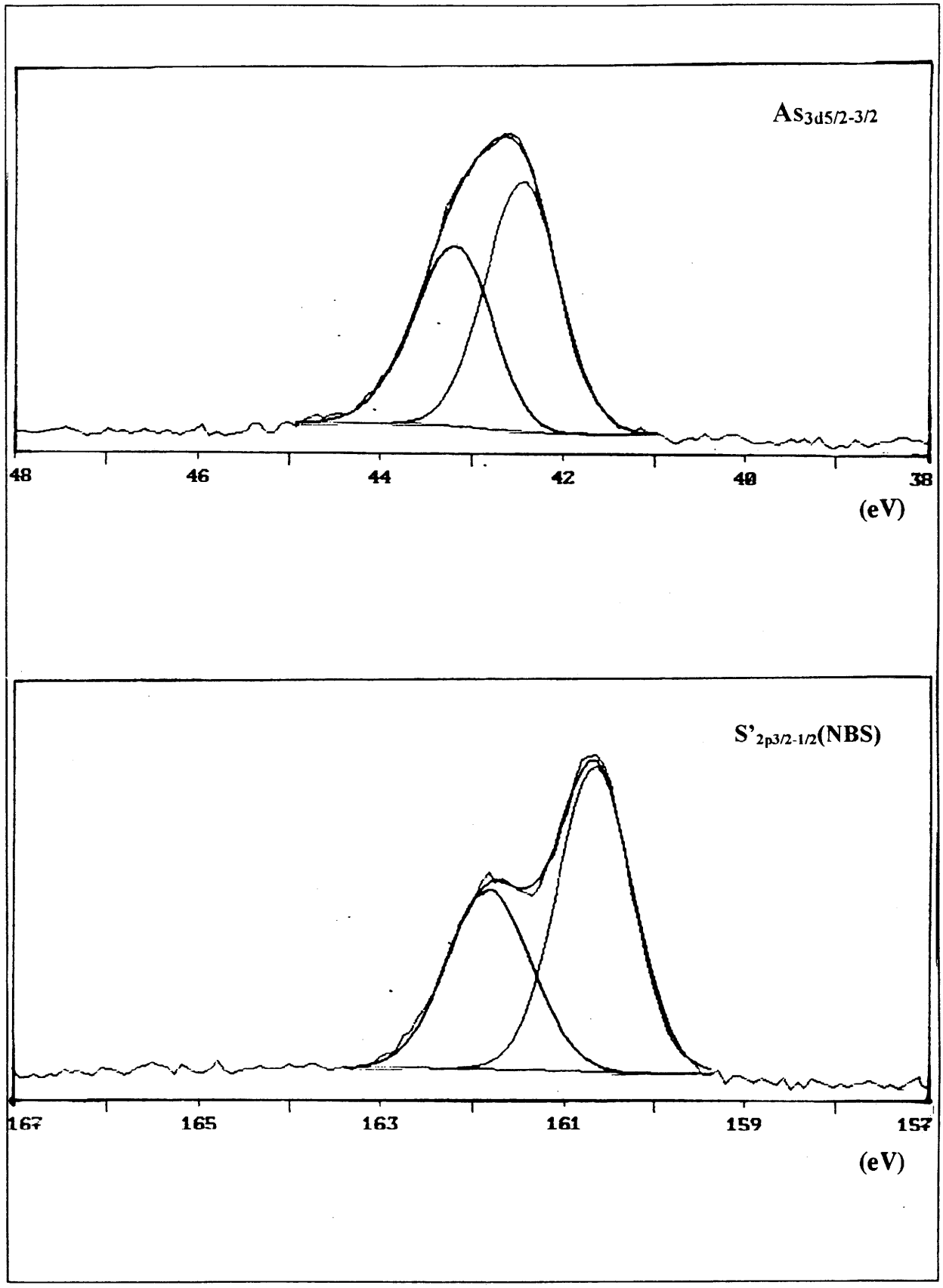

Fig. III.7-b) XPS spectra of As_{3d} and $S_{2p3/2-1/2}$ for c-Li_3AsS_3.

The decomposition of the S_{2p} peak reveals two sets of peaks $S_{2p3/2-1/2}$ and $S'_{2p3/2-1/2}$. The electronic density around the non-bridging sulphur atoms is expected to be higher than that of bridging sulphur atoms due to their higher negative character. Consequently, and as expected, the measured binding energy is found to be smaller than that of bridging sulphur atoms.

On the other hand, Li_3AsS_3 crystals show only one S_{2p} doublet indicating the presence of only one type of sulphur atom. Table III.7 shows the binding energies and the percentage of each type of sulphur atoms, bridging and non-bridging, for both crystals.

	Li_2S		$LiAsS_2$		Li_3AsS_3	
	B.E (eV)	**At. %**	**B.E (eV)**	**At. %**	**B.E (eV)**	**At. %**
$As_{3d5/2-3/2}$	-	-	43 - 43.7 (0.9) (0.9)	100	42.2 - 42.9 (1.0) (1.0)	100
$S_{2p3/2-1/2}$ (BS)			161.7-162.9 (1.1) (1.1)	49		
$S'_{2p3/2-1/2}$ (NBS)	160.7-161.9 (1.2) (1.2)	100	160.9-162.1 (1.0) (1.0)	51	160.7-161.9 (1.0) (1.0)	100

( ); Calibration with C1s peak with the carbon contaminated on the surface.

Table III.7 Summary of XPS results for $LiAsS_2$ and Li_3AsS_3 crystals compared with Li_2S.

The binding energy of a non-bridging sulphur is noted to be similar in both crystals and Li_2S, which reveals their stronger negative character. This table includes also the ratio between non-bridging and bridging sulphur atoms in $LiAsS_2$ crystal. The atomic percentage ratio of bridging sulphur to non-bridging sulphur determined by XPS is 49:51 which is close to the expected ratio of 1:1.

III.3.2 Raman spectroscopy

III.3.2.1 Li_3AsS_3 crystal

Raman experiments were done with the help of M. Couzi and R. Cavagnat in the Laboratoire de Spectroscopie Moléculaire et Crystalline, Univ. Bordeaux I. The laser beam

wavelength used to excite the phonons was 514.5 nm at ~50 mW. The sample was a block of crystals stacked together, the random orientation making it impossible to determine the direction of the crystallographic axis. Furthermore, it was impossible to obtain well polarized Raman spectra. The samples were introduced into a sealed glass capillary (ϕ; 0.5 mm) because of their hygroscopic nature.

Li_3AsS_3 has 28 atoms per unit cell and 81 vibrational (78 optical and 3 acoustic) modes. The unit cell is orthorhombic and the space group is $Pna2_1$ as shown in III.1. The four AsS_3^{3-} pyramids are crystallographically equivalent, the Li atom is in a C_1 site connected to AsS_3^{3-} pyramids via S-Li-S bonds. However, there is no direct bond between the pyramids, so the treatment has been carried out as for isolated units. The calculated irreducible representation of the internal mode of AsS_3^{3-} is given in Table III.8. The obtained Raman spectra are shown in Fig. III.8-a) and b) for different polarizations. The assignment of the peaks are therefore difficult because of the unknown direction of the crystallographic axes. However, qualitative assignment can be made by using the symmetry coordinates and characteristic vibrational frequencies of isolated molecular entities.

C_{3v}	C_1	C_{2v}	**Active mode**
A_1		A_1	IR, R
A_2	A	A_2	- R
E		B_1	IR, R
		B_2	IR, R

Table III.8. Irreducible representation of internal mode of the AsS_3^{3-} pyramid.

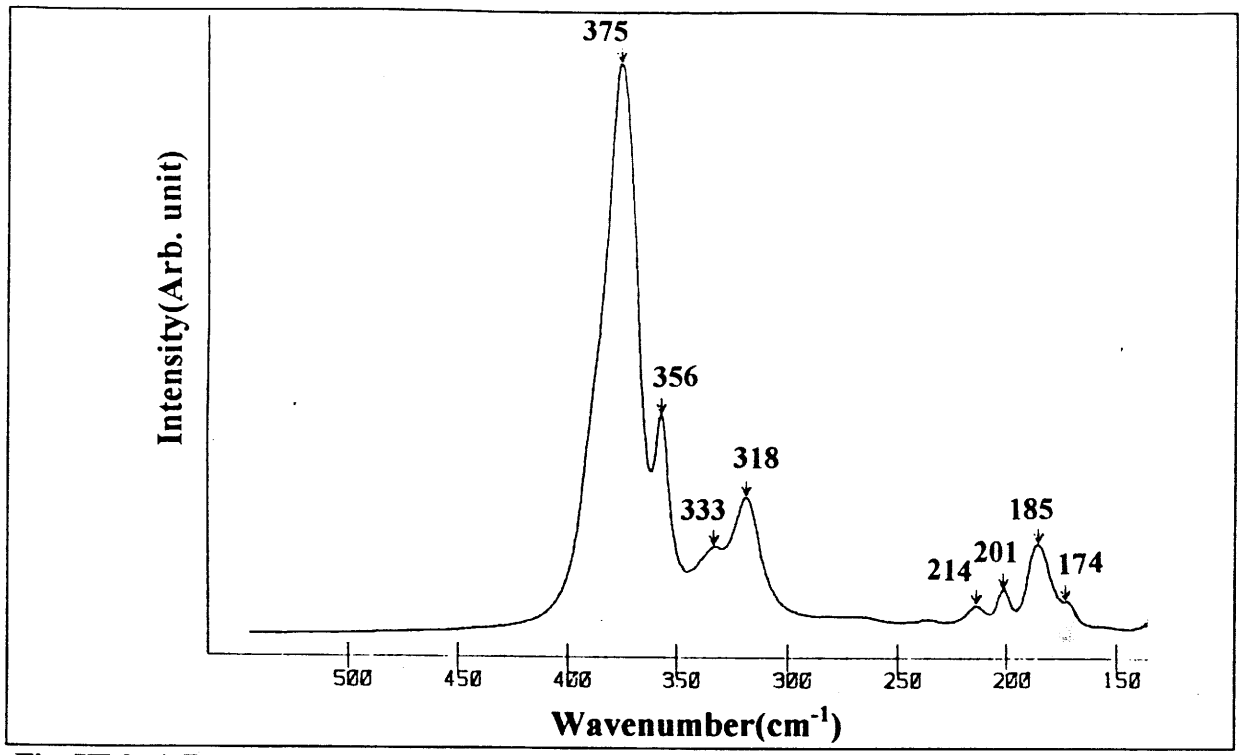

Fig. III.8-a) Raman spectrum for c-Li_3AsS_3 (the direction of plane is arbitrary and the beam is right angle polarized to incident plane).

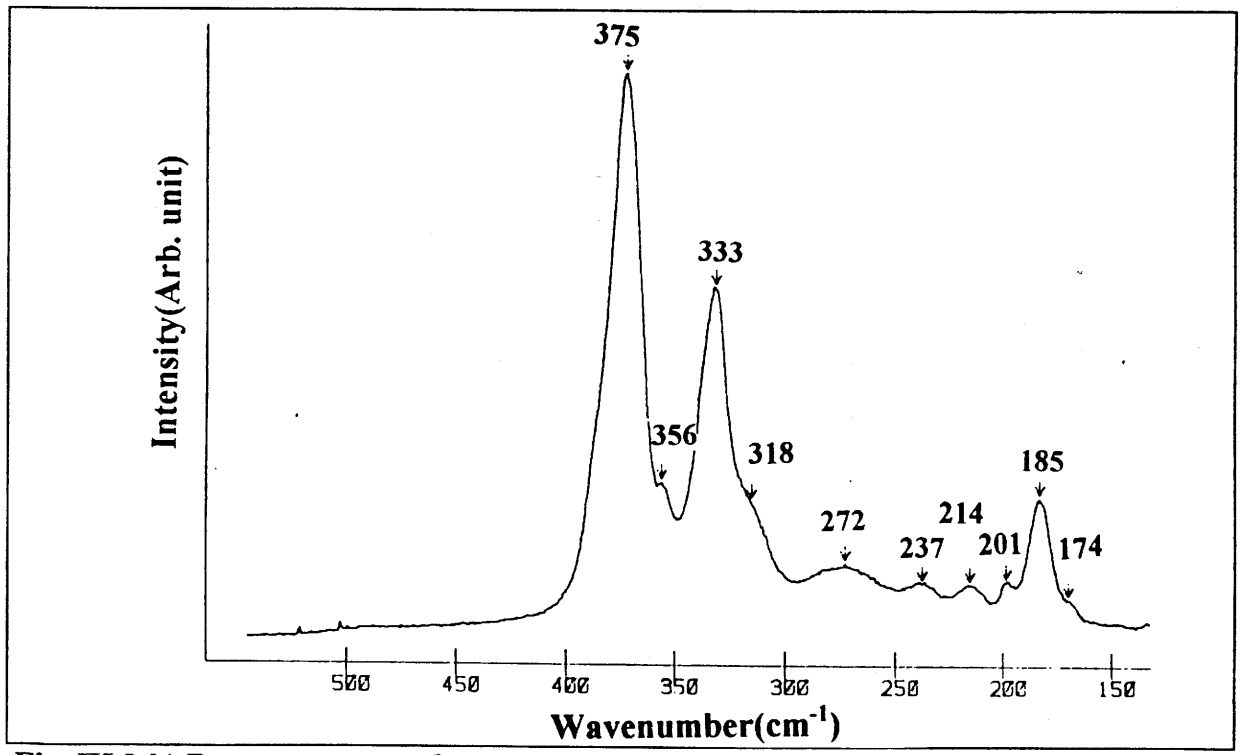

Fig. III.8-b) Raman spectrum for c-Li_3AsS_3 (the beam is polarized parallel to incident plane).

We have observed mainly two groups of peaks. The first one appearing between 318 cm^{-1} and 375 cm^{-1}, which can be assigned to As-S stretching modes in AsS_3^{3-} pyramidal units. The second group appearing between 174 cm^{-1} and 214 cm^{-1} is expected to arise from an As-S bending mode and a Li-S stretching mode. These assignments are supported by comparisons with previous work done on As_2S_3 (15,16) and Ag_3AsS_3 (17) crystals in which the characteristic frequency range for As-S bond stretching and S-As-S angle bending are 318 - 375 cm^{-1} and 173 - 214 cm^{-1} respectively. The peaks appear at 237 and 272 cm^{-1} in Fig. 8-b) are unable to define clearly.

III.3.2.2 $LiAsS_2$ crystal

$LiAsS_2$ crystal has 8 atoms per primitive unit cell and 24 vibrational (21 optical and 3 acoustic) modes. As was shown previously, the unit cell is monoclinic with space group Cc. In this crystal, AsS_3 pyramids are bridged via As-S-As bonds. The crystallographic point group is Cs. The results of Raman experiments are shown in Fig. III. 9. Fig. III. 9-a) represents the back scattering polarized spectrum to the (1 0 0) plane and Fig. III. 9-b) represents the parallel polarized spectra to the (1 0 0) plane. The frequency at 402 cm^{-1} probably corresponds to the stretching mode of As-S (non-bridging sulphur atom). The 247 - 276 cm^{-1} frequencies may be assigned to the stretching mode involving As-S (bridging sulphur atom). The peaks between 101 - 200 cm^{-1} are expected to be due to the bending motion of the As-S bond. As in c-Li_3AsS_3, the As-S non-bridging stretching vibration has shifted to higher frequency compared to the As-S stretching vibration in c-As_2S_3 (ca. 350 cm^{-1}, (15,16)). The As-S bond distance of NBS in $LiAsS_2$ is 2.21 Å, which is shorter than the one found in c-Li_3AsS_3 (2.25 Å). The major reason for a higher frequency compared to c-Li_3AsS_3 is probably the shorter bond length of the As-S bond involving non-bridging sulphur. The comparison of c-Li_3AsS_3 and c-$LiAsS_2$ is presented in Table III.9.

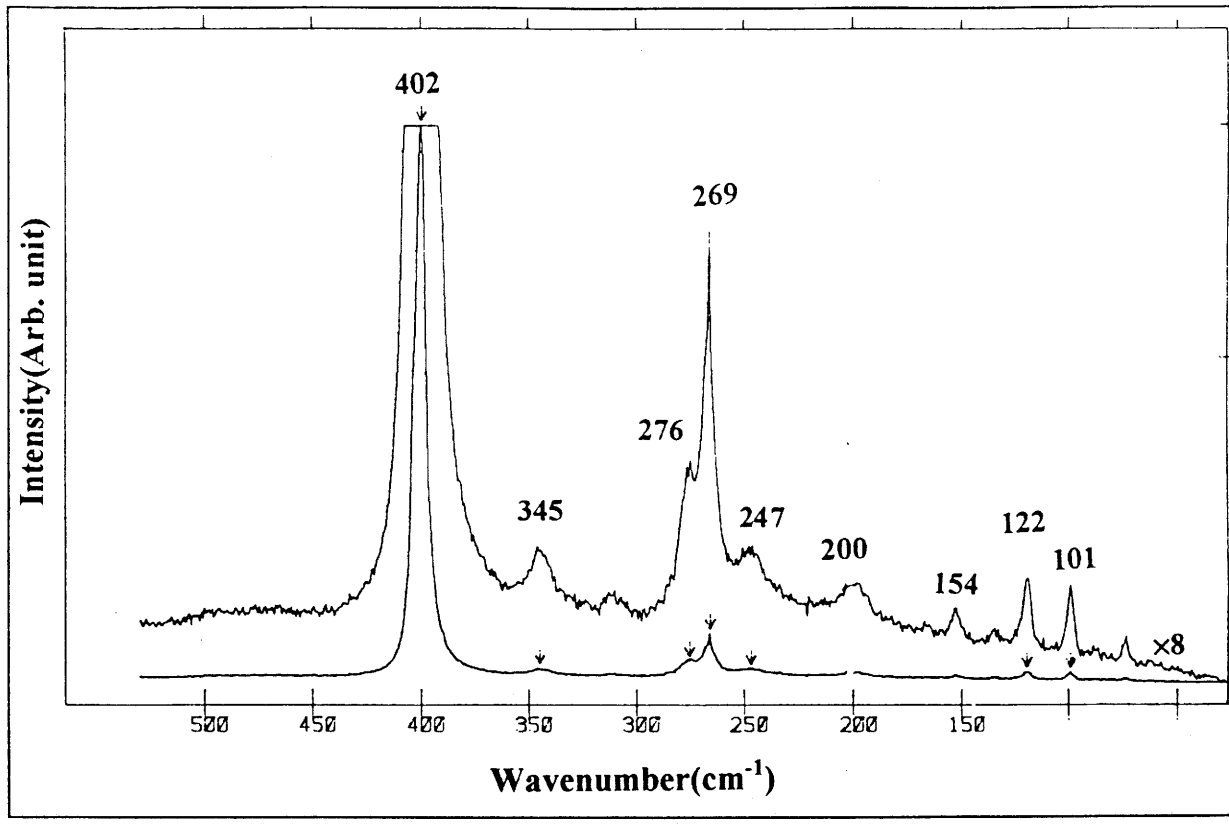

Fig. III.9-a) Raman spectrum for c-$LiAsS_2$ right angle polarized to (1 0 0) plane.

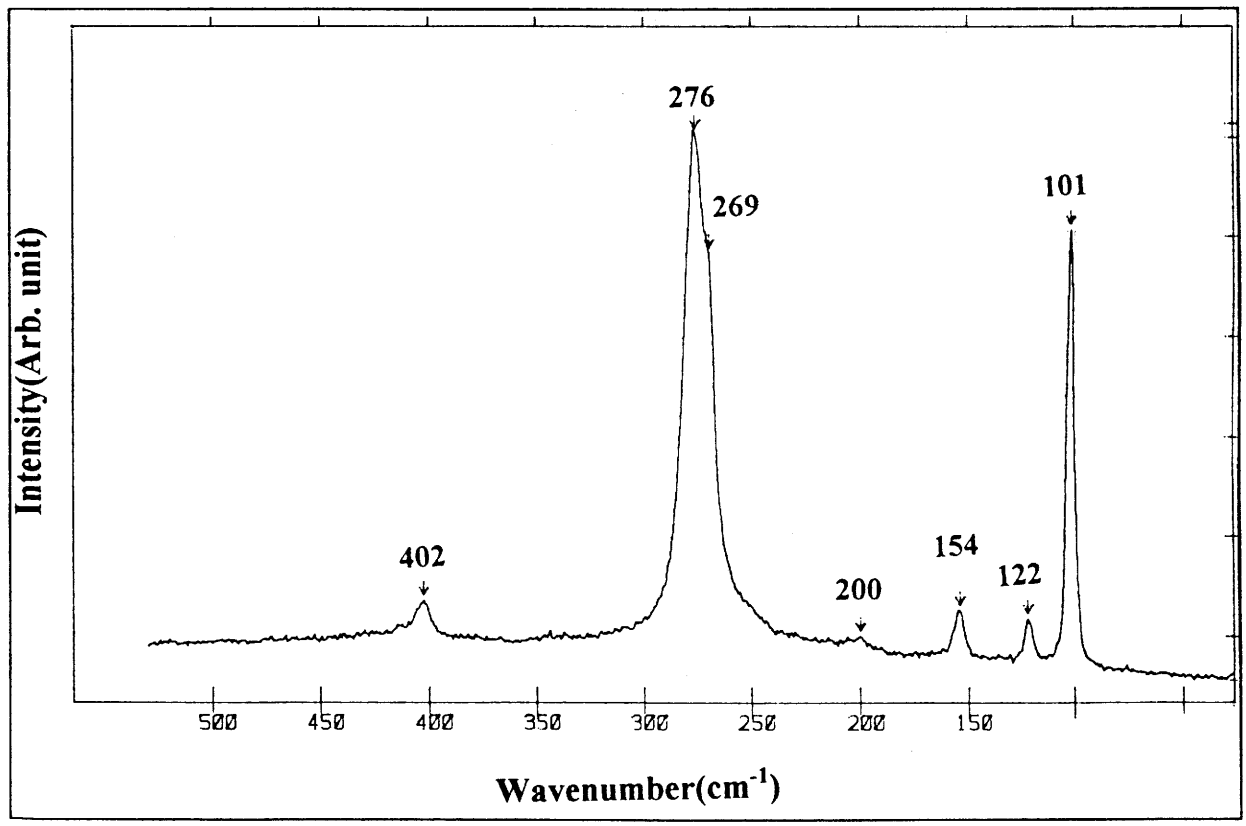

Fig. III.9-b) Raman spectrum for c-$LiAsS_2$ paralle polarized to (1 0 0) plane.

Mode	c-Li_3AsS_3 (cm^{-1})	c-$LiAsS_2$ (cm^{-1})
Stretching mode		
As-S	-	247 - 276
As-S$^-$	318 - 375	402
Bending mode	173 - 214	101 - 200

Table III.9 Vibrational comparison between c-Li_3AsS_3 and c-$LiAsS_2$.

II.3.3 IR spectroscopy

The IR spectroscopy measurements were performed with the help of J. C. Lassègues, at the Laboratoire de Spectroscopie Moléculaire et Cristalline, Univ. Bordeaux I.

The IR spectra obtained for $LiAsS_2$ and Li_3AsS_3 are shown in Fig. III.10. The spectrum of $LiAsS_2$ shows strong absorptions at 420, 330 and 300 cm^{-1}. The peak at 420 cm^{-1} may be assigned to the As-S stretching vibration of non-bridging sulphur involved in As-S pyramids, and the other two peaks originate from the As-S stretching vibration involving bridging sulphur. The IR spectrum of Li_3AsS_3 is not well defined and the only possible peak clearly observed is at 355 cm^{-1}. This value is similar to the one observed in Raman spectra (356 cm^{-1}). The broad spectral feature between 300 - 420 cm^{-1} may also be assigned to stretching As-S$^-$ vibrational motions in AsS_3^{3-} pyramids.

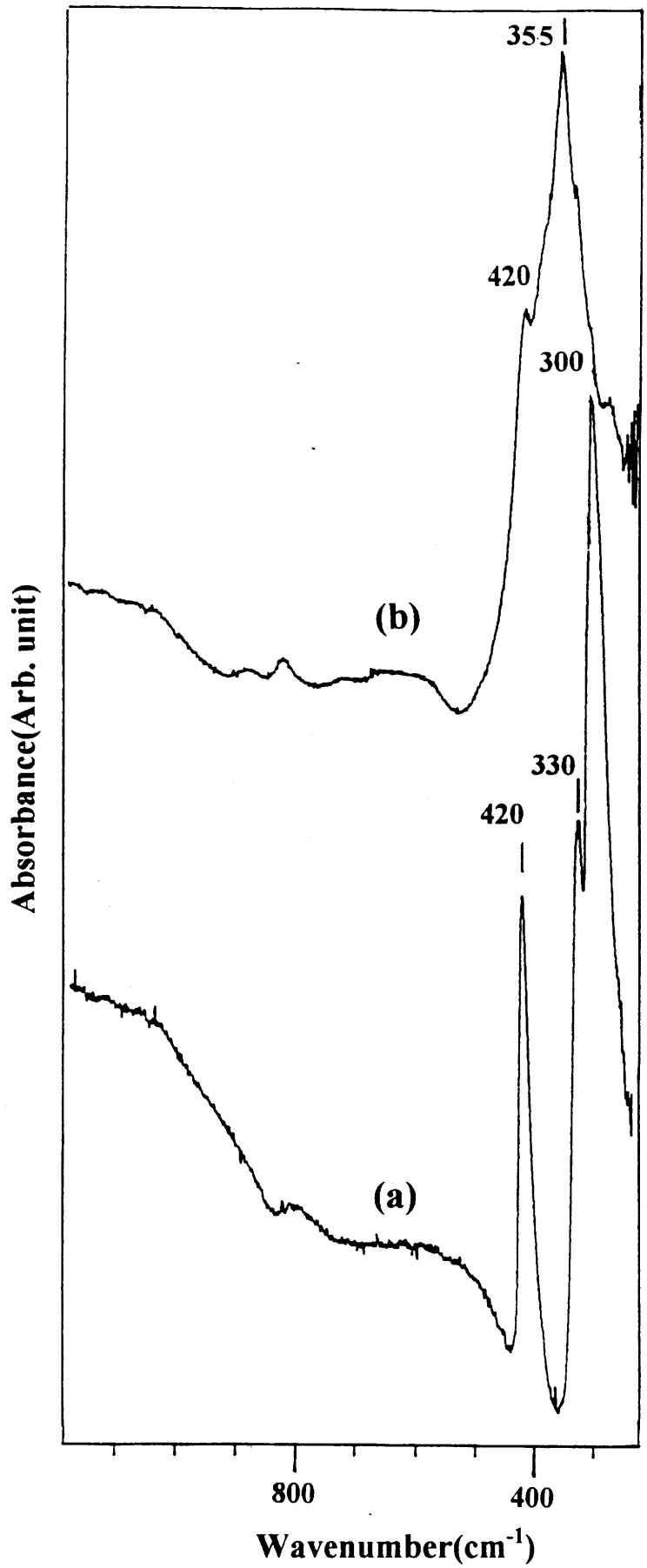

Fig.III.10 IR spectra for c-$LiAsS_2$ (a) and c-Li_3AsS_3 (b).

Conclusion

The crystal structure of Li_3AsS_3 has been determined with the use of three dimensional intensity data. The crystal was orthorhombic having the unit cell dimensions a = 8.052 Å, b = 6.632 Å and c = 9.814 Å with the space group $Pna2_1$. Four formula units are present in the cell. The crystal structure of Li_3AsS_3 shows AsS_3 pyramids where all sulphur atoms are non-bridging. Lithium atoms are involved partly in LiS_4 tetrahedra and LiS_4 pyramids. Arsenic atoms have three nearest S neighbours at an average distance of 2.25 Å which form trigonal AsS_3 pyramids. The Li-S average distance in these tetrahedra are 2.45 Å and 2.51 Å respectively, and 2.50 Å in the pyramids.

The structure of $LiAsS_2$ has been partly determined. The crystal is monoclinic having unit cell dimensions: a = 11.869 Å, b = 5.382 Å, c = 5.348 Å and β = 113°36', the space group is Cc. There are also 4 formula units in the unit cell. The crystal structure of $LiAsS_2$ is constituted of AsS_3 pyramids with one NBS and two bridging sulphurs. The average As-S bond length corresponding to bridging sulphur atoms is 2.33 Å and the one corresponding to non-bridging sulphurs is 2.21 Å. Lithium has three nearest S neighbours between 2.34 Å to 2.48 Å and forms a pyramid with them on the base. The framework of this structure is probably right; remains an ambiguity concerning a small part of lithium atoms.

From XPS studies on these two crystals, two kinds of sulphur atoms were clearly identified, one corresponding to NBS and another to BS. These results fit well the crystallographic ones and seems to confirm that the structure of $LiAsS_2$ is correct. The main peaks observed on Raman and IR spectra were assigned but few references are available, thus not allowing precise assignments of the observed peaks.

References

1. M. C. R. Shastry, M. Ménétrier and A. Levasseur, Solid State Comm., **85** (1993) 887

2. G. M. Sheldrick, *SHELX 76*, Program for Crystal Structure Determination
(Univ. Cambridge, England, 1976)

3. N. Walker and D. Stuart, Acta Cryst., **A39** (1983) 158

4. F. Ugozzoli, Comput. Chem., **11** (1987) 109

5. International Table for X-ray Crystallography, **Vol.4** (Kynoch Press, Birmingham, 1974)

6. R. G. Wyckoff, *Crystll Structure*, **Vol. 2** (New York, Wiley 1957) 26

7 D. Harker, J. Chem. Phys., **4** (1936) 381

8. Z. M. Yang and F. Pertlik, J. Alloys Comp., **216** (1994) 155

9. P. Vinatier, Ph. D. Thesis, Univ. Paris XI Orsay, (1995)

10. P. Vinatier, P. Gravereau, M. Ménétrier, L. Trut and A. Levassur,
Acta Cryst., **C50** (1994) 1180

11. Molecular Simulations, *CERIUS* Version 3.1
(St Johns Innovation Center, Cambridge, England, 1993)

12. A. Zemann and J. Zemann, Acta Cryst., **12** (1959) 1002

13 T. Matsumoto and W. Nowacki, Z. Kristallogr., **129** (1969) 163

14. G. Ertl and J. Küppers,
Low Energy Electrons and Surface Chemistry (VCH Verlagsgesellschaft mbH, 1985)

15 R. Zallen, M. L. Slade and A. T. Ward, Phys Rev., **B 3** (1971) 4257

16 A. P. DeFonzo and J. Tauc, Phys. Rev., **B 18** (1978) 6957

17 H. H. Byer, L. C. Bobb, I. Lefkowitz and B. S. Dearer Jr., Ferroelectrics, **5** (1973) 207

Chapter IV. Structural study of LiI-Li_2S-As_2S_3 glasses

Introduction

Ionic conducting glasses, usually in oxide glasses, are considered to be made up of covalent network formers such as SiO_2, B_2O_3, P_2O_5, GeO_2, Sb_2O_3, As_2O_3 etc., which give rise to a random corner linked tetrahedra arrangement, and of the network modifiers such as Ag_2O, Li_2O and Na_2O. It is well known that the network modifiers lead to the fragmentation of structural entities (1). More recently, similar studies have been carried out on alkali thioborate glasses (2-7), alkali phosphate glasses (8-10) and alkali germanate glasses (11,12). Chalcogenide based glasses with heavy metal halides (Cl, Br and I) and As_2X_3 have been investigated widely because of their excellent electrical and optical properties, and good chemical stability (13,14). However, compared to the other covalent network formers, alkali modified As_2S_3 based glasses have not been studied as extensively and the structural modification by Li_2S was only recently known partly by the work done by Shastry in this laboratory (15,16). Furthermore, a study of LiI doped Li_2S-As_2S_3 binary glasses was reported previously by J. H. Kennedy et al. (17) on the ionic character of this material.

This chapter is devoted to the detailed modification processes occurring in As_2S_3 based glasses. The short range order found in $LiAsS_2$ and Li_3AsS_3 crystals is compared to the short range order expected in glasses by means of techniques sensitive to SRO. Additionally, the LiI doping effect on Li_2S-As_2S_3 binary glass is studied.

IV.1 Physical characterisation of LiI-Li_2S-As_2S_3 glasses

IV.1.1 Chemical analysis

The glasses obtained by quenching between two stainless steel plates (cf. I.5) were analyzed and the results are shown in Table IV.1. The analyzed and nominal compositions are well within experimental error.

xLi_2S-$(1-x)As_2S_3$ glass		Weight (%)				Atomic ratio		
		Li	As	S	O, C	S/As	Li/A_S	Li/S
x = 0.67	Exp.	8.2	43.4	45.9	2.7	2.47	2.02	0.82
	Nom.	8.3	44.2	47.5	-	2.50	2.00	0.80
x = 0.70	Exp.	8.7	40.3	48.2	2.8	2.77	2.31	0.83
	Nom.	9.2	42.4	48.4	-	2.75	2.50	0.91
x = 0.75	Exp.	11.0	39.6	46.2	3.2	2.71	2.98	1.10
	Nom.	10.8	39.1	50.1	-	3.0	3.0	1.0

Table IV.1 Chemical analysis of xLi_2S-$(1-x)As_2S_3$ glasses (x = 0.67, 0.70, 0.75).

IV.1.2 Evolution of the glass transition temperature (Tg) versus composition for LiI-Li_2S-As_2S_3 glasses

IV.1.2.1 Effect of modifier

The Tg's were determined by Differential Scanning Calorimetry (DSC). The measured glass transition temperature (Tg) and melting temperature (Tm) are given in Table IV.2.

xLi_2S-$(1-x)As_2S_3$	Tg(°C)	Tm(°C)
x = 0.67	173	409
x = 0.70	179	402
x = 0.75	185	394

Table IV.2 Variation of glass transition temperature (Tg) and melting temperature (Tm) as a function of composition for xLi_2S-$(1-x)As_2S_3$ glass system obtained by DSC.

The striking feature here is that Tg increases as the Li_2S content increases. This kind of behaviour is observed in the low alkali modifier region of oxide glasses (18). Generally, it is considered that Tg decreases because of structural fragmentation into smaller discrete units as the modifier content increases, which in turn also leads to an increase in the proportion of NBS. Following the crystal structure determination (cf. III.1), we suppose that for x = 0.75 the glass is formed by AsS_3^{3-} entities. Each unit makes weak bonds with Li cations. It is therefore expected that the fraction of non-bridging sulphurs increases with increasing modifier content in this binary glass as in other cases (2-10). This evaluation, however, is contrary to the trends in Tg in xLi_2S-$(1-x)As_2S_3$ glasses.

From previous studies on the crystal structure of $LiAsS_2$ and Li_3AsS_3, we observed two behaviours; firstly, the fragmentation of the framework as just described, and secondly, the coordination of Li^+-ions increases with Li_2S content. Two kinds of lithium were found; two thirds are tetrahedrally and one third is three coordinated (Li being at the apex of a pyramid). The evolution of Li coordination between the two crystals may occur also in the corresponding glasses and could explain the increase in Tg. Despite the apparent fragmentation of the framework, the evolution of the lithium coordination from 3 to 4 causes the framework to become more and more rigid and, as a consequence, Tg increases.

IV.1.2.2 Effect of dopant salt

The variation in glass transition temperature (Tg) in the LiI-Li_2S-As_2S_3 ternary system is shown in Table IV.3, and Fig. IV.1.

Composition	Tg(°C)	
y	yLiI-(1-y)(0.70Li_2S-0.30As_2S_3)	yLiI-(1-y)(0.75Li_2S-0.25As_2S_3)
0	179	185
0.1	165	173
0.2	156	160
0.3	143	142
0.4	127	123
0.5	101	108

Table IV.3 Evolution of Tg with LiI content in the yLiI-(1-y)(xLi_2S-(1-x)As_2S_3) glass systems.

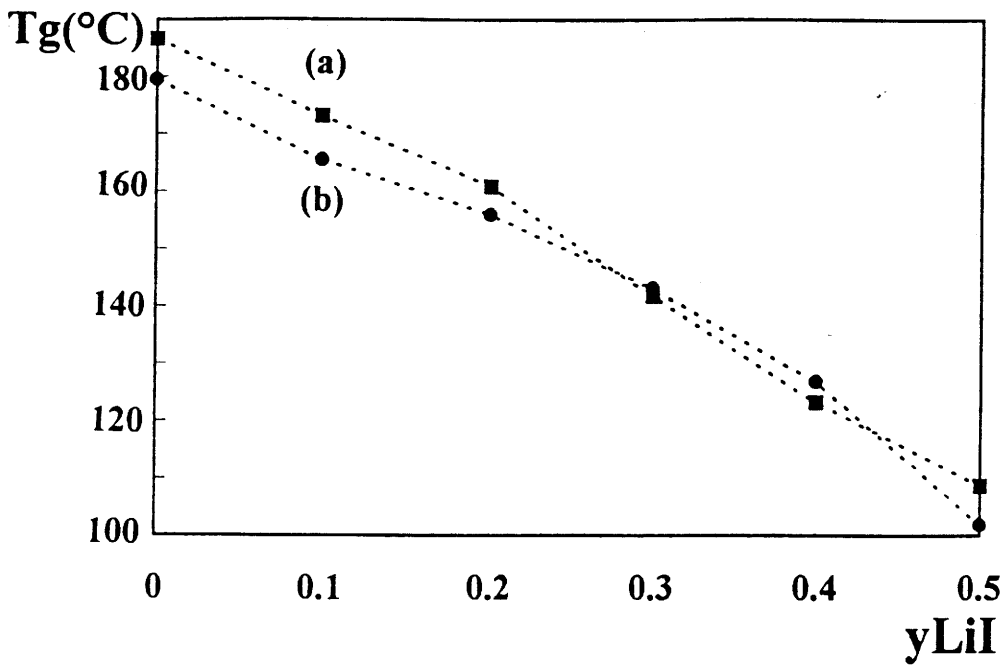

Fig. IV.1 Glass transition temperature (Tg) versus LiI content.
(a) yLiI-(1-y)[0.70Li_2S-0.30As_2S_3], (b) yLiI-(1-y)[0.75Li_2S-0.25As_2S_3].

As we can see from Table IV.3 and Fig. IV.1, the glass transition temperature Tg decreases when the LiI content increases. In this ternary glass, there is no apparent structure modification of host glass matrix (binary Li_2S-As_2S_3 glass) as we will see later in the spectroscopic study section (cf. IV.4). This trend is very usual, and we can consider that LiI is diluted in the vitreous matrix without detectable alteration in the nature of the matrix (19).

IV.1.3 Density trends in LiI-Li_2S-As_2S_3 glasses

IV.1.3.1 Effect of modifier

The density results, and calculated Li^+-ion concentration are listed in Table IV.4.

xLi_2S-$(1-x)As_2S_3$	ρ(mg/mm^3)	Li^+ concentration* (10^{-2} mole cm^{-3})
0.67	2.52	3.02
0.70	2.45	3.24
0.75	2.33	3.64

* Li^+ concentration = number of Li atom per formula unit × density / molecular weight

Table IV.4 Variation of density (ρ) and Li^+-ion concentration for various xLi_2S-$(1-x)As_2S_3$ glasses as obtained by Archimedes method.

As we can see from Table IV.4, the glass matrix becomes less dense when the Li_2S modifier content increases concurrent with an increment in Li^+-ion concentration. Following this result, we expect a decrease of the Li^+-Li^+ distance in the Li_2S-As_2S_3 binary glasses, which will affect the ionic conductivity as we will see later.

IV.1.3.2 Effect of dopant salt

We measured the density of yLiI-(1-y)[$0.70Li_2S$-$0.30As_2S_3$] ternary glasses, the results of which are listed in Table IV.5 with the calculated Li^+-ion concentrations.

y	ρ (mg/mm^3)	Li^+ concentration (10^{-2} mole cm^{-3})
0	2.45	3.24
0.1	2.57	3.21
0.2	2.66	3.15
0.3	2.69	3.01
0.4	2.88	3.05
0.5	3.02	3.02

Table IV.5 Trends in density (ρ) and Li^+-ion concentration with composition for yLiI-(1-y)(0.70Li_2S-0.30As_2S_3) ternary glasses.

In Table IV.5, the density is noted to increase on adding LiI. The Li^+ concentration decreases from y = 0 to y = 0.3 after which it remains relatively constant. The first part of this trend has been observed previously in thioborate based glasses (19). The plateau starting at y = 0.3 may be explained by the presence of LiI aggregates, too small to be detected by XRD. Presence of such clusters was shown in LiI-Li_2S-B_2S_3 glasses (20).

IV.2 X-ray absorption spectroscopy (XAS)

IV.2.1 As K-edge EXAFS of xLi_2S-(1-x)As_2S_3 glasses

Fig. IV.2 and Fig. IV.3 show the As K-edge EXAFS, χ(k) weighted by k^3 for these binary glass systems, and Fourier Transforms (FTs) over a k space range of 2.5 to 13 $Å^{-1}$ respectively. Arsenic K-edge energy was taken at the maximum derivative point of the white radiation. As can be seen in Fig. IV.3, additional small peaks appear before the main one

(which corresponds to interactions with nearest neighbour sulphur atoms). Therefore, the curve fitting of the inverse Fourier transformed $k^3\chi(k)$ was performed with a two shell model. The best-fitted and experimental EXAFS spectra are compared in Fig. IV.4 and the fitted structural parameters are presented in Table IV. 6.

The bond length corresponding to the first small peak which appears in Li_2S modified glasses may be attributed to the As-O bond (1.79 Å) in As_2O_3 (21). However, the number of As-O bonds greatly exceeds that which corresponds to the composition (~3 %) known to be present in the glass. Therefore, a large impurity content may be due to the deterioration by the moisture during XAS measurements. In spite of this deterioration, however, the variation of the As-S bond length with the lithium content can be clearly observed, even although the As-S distances with BS and As-S^- distances with NBS cannot be differentiated. The average lengths of As-S bonds at x = 0.67, 0.70 and 0.75 correspond to 2.25 Å, 2.19 Å and 2.18 Å respectively.

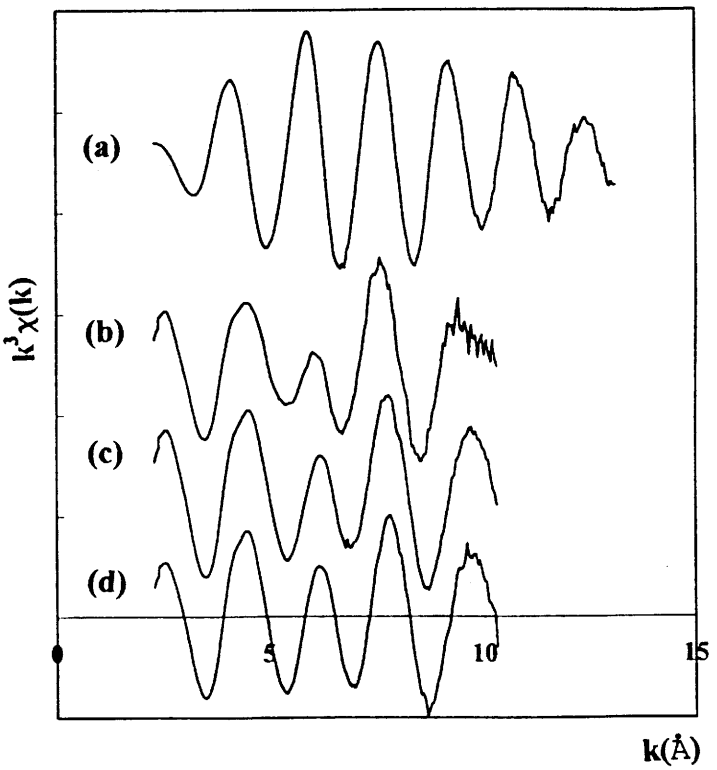

Fig. IV.2 Experimental As K-edge EXAFS spectra, $k^3\chi(k)$, for (a) v-As_2S_3, and (b) x = 0.67, (c) x = 0.70, (d) x = 0.75 in xLi_2S-(1-x)As_2S_3 binary glasses.

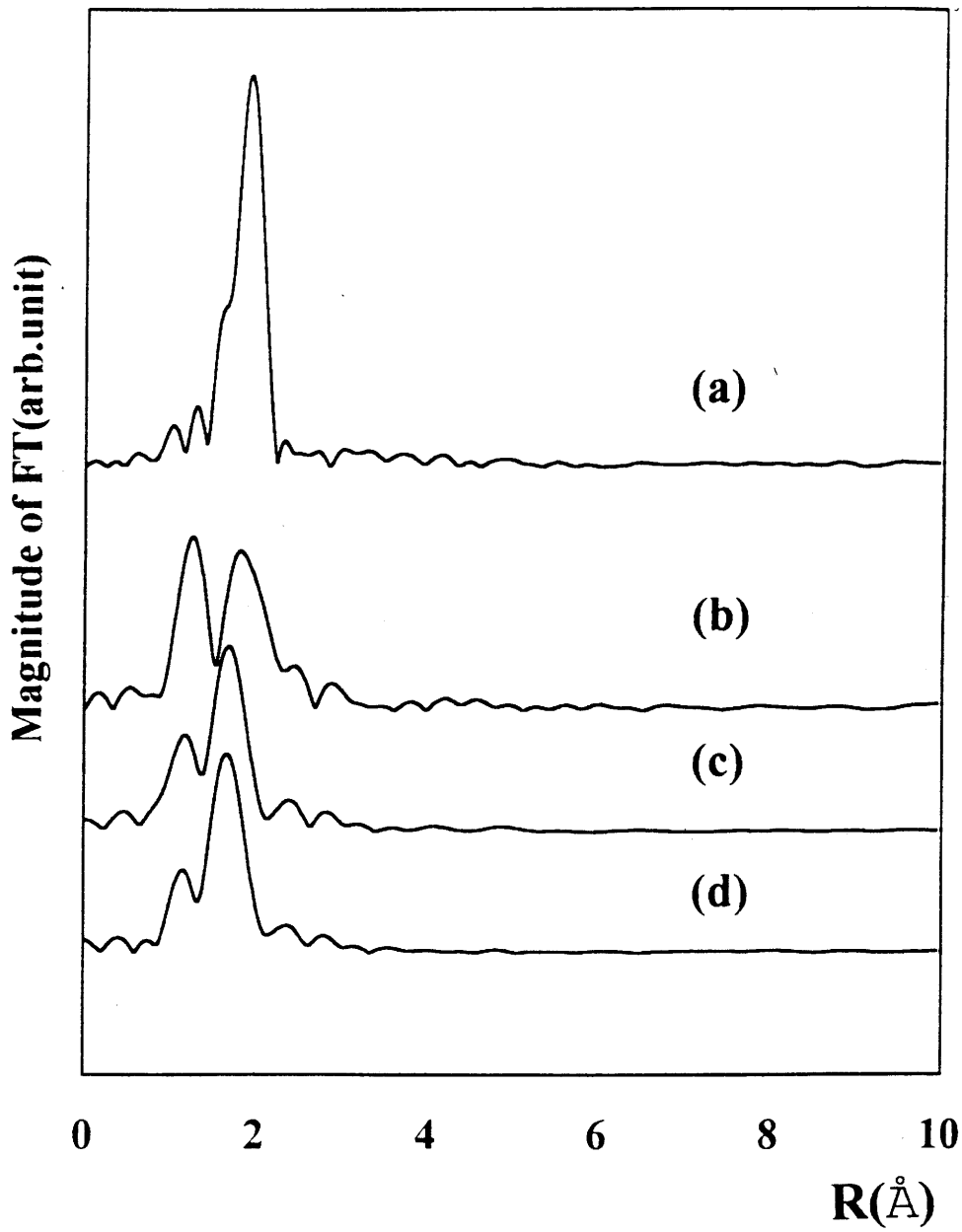

Fig. IV.3 Magnitude of FTs in the range ~2.5 Å^{-1} < k < ~13 Å^{-1} of $k^3\chi(k)$ for (a) v-As_2S_3 and (b) x = 0.67, (c) x = 0.70, (d) x = 0.75 in xLi_2S-(1-x)As_2S_3 binary glasses. The binary glasses include a peak corresponding to As-O bond at 1.2 - 1.4 Å.

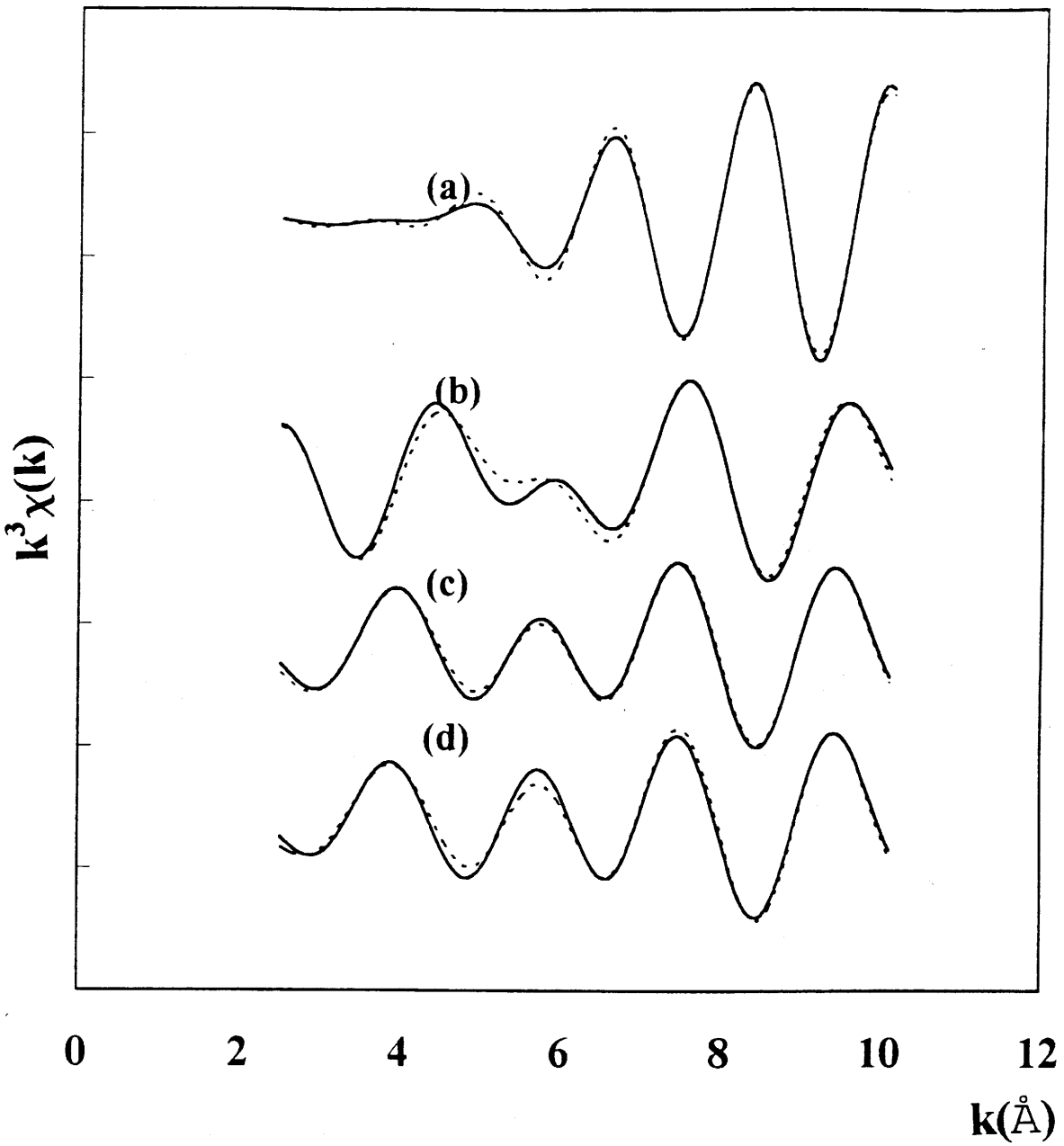

Fig. IV.4 Best fitted (dotted line) and experimental inverse transform $k^3\chi(k)$ for the range ~0.8 Å < R < ~2.2 Å for the FTs of Fig. IV.3 for (a) v-As_2S_3 and (b) x = 0.67, (c) x = 0.70, (d) x = 0.75 in xLi_2S-(1-x)As_2S_3 binary glasses.

x	Bonding pair	C.N	R(Å)	$\sigma^2(10^{-3}/Å)$	E_0(eV)
0	**As-S**	**2.8**	**2.28**	**3.6**	9.3
0.67	As-O	1.7	1.68	2.1	12.3
	As-S	**2.1**	**2.25**	**6.4**	
0.70	As-O	1.0	1.67	1.5	-7.3
	As-S	**1.6**	**2.19**	**3.3**	
0.75	As-O	0.8	1.67	0.8	-10.1
	As-S	**1.7**	**2.18**	**2.8**	

Table IV.6 Best fitted structural parameters of the arsenic K-edge for the binary glass system xLi_2S-$(1-x)As_2S_3$ (C.N. = coordination number; R = radial distance; σ = Debye-Waller factor; E_0 = threshold energy).

The modifying process of Li_2S-As_2S_3 glass under introduction of Li_2S, is to break -As-S-As- chains by creating non-bridging sulphurs. Thus, we can expect the following process;

$As_2S_3 + Li_2S$ creates 1 non-bridging sulphur

$As_2S_3 + 2Li_2S$ creates 2 non-bridging sulphurs

and $As_2S_3 + 3Li_2S$ creates 3 non-bridging sulphurs

Only the last case gives AsS_3^{3-} entities exclusively. From the previous crystalline structural study, it was shown that the As-S bond lengths involving NBS were averaged to be 2.211 Å and 2.253 Å respectively in $LiAsS_2$ and Li_3AsS_3 crystals. However, the As-S bond lengths involving bridging sulphurs average 2.327 Å in $LiAsS_2$ crystals. Thus, the As-S bond length associated with non-bridging sulphurs is shorter than that associated with bridging sulphur. In summary of this point, in Li_2S-As_2S_3 glasses, increasing the Li_2S modifier content, causes an increase in the number of non-bridging sulphurs and the average As-S bond length is thus

expected to decrease. Shastry et al. (16) stated that the glass modification is maximised at x = 0.75. Consequently we therefore propose that all As-S bonds involve NBS with an As-S bond length of 2.18 Å. This value is a shorter than that found in crystalline Li_3AsS_3. In the case of glassy and crystalline Ag_3AsS_3 (22), there is no difference in the As-S bond lengths. If we consider the maximum error range generally estimated to be ±0.05 Å (23), the 2.18 Å value found in our glass is smaller (by about 0.2 Å) than that in crystalline Li_3AsS_3. This result is considered to come from the imperfection of curve decomposition between As-O and As-S overlapping peaks.

IV.2.2 As K-edge XANES of xLi_2S-$(1-x)As_2S_3$ glasses

As shown in Fig. IV.5, the normalized As K-edge XANES spectra for the binary glass Li_2S-As_2S_3 system exhibits complicated features due to the large amount of oxide impurity, but as we will see later from XPS experiments, there is no change in the valence state of As atoms during the modifying process.

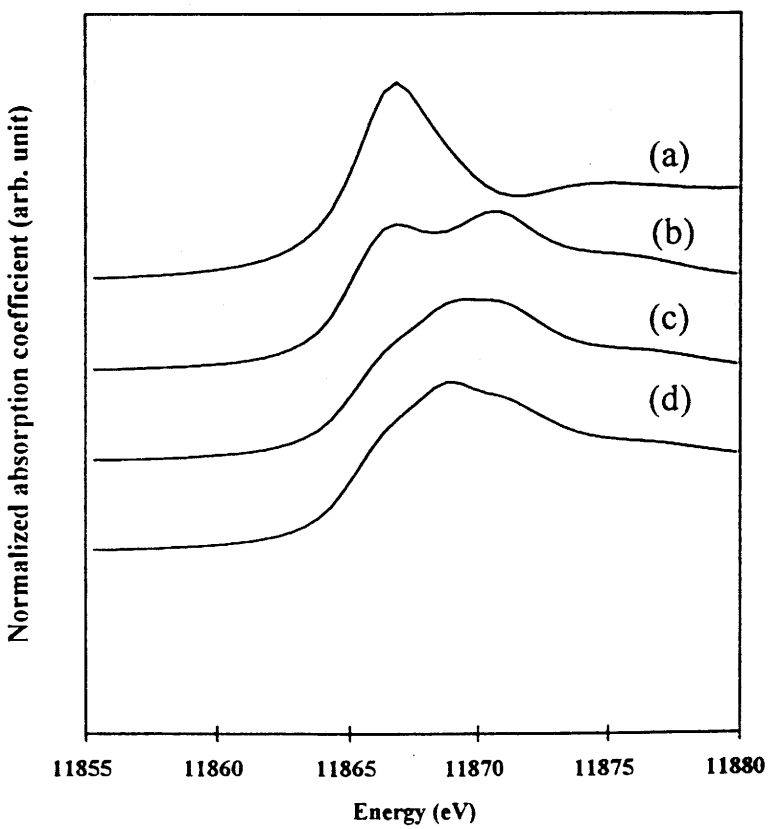

Fig. IV.5 Normalized As K-edge XANES spectra of (a) v-As_2S_3, (b) x = 0.67, (c) x = 0.70, (d) x = 0.75 in xLi_2S-$(1-x)As_2S_3$ binary glasses.

IV. 3 X-ray photoelectron spectroscopy (XPS) of binary glasses

Several XPS studies on oxide glasses have shown a characteristic chemical shift between the O1s photoelectron lines of bridging and non-bridging oxygen atoms. Such investigations have demonstrated that XPS is well adapted to the study of the local structure of glasses (24,25).

The generation of non-bridging sulphur atoms upon addition of lithium sulphide is generally accepted, however, the direct determination of the concentration of non-bridging sulphur atoms using XPS has been reported only recently (26-28). A differentiation in electronic states between bridging and non-bridging sulphur atoms in Li_2S-As_2S_3 glass has been achieved by XPS.

In As_2S_3 glass, each of the three sulphur atoms is bonded to another As atom to form a three dimensional network structure, in which all the sulphur atoms are bridging.

Fig. IV.6-a) shows the S_{2p} XPS spectra for different amounts of Li_2S modifier. The figure shows that the S_{2p} doublet peak shape changes with Li_2S content and this change is expected to be due to the formation of non-bridging sulphur atoms exhibiting a different chemical shift. The simulation of the experimental curve using a combination of Gaussian (80%) and Lorentzian (20%) shapes leads to one S_{2p} doublet for pure As_2S_3. The higher binding energy side is attributed to the $S_{2p1/2}$ spin orbital component while the lower one is due to the $S_{2p3/2}$ component. Further decomposition of S_{2p} peaks of x = 0.67 glass leads to two sets of peaks $S_{2p3/2\text{-}1/2}$ and $S'_{2p3/2\text{-}1/2}$. The electronic density around the non-bridging sulphur atoms is expected to be higher compared to that of bridging sulphur atoms due to their increased negative character as we have confirmed from the experiment on the crystalline composition. A similar phenomenon has been observed in some chalcogenide glasses, Tl_2S-As_2S_3 (26), Tl_2S-Ge_2S (27), and Li_2S-B_2S_3 (28). Therefore, the measured binding energy of NBS is smaller than

that of bridging sulphur atoms. Table IV.7 lists the binding energies and the atomic percentage of each species.

In pure As_2S_3 glass, all the sulphur atoms are bridging. For x = 0.67, the NBS / BS ratio is 78:22. This value is similar to the ratio which can be calculated from chemical formula, 80:20 which is within experimental error (±10 %). For x = 0.70, the ratio, 88:12, is comparable to the calculated ratio of 91:9. For x = 0.75, we could not find the bridging sulphur peak because all the sulphur atoms are non-bridging as expected. The results also show that the binding energy (B.E.) difference between bridging and non-bridging sulphur atoms is approximately 0.7 eV. The B.E. of NBS are quite similar to the B.E. of sulphur atoms in Li_2S indicating a strong negative character of these NBS. The B.E. of BS and arsenic in binary glass (Fig. IV.6-a and Fig. IV.6-b) is lower than the B.E. of sulphur and arsenic in v-As_2S_3. This difference which is frequently observed (29,30) can be associated with the presence of alkali cations.

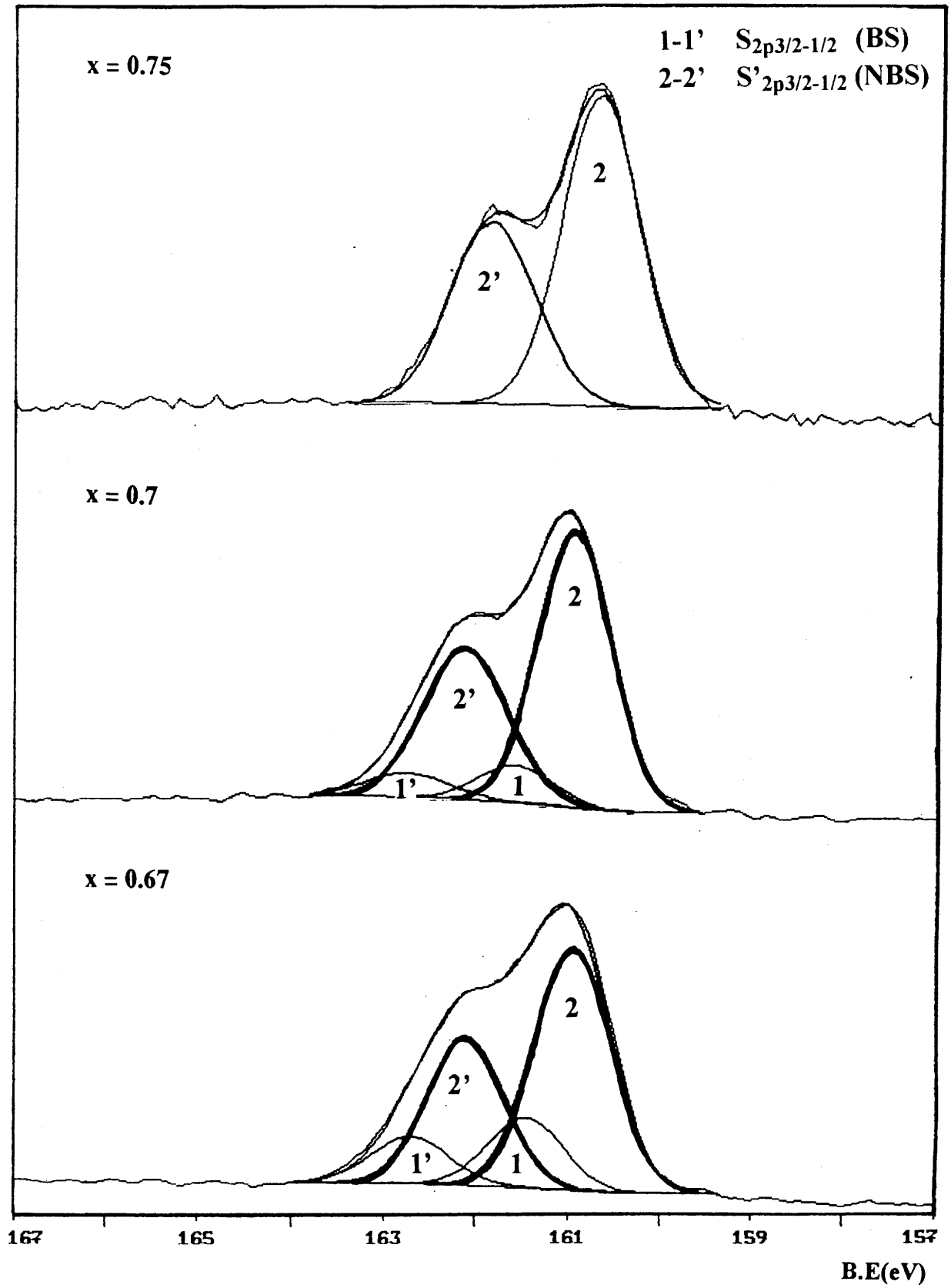

Fig. IV.6-a) XPS spectra of the $S_{2p3/2-1/2}$ peak in xLi_2S-$(1-x)As_2S_3$ binary glasses.

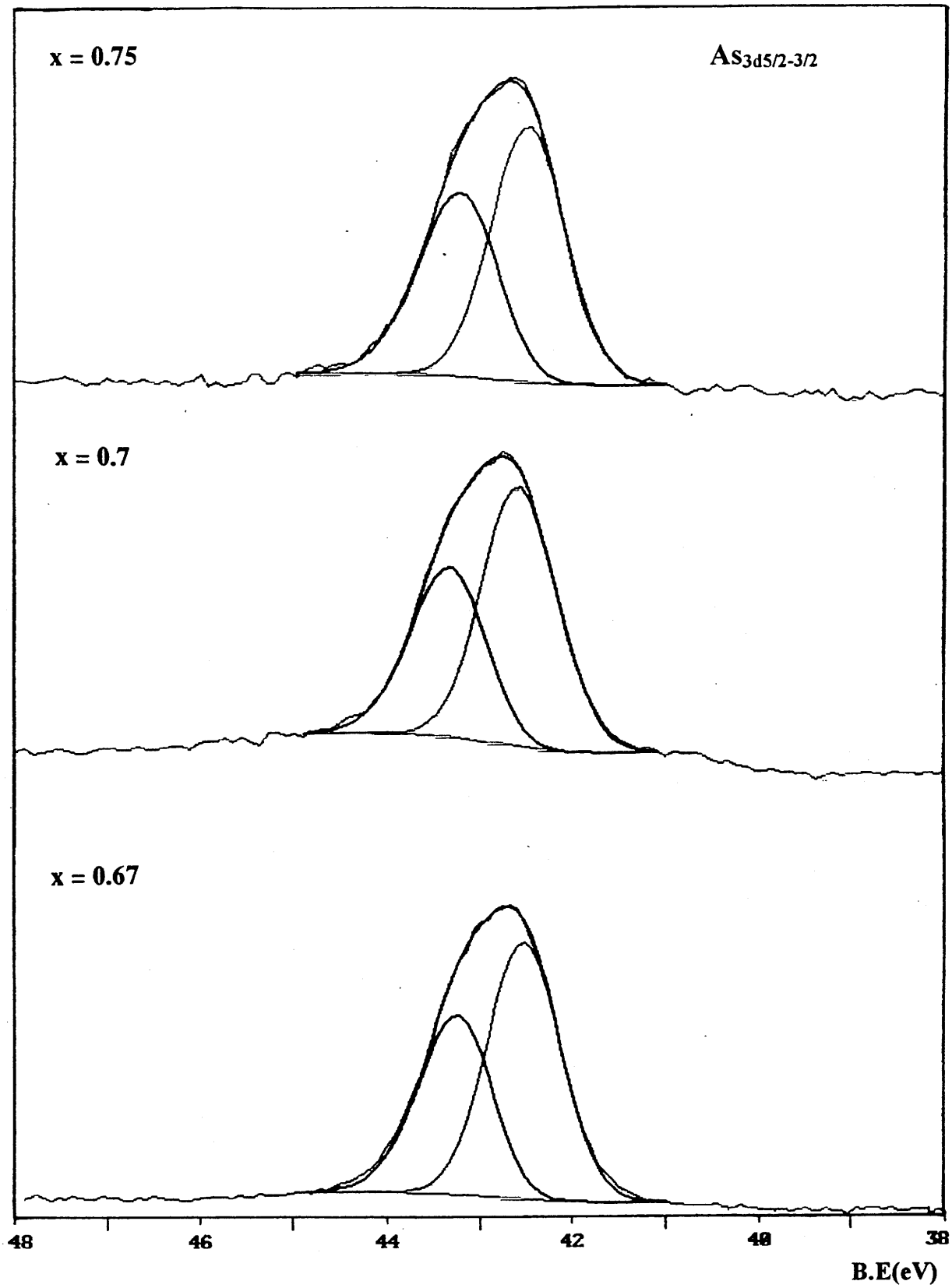

Fig. IV.6-b) XPS spectra of the $As_{3d5/2-3/2}$ peak in xLi_2S-$(1-x)As_2S_3$ binary glasses.

	As_2S_3	Li_2S	x=0.67		x=0.70		x=0.75	
	B.E(eV)	B.E(eV)	B.E(eV)	At. %	B.E(eV)	At. %	B.E(eV)	At. %
$As_{3d5/2-3/2}$	43.6 - (1) 44.3 (1)		42.6 - (1) 43.3 (1)		42.5 - (1) 43.2 (1)		42.2 - (1) 42.9 (1)	
$S_{2p3/2-1/2}$	162.5 - (1) 163.7 (1)	-	161.5 - (1) 162.6 (1)	22	161.6 - (1) 162.7 (1)	12		
$S'_{2p3/2-1/2}$	-	160.7 - (1.2) 161.9 (1.2)	160.9 - (1) 162.1 (1)	78	160.9 - (1) 162.1 (1)	88	160.7 - (1) 161.9 (1)	100

Table VI.7 XPS results for xLi_2S-(1-x)As_2S_3 glasses versus composition.

IV.4 Raman spectroscopy

IV.4.1 Li_2S-As_2S_3 binary glasses

As we have seen in XAS and XPS experiments, the structural entities in Li_2S-As_2S_3 glass change depending on the amount of Li_2S. At x = 0.67, the presence of pyramidal units in which As atoms are bonded to bridging and non-bridging sulphur atoms is expected. The most modified glass (x = 0.75) revealed the presence of only non-bridging sulphur atoms. To obtain more information on these "molecular" units a Raman spectroscopic study was carried out. A similar study was previously reported by Shastry et al. (16). The reported Raman spectra of Li_2S-As_2S_3 are shown at Fig. IV.7. The spectrum of v-As_2S_3 exhibits a dominant peak at 340 cm^{-1}, and as reviewed in chapter II, this peak corresponds to the ν_1 symmetric stretching mode in the AsS_3 pyramidal unit. Li_2S modified glasses show their main peak at 380 cm^{-1} with a shoulder at 350 cm^{-1}. These peaks were assigned by Shastry et al.(16) after comparison with the polarized Raman spectrum reported in Fig. IV.8 as the ν'_1 and ν'_3 stretching modes of As-

S^- in AsS_3^{3-} pyramids. As noted by Shastry et al., the broad shoulder around 270 - 360 cm^{-1} and 120 - 200 cm^{-1} may be a manifestation of the number of different units present for this composition. This is substantiated by comparison of the Raman spectra between $LiAsS_2$ and Li_3AsS_3 crystals (cf. III.3). The As-S stretching mode frequencies were reported at 270 - 402 cm^{-1} in $LiAsS_2$ crystal and at 318 - 375 cm^{-1} in Li_3AsS_3. The As-S bending modes frequencies appeared at 101 - 200 cm^{-1} in crystalline $LiAsS_2$ and 173 - 214 cm^{-1} in crystalline Li_3AsS_3.

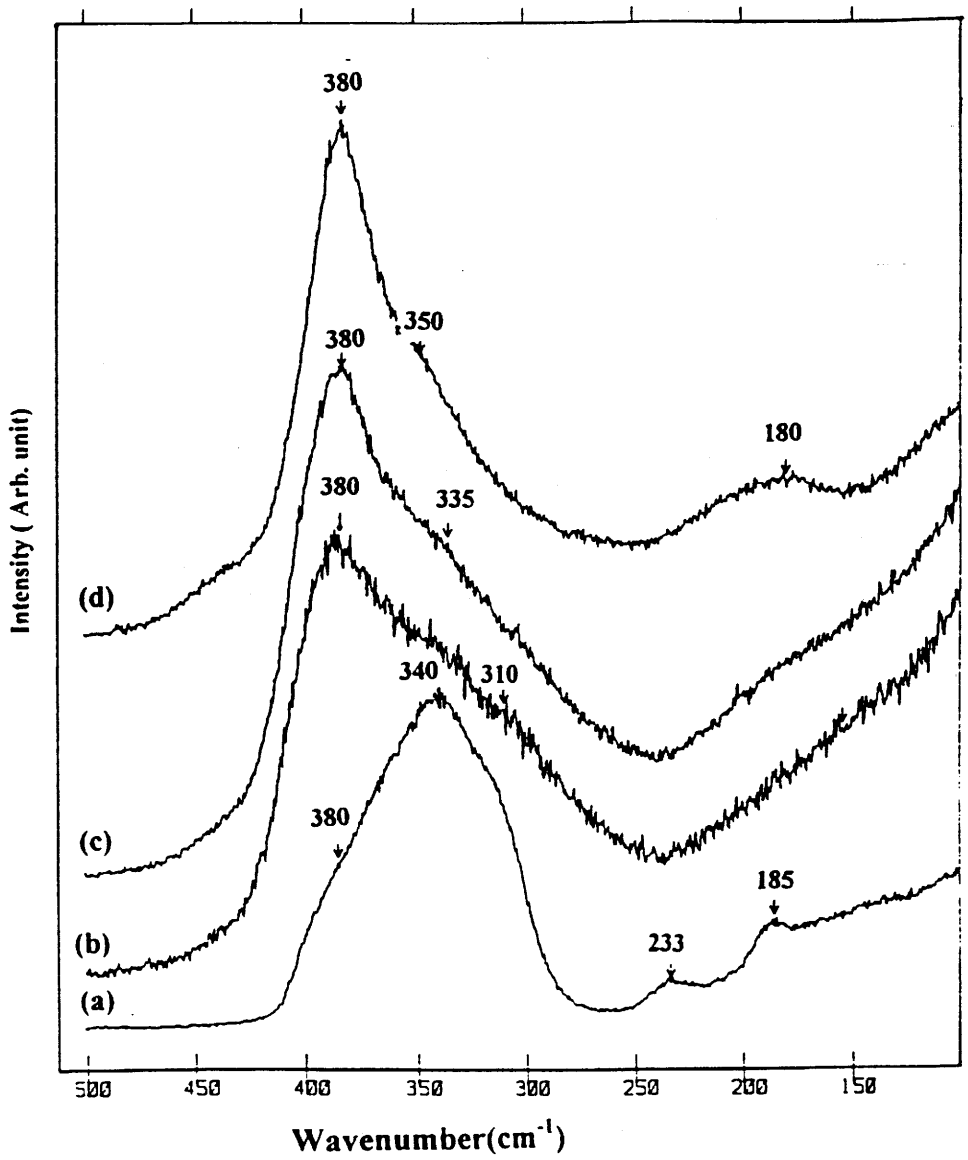

Fig. IV.7 Raman spectra obtained for (a) v-As_2S_3, (b) x = 0.67, (c) x = 0.70, (d) x = 0.75 in binary glass xLi_2S-(1-x)As_2S_3 system (16).

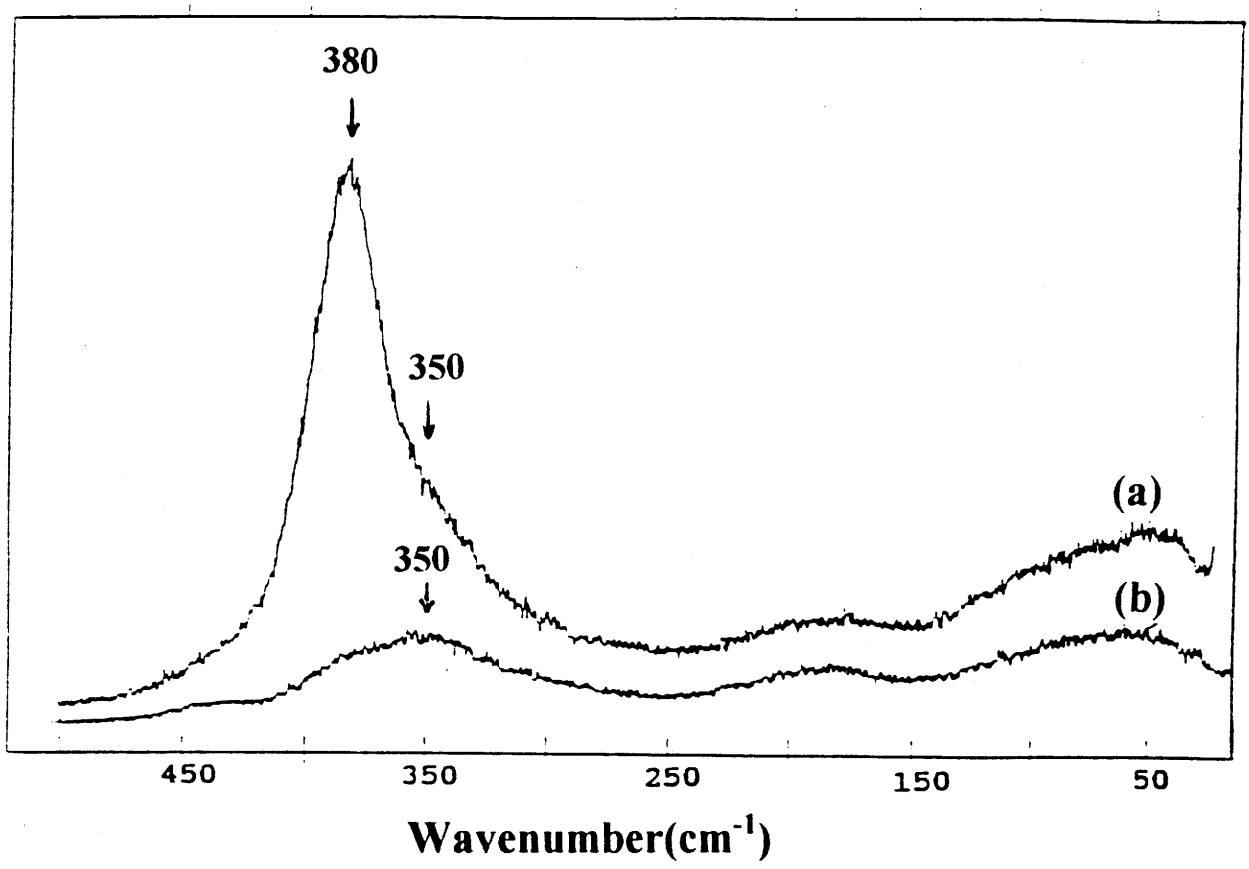

Fig. IV.8 Raman spectra of $0.75Li_2S$-$0.25As_2S_3$ glass in VV (a) and VH (b) geometries (16).

Fig. IV.9 illustrates the Raman spectra of the x = 0.75 glass and of the Li_3AsS_3 crystal. They are noted to be similar. From chapter III.3, the 375 cm^{-1} and 356 cm^{-1} peaks were assigned to the As-S stretching modes of As-S^- in AsS_3^{3-} pyramidal units. From the comparison of the glass and crystalline phases, it can be estimated that the 380 cm^{-1} and 350 cm^{-1} peaks of the glass may be assigned to stretching modes of As-S^- bond, which is in accordance with the assignment made by Shastry et al. (16). The comparison to the As-S bending mode in the AsS_3^{3-} pyramid also shows a strong similarity between glassy and crystalline Li_3AsS_3. These comparisons lead to the conclusion that the AsS_3^{3-} structural units exist in both Li_3AsS_3 crystal and in the corresponding glass (x = 0.75).

IV.4.2 LiI-Li_2S-As_2S_3 ternary glasses

When AsI_3 is added to crystalline As_2S_3, some As-S bonds are broken with the formation of As-I and S-S bonds. This bond breaking disrupts the cross-linked structure in the layers, forming individual chains and leading to a marked decrease in the viscosity (31). On the other hand, as can be seen in the case of addition of LiI doping salt to Li_2S-B_2S_3 glass, LiI does not induce any change in the structure of the host matrix (5). Similar behavior has been observed in other sulphide based glasses such as LiI-Li_2S-P_2S_5 (8,32).

Figure IV.10-a) shows the Raman spectra for x = 0.70 (y = 0, 0.2 and 0.5) and Fig. IV.10-b) for x = 0.75 (y = 0, 0.3 and 0.5). As expected, these spectra do not exhibit any modification upon introduction of LiI doping salt. In addition, there is no signal showing the formation of S-S bonds or As-I bonds which were observed in the As-S-I glass system (31, 33). The addition of LiI does not affect the structure of the host glass, and the general expectation of dissolving LiI into glass matrix as an ionic species is again confirmed.

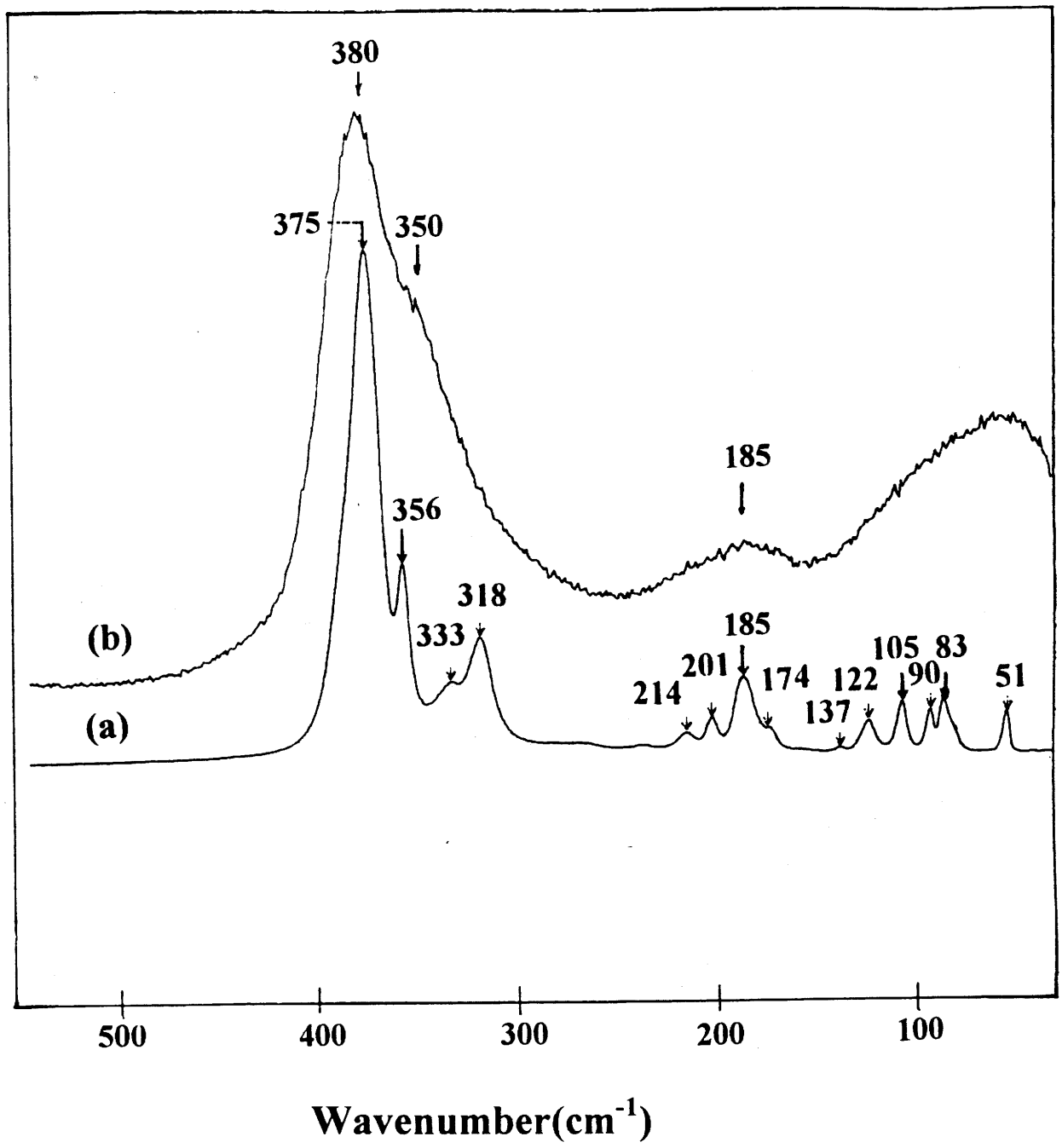

Fig. IV.9 Raman spectra obtained from (a) c-Li_3AsS_3 and (b) 0.75Li_2S-0.25As_2S_3 glass. The c-Li_3AsS_3 spectrum is right angle polarized to incident plane.

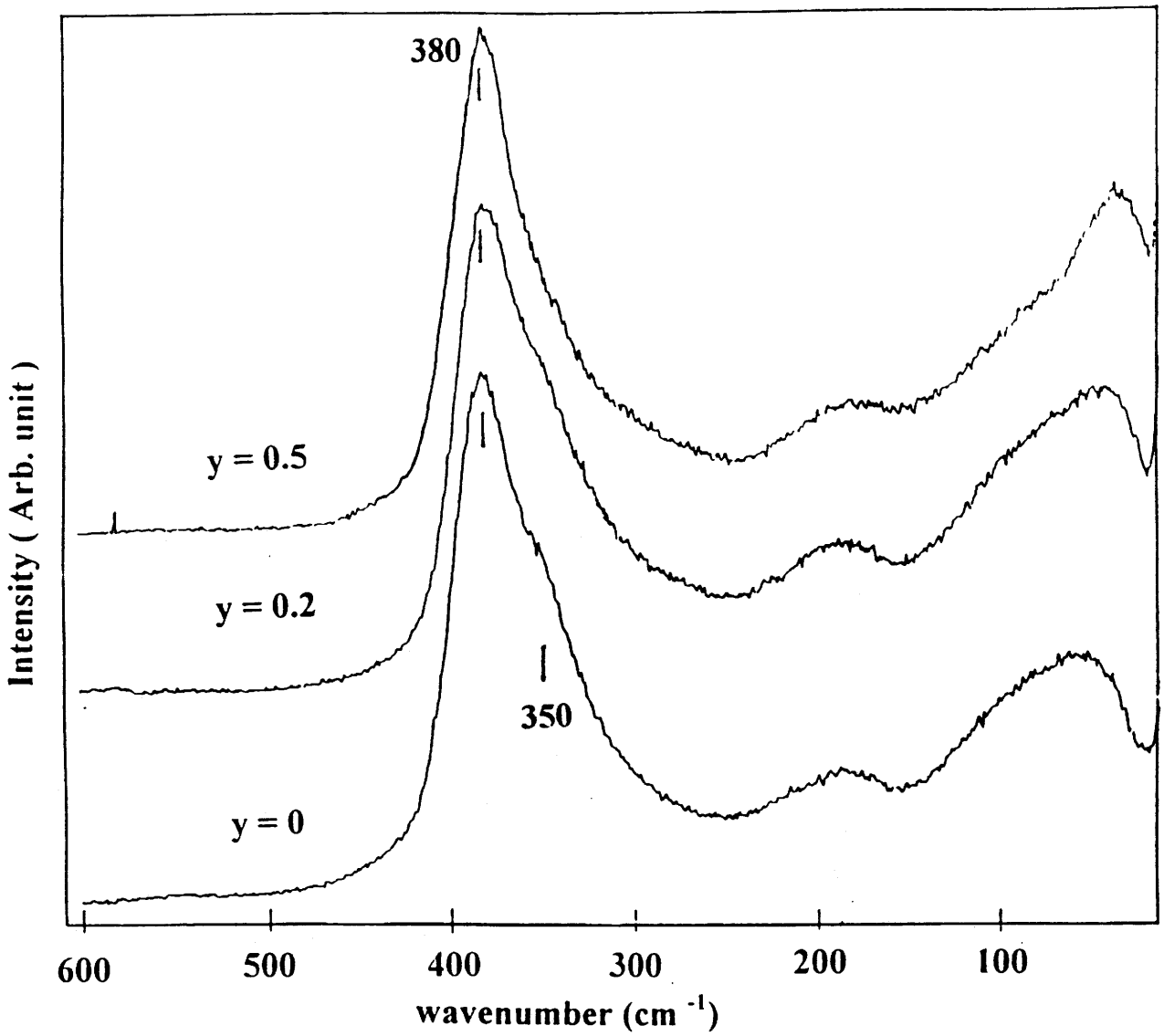

Fig. 10-a) Raman spectra obtained from yLiI-(1-y)(0.70Li_2S-0.30As_2S_3) glasses.

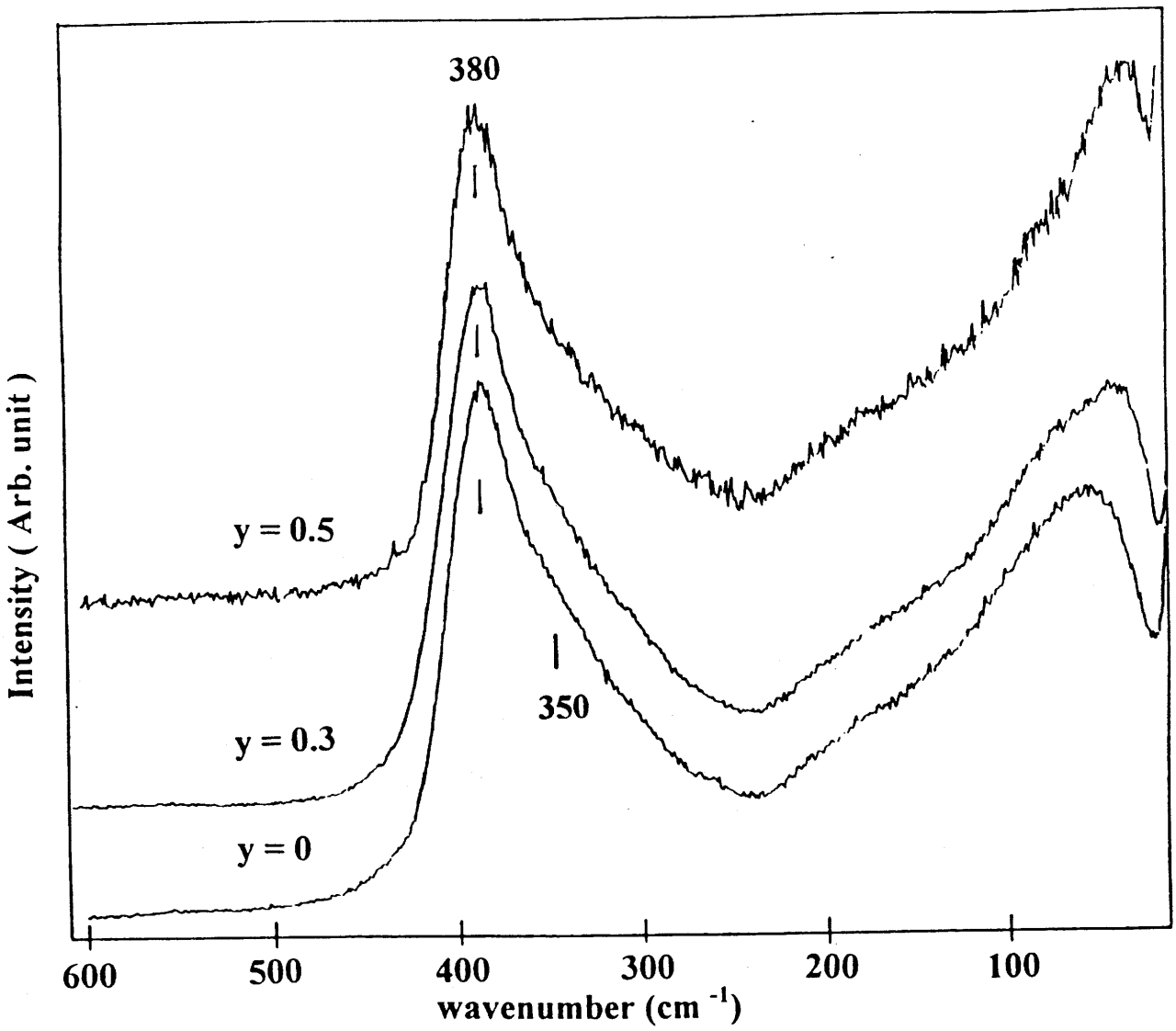

Fig. 10-b) Raman spectra obtained from yLiI-(1-y)(0.75Li_2S-0.25As_2S_3) glasses.

IV.5 IR spectroscopy of Li_2S-As_2S_3 binary glasses

The spectra obtained from xLi_2S-$(1-x)As_2S_3$ glasses are shown in Fig. IV.11. The general feature of these spectra upon addition of Li_2S to As_2S_3 glass is the strong enhancement in absorption around 370 cm^{-1} . In the previous section, we observed that Raman spectra exhibit a large and broad peak around 380 cm^{-1} ; for x = 0.75 all the units are expected to be AsS_3^{3-} pyramids. Fig. IV.12 shows a comparison of the IR spectrum of crystalline Li_3AsS_3 and that of the corresponding glass. These are noted to be similar. In Chapter III, the 355 cm^{-1} peak of Li_3AsS_3 was assigned to a stretching vibration mode of $As\text{-}S^-$ in AsS_3^{3-} pyramids. Consequently, the 370 cm^{-1} peak observed in Li_2S-As_2S_3 glass seems to be a comprise of the $As\text{-}S^-$ stretching vibration in AsS_3^{3-} pyramids. The higher shift of the $As\text{-}S^-$ stretching vibration frequency in Li_2S-As_2S_3 glasses compared to that in Li_3AsS_3 crystal may stem from the shorter $As\text{-}S^-$ bond distance found in glass. The observed broad peak around 400 - 500 cm^{-1} in glass would contribute to the shoulder at 420 cm^{-1} in crystalline Li_3AsS_3. However, the origin of this peak remains unverified.

The overall spectral feature of crystalline Li_3AsS_3 is conserved in the x = 0.75 glass. These results confirm that the structure of the x = 0.75 glass contains similar AsS_3^{3-} trigonal pyramidal units as previously observed by Raman experiments.

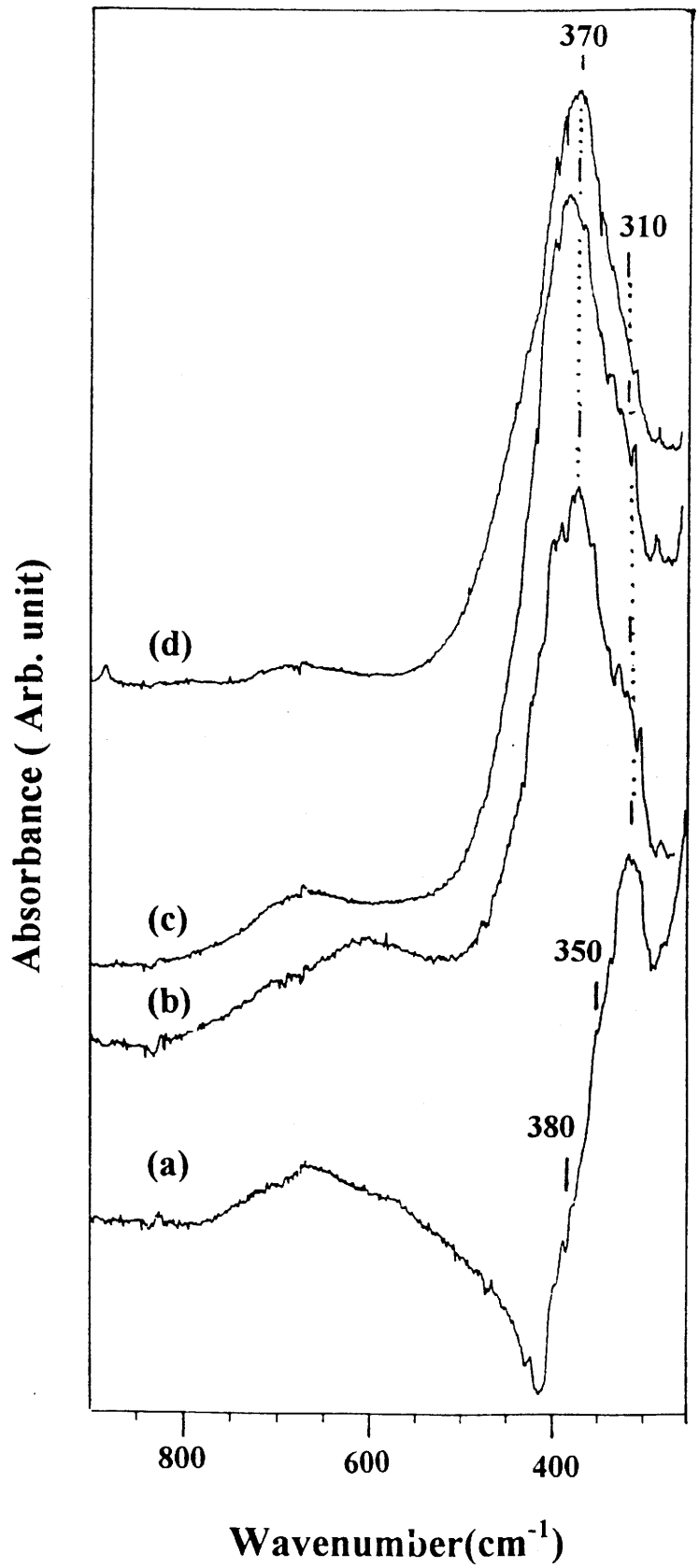

Fig. IV.11 Dispersive IR spectra for (a) v-As_2S_3, (b) x = 0.67, (c) x = 0.70 and (d)x = 0.75 in xLi_2S-(1-x)As_2S_3 binary glasses.

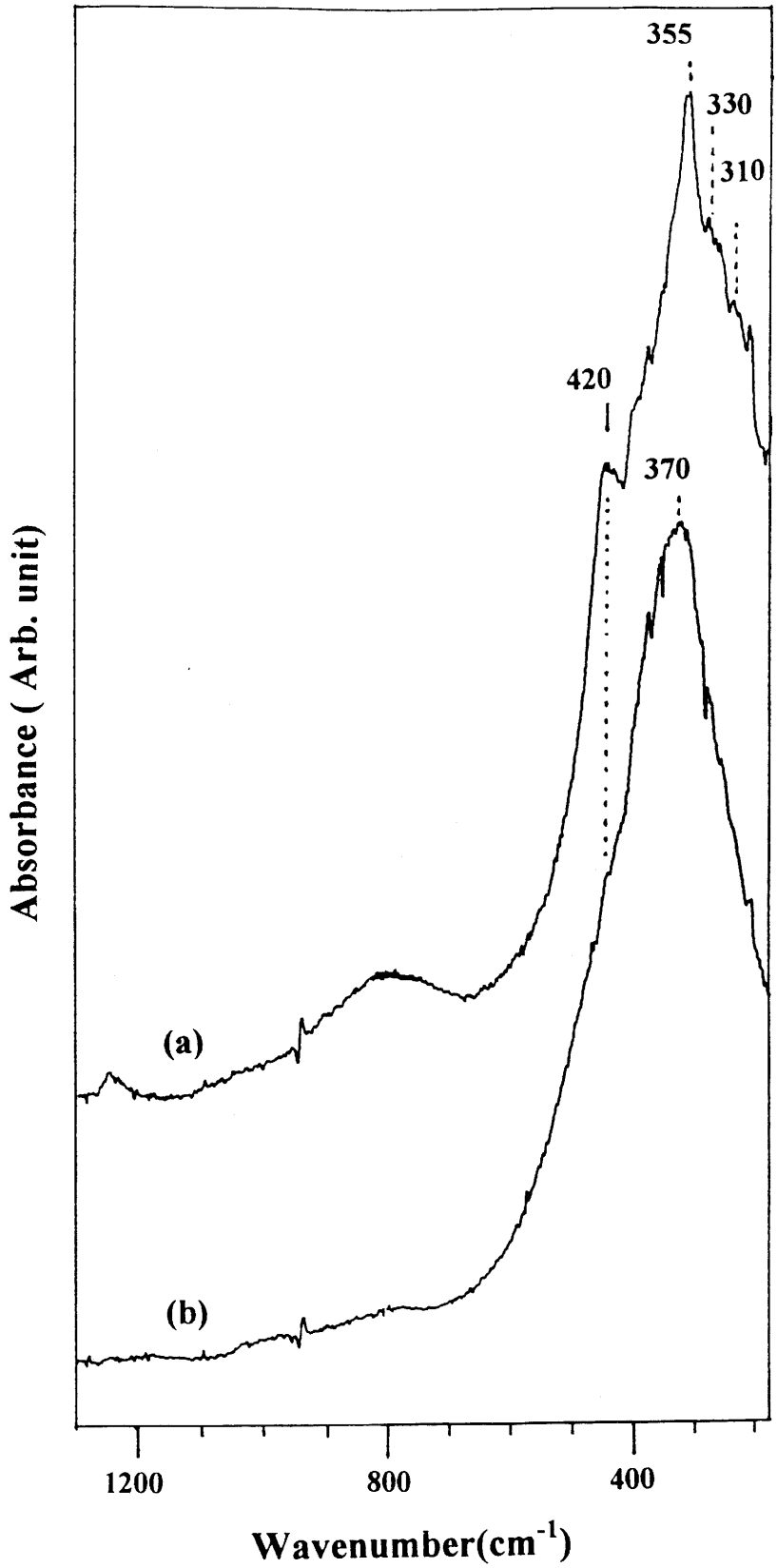

Fig. IV.12 Dispersive IR spectra obtained for (a) c-Li_3AsS_3 and (b) 0.75Li_2S-0.25As_2S_3 glass.

Conclusion

The structural modification process upon introduction of Li_2S to As_2S_3 glass was confirmed by physical characterization and spectroscopic experiments.

In xLi_2S-$(1-x)As_2S_3$ binary glasses, the glass transition temperature increases with Li_2S modifier content. This behaviour was explained by comparing the variation in the structure of the crystalline phases of c-$LiAsS_2$ to c-Li_3AsS_3, which originates from the change in structural dimension and local coordination of Li polyhedra. Li_2S modifier in As_2S_3 glass creates non-bridging sulphurs and its ratio to bridging sulphur atoms was similar to that calculated for corresponding compositions. In addition the As-S^- bond distance was shorter than that associated with bridging sulphurs. The molecular frame of AsS_3 pyramid was conserved even in modification as AsS_3^{3-}. In the x = 0.75 glass, all the terminating sulphur atoms were non-bridging as determined by comparing between c-Li_3AsS_3 and the x = 0.75 glass.

In LiI-Li_2S-As_2S_3 ternary glass, there was no evidence of a structural change in the Li_2S-As_2S_3 host matrix upon doping with LiI salt.

References

1. R. H. Doremus, *Glass Science* (John Wiley & Sons, 1973)

2. S. Susman, L. Boehm, K. J. Volin and C. J. Delbecq, Solid State Ionics, **5** (1982) 21

3. D. E. Hintenlang and P. J. Bray, J. Non-Cryst. Solids, **69** (1985) 243

4. K. S. Suh, A. Hojjaji, G. Villeneuve, M. Ménétrier and A. Levasseur,
J. Non-Cryst. Solids, **138** (1991) 13

5. M. Ménétrier, A. Hojjaji, A. Levasseur, M. Couzi and K. J. Rao,
Phys. Chem. Glasses, **33** (1992) 222

6. J. A. Sills, S. W. Martin, D. R. Torgeson, J. Non-Cryst. Solids, **168** (1994) 86

7. C. Estournès, A. P. Owen, M. Ménétrier, A. Levasseur, K. J. Rao and S. R. Elliott,
J. Non-Cryst. Solids, **171** (1994) 80

8. J. P. Malugani and G. Robert, Solid State Ionics, **1** (1980) 519

9. R. Mercier. J. P. Malugani, B. Fahys and G. Robert, Solid State Ionics, **5** (1981) 663

10. S. J. Visco, P.J. Spellane and J. H. Kennedy, J. Electrochem. Soc., **132** (1985) 751

11. E. R. Plumat, J. Am. Ceram. Soc., 9 (1968) 499

12. B. Barrau, M. Ribes, M. Maurin, A. Kone and J. L. Souquet,
J. Non-Cryst. Solids, **37** (1980)

13. L. Jun, J. J. Videau, J. M. Reau, B. Tanguy, J. Portier and P. Hagenmuller,
J. Non-Cryst. Solids, **111** (1989) 43

14. L. Zhenhua and C. Jijian, J. Non-Cryst. Solids, **136** (1991) 205

15. M. C. R. Shastry, M. Ménétrier and A. Levasseur, Solids State Commun., **85** (1993) 887

16. M. C. R. Shastry, M. Couzi, A. Levasseur, M. Ménétrier, Phil. Mag. **B 68** (1993) 551

17. S. J. Visco, P. J. Spellane and J. H. Kennedy, J. Electrochem. Soc., **132** (1985) 1766

18. S. W. Martin and C. A. Angell, J. Non-Cryst. Solids, **66** (1984) 429

19. M. Ménétrier, C. Estournès, A. Levasseur and K. J. Rao,
Solid State Ionics, **53-56** (1992) 1208

20 P. Vinatier, M. Ménétrier and A. Levasseur, accepted in Solid State Ionics (1995)

21. A. F. Wells, *Structural Inorganic Chemistry*,
5th Ed (Oxford University Press, New York, 1984)

22. M. Okuno, H. Sugaya and T. Matsumoto, J. Non-Cryst. Solids, **150** (1992) 356

23. A. V. Chadwick, Lecture note, Univ. of Canterbury, Kent

24. R. Brückner, H. U. Chun and H. Goretzki, Glasstech. Ber., **51** (1978) 1

25. P. I. K. Onorato, M. N. Alexander, C. W. Struck, G. W. Tasker and D. R. Uhlmann,
Comm. Am. Ceram. Soc., **68** (1985) C148

26. J. Heo, J. S. Sanghua and J. D. Mackenzie, J. Non-Cryst. Solids, **101** (1988) 23

27. R. M. Almeida, H. Nasu, J. Heo and J. D. Mackenzie, J. Mat. Sci. Lett., **6** (1987) 701

28. P. Vinatier, Ph. D. Thesis, Univ. Paris XI Orsay, (1995)

29. T. A. Clarke and E. N. Rizhalla, Chem. Phys. Lett., **37** (1976) 523

30. R. Gresch, W. Müller-Warmuth and H. Dutz, J. Non-Cryst. Solids, **34** (1979) 127

31. T. E. Hopkins, R. A. Pasternak, E. S. Gould and J. R. Herndon,
J. Phys. Chem. **66** (1962) 733

32. G. Robert. J. P. Malugani and A. Soida, Solid State Ionics, **3-4** (1981) 311

33. Y. Kameda, Y. Sugawa and O. Uemura, J. Non-Cryst. Solids, **156** (1993) 725

Chapter V. Ionic conductivity study of LiI-Li_2S-As_2S_3 glass

Introduction

In the last two decades, interest has centred on the investigation of fast ion conductors (FIC) or superionic conductors, in which the value of the ionic conductivity is comparable to that of molten salts or of concentrated ionic solutions ($\sigma \geq 10^{-2}\ \Omega^{-1}cm^{-1}$) (1). Generally FIC's containing singly charged cations such as Ag^+, Li^+ and Na^+-ions tend to show high conductivities, Ag^+ containing FIC's having the highest conductivity (2-4). Some cationic FIC's have values of ionic conductivity comparable to those of their crystalline superionic counterparts, but it is noticeable that the highest conductivities in the glasses are achieved by the introduction of doping salts, i.e. β-AgI (3) or LiI (5) which by themselves are not superionic conductors in the crystalline state.

The ionic conductivitiy of a glass is largely dependent on composition but its mechanism is not so well known as crystalline ionic solids. The difficulties of understanding transport mechanisms in glass is principally due to the complexity of the structure, the framework and local environment of ions.

The correlation of conductivity with glass structure and composition has long been studied and there were several models proposed to explain the conduction mechanism. However, many such models seek to describe the situation in specific ionic conducting glasses, but the various types make it difficult to unify these into a single model. Given such difficulties, there has still been remarkable progresses in glass study. There is still, however, a certain lack of confidence in the explanation of the conduction mechanisms of glasses. We have tried here

to apply the classical models to sulphide glasses in order to explain the correlation between conductivity and composition. The structural information already presented in Chapter IV has been successful in explaining the conduction mechanisms in highly modified sulphide glasses.

Studies of ionic conduction in glasses have been carried out on xLi_2S-$(1-x)As_2S_3$ binary and $yLiI$-$(1-y)[xLi_2S$-$(1-x)As_2S_3]$ in the range $x = 0.70$ at $0 < y < 0.5$ and $x = 0.75$ at $0 < y < 0.5$, respectively.

V.1 Ionic conduction models

The ionic conductivity of a glass is strongly affected by composition, increasing by several orders of magnitude for a relatively modest increase in the modifier cation content. The conductivity may be expressed as the product of the concentration of charged carriers and their mobility as follows :

$$\sigma = Ze n \mu, \qquad \text{(Eq. V.1)}$$

where Ze is the electric charge number, n is the mobile carrier concentration, and μ is their mobility. It is generally agreed that compositional influences on both of these terms may contribute to the overall composition dependence of the conductivity (6). The general expression for the concentration of thermally activated mobile carriers is $n = N_0 \exp(-Ec/kT)$, where N_0 is the total number of modifier cations and Ec is the creation energy of mobile carriers. The temperature dependence of the ionic conductivity below the glass transition temperature, appears to obey an Arrhenius law as :

$$\sigma \text{ (or } \sigma T) = \sigma_0 \exp(-E_A/k_B T) \qquad \text{(Eq. V.2)}$$

However, if either n or μ in (Eq. V.1) becomes dominant, then this general agreement is broken.

A number of models have been proposed accounting for various aspects of ionic conduction in glasses, in particular the behaviour of the d.c. conductivity activation energy. These may be categorised classically into the strong electrolyte, the weak electrolyte and defect models.

V.1.1 Strong electrolyte model

This model supposes that all modifying cations contribute to the conductivity, and as is shown in (Eq. V.1) the conductivity linearly depends upon the concentration of cations. The experimentally determined exponential dependence on composition is believed to indicate dominance on the mobility term. Classically, Anderson and Stuart (7) considered the activation energy as the sum of the energy required to overcome cation-anion binding energy Eb and the energy required to open up doorways Es when the ion passes through. According to the theory:

$$E_A = Eb + Es \qquad \text{(Eq. V.3)}$$

The solution of the strain energy term Es was based on Frenkel's calculations (8) which is applicable to a close-packed liquid, and then modified for the glassy structure as :

$$Es = 4\pi G r_D (r - r_D)^2, \qquad \text{(Eq. V.4)}$$

where G is the shear modulus, r_D is the doorway radius and r is the cation radius. The electrostatic binding energy term Eb was expressed by :

$$Eb = (\beta/\gamma)(ZZ_0e^2)/(r + r_0), \qquad \text{(Eq. V.5)}$$

where β and γ are covalency parameters arbitrarily taken equal to the relative permittivity, εr, Z_0 and r_0 are the charge and radius of counter anion respectively, Z and r are the charge and radius of the cation respectively. On the basis of such assumptions, the activation energy of ionic conduction proposed by Anderson and Stuart can be written as :

$$E_A = (\beta/\gamma)(ZZ_0e^2)/(r + r_0) + 4\pi G r_0 (r - r_D)^2 \qquad \text{(Eq. V.6)}$$

Later, McElfresh and Howitt (9) modified the strain energy term, Es, as the enlargement of a cylindrical hole of length *l* from a radius r_D to r, such that $Es = \pi G l(r-r_D)^2 / 2$. The pictorial view of this model considered by Martin and Angell is illustrated in Fig. V.1 (10). This model was able to calculate the variation of E_A with composition in some alkali silicate glasses (11).

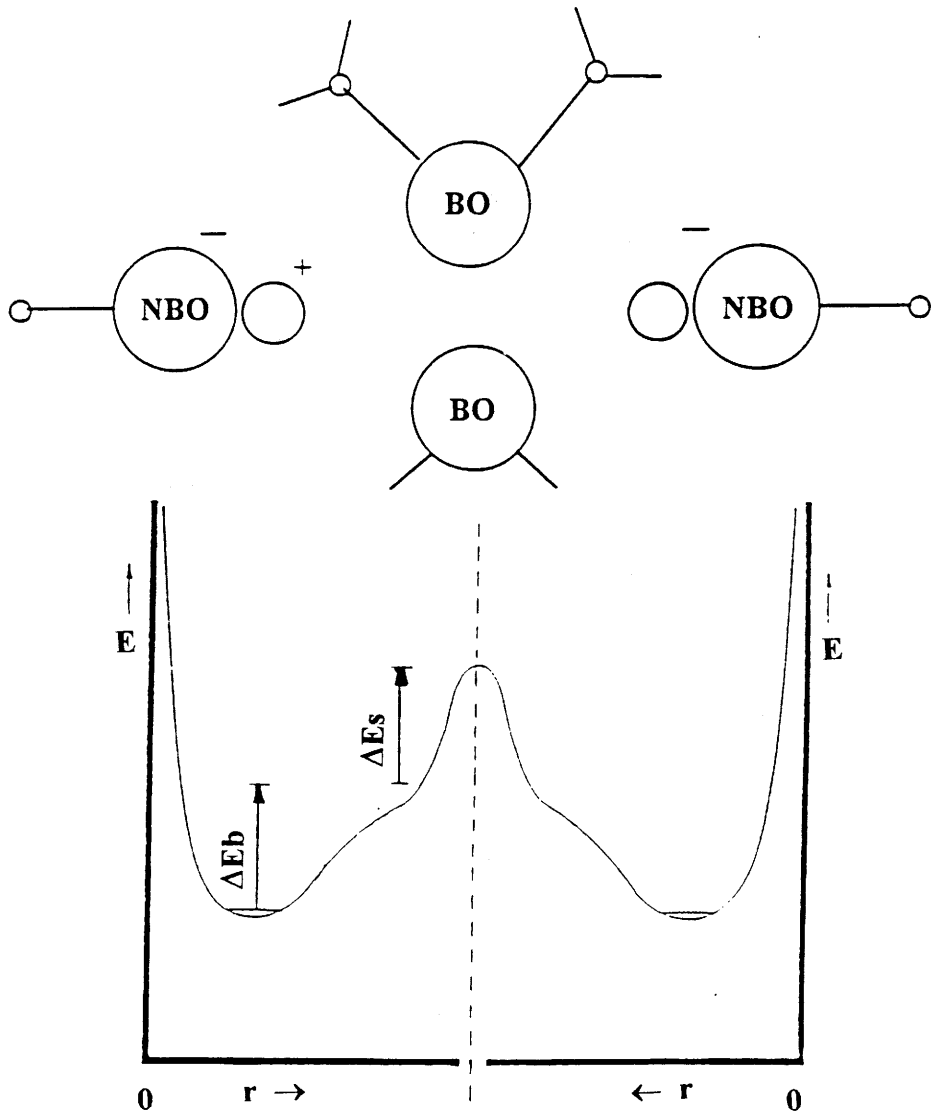

Fig. V.1 Potential energy surface experienced by a mobile cation in an oxide glass as described by the strong electrolyte model as visualised by Martin and Angell (10).

V.1.2 Weak electrolyte model

The weak electrolyte model was developed by Ravaine and Souquet (12,13). This model supposes that only a small number of cations (or anions) are contributing at a given time to conduction and that the mobility is compositionally independent. It also supposes that the activation energy represents the binding energy which holds the ions in their equilibrium positions and once an ion has dissociated away from its site, it is thought to experience no other energy barrier for motion.

Ionic conductivity of electrolytes is often expressed as a product of concentration and mobility as described by equation (V.1). Ravaine and Souquet (12,13) have extended the weak electrolyte theory to glasses by observing the relation, $\sigma = A\,(aNa_2O)$, in Na_2O-SiO_2 glasses. A is a constant. By assuming the dissociation equilibrium to be $Na_2O \Leftrightarrow Na^+ + NaO^-$ and from thermodynamics $\mu Na_2O = \mu^\circ Na_2O + RTln[Na^+]^2$ under constant activity coefficient and charge neutrality, it can be deduced that :

$$\sigma = \text{const. } [Na^+] \qquad \text{(Eq. V.7)}$$

This shows clearly that the mobility is independent of glass composition. Kone et al. (14) took the argument a stage further, and wrote :

$$E_A(\sigma) = Em + \Delta H/2 + 1/2\,\alpha(1-x)^2, \qquad \text{(Eq. V.8)}$$

where ΔH is the enthalpy of reaction, Em is the "true" activation energy, and x is the mole fraction of alkaline component. The validity of this equation has been checked for $AgPO_3$-AgI (15) and lithium borate glasses (16). Thus, a main consequence of this model is that the conductivity is dependent on the concentration of the free cations, but not all modifier cations are equally mobile. Martin and Angell (10) proposed that the strong and weak electrolyte theories could be reconciled if the dissociation energy of free cations could be identified with the electrostatic binding energy and the mobility energy with elastic strain energy. This structural model is shown in Fig. V.2. In both the weak electrolyte and Anderson-Stuart (A-S)

models, a strain energy barrier is always presumed to be present because of the volume requirement of the migrating cation. To account for the dissociated and undissociated states in the weak electrolyte model, the availability of metastable sites of higher energy, rather than the bound lowest energy sites as in Fig. V.2 was suggested.

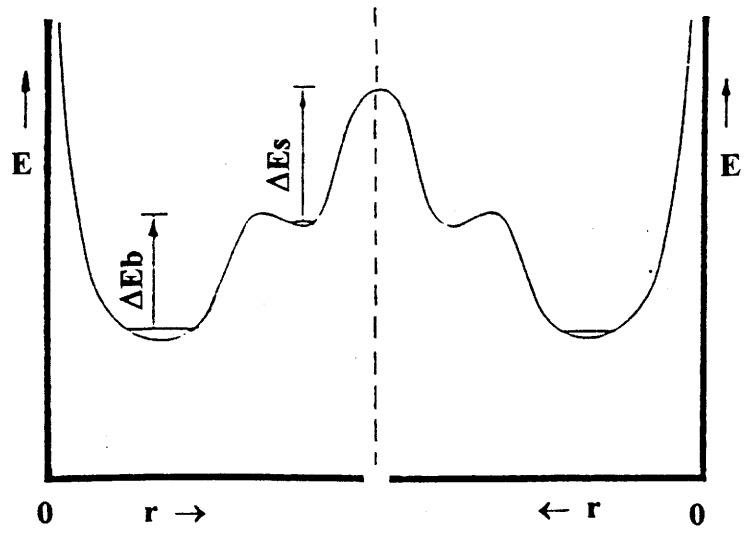

Fig. V.2 Potential energy surface described by the weak electrolyte model (10).

V.1.3 Defect models

This model utilises concepts employed in the study of crystalline ionic conductors, where the emphasis is on the particular sites in the structure participating in the diffusion process.

Ionic transport in crystals usually involves the migration of defects. Interstitial cations may hop in a direct interstitial mechanism (hop directly between interstitial sites) or in a pair-

wise (interstitialcy) mechanism displacing a cation from a neighbouring lattice site. The cation pairs are variously called split interstitials, interstitial pairs, or interstialcies. Here an interstitial ion displaces one of its nearest neighbours out of its lattice position into an adjacent interstitial site, the incoming interstitial ion then occupies the related lattice vacancy.

V.1.3.1 Haven-Verkerk model

This model was proposed by Haven and Verkerk in 1965 (17) to compare the difference in diffusion coefficient between tracer ions and the diffusion conductivity defined by the Nernst-Einstein equation. When the electrical conductivity arises from a diffusion mechanism as in ionic conduction, a conductivity diffusion coefficient, D_σ, may be defined by the Nernst-Einstein equation :

$$D_\sigma = kT\sigma/ne^2 \qquad \text{(Eq. V.9)}$$

When ionic motion involves both direct and indirect interstitial mechanisms, a correlation factor f is included in the Nernst-Einstein equation (18,19). Thus the expression becomes $D^* = fkT\sigma/ne^2$. In general, the tracer diffusion coefficient D^* will not be equal to D_σ if correlation effects are important; the correlation factor being expressed by the Haven ratio $H_R = D^*/D_\sigma$ ($H_R \leq 1$).

In the case of sodium silicate glasses, the experimental H_R value lies between 0.45 and 0.55, and the displacement mechanism was explained as an indirect interstitial mechanism (17,20,21). The interstitial cation could be regarded either as an ion in a high energy site or else it could be inserted as an extra cation creating a region of higher than average cation density. The crowd ion defect could migrate by co-operative processes related to fluctuation in cation density in the glass.

Diffusion measurement using ^{22}Na and ^{24}Na isotopes (22) led to the conclusion that the same diffusion (indirect interstitial) mechanism was present in both sodium silicate glass and AgBr crystals.

V.1.3.2 Paired Interstitial model

Ingram and co-workers identified Na_2^{++} pairs as the mobile entities in the weak electrolyte theory (23-25). In a normal arrangement, only one cation is near each non-bridging oxygen (NBO). However, an interstitial pair exists when two cations are associated with one NBO and a cation vacancy is created elsewhere like $2M^+ + h^* \Leftrightarrow (M_2^*)^{++} + h$ (M^+: alkali ion at normal site, $(M_2^*)^{++}$: interstitial pair, h and h*: vacant and normal interstitial site respectively). The values of the equilibrium constants and of the corresponding defect concentrations and mobilities are normally obtained from aliovalent doping experiments. As an example, introduction of Cd^{2+} ions into AgBr crystals creates vacancies and suppresses the concentration of mobile interstitials (26).

Moynihan, Lesikar, and Ingram (23) applied the concept of doping to the mixed alkali effect. They explained the rapid fall in conductivity seen in the dilute foreign alkali region by the removal of mobile interstitials, M* or $(M_2)^*$, and their replacement either by foreign cations in interstitial sites, Li^+, or by relatively immobile mixed alkali pairs, (LM)*. The homovalent doping was applied first to K_2O-3SiO_2 glasses (27) and subsequently to other Na^+ ion conducting glasses (28) and β-alumina (29). The object is to study the effect of foreign cations on reaction equation (V.9). Taking the simplest case, where foreign cations, L, enter regular interstitial sites. The results of homovalent doping experiments have been found be consistent with theory.

In, for example Na_2O-2SiO_2 glass (30) the value of the defect creation energy obtained is Ec ≈ 11.7 kJ $mole^{-1}$. The migration energy was obtained by difference Em = E_A - Ec = 43 kJ $mole^{-1}$, thus Em ≈ 4Ec was obtained. This result is inconsistent with the expectation of the A-S model theory where ΔH/2 > Em and Eb ≈ 4 Es.

V.2 Ionic conductivity of LiI-Li_2S-As_2S_3 glass

V.2.1 Evolution of ionic conductivity in Li_2S-As_2S_3 binary glasses

The results of conductivity measurements for Li_2S-As_2S_3 binary glasses are listed in Table V.1.

Composition	E_A(eV)	Log σ_0($(\Omega cm)^{-1}$)	Log σ_{25}($(\Omega cm)^{-1}$)
x = 0.67	0.45	4.91	-5.20
0.70	0.46	5.34	-4.96
0.75	0.51	6.21	-4.86

Table V.1. Conductivity and activation energy as a function of composition for the xLi_2S-$(1-x)As_2S_3$ binary glass system.

The results of the ionic conductivity exhibit Arrhenius behaviour. Table V.1 shows an increase in the activation energy E_A and the pre-exponential factor σ_0 when the Li_2S modifier content increases. The room temperature conductivity σ_{25} also increases in the same manner. Generally highly modified glasses (including oxide glasses) show a decrease in activation energy when the modifier content increases. There are, however, some cases which reveal a simultaneous increase of both E_A and σ_0 (31-34). There are even cases reported in which the activation energy increases then decreases with modifier content (35,36). The ionic conduction in Li_2S-B_2S_3 (34) may be a typical example of the second case in sulphide glass. However, the structured changes occuring with the modifier concentration is quite different in Li_2S-As_2S_3 glass. To determine the conduction behaviour, it is necessary to consider the framework of the Anderson-Stuart model in (Eq. V.6) with the interpretation of Martin and Angell (31).

$$E_A = (\beta/\gamma)(ZZ_0e^2)/(r + r_0) + 4\pi G r_D(r - r_D)^2 \qquad \text{(Eq. V.6)}$$

With addition of alkali, some sulphur atoms are converted into NBS, which carry a localised electron density. This was confirmed by XPS experiments (cf. III.3 & IV.3). Following this, the first part of the equation, $ZZ_0e^2/(r + r_0)$, increases and leads to an increase in the activation energy. Normally the second term, Es, can be estimated from gas diffusion and modulus data, unfortunately neither are available for this binary glass. However, Brandt and Kim (37) found that the activation energy for the diffusion varies proportionally with Tg for binary lithium borate glasses. Since Es depends on the interstitial window radius, r_D, it may be expected that r_D follows Tg. DSC measurements (cf. IV.1), showed an increase in Tg for such binary glasses. Therefore, the interstitial window radius may be expected to increase as a function of the alkali content. However, it is difficult to estimate the variation of $r_D(r - r_D)^2$.

Also to be considered is the variation of shear modulus (G) dependent on parameters such as; P. ρ/M, where P is the number of total atoms present in one formula mole of the glass, M is the molecular mass, and ρ its density (38). G is shown to increase with the modifier content, as illustrated in Table V.2. This result is consistent with variations in Tg and follows the predictions of Brandt and Kim (37).

xLi_2S-$(1-x)As_2S_3$	ρ(mg/mm^3)	Li^+ concentration (10^{-2} mole cm^{-3})	P.ρ/M
0.67	2.52	3.02	8.24
0.70	2.45	3.24	8.32
0.75	2.33	3.64	8.50

Table V.2 The variation of the P.ρ/M versus x for the xLi_2S-$(1-x)As_2S_3$ glass system.

The second term, therefore, of the A-S model will increase with the modifier content in this binary glass. Totally, the activation energy Ea will increase, as we have confirmed.

The variation of the pre-exponential term σ_0 is not so easy to estimate. According to Elliott (3), under assumption of independent jumping of the ions, σ_0 is given by $(Ze)^2\lambda^2\nu_0N_0$

/6kT (Ze; charge of the mobile ion, λ; intersite spacing, and ν_0; jump frequency). Since an increase in the alkali content will lead to an increase in the number of cation sites, the jump distance between sites is expected to decrease. This may also affect the vibrational force constant describing the mobile cation-anion interactions. In this study we were unable to determine the cation vibrational frequency. However, works observing a progressive shift to higher frequencies of the cation-anion cage vibration mode (39-43) were located. Consequently, the pre-exponential factor which depends in part upon the vibrational frequency may increase. If we compare the order of magnitude of the variation of the total Li^+ ion concentration N_0, then it is comparable to that of σ_0. From these results, we may suggest that the increase in the pre-exponential factor and the ionic conduction in xLi_2S-$(1-x)As_2S_3$ glass system can be approximately explained using the A-S model.

V.2.2 Effects of dopant salt

Conductivity results are shown in Table V.3, and Fig. V.3 for $yLiI$-$(1-y)(0.70Li_2S$-$0.30As_2S_3)$ and $yLiI$-$(1-y)(0.75Li_2S$-$0.25As_2S_3)$ ternary glass systems. The maximum room temperature ionic conductivity (σ_{25}) obtained was $\sim 10^{-4}(\Omega cm)^{-1}$ for both systems. It is noted that σ_{25} increases with the LiI salt concentration. The variation in conductivity corresponds to the activation energy variation in the low alkali doped region, but in highly doped regions ($y \geq 0.3$), the conductivity seems to be strongly influenced by the pre-exponential factor σ_0. Such a minimum in the activation energy was also observed in LiI-Li_2S-B_2S_3 glasses (44).

Composition y	E_A(eV)	Log σ_0($(\Omega cm)^{-1}$)	Log σ_{25}($(\Omega cm)^{-1}$)
$0.70Li_2S$-$0.30As_2S_3$			
0.0	0.43	2.39	-4.96
0.1	0.37	1.82	-4.93
0.2	0.35	1.05	-4.92
0.3	0.33	0.84	-4.66
0.4	0.38	1.96	-4.51
0.5	0.42	2.63	-4.38
$0.75Li_2S$-$0.25As_2S_3$			
0.0	0.48	3.27	-4.86
0.1	0.45	3.02	-4.30
0.2	0.42	2.38	-4.69
0.3	0.34	1.17	-4.53
0.4	0.35	1.73	-4.19
0.5	0.38	2.59	-3.9

Table V.3 Conductivity results as a function of composition in yLiI-(1-y)($0.70Li_2S$-$0.30As_2S_3$) and yLiI-(1-y)($0.75Li_2S$-$0.25As_2S_3$) ternary glass systems.

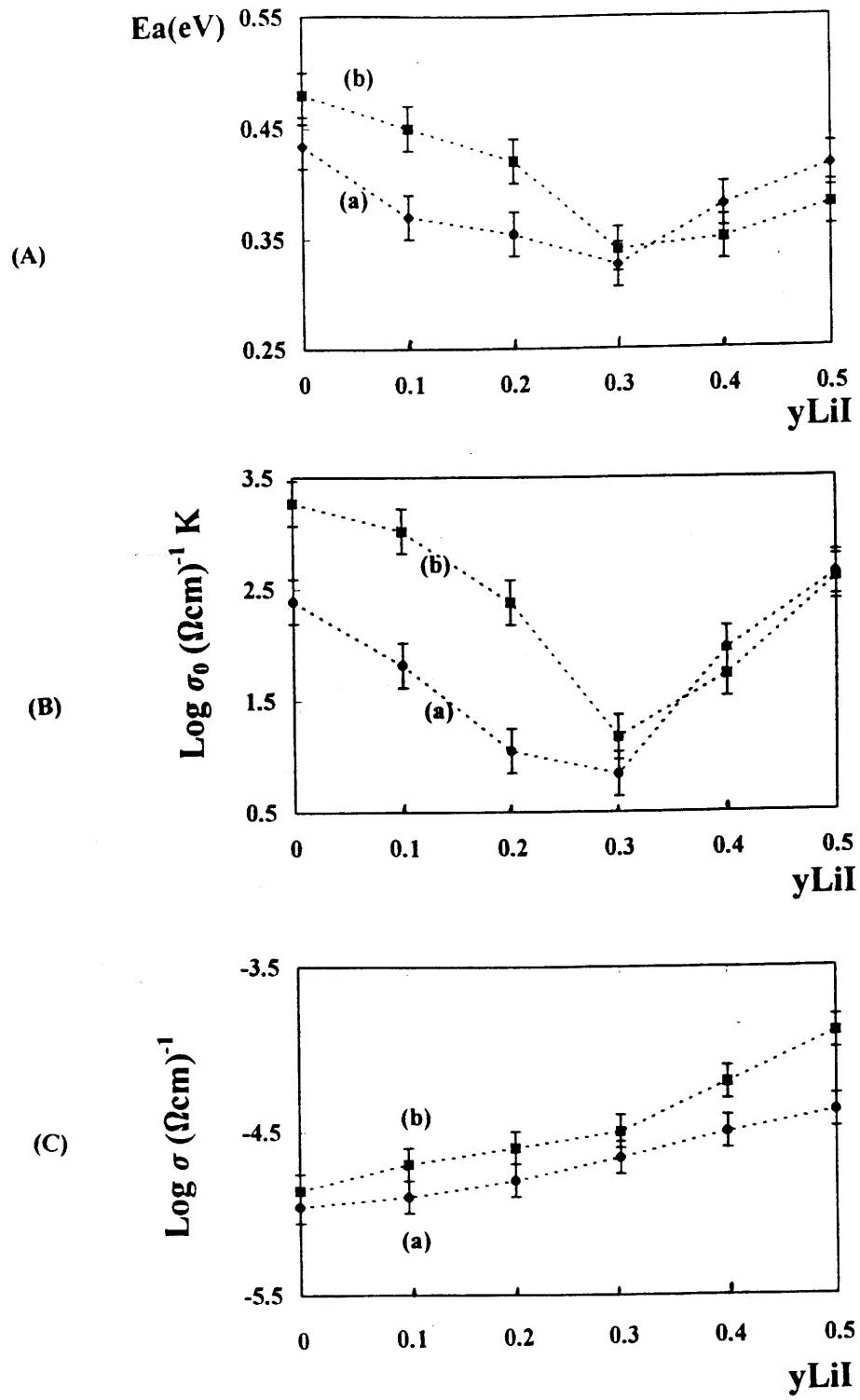

Fig. V.3 Ionic conductivity of yLiI-(1-x)[xLi_2S-(1-x)As_2S_3] glasses;

(A) activation energy variation, (B) pre-exponential factor variation, (C) ionic conductivity variation versus composition, (a) y = 0.70, (b) y = 0.75.

Let us now reconsider the interpretation of the results from the LiI-Li_2S-B_2S_3 system based on the strong electrolyte model (44). In Li_2S-As_2S_3 glasses, the counter-anion can only be a non-bridging sulphur (NBS). In the ternary system, the electrostatic binding energy term of (Eq. V.6) may be determined to be a competition between the newly added counter anion I^- and the original counter-anion NBS. When we compare the ionic radius of I^- (2.1 Å) and S^- (1.3 Å), it can be easily estimated that the dissociation energy of a Li^+-ion from I^--ion is lower than that for an Li^+ associated with a NBS. Thus, if the relative amount of I^- versus NBS increases, one would expect a decrease in Eb upon addition of LiI.

For the second term in (Eq.V.6), $4\pi G r_D(r - r_D)^2$, the estimation of $r_D(r - r_D)^2$ is difficult as we have already observed in the Li_2S-As_2S_3 system. However, the shear modulus (G) varies as P.ρ/M, such that G decreases as the LiI content increases as shown in Table V.4. The combination of both electrostatic and strain energy terms always results in a decrease in activation energy.

y	ρ (mg/mm^3)	Li^+ ion content. (10^{-2} mole cm^{-3})	P.ρ/M
0.0	2.45	3.24	8.32
0.1	2.57	3.21	8.13
0.2	2.66	3.15	7.82
0.3	2.69	3.01	7.34
0.4	2.88	3.05	7.28
0.5	3.02	3.02	7.04

Table V.4 The variation of density (ρ), Li^+-ion concentration, and shear modulus represented by (P.ρ/M) as a function of composition for the yLiI-(1-y)(0.70Li_2S-0.30As_2S_3) ternary glass system.

The limit of the vitreous domain as LiI is added to each binary glass is determined as the maximum content of doping salt in which no X-ray diffraction lines are observed. When more LiI is added, lines associated with LiI appear in the diffraction pattern. This means that the glass is saturated with LiI and that the excess salt has crystallised during quenching or precipitated from the melt when the temperature decreased. If the LiI excess is reduced, the aggregates formed in this way may be smaller and consequently be undetectable by X-ray diffraction. On the basis of what was observed in LiI-Li_2S-B_2S_3 glasses (45), we can assume the formation of small LiI aggregates which are not detectable by X-ray diffraction exist in the vitreous domain. This assumption would lead to the existence of two different regimes.

(1) At low concentration of LiI, LiI is dissolved into the glass, i.e. the I^--ions are dispersed among the pre-existing structural entities of the binary glass.

(2) At higher concentrations of LiI, small size aggregates of LiI which do not produce any X-ray diffraction peak are present in the glass.

In the first case, E_A decreases upon addition of LiI as a result of decreases in coulombic attraction. The decrease in the number of cation sites caused by dissolving LiI can lead to an increase in the jump distance between sites. Meanwhile, spectroscopic experiments (cf. IV.4 & IV.5) did not show any structural change in the host glass matrix. This suggests that the jumping frequency remains constant or changes very little. Altogether, one expects that the pre-exponential factor decreases as a decreasing function of the LiI content.

For the second case, the forming of the LiI aggregates may lead to reduced dissociation of LiI in the glass phase. The non-conducting property of LiI clusters (conductivity of cubic LiI $\sim 5.5\times10^{-5}\ \Omega^{-1}\ cm^{-1}$) leads to a general increase in activation energy. This is in opposition to the case in AgI doped glasses, where AgI plays the role of a good conductor.

At first sight, the simultaneous increase in the pre-exponential factor is also difficult to understand. We propose that it may originate from a conduction enhancement as an interface

effect between the glass and the LiI clusters, as proposed by C.C. Liang (46). He measured the conductivity of Al_2O_3-LiI composites, and showed that the defects at the interfaces provide free sites for hopping, which leads to an increase in the hopping frequency. We might, therefore, imagine this causes an increase in σ_0, but this requires further verification.

Conclusion

We have reviewed the classical models of ionic conduction in glasses before considering the Li^+-ionic conductivity in Li_2S-As_2S_3 and LiI-Li_2S-As_2S_3 glasses, which provides us with a basic understanding of the ionic motion in glasses.

We have considered the conduction mechanism of Li^+-ion conductivity in sulphide glasses. The behaviour in binary Li_2S-As_2S_3 glasses is interpreted by a modified A-S model,

References

(1) H. L. Tuller, D. P. Button and D. R. Uhlmann, J. Non-Cryst. Solids, **40** (1980) 93

(2) E. Robinel, B. Carette and M. Ribes, J. Non-Cryst. Solids, **57** (1983) 49

(3) S. R. Elliott,

Physics of Amorphous Materials, 2nd ed. (Longman Scientific & Technical, 1990)

(4) C. C. Hunter and M. D. Ingram, Solid State Ionics, **14** (1984) 31

(5) D. Ravaine, J. Non-Cryst. Solids, **73** (1985) 287

(6) S. W. Martin, J. Am. Ceram. Soc., **74** (1991) 1767

(7) O. L. Anderson and D. A. Stuart, J. Am. Ceram. Soc., **37** (1954) 573

(8) J. Frenkel, *Kinetic Theory of Liquids* (Oxford University Press, New York, 1947)

(9) D. K. McElfresh and D. G. Howitt, J. Am. Ceram. Soc., **69** (1986) C237

(10) S. W. Martin and C. A. Angell, J. Non-Cryst. Solids, **83** (1986) 185

(11) S. W. Martin, J. Am. Ceram. Soc., **71** (1988) 438

(12) D. Ravaine and J. L. Souquet, Phys. Chem. Glasses, **18** (1977) 27

(13) D. Ravaine and J. L. Souquet, Phys. Chem. Glasses, **19** (1978) 115

(14) A. Kone, J. L. Souquet, Solid State Ionics, **18/19** (1986) 454

(15) J. C. Reggiani, J. P. Malugani and J. Bernard, J. Chem. Phys., **75** (1978) 245

(16) A. Levasseur, J. C. Brethous, M. Kbala and P. Hagenmuller,

Solid State Ionics, **5** (1981) 651

(17) Y. Haven and B. Verkerk, Phys. Chem. Glasses, **6** (1965) 38

(18) K. Compaan and Y. Haven, Trans. Faraday Soc., **52** (1956) 786

(19) K. Compaan and Y. Haven, Trans. Faraday Soc., **54** (1958) 1498

(20) C. Lim and D. E. Day, J. Am. Ceram. Soc., **60** (1977) 198

(21) C. Lim and D. E. Day, J. Am. Ceram. Soc., **61** (1978) 99

(22) L. Barr, J. Mundy and A. Rowe,

Amorphous Materials, R. Douglas and B. Ellis Ed. (Wiley Science, London, 1972)

(23) M. D. Ingram, C. T. Moynihan, A. V. Lesikar, J. Non-Cryst. Solids, **38/39** (1980) 371

(24) M. D. Ingram, J. Am. Ceram. Soc., **63** (1980) 248

(25) M. D. Ingram and C. T. Moynihan, Phys. Chem. Glasses, **28** (1985) 132

(26) J. Teltow, Am. Phys. Lpz., **5** (1949) 71

(27) C. T. Moynihan and A. V. Lesikar, J. Am. Ceram. Soc., **64** (1981) 40

(28) J. A. Bruce, M. D. Ingram, M. A. Mackenzie and R. Syed,

Solid State Ionics, **18/19** (1986) 410

(29) M. D. Ingram, Solid St. Commun., **37** (1981) 791

(30) A. Kone, Ph. D. Thesis, Grenoble, (1986)

(31) S. W. Martin and C. A. Angell, Comm. Am. Ceram. Soc., **67** (1984) 429

(32) G. Chiodelli, G. Comparavignano, G. Flor, A. Magistris and M. Villa,

Solid State Ionics, **8** (1983) 311

(33) C. A. Angell, Solid State Ionics, **18/19** (1986) 472

(34) M. Ménétrier, A. Hojjaji, C. Estournès and A. Levasseur,

Solid State Ionics, **48** (1991) 325

(35) M.R. Mallace, Ph. D. Thesis, Univ. of Aberdeen (1994)

(36) C. L. Kraevski, T. F. Jeudokimova, V. F. Solinov, E. V. Schschmentseva,

Fiz. Khim. Stekla, 4 (1978) 326 (Russ.)

(37) W. W. Brandt and Y. K. Kim,

Proc. 6th Intn'l. Symp. Reactivity Sol. Schectady, N. Y. 1968 (Wiley, New York, 1969)

(38) O. L. Anderson, *Physical Acoustics*, ed. W. P. Mason,

Vol. 3B (Academic Press, New York, 1965)

(39) G. J. Exarhos and W. M. Risen, Chem. Phys. Lett., **10** (1971) 484

(40) G. J. Exarhos and W. M. Risen, Solid State Comm., **11** (1972) 755

(41) E. I. Kamitsos, G. D. Chryssikos and M. A. Karakassides,
Phys. Chem. Glasses, **29** (1988) 121

(42) M. D. Ingram, G. D. Chryssikos and E. I. Kamitsos,
J. Non-Cryst. Solids, **131/133** (1991) 1089

(43) E. I. Kamitsos, G. D. Chryssikos, A. P. Patsis and M. A. Karakassides,
J. Non-Cryst. Solids, **131/133** (1991) 1092

(44) M. Ménétrier, C. Estournès, A. Levasseur and K. J. Rao,
Solid State Ionics, **53/56** (1992) 1208

(45) P. Vinatier, M. Ménétrier and A. Levasseur, accepted in Solid State Ionics (1995)

(46) C. C. Liang, J. Electrochem. Soc., **126** (1973) 1963

Chapter VI. Study of Li_2S-B_2S_3-As_2S_3 ternary glass system

Introduction

Ternary glasses could be classified into three types depending on the agent added to the binary glasses which are themselves formed by a glass former and a glass modifier.

1) Doped glasses; To improve the ionic conductivity, a lithium salt (generally alkali halides) can be added to a binary glass. These are called doping salts because they are diluted in the vitreous matrix without detectable interaction with the binary glass. (cf. Ch IV, where glasses belonging to LiI-Li_2S-As_2S_3 system are studied).

2) Stabilised glasses; This group of glasses use stabilisers (like Al_2O_3 or Al_2S_3) which do not give glasses by themselves but, when associated with a glass former, can easily be incorporated into a glass. An example of a stabilising framework is presented in Fig. VI.1. The typical examples are Na_2O-Al_2O_3-SiO_2 (1), Na_2O-Al_2O_3-B_2O_3 (2), and Li_2S-Al_2S_3-SiS_2 (3) glasses. Generally the effect of stabilisation is to improve not only the ionic conductivity but also the chemical durability of the glass.

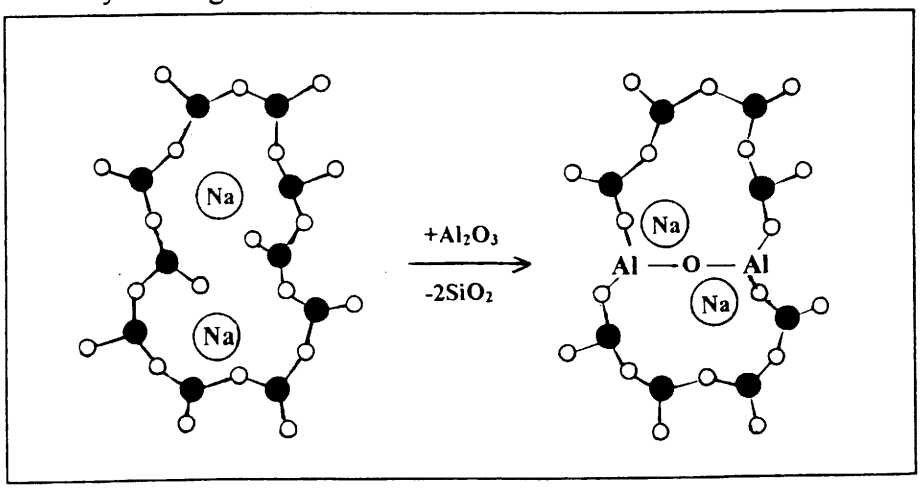

Fig. VI.1 Schematic representation of the substitution of Al_2O_3 into the sodium silicate glass (the 4th bonding is considered to be upper or down to the plane of the figure) (1).

3) Mixed former glasses; In these type of glasses, one former is partially substituted by another former. An increase in conductivity is often the aim of such a substitution. Such glasses can show two different ionic conduction behaviours, which depend upon the glass composition. One type exhibits two conductivity maxima which exist on the curve versus composition, as in Na_2O-B_2O_3-P_2O_5 (4), Ag_2O-B_2O_3-P_2O_5 (5), and Li_2O-B_2O_3-TeO_2 (6) glasses. The other type of behaviour shows only one conductivity maximum on the curve versus composition, as in Li_2O-B_2O_3-SiO_2 (7,8), Li_2S-GeS_2-SiS_2 (9) and Li_2O-B_2O_3-P_2O_5 (10). Sometimes, this mixed former effect involves a mixed anion effect such as is observed in $LiBS_2$-$LiBO_2$ glass (11), which can also be written as Li_2O-B_2O_3-Li_2S-B_2S_3.

This chapter is devoted to the study of the local structural modification due to the introduction of a second glass former into a vitreous matrix: we approach the problem from two directions. The first is to ascertain whether the second glass former is substituted into the host glass matrix and actually makes a mixed former glass. The second is how structural entities in general affect the variation in conductivity. As we have seen in Chapter I, xLi_2S-$(1-x)[(1-y)B_2S_3$-$yAs_2S_3]$ glasses showed little "solubility" of As_2S_3 in a Li_2S-B_2S_3 glass matrix and vice versa, which limits the domain in which glasses can be obtained. The studied glass domains were $x = 0.67$, $0 \leq y \leq 0.3$ and $x = 0.70$, $0 \leq y \leq 0.3$, respectively. The obtained glasses were characterised using methods such as ^{11}B NMR, IR and Raman spectroscopies.

Because of the difficulties found in the evaluation of the local environment of arsenic atoms, X-ray absorption spectroscopy (XAS) method was used.

VI.1 Physical properties of Li_2S-B_2S_3-As_2S_3 ternary glasses

VI.1.1 Evolution of glass transition temperature versus composition

Glass transition temperature (Tg) is known to be a sensitive measure of the "rigidity" of a glass matrix; the evolution of Tg in a mixed former glass is interesting in order to determine whether the structure is affected by the change in the ratio between formers. A good example is given by Tatsumisago et al. who found a parallel evolution of Tg and ionic conductivity with the ratio of two oxide formers (8).

In the first instance, two binary glasses Li_2S-B_2S_3 and Li_2S-As_2S_3 were studied. In the Li_2S-B_2S_3 binary glasses, we obtained results very similar to previously published work (12), i.e. increasing the modifier content decreases Tg (we do not see evidence of an exothermic peak between Tg and crystallisation temperature which was observed by Kennedy et al. (13)). On the contrary, in Li_2S-As_2S_3 binary glasses, the transition temperature slightly increases as the modifier content increases. The reason for this behaviour is not yet clear, but we can suppose that there is creation of strong ionic bonding between discrete AsS_3 units and lithium (Li^+)(cf. IV.1).

For the mixed former xLi_2S-$(1-x)[(1-y)B_2S_3$-$yAs_2S_3]$ glasses, as we have seen in Chapter I for $x = 0.67$ and $x = 0.70$, we could prepare glasses without crystallinity in the range $0 \leq y \leq 0.3$, but for $x = 0.75$ we obtained glasses only in the range $0 \leq y \leq 0.1$. The homogeneous glasses which have one Tg are formed in the region $0 \leq y \leq 0.2$, and $0 \leq y \leq 0.1$ for $x = 0.67$ and $x = 0.70$ respectively, outside this range the DSC traces show two Tg's, i.e., the glasses are not homogeneous. Fig.VI.2 shows the compositional dependence of Tg. Beyond the homogeneous zone there is a phase separation indicated by the presence of two Tg's. The XRD patterns show that the crystalline peak appearing outside the vitreous domain

is always due to $LiAsS_2$. These results show that the limit of "mutual solubility" between B_2S_3 and As_2S_3 causes phase separation.

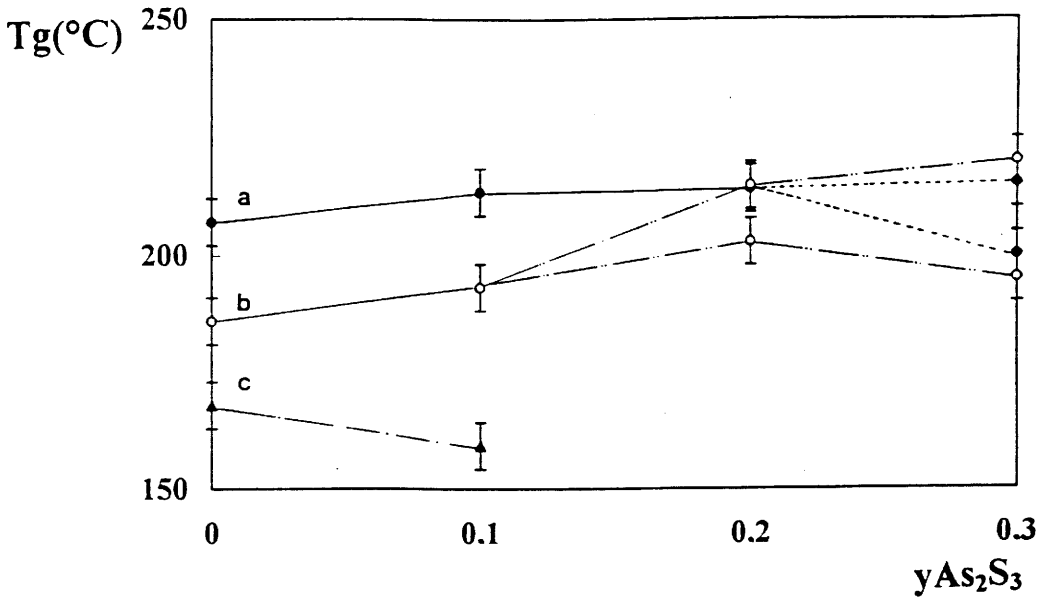

Fig. VI.2 Tg versus As_2S_3 content for xLi_2S-(1-x)[(1-y)B_2S_3-yAs_2S_3] glasses for (a) x = 0.67, (b) 0.70 and (c) 0.75. (—— ; homogeneous, —·—·—, —— —, ----- ; inhomogeneous)

VI.1.2 Evolution of density versus composition

Table VI.1 shows the evolution of density with glass composition. The density of the glasses increases with the addition of As_2S_3 into a Li_2S-B_2S_3 matrix.

Composition	Density(mg/mm^3)	Homogeneous	Heterogeneous
0.67/0.33			
y=0.0	1.82	X	
y=0.1	1.94	X	
y=0.2	2.06	X	
y=0.3	2.07		X
y=1.0	2.52	X	
0.70/0.30			
y=0.0	1.79	X	
y=0.1	1.91	X	
y=0.2	1.96		X
y=0.3	2.01		X
y=1.0	2.45	X	

Table VI.1 Measured densities for $0.67Li_2S$-0.33[(1-x)B_2S_3-xAs_2S_3] glasses and $0.70Li_2S$-0.30[(1-x)B_2S_3-xAs_2S_3] glasses.

VI.2 Structural study of Li_2S-B_2S_3-As_2S_3 ternary glass system

VI.2.1 Local structural study of Li_2S-B_2S_3-As_2S_3 ternary glass system

xLi_2S-$(1-x)B_2S_3$ binary glasses have been studied during the last ten years in this laboratory (12,14-16). The local order modification versus composition is well understood from several experimental results. In the present work the competition between B_2S_3 and As_2S_3 for Li_2S modifier was studied using NMR, Raman and IR spectroscopies on xLi_2S-$(1-x)[(1-y)B_2S_3$-$yAs_2S_3]$ ternary glasses in the range $x = 0.67$, $0 \leq y \leq 0.3$ and $x = 0.70$, $0 \leq y \leq 0.3$, respectively.

VI.2.1.1 ^{11}B NMR on Li_2S-B_2S_3-As_2S_3 ternary glasses

The ^{11}B NMR study of Li_2S-B_2S_3 glass (13,15,17-19) has revealed valuable information concerning the coordination of B atoms in alkali borate glasses. The addition of Li_2S to B_2S_3 changes 3-coordinated boron, B(3), to 4-coordinated boron, B(4) in the range $x < 0.5$, and changes from B(4) to B(3) in the range $x > 0.5$. The former case was confirmed through the study of crystalline materials, and the latter evolution has been supported by Raman spectroscopy (16). Structural hypotheses on this binary glass system have been developed. These structural entities may exist in xLi_2S-$(1-x)B_2S_3$ binary glasses proposed by A. Hojjaji (20), and are shown in Fig. VI.3. This proposed model was confirmed in the composition range $0.55 \leq x \leq 0.75$, which shows a fragmentation of the structural entities present in B_2S_3 into smaller ones upon increasing the Li_2S amount. Thus, as x increases, terminating B-S^- groups are formed by the insertion of S^- ions into B-S-B links and also by the simultaneous conversion of $(BS_{4/2})^-$ tetrahedra into $BS_{2/2}S^-$ triangles. Increasing x yet further leads to an increasing number of non-bridging sulphurs, and finally only BS_3^{3-} triangles are present for $x = 0.75$.

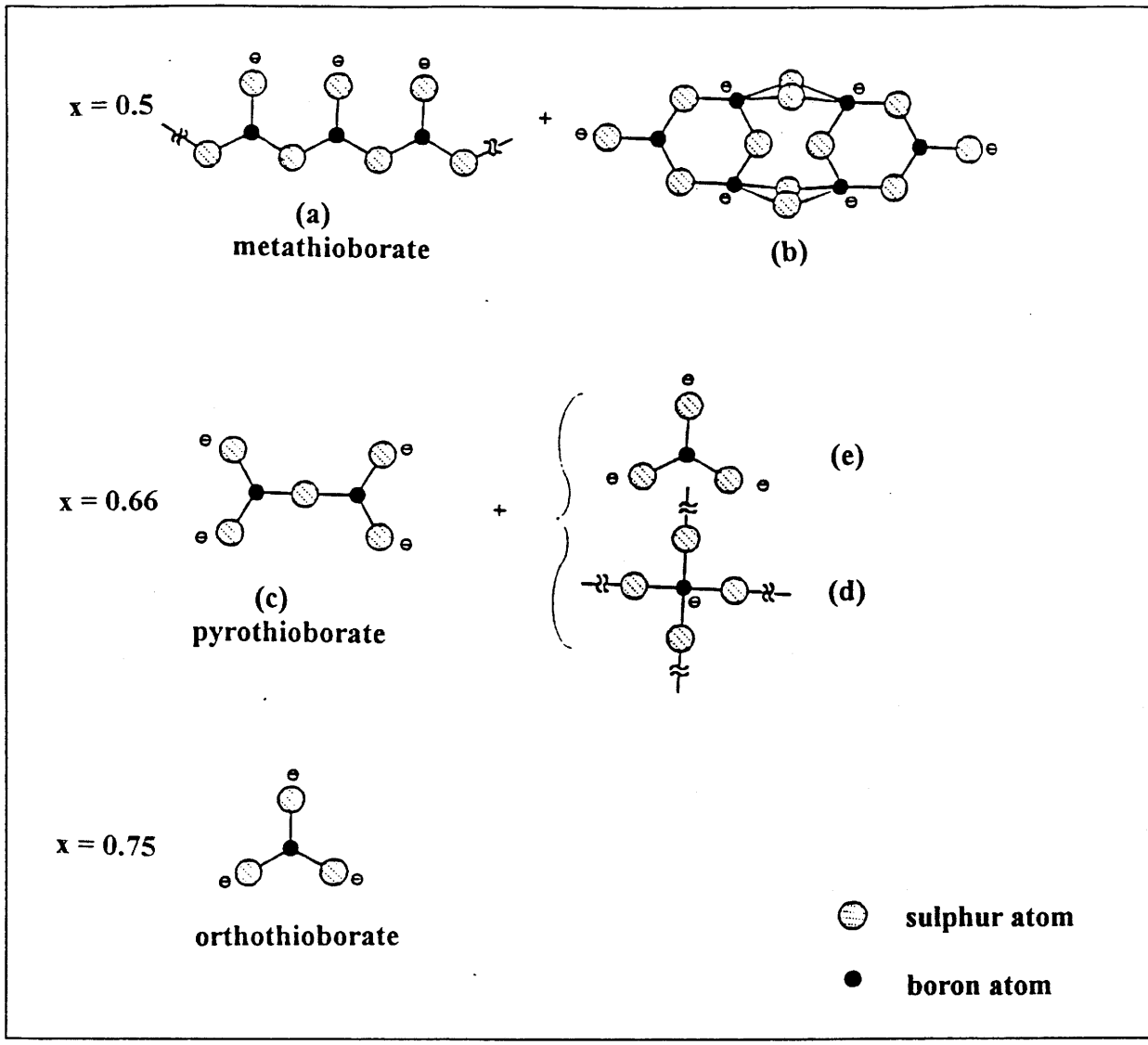

Fig. VI.3 Structural hypothesis proposed for xLi_2S-$(1-x)B_2S_3$ glasses (20).

The characteristic ^{11}B NMR spectra for this glass system exhibit a superposition of tetrahedral, B(4) and triangular, B(3) boron signals as illustrated in Fig. VI.4. Indeed, I = 3/2 nucleus like boron is sensitive to on EFG (electric field gradient) at the nuclear site. Closed shells of electron, however, do not generate an EFG, and the major contribution to the EFG arises from bonding electrons. The quadruple interaction perturbs the Zeeman interaction and the shift of each Zeeman level depends not only on the quadruple moment eQ of the nucleus and the component eq_{zz} of the EFG but also on the orientation of the magnetic field H with

respect to the principal axis of the EFG. If the quadrupole interaction is sufficiently small to be treated as a first order perturbation, the m = 1/2 ⇔ m = -1/2 (m; magnetic quantum number) or central transition is not affected in the first order, but the transition between m = ±3/2 and m = ±1/2 or satellite transitions are spread out. When the quadrupole interaction is large, then the interaction must be treated with second order perturbation theory, and the central transition(1/2 ⇔ -1/2) is affected. In this case, the resonance line shape becomes as in Fig. VI.5 (21). In ^{11}B NMR on xLi_2S-$(1-x)B_2S_3$ glasses, the B(4) signal is characterised by three transitions (3/2 ⇒ 1/2, 1/2 ⇒ -1/2 and -1/2 ⇒ -3/2), which leads to a single symmetric line since the spherical symmetry suppresses any quadrupolar effect. On the other hand, B(3) atoms experience an electric field with cylindrical symmetry, so that the central line is split by second order quadrupolar effects, while the two quadrupole satellites are not visible in the spectrum.

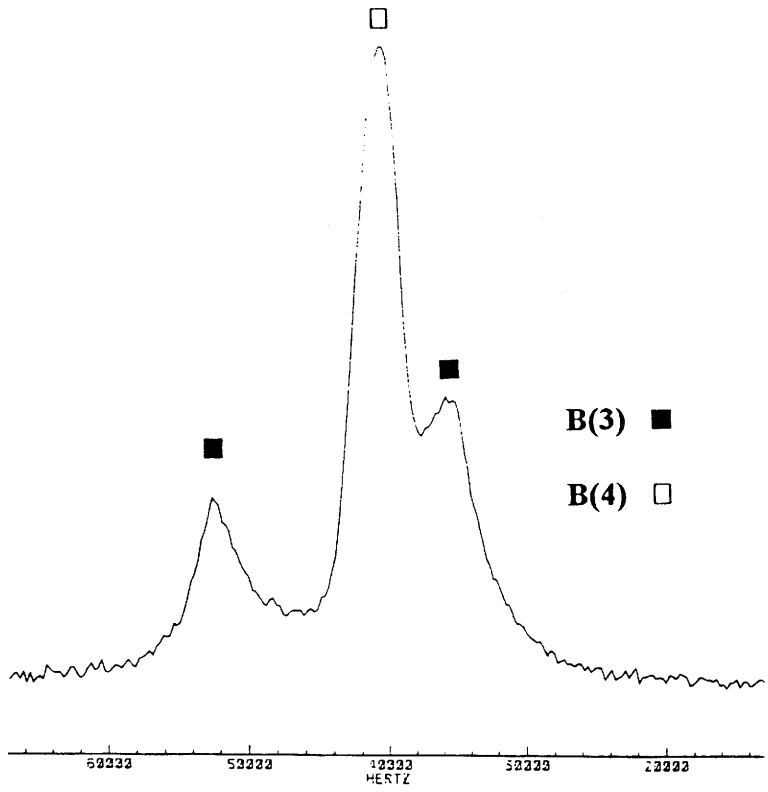

Fig. VI.4 Example of superposition of tetrahedral B(4) and triangular B(3) spectrum obtained by ^{11}B NMR for $0.67Li_2S$-$0.33B_2S_3$ binary glass.

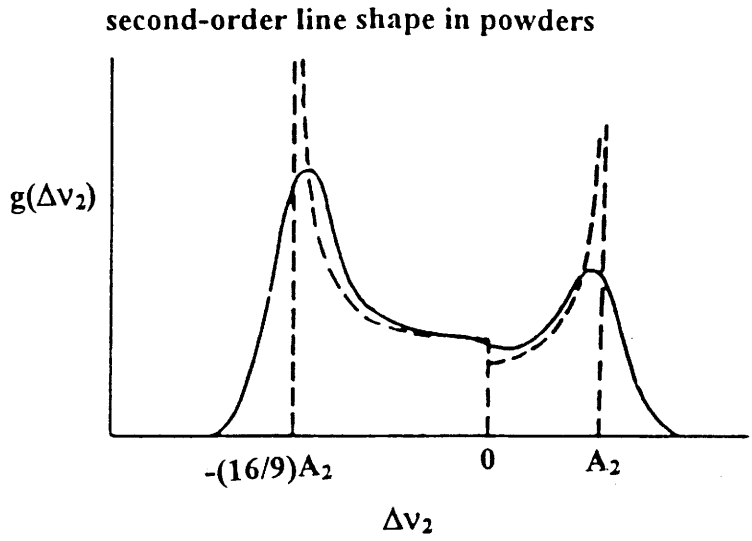

Fig. VI.5 Resonance line shape (solid curve) for a nucleus with a large quadrupole interaction in a glass or polycrystalline powder. $A_2=(9/64)\{(2I+3)/4I^2(2I-1)\}(e^2qQ)^2/\nu_0$,where the quadrupole coupling constant $Q_{cc}=e^2qQ$ and ν_0 is the resonance frequency in the absence of quadrupolar effects (21).

Fig. VI.6 shows the evolution of ^{11}B NMR spectra for Li_2S-B_2S_3-As_2S_3 ternary glasses. Each NMR spectrum exhibits a superposition of tetrahedral, B(4) and triangular, B(3) boron signals, as in Li_2S-B_2S_3 binary glasses. A quantitative study of the two kinds of boron atoms would require standardisation using samples with known amounts of the same type of B(3) and B(4). However, the qualitative trend can be seen clearly on the spectra for x = 0.70 series (Fig. VI.6-b). Thus, the samples with a higher y value contain a smaller proportion of B(3) than the y = 0 one. From this, we can assume that the B-S matrix is affected by the introduction of As_2S_3, where B(3) are converted into B(4). However, for the x = 0.67 series no significant change in the B(3)/B(4) ratio is in evidence in the homogeneous range ($y \leq 0.1$).

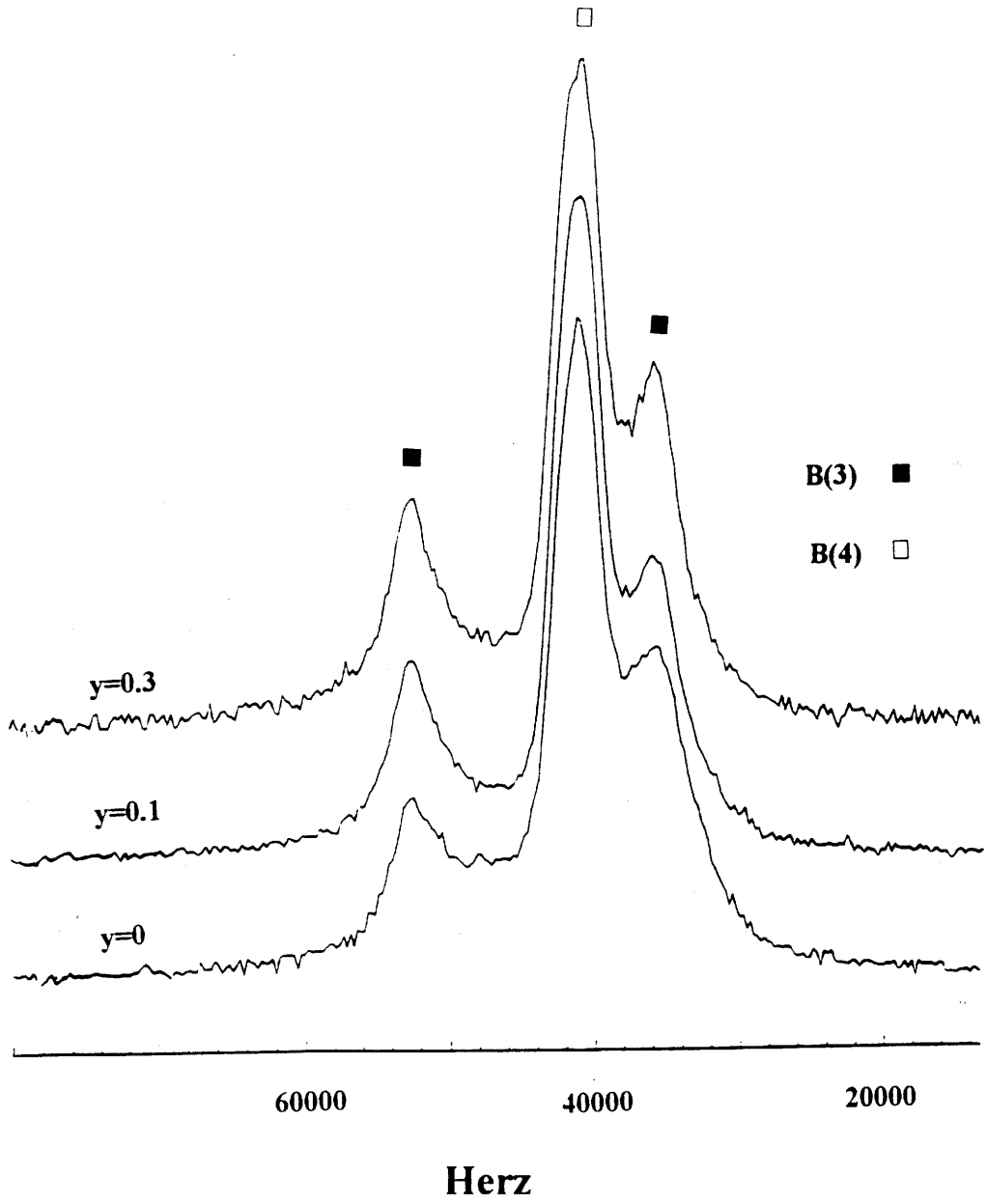

Fig. VI.6-a) ^{11}B NMR spectra of $0.67Li_2S$-$0.33[(1-y)B_2S_3$-$yAs_2S_3]$ glasses for y = 0, 0.1 and 0.3.

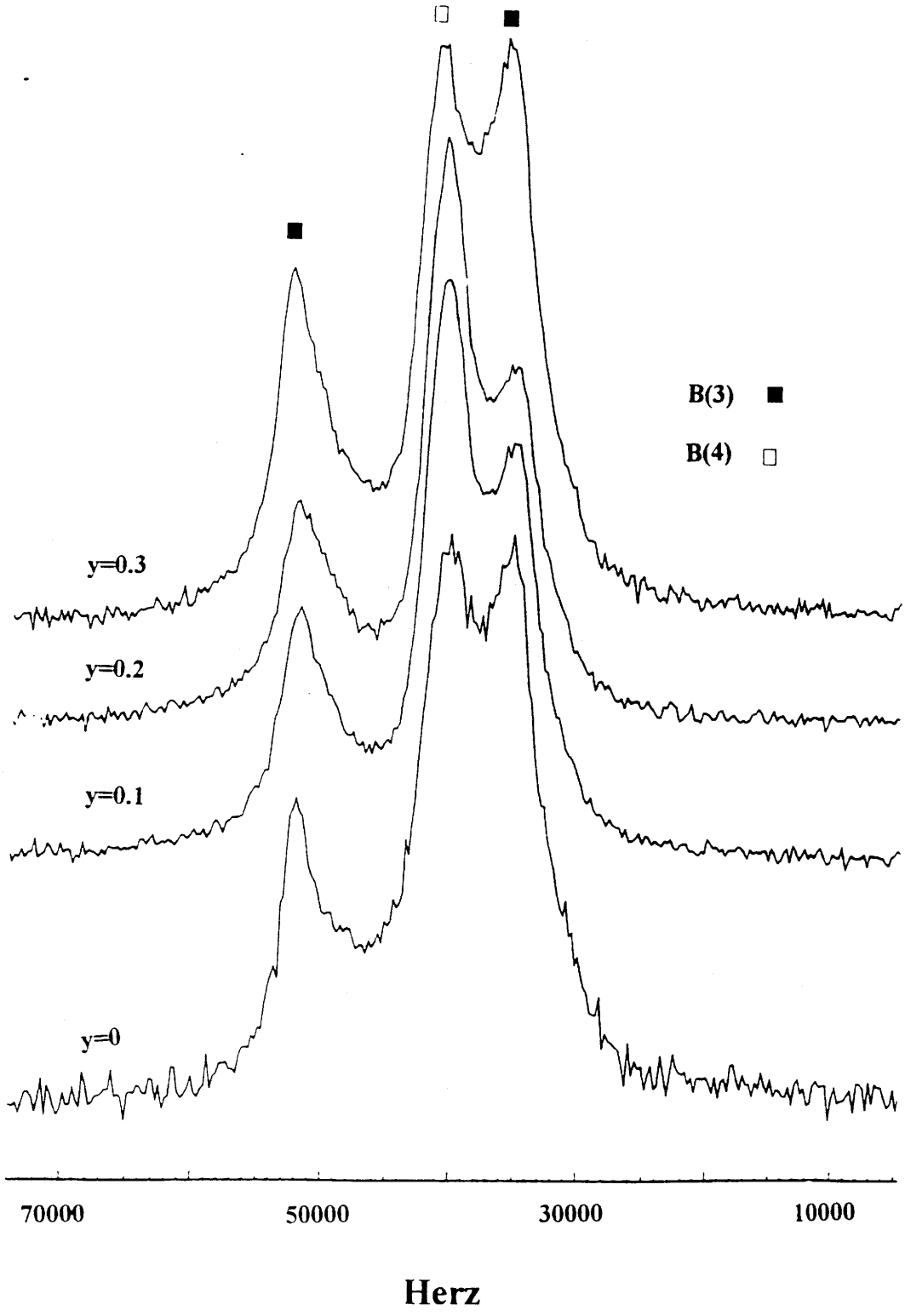

Fig. VI.6-b) ^{11}B NMR spectra of $0.70Li_2S$-$0.30[(1-y)B_2S_3$-$yAs_2S_3]$ glasses for y = 0, 0.2 and 0.3.

For higher As_2S_3 amounts, the glasses become inhomogeneous giving a mixture of two different glasses, which cannot be more precisely defined. This kind of behaviour of boron atom modification was observed in Li_2S-B_2S_3-P_2S_5 ternary glass (13), and there was also the B(3) transformation to B(4) in boron rich and in phosphorus rich glass compositions for which only 4-coordinated borons were observed. The ^{31}P MAS-NMR changes very little over a wide range of phosphorus content, indicating the presence of 4-coordinated P only. They further reported that the introduction of 4-coordinated P into the boron network shifts the B(4)/B(3) ratio to higher values. Here the effect of As_2S_3 introduction can be envisaged in three directions. (1) The restricted substitution of As atoms into B atomic sites; further introduction of As_2S_3 would cause phase separation into Li_2S-B_2S_3-As_2S_3 and Li_2S-As_2S_3 (or complementary Li_2S-B_2S_3) phases. (2) A phase separation happens immediately into vitreous Li_2S-B_2S_3 and Li_2S-As_2S_3 upon introduction of As_2S_3. In this case, the observation of one Tg may be due to the limited sensitivity of DSC instrumentation, the contribution of Li_2S-As_2S_3 glass being probably less than 10%. Thus, these assumptions include the competition between B_2S_3 and As_2S_3 for Li_2S modifier. (3) The formation of a mixed former glass with a different structure (As is not substituted into B sites). Here, the coordination of each cation is probably conserved in their own environment.

VI.2.1.2 IR spectroscopy

IR study for these ternary glasses was done by considering the structural modification of B_2S_3 by Li_2S, and the structural modification of As_2S_3 by Li_2S.

Fig. VI.7 shows the disperse IR spectra for different x values of xLi_2S-(1-x)B_2S_3 glasses. In this figure, spectra can be divided into three groups of peaks as suggested by J. Cho and S. W. Martin (22,23). The first group (950 ~ 900 cm^{-1}) can be assigned to three coordinated borons with all sulphur atoms considered to be BS, the second group (840 ~

810 cm^{-1}) to three coordinated boron where all sulphur atoms are considered as NBS (orthothioborate entities).

The third group at (740 ~ 690 cm^{-1}) can be assigned to metathioborate and entities including 4 coordinated boron (Fig. VI.7-a & b). This figure also shows that an increase in Li_2S content leads to a growth of the corresponding orthothioborate peaks. In other words, the number of three coordinated borons corresponding to BS_3^{3-} entities increase upon increasing Li_2S content. It should be noticed that there are no peaks corresponding to As_2S_3 or Li_2S-As_2S_3 glasses in the 600 - 1200 cm^{-1} range (cf. IV.5). The peak at 350 cm^{-1} may be related on Li^+-S cationic vibration, however there is not evidence references to explain this peak. The peak at 460 cm^{-1} is also found in Far-IR spectrm in 470 cm^{-1}, and will be discussed later.

Fig. VI.8 shows the IR spectra of Li_2S-B_2S_3-As_2S_3 ternary glasses. Both Fig. VI.8-A) and B) reveal that there is no significant change of the B-S matrix in the homogeneous glass forming region (a, b and c). Of note in Fig. VI.8-B) is the inhomogeneous glass (d) which shows some spectral change, when compared to glasses b and c. From the ^{11}B NMR results, for x = 0.70 glass, revealed a decrease in the ratio B(3)/B(4) when y increases from 0 to 0.1. Further introduction of As_2S_3 leads to an increase in the ratio. However in IR spectra, there is no modification of the spectrum irrespective of the value of y in the homogeneous domain (a, b and c). The broad peak appearing at 370 cm^{-1} is difficult to explain clearly. Fig.VI.9 shows the Far-IR spectra for the glasses in which x = 0.67 for differing amounts of As_2S_3. The spectral evolution versus As_2S_3 content appears as following; 1) 470 cm^{-1} peak decreases, 2) 420 cm^{-1} peak appears, 3) 340 cm^{-1} peak shifts to 360 cm^{-1}.

It is difficult at this stage to assign precisely all the peaks. It is possible that the peak at 470 cm^{-1} originates from the B-S bond as observed in $LiBS_2$-$LiBO_2$ glass (11), Li_3BS_3 glass and single crystal (24). The IR spectrum of Li_3AsS_3 crystal (cf. III.3) shows the main

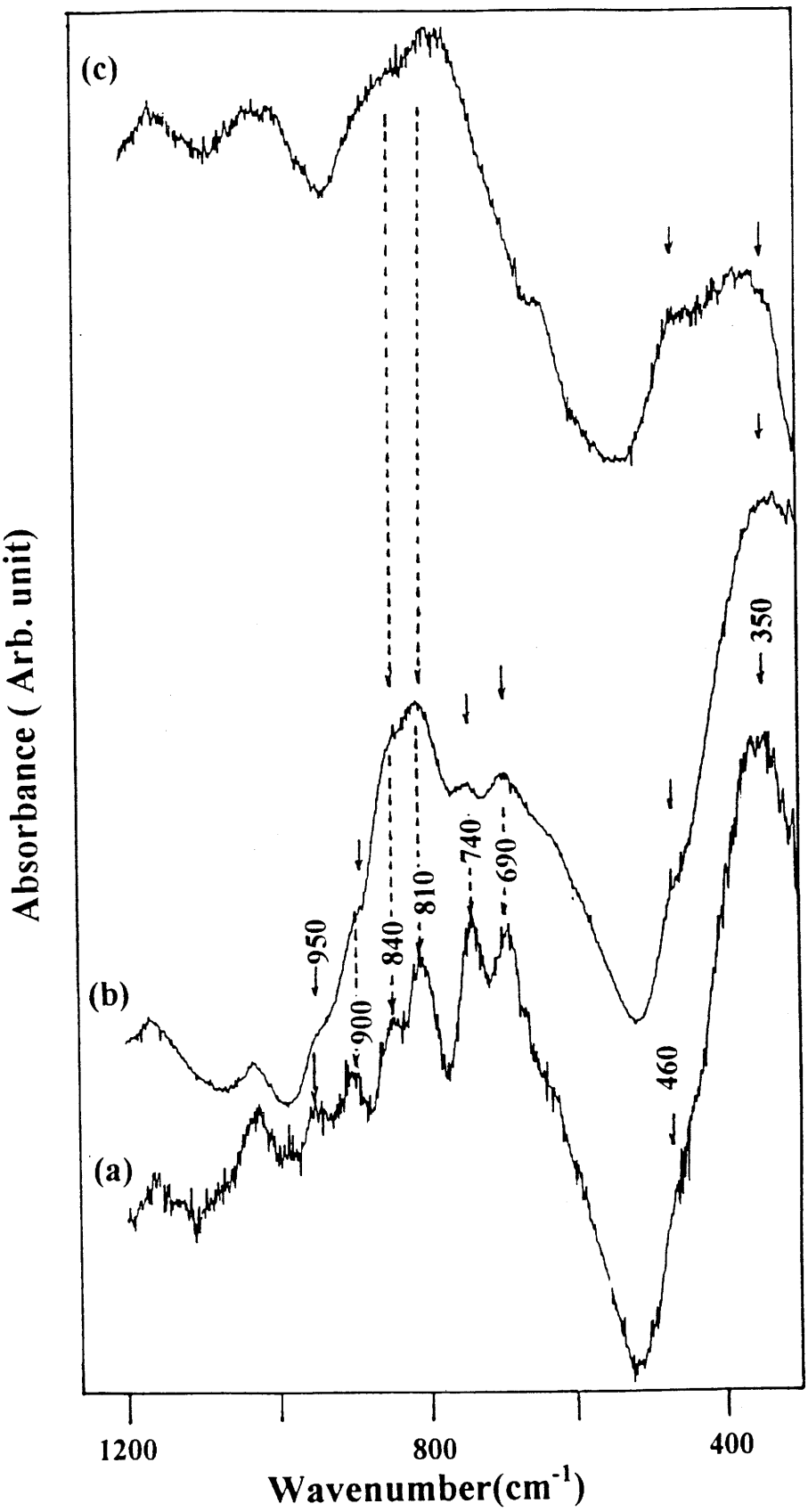

Fig. VI.7 IR spectra of xLi_2S-$(1-x)B_2S_3$ glasses for (a) x = 0.67, (b) x = 0.70 and (c) x = 0.75.

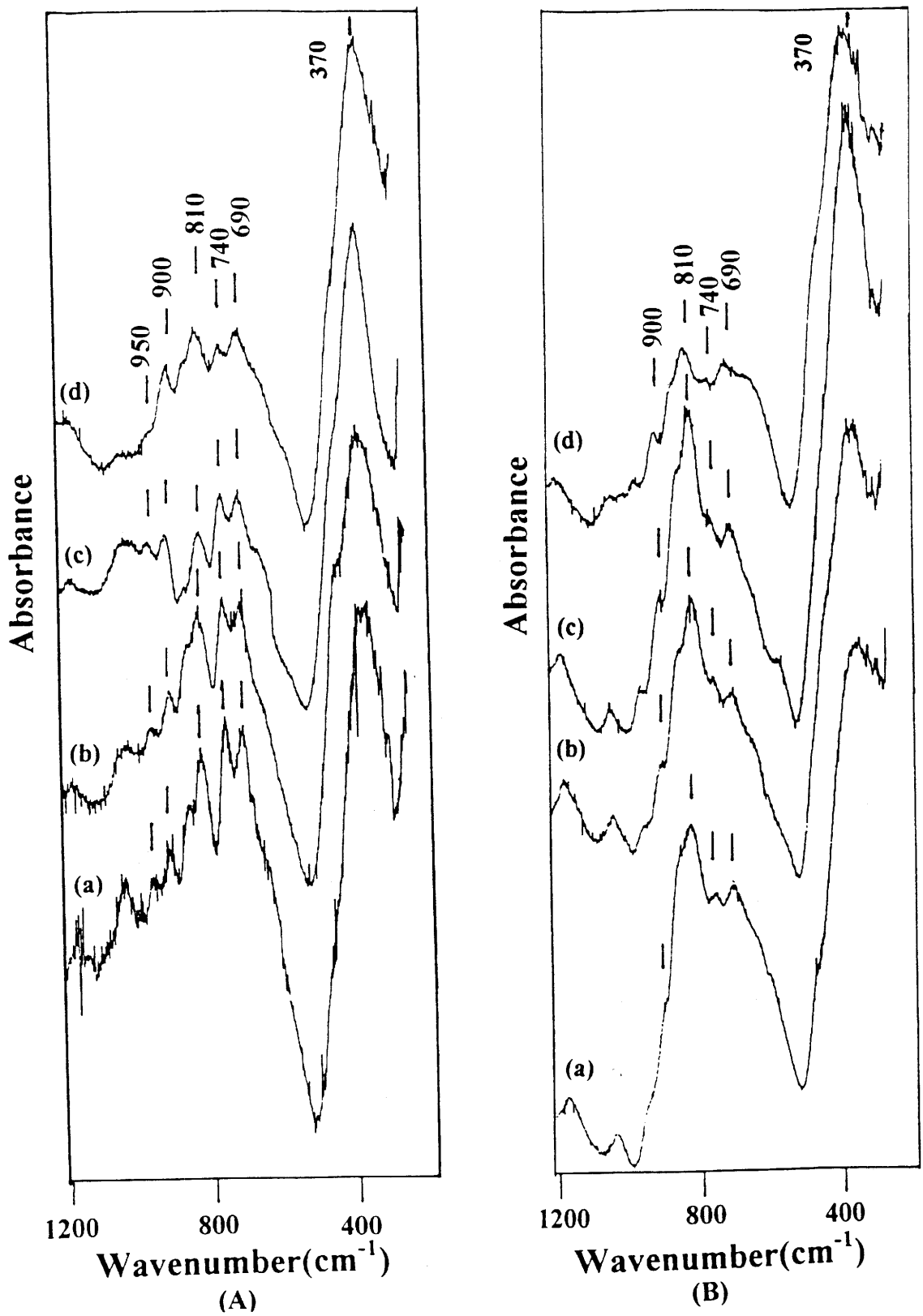

Fig. VI.8 IR spectra of xLi_2S-(1-x)[(1-y)B_2S_3-yAs_2S_3] glasses. (A); (a) y = 0, (b) 0.1, (c) 0.2 and (d) 0.3 with x = 0.67. (B); (a) y = 0, (b) 0.1, (c) 0.2 and (d) 0.3 with x = 0.70.

peak at 355 cm^{-1} and a shoulder at 420 cm^{-1}. The IR spectra of Li_2S-As_2S_3 glasses (cf. IV.3) similarly shows a main peak at 370 cm^{-1} and broad enhancement between 400 ~ 500 cm^{-1}.

Following these results, both the 420 cm^{-1} and 360 cm^{-1} peaks may be assigned to the stretching vibration of As-S^- in AsS_3^{3-} pyramids present in this glass. It was observed that there was no dramatic change in the spectra between the homogeneous and heterogeneous domain. In both NMR and IR, all these evolutions and observations can be interpreted using two explanations. A small amount of As atoms are substituted into B atom sites, the matrix consists of Li_2S-B_2S_3-As_2S_3 glass which results in a true mixed former glass in the homogeneous domain or a mixed glass with a different structure. However, the former case is difficult to happen, because the existing lone pairs in arsenic makes it difficult to bond the four coordinated arsenic with sulphur. The second possibility is that phase separation occurs immediately upon introduction of As_2S_3 into Li_2S-B_2S_3 glass. In this case, two phases are present, Li_2S-B_2S_3 and Li_2S-As_2S_3 glasses, throughout the glass forming range.

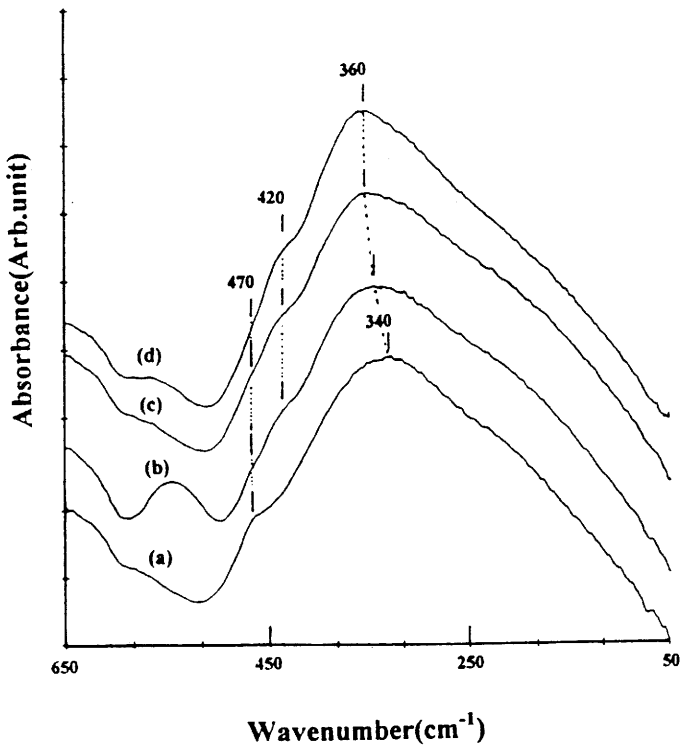

Fig. VI.9 Far-IR spectra of 0.67-0.33[(1-y)B_2S_3-yAs_2S_3] glasses, (a) y = 0, (b) 0.1, (c) 0.2 and (d) 0.3.

VI.2.1.3 Raman spectroscopy

The Raman spectrum of Li_2S-B_2S_3 binary glass is characterised by two dominant peaks at 448 cm^{-1} and 495 cm^{-1}. As previously shown, these glasses have two kinds of structural entities, three coordinated boron atoms carrying one, two or three bridging sulphurs and four coordinated boron atoms. Hojjaji et al.(20) assigned the peak at 448 cm^{-1} to the totally symmetric A_1' stretching mode of 3-coordinated boron atoms (D_{3h} symmetry), and the peak at 495 cm^{-1} to the stretching of B-S bonds around 4-coordinated boron atoms (Td symmetry). The vibration peak resulting from the B-S bonds is discernible because it appears in the same frequency region as $BS_{3/2}$ and BS_3^{3-}. Following this description, it is difficult to specify the contribution to the spectrum of three coordinated borons with bridging sulphur and that of non-bridging sulphurs. Fig. VI.10 shows Raman spectra obtained from Li_2S-B_2S_3-As_2S_3 ternary glasses. In these ternary mixed former glasses, 495 cm^{-1} and 448 cm^{-1} peaks are present, but less and less so when the As_2S_3 content increases. In addition a new peak at 380 cm^{-1} becomes more and more evident.

In the binary Li_2S-As_2S_3 glass system, Raman spectra exhibit a main peak at 380 cm^{-1} which corresponds to symmetric stretching vibration mode of As-S^- in AsS_3^{3-} pyramidal units (25) and a shoulder at 350 cm^{-1} which corresponds to antisymmetric stretching vibration mode of As-S^- in the same pyramidal units. These peaks are also present in c-Li_3AsS_3 (cf. III.3). The large band appearing between 200 cm^{-1} and 300 cm^{-1} may therefore correspond to an As-S^- bending mode in AsS_3^{3-} pyramidal units (24).

As we have seen in IR spectra, the Raman spectra are the superposition of Li_2S-B_2S_3 and Li_2S-As_2S_3 binary features. This fact again represents implicitly the possibility that the ternary glasses are composed of two separated phases.

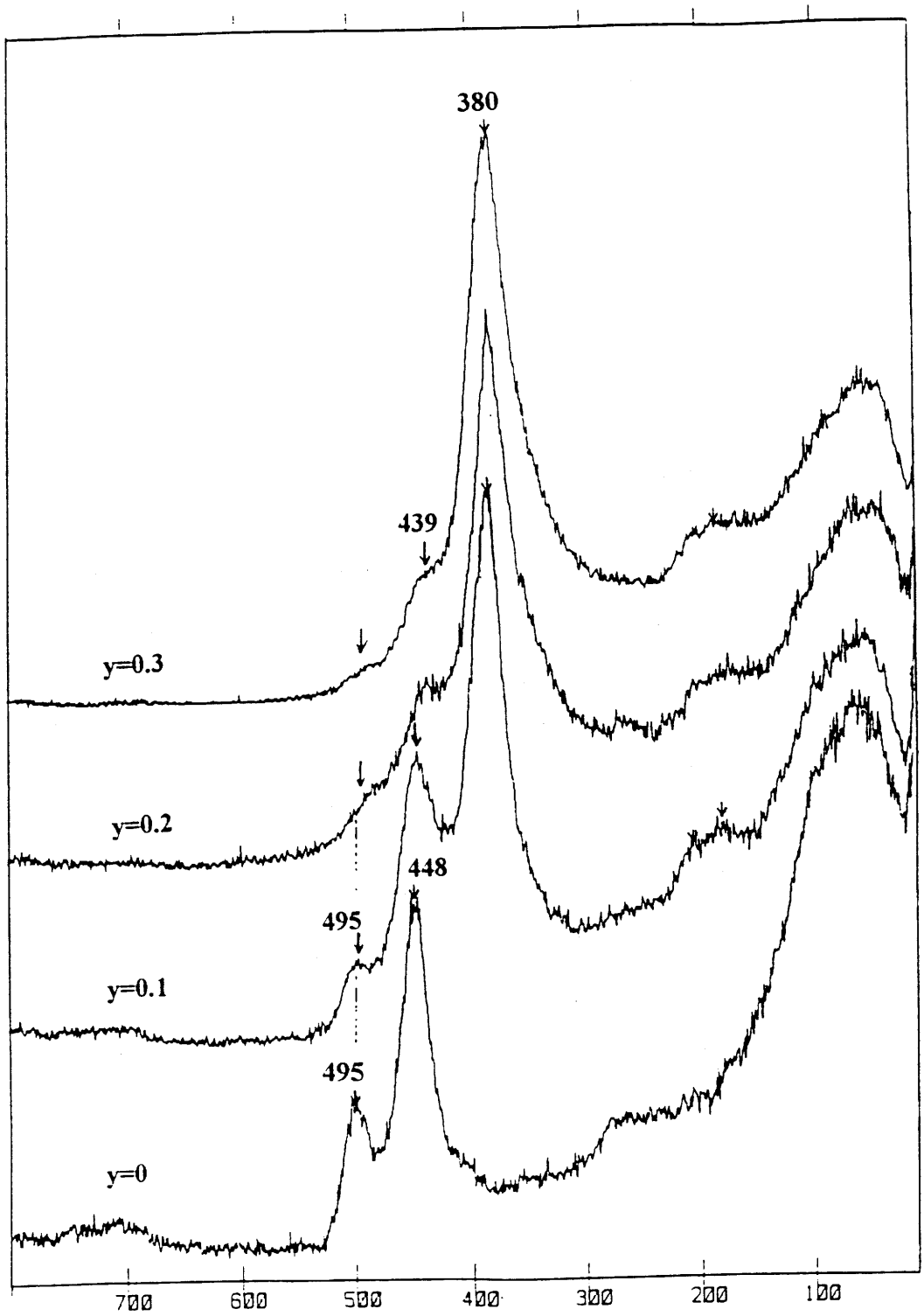

Fig. VI.10-a) Raman spectra of $0.67Li_2S$-$0.33[(1-y)B_2S_3$-$yAs_2S_3]$ glasses.

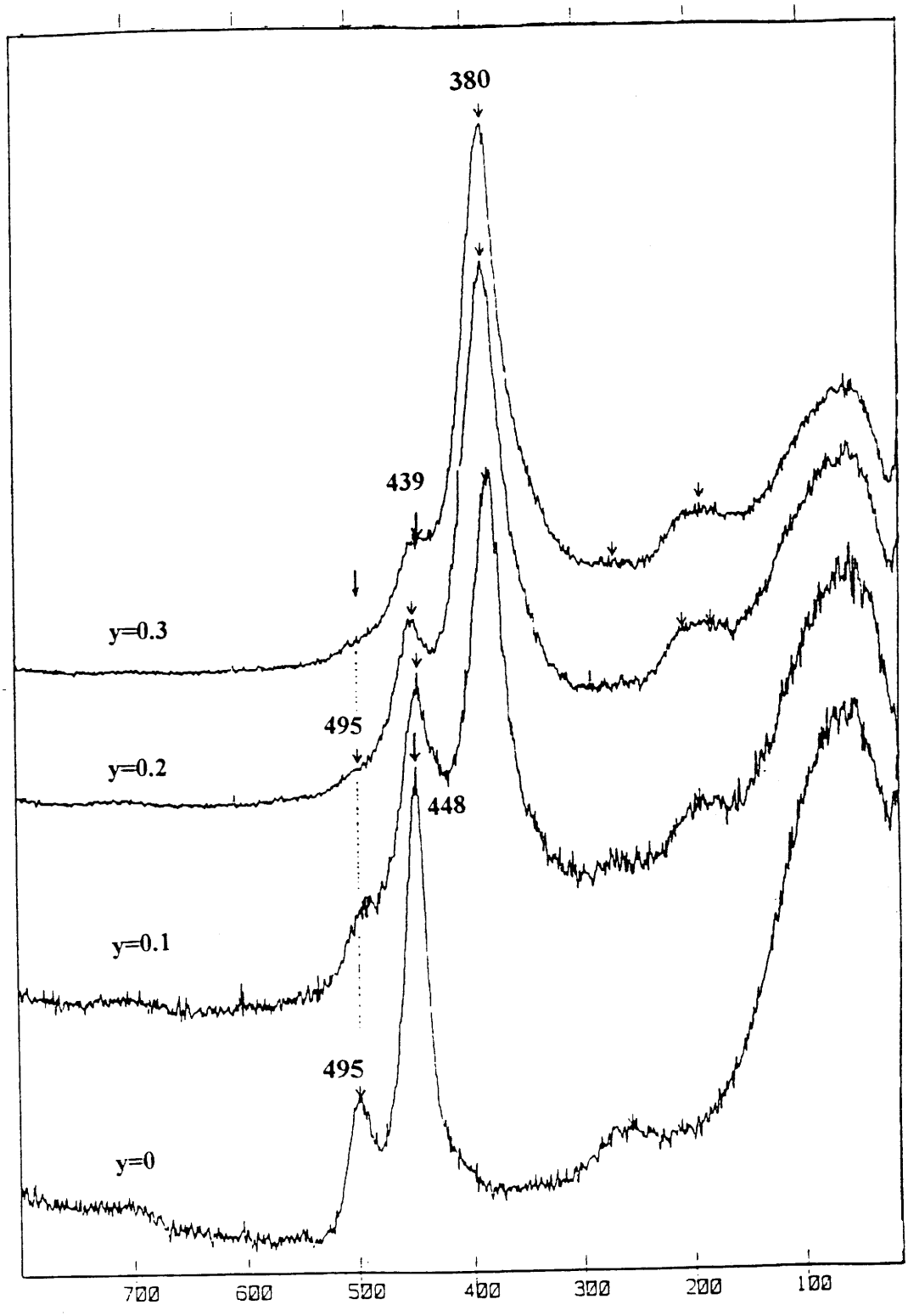

Fig. VI.10-b) Raman spectra of $0.70Li_2S$-$0.30[(1-y)B_2S_3$-$yAs_2S_3]$ glasses.

VI.2.2 XAS study on As atoms in the Li_2S-B_2S_3-As_2S_3 ternary glass system

In this work X-ray absorption spectroscopy (XAS) at the As K-edge was used to investigate the variation of structural parameters in xLi_2S-(1-x)[(1-y)B_2S_3-yAs_2S_3] (x = 0.67, 0.70; y = 0.1, 0.2, 0.3)

VI.2.2.1 As K-edge EXAFS study of xLi_2S-(1-x)[(1-y)B_2S_3-yAs_2S_3] (x = 0.67, 0.70; y = 0.1, 0.2, 0.3)

In glassy As_2S_3, each As atom is bonded to three S atoms in a trigonal pyramidal arrangement with the As atom at the apex and the three S atoms forming the base. When Li_2S modifier is added, the linked AsS_3 pyramids in the unmodified state change to discrete AsS_3^{3-} units in the modified state (25), resulting in the creation of non-bridging sulphurs.

The As K-edge EXAFS μ(k) weighted by k^3 are shown in Fig. VI. 11. The magnitude of the Fourier transform (FT) of the EXAFS data shown in Fig. VI.12 were obtained by transforming over a k space range of 2.5 to 13 $Å^{-1}$. As is typical for amorphous compounds with very short range ordering, the FTs for all compositions consist of only a main peak related to the first As-S coordination sphere and of negligible contributions from more distant shells such as the As-As interaction. In order to determine the local structural parameters between arsenic and sulphur atoms, the main peak in the FT was inverse Fourier transformed into k space and then the curve-fitting was done using theoretical amplitude and phase functions determined from FEFF 5 code. At first, in order to differentiate non-bridging sulphur (NBS) and bridging sulphur (BS), curve-fitting was done under the assumption that there are two bond distances between arsenic and sulphur atoms, (except for glassy As_2S_3). However, the fitted structural parameters did not have any physical meanings and we performed one-shell fitting.

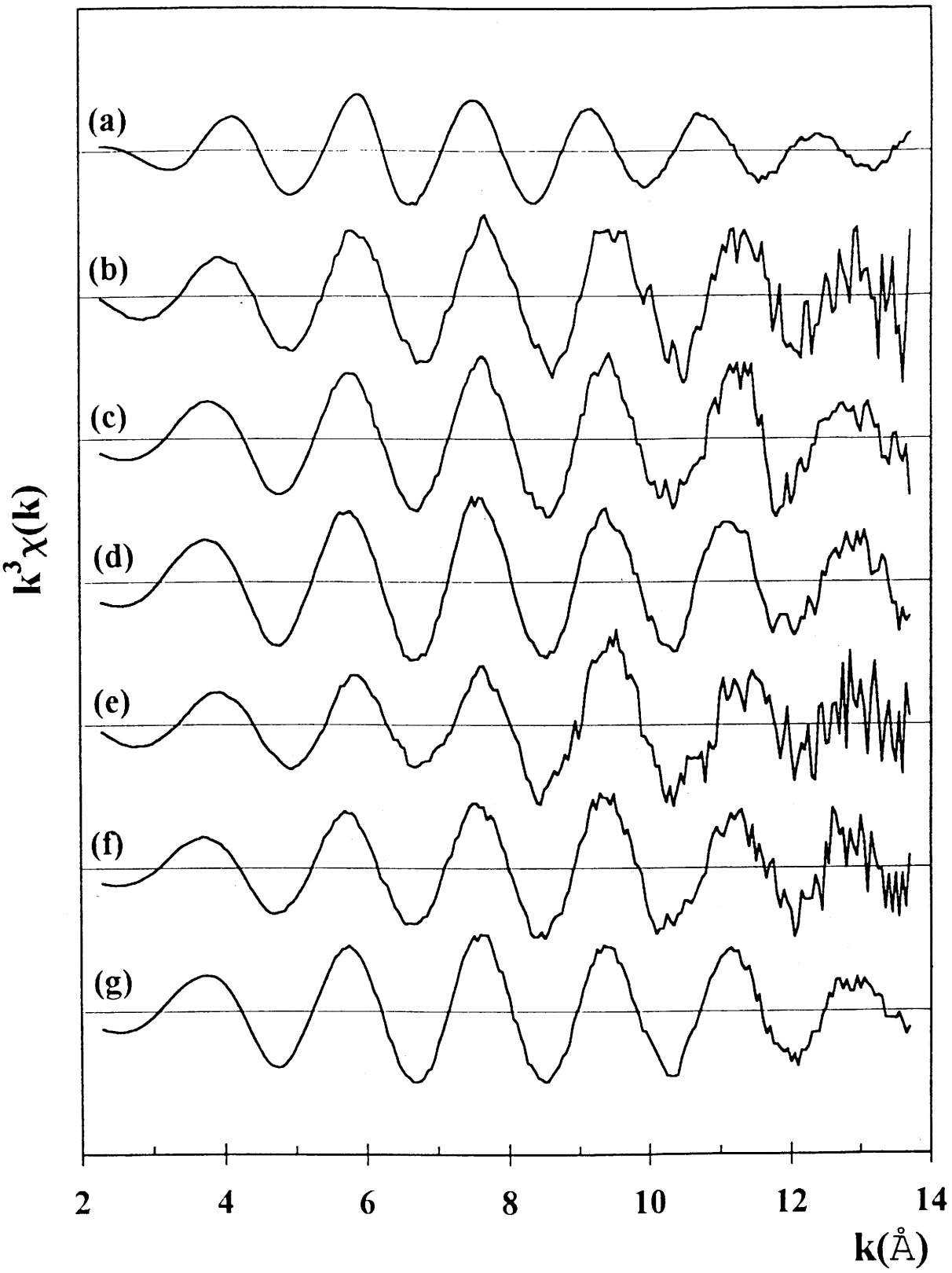

Fig. VI.11 Experimental As K-edge EXAFS spectra, $k^3\chi(k)$, of (a) v-As_2S_3, and (b) y = 0.1, (c) y = 0.2, (d) y = 0.3 with x=0.67, and (e) y = 0.1, (f) y = 0.2, (g) y = 0.3 with x=0.70 for the xLi_2S-(1-x)[(1-y)B_2S_3-yAs_2S_3] ternary glass system.

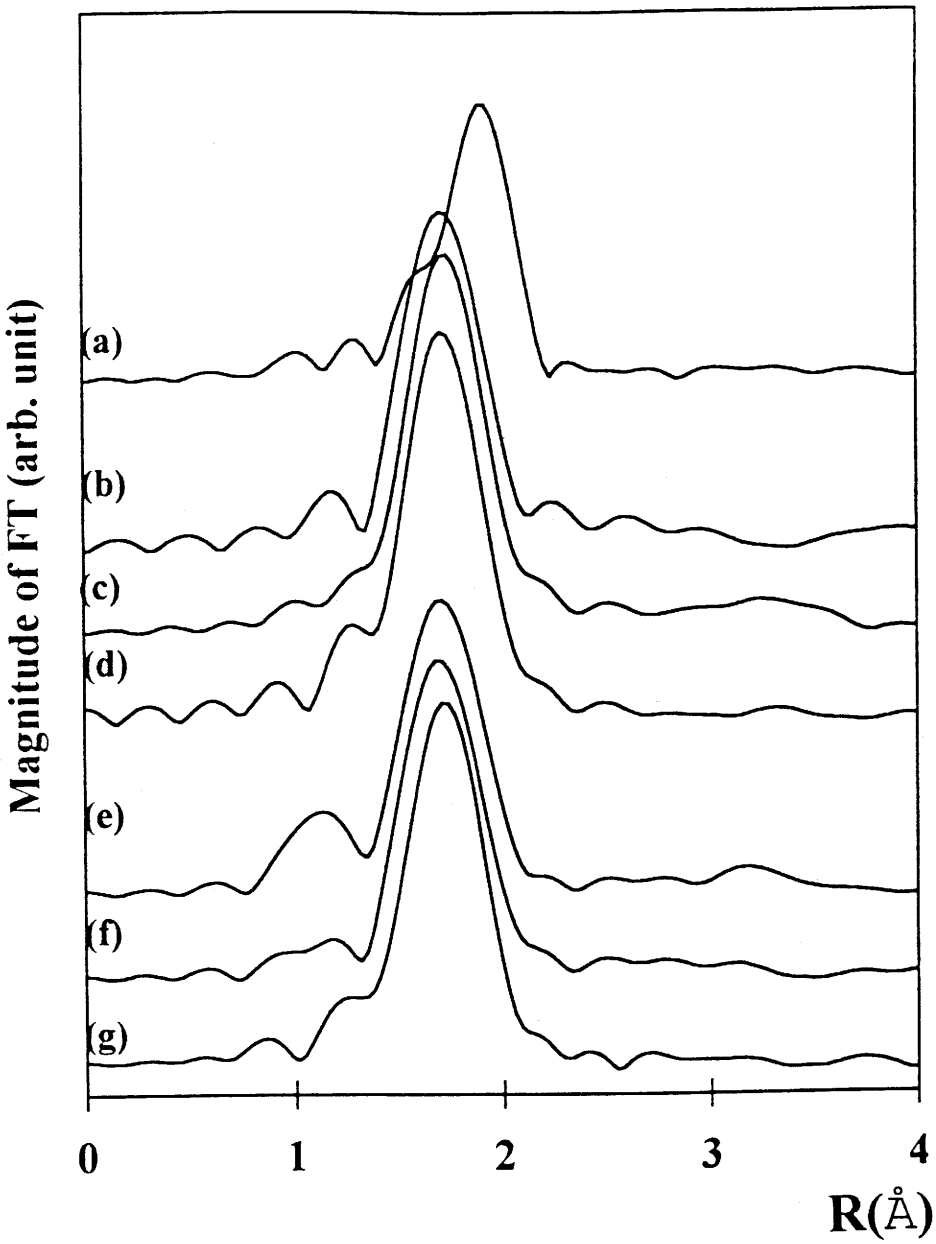

Fig.VI.12 Magnitudes of FTs in the range ~2.5 Å^{-1} < k < ~13Å^{-1} of $k^3\chi(k)$, of (a) v-As_2S_3, and (b) y = 0.1, (c) y = 0.2, (d) y = 0.3 with x=0.67, and (e) y = 0.1, (f) y = 0.2, (g) y = 0.3 with x=0.70 for xLi_2S-(1-x)[(1-y)B_2S_3-yAs_2S_3] glasses.

The best one-shell fitting result and experimental $k^3\chi(k)$ are compared in Fig. VI.13 and the fitted structural parameters can be seen in Table VI.2. The experimental and fitting results of the main peaks are shown in Fig.VI.14. The fitted As-S bond distance and the number of sulphur atoms surrounding the arsenic atom for v-As_2S_3 are in good agreement with those for the well known crystalline As_2S_3 (26). The As K-edge EXAFS analyses of the two ternary Li_2S-B_2S_3-As_2S_3 glass systems do not exhibit any noticeable variation of As-S bond distances with the compositional ratio within experimental error limits. There is however for x = 0.70 a slight shortening of the As-S bond distances determined for x = 0.67. Comparing this with the previous results obtained from spectroscopic experiments (cf. VI.1.1), we conclude that the shorter As-S bond distances found in ternary glass systems compared to As_2S_3 indicate that most of the As-S bonds in AsS_3 pyramids are modified to a non-bridging termination state as As-S^-.

Composition x	y	**C.N.$_{As\text{-}S}$(Å)**	**$R_{As\text{-}S}$(Å)**	**$\sigma_{As\text{-}S}^2(10^{-3}$/Å)**	**E_0(eV)**
0	1	2.8	2.28	3.6	9.3
0.67	0.1	3.1	2.16	1.7	-7.4
	0.2	3.5	2.17	1.8	-10.4
	0.3	4.2	2.17	2.8	-11.3
0.70	0.1	2.5	2.15	1.2	-12.5
	0.2	3.1	2.16	1.9	-15.7
	0.3	2.8	2.17	2.7	-13.3

Table VI.2 Best fitted structural parameters at the arsenic K-edge for the xLi_2S-(1-x)[(1-y)B_2S_3-yAs_2S_3] ternary glass system.

It is well known that there is a strong correlation in EXAFS amplitude between C.N. and σ_i^2 which can sometimes give rise to large C.N. and a simultaneously large σ_i^2 in the curve-fitting or vice versa. Therefore, we have tried curve-fitting with a fixed value of C.N. or σ_i^2 in

order to examine whether the tendency of C.N. or σ_i^2 with the value y is due to their noted correlation. However, the resultant curve-fittings did not present any good fit. Moreover, we have found from a series of the present curve-fitting that the curve-fittings with fixed C.N. show relatively good fits in the low k region, while those with fixed σ_i^2 show relatively good fits in the high k region contrary to the former case. In addition, because the weighting scheme of k^n, in which higher n values put more emphasis on the high k region, can also influence EXAFS analysis, we have carried out EXAFS analyses for the cases of n = 0, 1, and 2, and the same tendency of C.N. and σ_i^2 values as for n = 3 were obtained. These facts indicate that the fitted C.N. and σ_i^2 values might be attributed not to their strong correlation, but to the intrinsic structural nature around the arsenic atom in the present glass systems. In Table VI.2, the C.N. of arsenic seems to increase upon increasing the As_2S_3 and decreasing the Li_2S content, but the maximum error for EXAFS experiment (~30 %, (27)) does not allow full confidence in such a variation. Nevertheless, the amount of Li_2S modifier seems to influence the C.N. of arsenic but it requires further investigation for confirmation. Consequently, though the exact local symmetry around arsenic is not clear at this moment, we propose that arsenic atoms are coordinated to three sulphur atoms, and borons are four- or three-coordinated according to the amount of Li_2S modifier in the binary glass system of Li_2S-B_2S_3 previously reported on the basis of results by ^{11}B NMR and neutron diffraction (15,28).

The Debye-Waller factor σ_i^2 increases with increasing As_2S_3 and decreasing Li_2S contents in the same manner as the change of coordination number, which implies that the As-S bond becomes less covalent at higher arsenic concentrations. These variations of C.N. or Debye-Waller factors σ_i^2 may not have any physical meaning at this moment since their fitting was performed for free values, but they do give us some reference guide in considering the structural variation of this ternary glass.

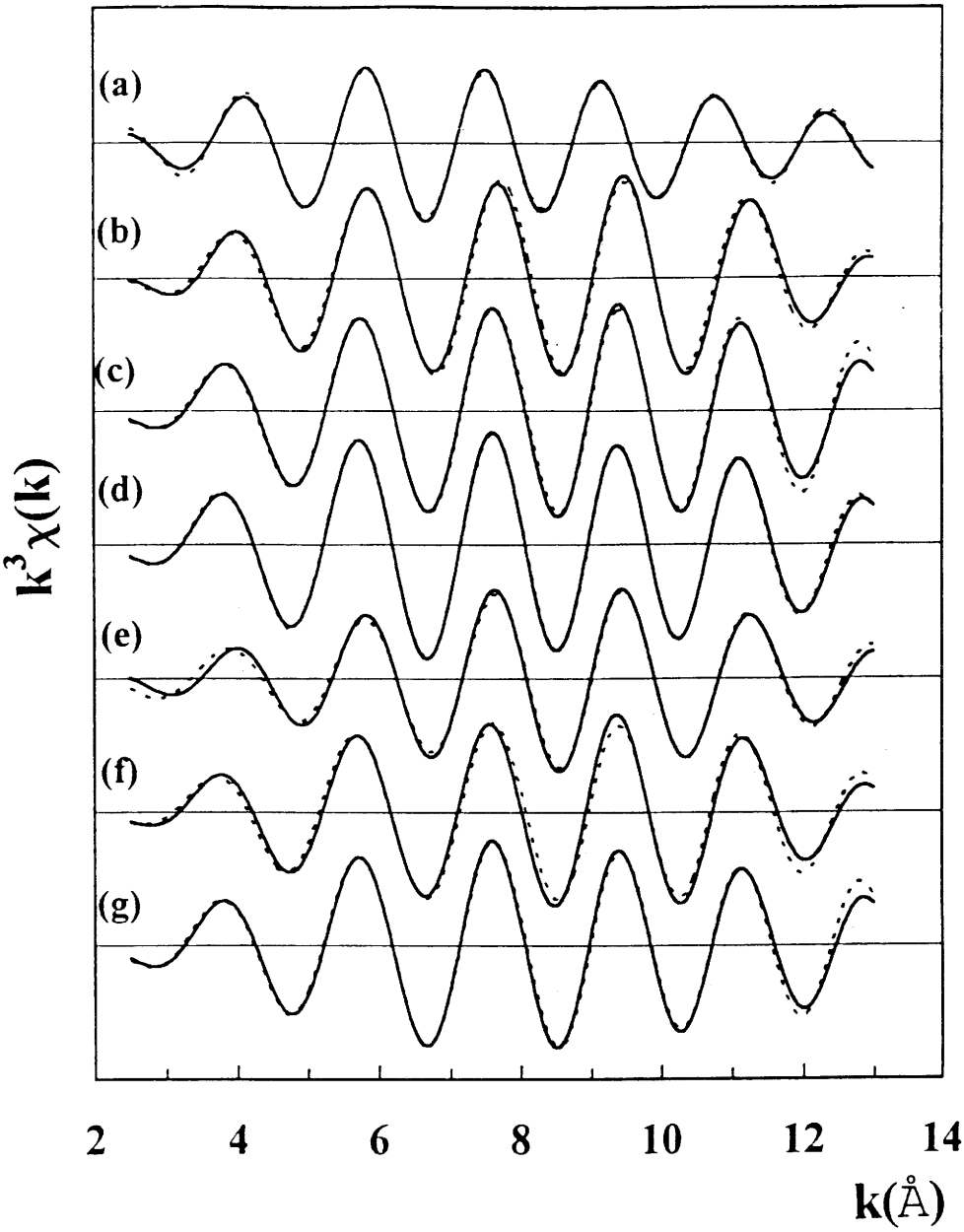

Fig. VI.13 Best-fitted (dotted curve) and experimental (solid curve) inverse Fourier transformed $k^3\chi(k)$, for the first shell in the FTs of Fig.VI.12 for (a) v-As_2S_3, and (b) y = 0.1, (c) y=0.2, (d) y = 0.3 with x = 0.67, and (e) y = 0.1, (f) y = 0.2, (g) y = 0.3 with x=0.70 for the xLi_2S-(1-x)[(1-y)B_2S_3-yAs_2S_3] ternary glass system.

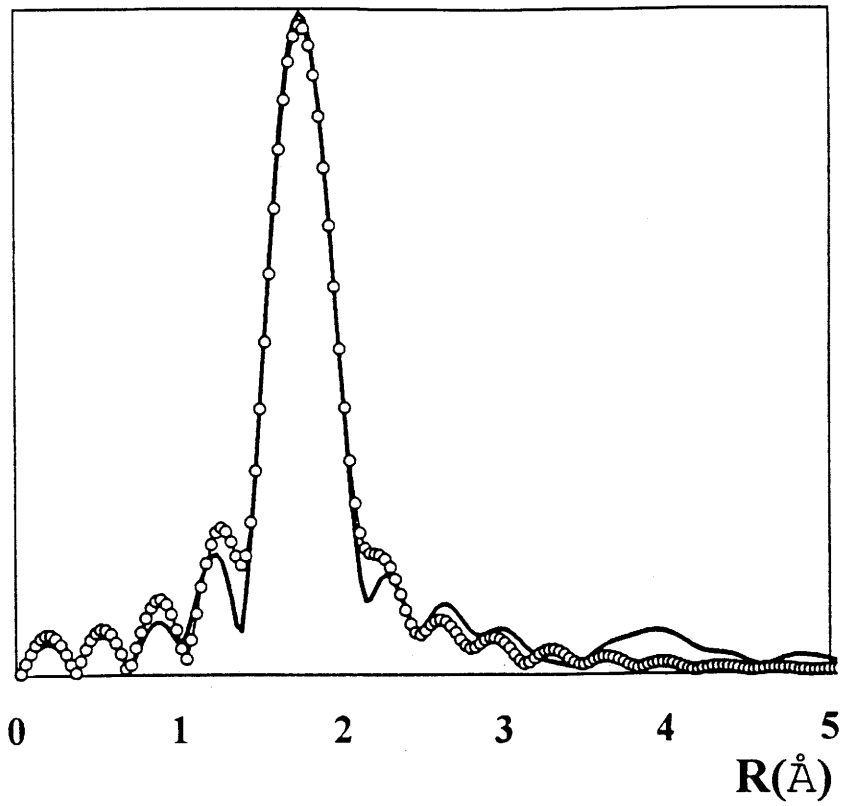

(a)

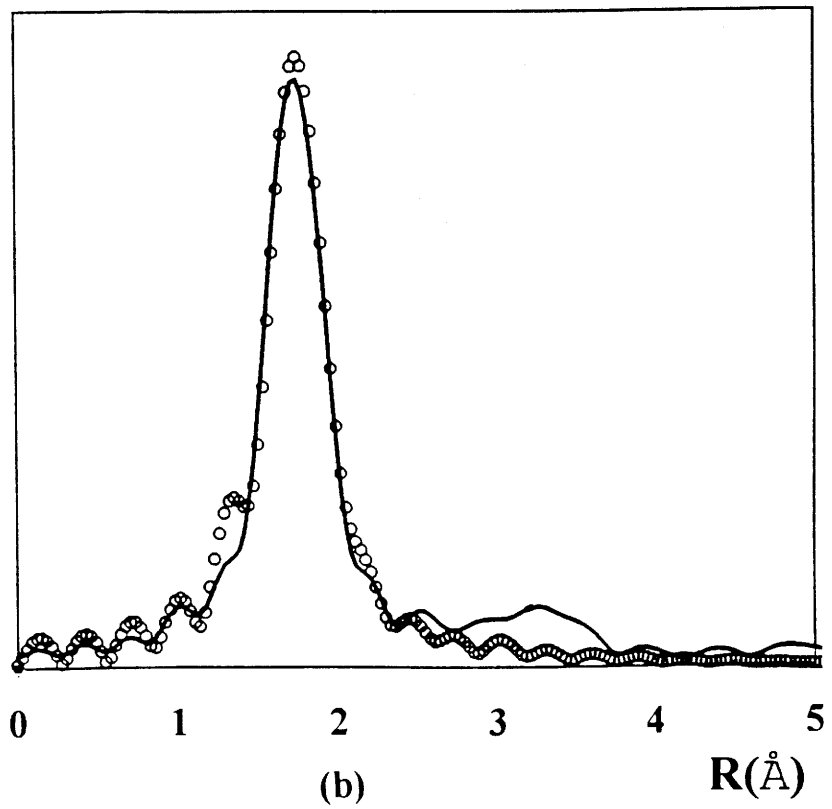

(b)

Fig. VI.14 Experimental (solid curve) and fitted results (dotted curve) of the main peaks (a) y = 0.1, (b) 0.2 with x = 0.67.

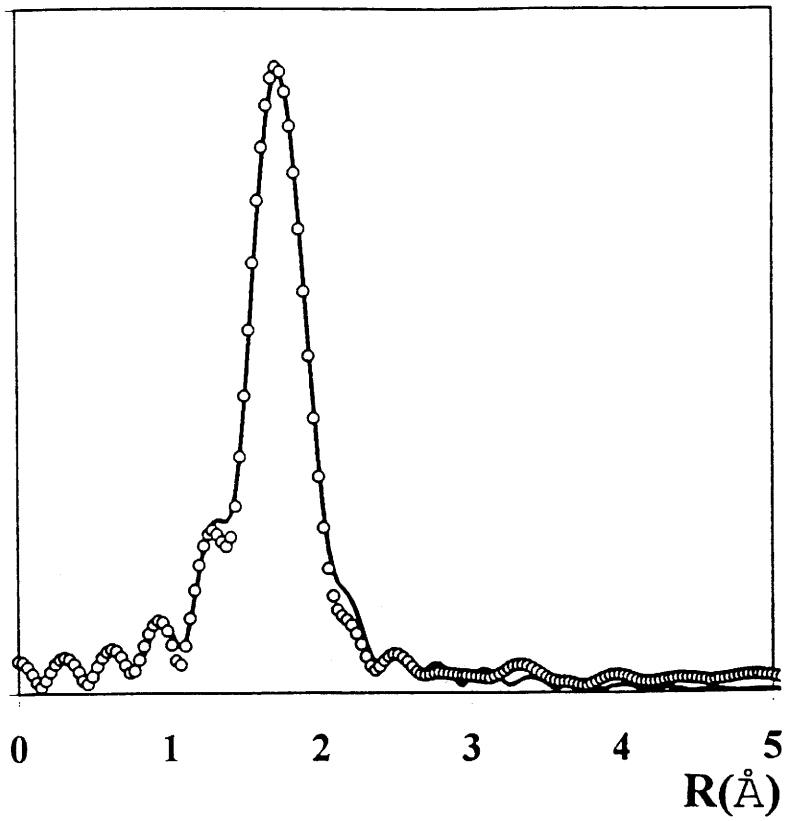

(c)

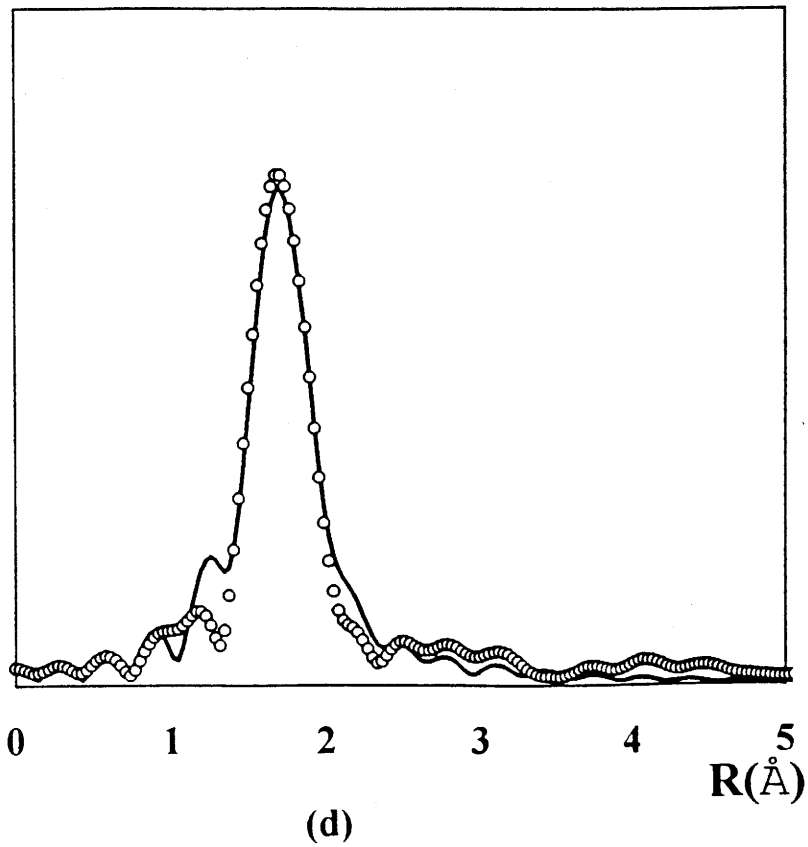

(d)

Fig. VI.14' Continued over Fig. VI.14 (c) 0.3 with x = 0.67 and (d) 0.1with x = 0.70.

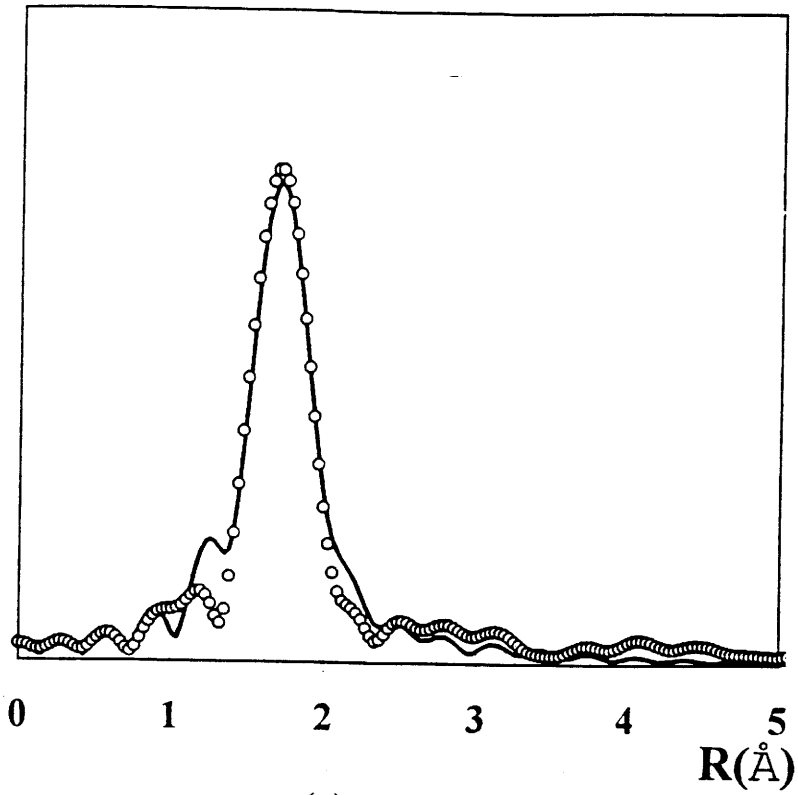

(e)

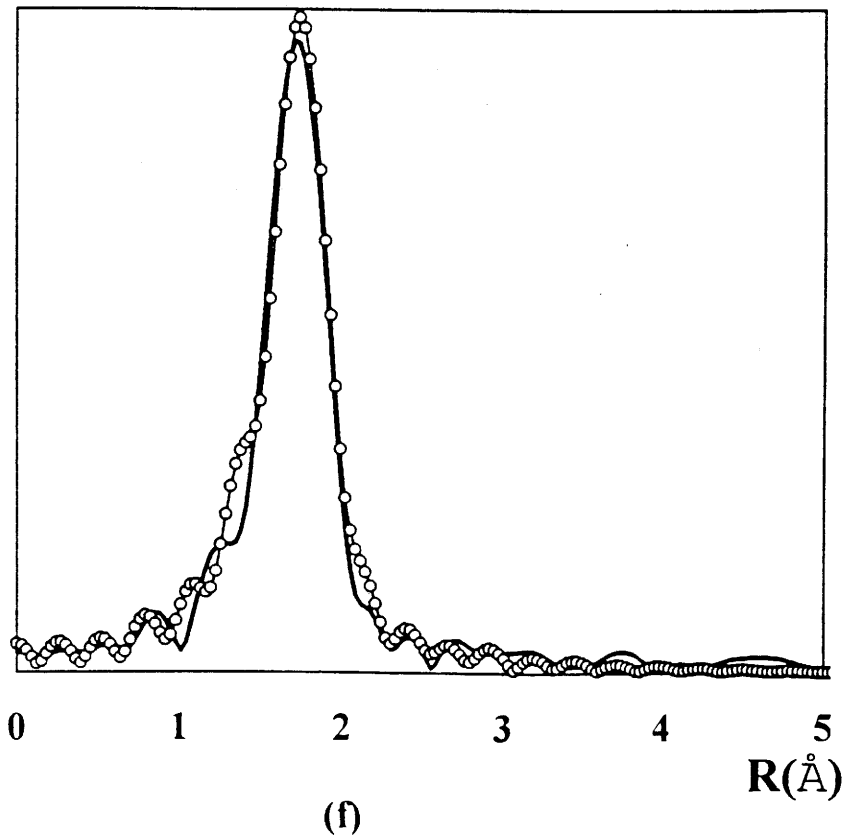

(f)

Fig. VI.14'' Continued over Fig. VI.14 (e) 0.2, (f) 0.3 with x = 0.70.

VI.2.2.2 As K-edge XANES for xLi_2S-$(1-x)[(1-y)B_2S_3$-$yAs_2S_3]$ (x = 0.67, 0.70; y = 0.1, 0.2, 0.3)

Fig. VI.15 shows the normalised As K-edge XANES spectra, in which the main peak corresponds to the transitions from the 1s core state to the final unoccupied 4p state and is associated with the antibonding sp^3 state. It can be clearly seen that the main peak for the ternary glass system exhibits a higher shift ($\Delta E > 1$ eV) compared to that for glassy As_2S_3, indicating that the arsenic atoms achieve a more positive valence state. In parallel, sulphur atoms become more negative as was observed for the binary glasses by XPS, and it represents the formation of ionic As-S^- bonds including NBS for the ternary glass systems. Moreover, it should be noted that the main peak has a higher energy for higher concentrations of modifier. For a constant modifier content, the peak shifts to lower energy upon increasing the As_2S_3 content. The variation of the main peak positions with different lithium (x) and arsenic (y) concentrations is plotted in Fig. VI.16. Although lithium influences more strongly the ionicity of the As-S bond as in binary Li_2S-As_2S_3 glass systems, it can be suggested that boron, which competes with arsenic in the formation of glass, also influences the As-S bonding character. Of note is that the homogeneous/inhomogeneous phase change does not cause any change in the variation of the spectrum as we observed in the previous spectroscopic studies. Considering this fact, these XANES spectra indicate the possibility of the occurrence of a limited mixed former effect at low As_2S_3 contents (perhaps below y = 0.1). In addition, they suggest the existence of the Li_2S-As_2S_3 phase through-out the composition range.

Consequently, in spite of little variation of bond distance upon differing amounts of lithium and boron in the present compositional range, the changes of Debye-Waller factors in EXAFS analyses and the peak positions in XANES spectra suggest that the nature of the neighbours should be related to the bonding character of the As-S bond.

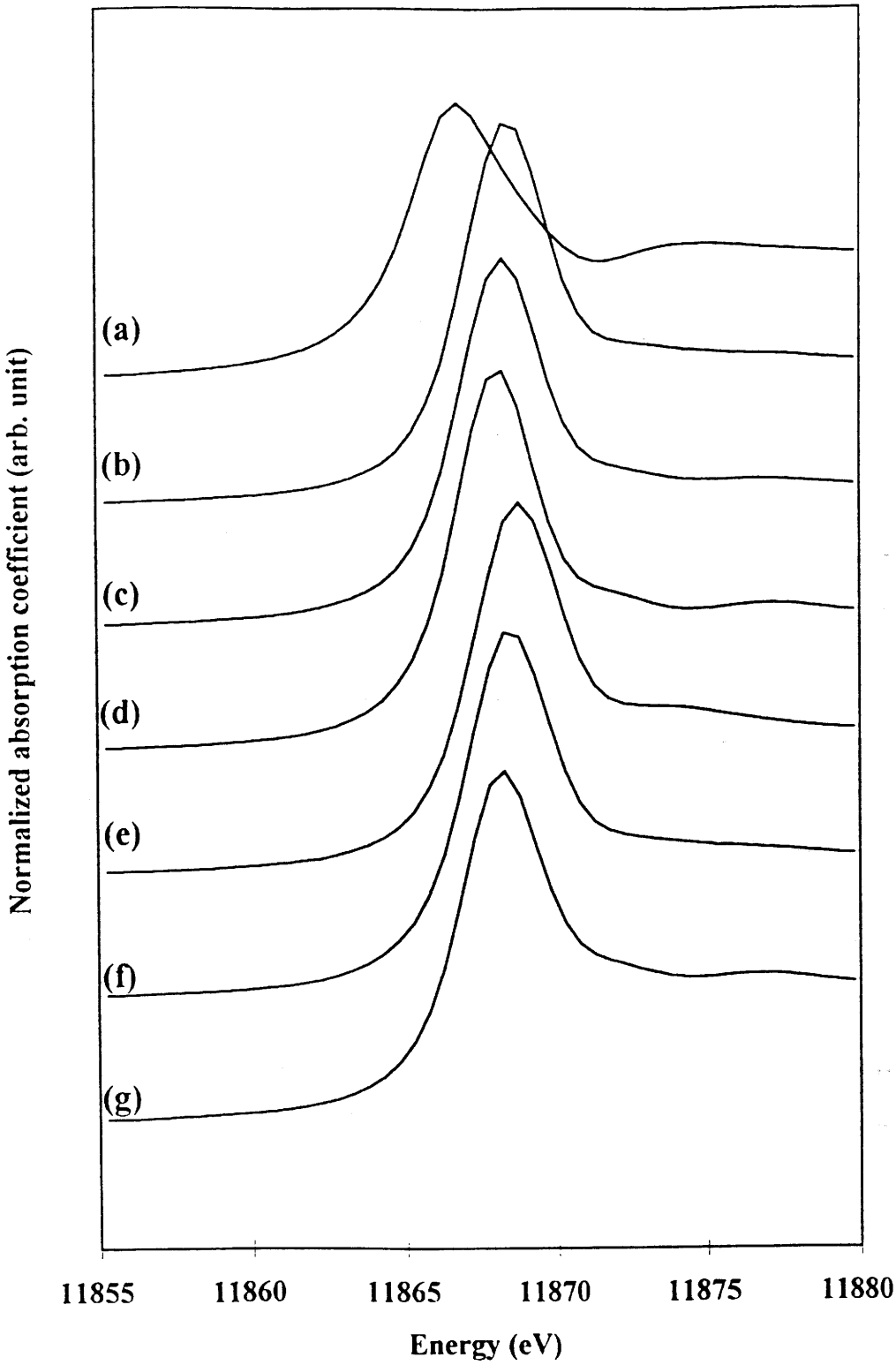

Fig. VI.15 Normalised As K-edge XANES spectra for (a) v-As_2S_3, and (b) y = 0.1, (c) y = 0.2, (d) y = 0.3 with x=0.67, and (e) y = 0.1, (f) y = 0.2, (g) y = 0.3 with x=0.70 for the xLi_2S-(1-x)[(1-y)B_2S_3-yAs_2S_3] ternary glass system.

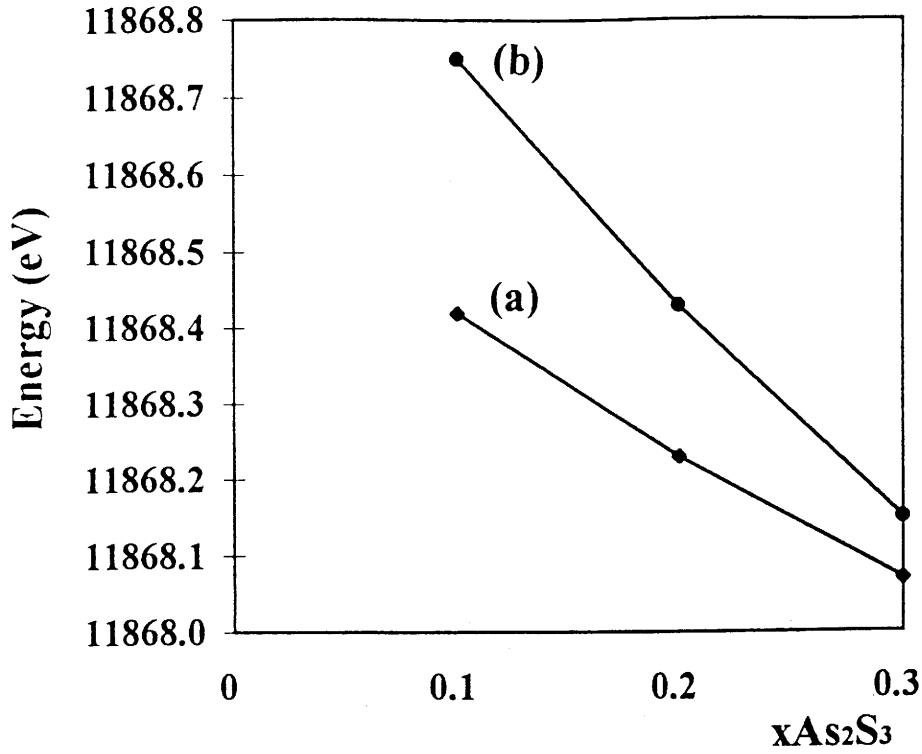

Fig. VI.16 Variation of main peak position with respect to x- and y-values in the As K-edge XANES spectra for the ternary glass system, xLi_2S-(1-x)[(1-y)B_2S_3-yAs_2S_3], (a) x = 0.67 and (b) x = 0.70.

VI.3 Ionic conductivity of Li_2S-B_2S_3-As_2S_3 ternary glasses

VI.3.1 Review of conduction models for mixed former glass

In this section we will review the models describing the mixed former effect which is found in several glasses. For the description of mixed former effect, one of the most representative model is the 'weak electrolyte model' for a homogeneous glass in which two conduction maxima are present. Another one is Liang's model for phase separated glasses with only one maximum in the conduction curve.

VI.3.1.1 Weak electrolyte model

This model was suggested by Kone (29) to explain the gain in conductivity in homogeneous glasses containing two formers. Basically, he considered the glass , MF_1F_2, as consisting of an endothermic mixing of limiting compositions of MF_1 and MF_2. The mixing is represented by a formalism of regular solution. In this case, because of kinetic reasons one cannot achieve the phase separation, and consequently he observed an increase in the thermodynamic activity related to the conductivity in such compounds. In this formalism, the enthalpy of mixing is $\Delta H_m = -\alpha x(1-x)$ and the free energy of mixing is $\Delta G_m = -\alpha x(1-x)+RT[x\mathrm{Ln}x + (1-x)\mathrm{Ln}(1-x)]$, where x and (1-x) are the mole fraction of components MF_1 and MF_2, and α is an enthalpy term representative for the rearrangement of chemical bonding. The probability for de-mixing is given by $P = P_0 \exp\{-(\Delta x^2 d^2\Delta Gm/d^2x)/2RT\}$, where P_0 is a characteristic kinetic constant for rearrangement of F_1 and F_2 components. This probability is low for $d^2\Delta Gm/d^2x > 0$ and becomes large for $d^2\Delta Gm/d^2x < 0$. In the latter case, de-mixing cannot happen as described above. The weak electrolyte theory predicts the ionic conductivity to be proportional to the square root of the activity of modifier cation, whereupon an increase in the activity must lead to a variation in conductivity in the same manner. The thermodynamic activities MF_1 and MF_2 pass through a maximum located near each composition limit, and following this fact, one can expect a double maximum on the curve of conductivity (cf. Fig. VI.17).

For example, $0.50Ag_2O$-$0.50P_2O_5$ and $0.50Ag_2O$-$0.50Te_2O_4$ or $0.30Ag_2O$-$0.70B_2O_3$ and $0.30Ag_2O$-$0.70Te_2O_4$ (30) do not present phase separation due to kinetic reasons. If one represents the limit formulations $0.50Ag_2O$-$0.50P_2O_5$ and $0.50Ag_2O$-$0.50Te_2O_4$ or $0.30Ag_2O$-$0.70B_2O_3$ and $0.30Ag_2O$-$0.70Te_2O_4$ by F_1Ag and F_2Ag (M = Ag), it is possible to simulate the variation of the thermodynamic activity for these compositions when they are mixed. This variation is represented in Fig. VI.17-a) and VI.17-b), which is supposed to exhibit

regular behaviour characterised by an enthalpy of mixing; $\Delta H_m = \alpha x(1-x)$ with $\alpha = 12kJ\ mole^{-1}$. In principle, those mixtures should lead to separate phases at $T < (\alpha/2)RT$, in this case, $T < 450°C$. If one supposes that the phase separation is avoided for kinetic reasons, the thermodynamic activities of each composition limit pass through a maximum. Thus, one can suppose that the variation of activity leads to a similar variation in conductivity. The existence of two activity maxima provides the justification for two maxima in conductivity. The creation of Ag^+ charge carriers results from the dissociation equilibrium as follows,

$F_1Ag \Leftrightarrow F_1^- + Ag^+ \quad [Ag^+] \propto a^{1/2}\, F_1Ag$

$F_2Ag \Leftrightarrow F_2^- + Ag^+ \quad [Ag^+] \propto a^{1/2}\, F_2Ag$

This is the hypothesis based on the weak electrolyte theory.

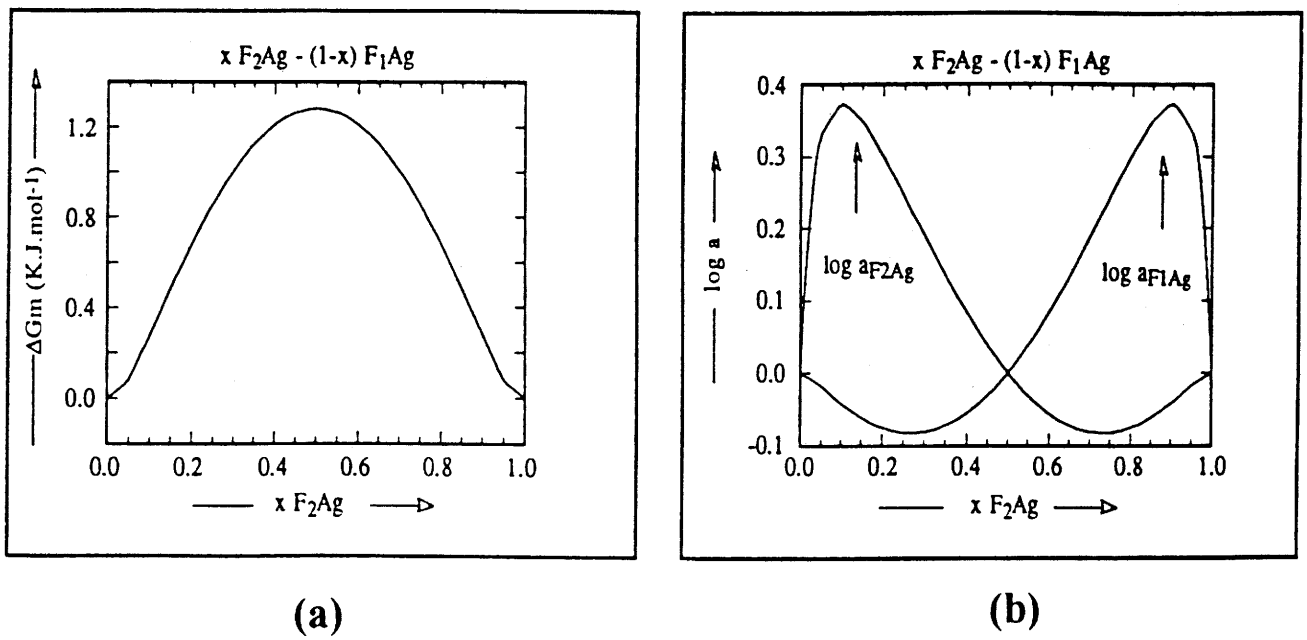

Fig. VI.17 a) Variation of free enthalpy of mixing versus the substitution ratio, b) variation of the activity of two limit compositions versus the ratio of substitution (30).

VI.3.1.2 Liang's model

The model of Liang was proposed to explain the increase of ionic conduction between pure LiI and Al_2O_3-LiI (31) or Al_2O_3-AgI (32) "composite" materials. In these composites, the interface between the insulator and the ionic conductor is expected to present a large number of defects, allowing the cation to move quickly. When the insulator is low in concentration, the conductivity found is the conductivity of the ionic conductor. When the amount of insulator increases, the interfacial conductivity becomes predominant. Finally, when the insulator component content is very large, the interfacial area decreases, the percolation between the different interfacial sites does not exist any longer and the ionic conductivity suddenly decreases. With this hypothesis, Roman et al. performed a Monte-Carlo simulation (33) showing the three variation regions described above, A, B, and C as represented in Fig.VI. 18. Only one conductivity maximum is present.

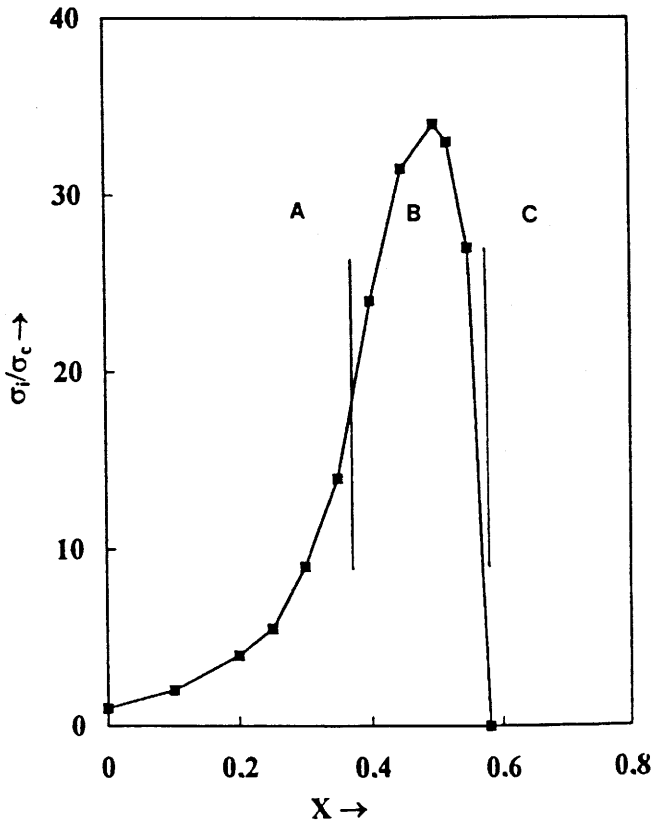

Fig. VI.18 Simulated variation of the ratio of ionic conductivity σ_i to interface conductivity σ_c versus the amount of isolator substitution in the conductor material (33).

VI.3.2 Influence of second former on ionic conductivity of Li_2S-B_2S_3-As_2S_3 glasses

The conductivity of these glasses obey the Arrhenius law $\sigma = \sigma_0 exp(-Ea/kT)$ over the temperature range studied (see Fig. VI.19). The room temperature conductivity σ_{25} is affected by both activation energy Ea and pre-exponential factor σ_0. As we can see from Fig.VI.19-a), Ea increases as the As_2S_3 content increases in the homogeneous glass forming region. The pre-exponential factor σ_0 increases slowly for x = 0.67 through the glass forming range, and for x = 0.70 σ_0 shows a maximum at y = 0.1 and then decreases. As we can see from other cases (5,10,34,35), introduction of a second glass former can cause a variation in the environment of the original glass former and also cause a variation in Tg. If these glasses follow these trends, we could expect that the introduction of As_2S_3 could change the coordination of boron atoms. This effect was suggested by ^{11}B NMR for x = 0.70 (cf. VI.1). It was found that the number of tri-coordinated borons decrease in the homogeneous domain and increases in the inhomogeneous region, for x = 0.70.

The activation energy evolution can be interpreted using the Anderson - Stuart ionic conduction model (36). The activation energy can be written as, Ea = Ec + Em, where Ec is the electrostatic activation energy and Em is the network strain energy. Ec represents the coulombic energy the mobile ion (Li^+) has to overcome in order to escape from the attraction of negative charges. Em, the strain energy, represents the energy necessary to enlarge a bottleneck (36). Negative charges are either B(4) (tetra-coordinated boron) or non-bridging sulphur (NBS) depending on the composition. The ionic radius of a B(4) (which is bonded to four bridging sulphur atoms) can be considered larger than a NBS. Therefore, for a Li^+ -ion associated with a NBS, Ec is higher than that for an Li^+ -ion associated with a B(4). As it has been observed (only for x = 0.70), the ratio B(3)/B(4) decreases upon addition of As_2S_3, and the number of NBS (necessarily associated with B(3)) therefore decreases, thus Ec is expected to decrease. The second term of the activation energy in the Anderson-Stuart model, Em, is

more difficult to quantify. This energy is required to enlarge passageways for Li^+-ions to pass through the bottlenecks present in the framework. Em can be directly related to the shear modulus of the glass (37) which varies as P.ρ/M (38) where P is the total number of atoms present in one mole of the glass, M is its molar mass and ρ its density. Table VI.3 shows the variation of the measured density, lithium concentration and the P.ρ/M factors with the As_2S_3 content. In the homogeneous region P.ρ/M increases i.e. Em is expected to increase also. The activation energy, in this domain, increases also. If the Anderson-Stuart model is applicable in this case, Em seems to be more important than Ec.

However, the vitreous domain is too small to allow an explanation of the conductivity evolution.

Homo-geneous	Hetero-geneous	Composition	Density (mmg/mm^3)	Li^+ concentration (10^{-2} mole cm^{-3})	P.ρ/M
		0.67/0.33			
X		y=0.0	1.82	3.50	9.56
X		y=0.1	1.94	3.52	9.60
X		y=0.2	2.06	3.53	9.65
	X	y=0.3	2.07	3.37	8.95
		0.70/0.30			
X		y=0.0	1.79	3.71	9.60
X		y=0.1	1.91	3.75	9.63
	X	y=0.2	1.96	3.65	9.38
	X	y=0.3	2.01	3.56	9.15

Table VI.3 Measured density, calculated Li^+-ion concentration, variation of P.ρ/M as a function of composition for the xLi_2S-(1-x)[(1-y)B_2S_3-yAs_2S_3] glass system.

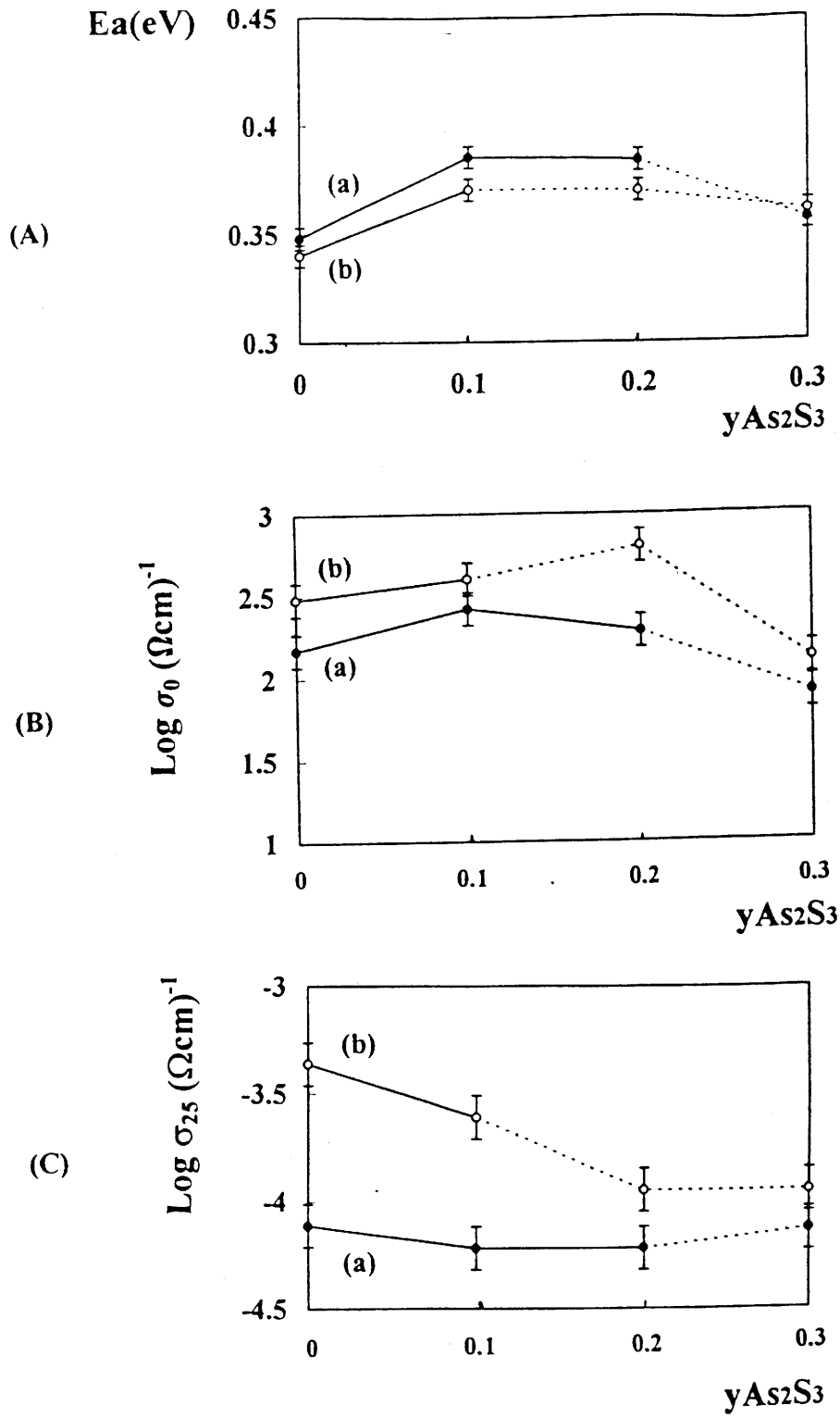

Fig. VI.19 Ionic conductivity of xLi_2S-(1-x)[(1-y)B_2S_3-yAs_2S_3] glasses; (A) activation energy variation; (B) pre-exponential factor variation ; (C) room temperature ionic conductivity variation versus composition (a) x=0.67 and (b) 0.70 (—— homogeneous, ----- inhomogeneous).

Conclusion

Li_2S-(1-x)[(1-y)B_2S_3-yAs_2S_3] ternary glasses in the range of x = 0.67, $0 \leq y \leq 0.3$, and x = 0.70, $0 \leq y \leq 0.3$ have been studied. In these ternary glasses, we have observed an increase in Tg upon addition of a second former species. From spectroscopic experiments, we raise a question whether this ternary glass is really formed by a ternary B-As-S phase, or composed of separate phases such as Li_2S-B_2S_3 and Li_2S-As_2S_3. The main results are summarised below:

(1) From ^{11}B NMR, the B(3)/B(4) ratio decreases on addition of As_2S_3 and then increases regardless of the presence of homogeneous or inhomogeneous phases, for x = 0.70. However, no significant change is observed for the x = 0.67 series.

(2) IR spectra showed the superposition of spectral features of Li_2S-B_2S_3 and Li_2S-As_2S_3 binary glasses regardless of the homogeneity of the material.

(3) The evolution of Raman spectra with the glass composition can be interpreted in the same manner as IR.

These facts show that the ternary glass may include both of Li_2S-B_2S_3 and Li_2S-As_2S_3 binary glass phases throughout the composition range. Furthermore, the competition between B_2S_3 and As_2S_3 for Li_2S modifier can lead to the modification of the B(3) and B(4) content, and Li_2S-As_2S_3 seems to exist when the As_2S_3 content is high.

On the other hand, As K-edge XAS showed that the main peak has a higher energy for higher concentrations of modifier. For an intermediate modifier content it shifts to a lower energy upon increasing the As_2S_3 content. It also showed that high As contents results in a progressive increase in the coordination number of As atoms. In view of these facts, the introduction of As_2S_3 might have the effect of substituting into the position of 4-coordinated boron atoms, B(4), resulting in the higher modified state. However, it is still not clear that As

changes its coordination with composition. Furthermore, the presence of lone pairs on arsenic atoms prevents the possibility of the substitution of As into boron sites.

The ionic conductivity behaviour showed similarities to Li_2S-B_2S_3 binary glasses, where the room temperature conductivity is affected by both activation energy and pre-exponential factor. It was also observed that the room temperature conductivity is more seriously affected by activation energy for homogeneous glass and by pre-exponential factor for inhomogeneous glass respectively. Such a conduction behaviour has been explained using classical Anderson-Stuart model.

The evolution of the ionic conductivity cannot be explained simply following the weak electrolyte or Liang's model, because these ternary glasses exhibit too small a glass forming domain.

References

1) H. Wakabayashi, Phys. Chem. Glasses, **30** (1989) 51

2) W. C. LaCourse, J. Non-Cryst. Solids, **21** (1976) 431

3) A. Pradel, Ph. D. Thesis, Univ. of Montpellier (1988)

4) T. Tsuchiya and T. Moriya, J. Non-Cryst. Solids, **38-39** (1980) 323

5) A. Magistris, G. Chiodelli and M. Duclot, Solid State Ionics, **9-10** (1983) 611

6) A. C. Martins Rodrigues and M. J. Duclot, Solid State Ionics, **28-30** (1988) 729

7) T. Minami, J. Non-Cryst. Solids, **73** (1985) 273

8) M. Tatsumisago, K. Yoneda, N. Machida and T. Minami,
J. Non-Cryst. Solids, **95-96** (1987) 857

9) V. K. Deshpande, A. Pradel and M. Ribes, Mat. Res. Bull., **23** (1988) 379

10) A. Magistris , G. Chiodelli and M. Villa, J. Power Sources, **14** (1985) 87

11) M. Tatsumisago, K. Yoneda and T. Minami, J. Am. Ceram. Soc., **71** (1988) 766

12) M. Ménétrier, A. Hojjaji, C. Estournès and A. Levasseur,
Solid State Ionics, **48** (1991) 325

13) Z. Zhang, J. H. Kennedy, J. Thompson, S. Anderson, D. A. Lathop and H. Eckert,
Appl. Phys., **A49** (1989) 41

14) A. Levasseur, R. Olazouga, M. Kbla, M. Zahir and P. Hagenmuller,
C. R. Acad. Sci., **293** (1981) 563

15) K. S. Suh, A. Hojjaji, G. Villeneuve, M. Ménétrier and A. Levasseur,
J. Non-Cryst. Solids, **128** (1991) 13

16) A. Hojjaji, M. Ménétrier, A. Levasseur, M. Couzi and K. J. Rao,
Phys. Chem. Glasses, **33** (1992) 1

17) D. E. Hintenlang and P. J. Bray, J. Non-Cryst. Solids, **69** (1985) 243

18) P. J. Bray and J. G. Okeefe, Phys. Chem. Glasses, **4** (1963) 37

19) K. S. Kim and P. J. Bray, J. Chem. Phys., **64** (1976) 4459

20) A. Hojjaji, Ph. D. Thesis, Univ. of Bordeaux I (1990)

21) P. J. Bray, J. Non-Cryst. Solids, **95-96** (1987) 45

22) J. Cho and S. W. Martin, J. Non-Cryst. Solids, **170** (1994) 182

23) S. W. Martin and D. R. Bloyer, J. Am. Ceram. Soc., **74** (1991) 1003

24) P. Vinatier, Ph. D. Thesis, Univ. of Paris XI, Orsay, (1995)

25) M. C. R. Shastry, M. Couzi, A. Levasseur and M. Ménétrier, Phil. Mag., **B68** (1993) 551

26) A. F. Wells, *Structural Inorganic Chemistry*, 5th Ed.,
(Oxford Univ. Press, New York, 1984)

27) B. K. Teo, *EXAFS; Basic Principles and Data Analysis* (Springer-Verlag, Berlin, 1986)

28) M. Ménétrier, C. Estournès, A. Levasseur and K. J. Rao,
Solid State Ionics, **53-56** (1992) 1208

29) A. Kone, Ph. D. Thesis, Grenoble (1986)

30) D. Coppo, Ph. D. Thesis, l'Institut National Polytechnique de Grenoble (1992)

31) C. C. Liang, J. Electrochem. Soc., **126** (1973) 1963

32) K. Shahi and J. B. Wagner Jr, J. Phys. Solids, **128** (1981) 6

33) F. W. Poulsen, A. N. Hessel, K. Clausen, S. Skaarup and S. D. Toft,
Proc. 6th Riso Int. Symp. on Metallurgy and Material Science (1985), 165

34) B. Krebs, Angew. Chem., **22** (1983) 113

35) B. V. R. Chowdari and S. K. Akhter, J. Non-Cryst. Solids, **116** (1990) 16

36) O. L. Anderson and D. A. Stuart, J. Am. Ceram. Soc., **37** (1954) 573

37) D. K. McElflresh and D. G. Howitt, J. Am. Ceram. Soc., **69** (1986) C237

38) O. L. Anderson, *Physical Acoustics*, ed W. P. Mason, **Vol. 3B**
(Academic Press New York 1965)

Chapter VII. Optical basicity(Λ) study of sulphide glasses using the absorption properties of the Pb^{2+} ion

Introduction

Glass structure and properties are strongly affected by the nature of the network former, network modifier or doping agent and their respective concentrations. A lot of effort has been expended to clarify the role of each component in the glass. The knowledge of the structure - various physical properties and the cross linking of the results obtained by techniques sensitive to local order - can lead to a better knowledge of the vitreous state.

The acid-base concept, following the Lewis concept, has long been studied, but only two decades ago this came to be applied to the interpretation of various aspects of the physics and chemistry of glass; such as refractivity, network coordination number changes, chemical durability, etc.(1). For oxide glasses, the "basic" nature of the oxygen atoms is an important feature and has a profound bearing on the physics and chemistry of glasses. To study this "basic" nature of oxygen atoms, the optical basicity concept was developed by Duffy and Ingram (1). Such a method, however, has been confined to oxidic medium and only recently been applied to a limited range of sulphide materials (2).

Generally, sulphide based glasses are expected to have more basic properties than oxide based glasses because of the higher polarizability and lower electronegativity of sulphur atoms as compared to oxygen. Sulphide based glasses are generally hygroscopic, and this property leads to difficulties in their characterisation.

In this chapter, we have reviewed the previous studies and developments of concepts concerning optical basicity. The polarizability of sulphide anions was obtained by measuring the refractive index for various compositions of arsenic and thioborate based glasses. We also attempted to measure the optical basicity by using a Pb^{2+} ion probe.

VII.1 General background

VII.1.1 Acid-base relationships in glass

The concept of acids and bases has several definitions. The Brönstead and Lowry theory (3-5) offered a definition of acids and bases to determine acid - base functions only in a protonic solvent. According to this theory, an acid is defined as a species which has a tendency to yield a proton and a base as a substance which can accept a proton. This definition can be represented by the equation AH (acid) + $H_2O \Leftrightarrow A^-$ (base) + H_3O^+ and the acid - base reaction can be represented by the equation, Acid(1) + Base(2) $\Leftrightarrow$ Acid(2) + Base(1). The equilibrium constant of this reaction is determined by the relative affinities of the bases for the proton. The essential nature of the neutralisation according to the proton transfer concept, must be viewed in terms of a complete proton transfer reaction. The acid - base theory of Lewis (6) considers acid - base functions and related processes independently of the solvent. An acid is any species that is capable of accepting a pair of electrons and a base is any species that can donate a pair of electrons to form a covalent bond with the acid. Neutralisation is then the formation of a coordinate covalent bond between the acid and base.

When compared to the investigation of acid - base phenomena in aqueous and non-aqueous chemistry, little has been done to determine acid - base relationships in glass. Initially it was believed that acidic oxides are glass formers, and basic oxides merely modify the properties of glass.

Certain metal ions undergo observable changes (for example, a colour change or a change of oxidation state) depending upon the degree of electron donation they receive from the oxygens. Therefore, they may be used as probes for basicity in glass. One of the earliest studies of glass basicity using metal probe ions was done by Weyl and Thümen (7) who exploited the Cr(III)/Cr(VI) equilibrium. Lüx and Rogler (8) studied acid-base relationships in Li_2O-Na_2O-B_2O_3 mixed alkali borate glasses using Cr(III)/Cr(VI) as colour indicators. In these glasses, the estimated competition of B_2O_3 and Li_2O leads to the conclusion that in certain composition ranges Li_2O behaves as a stronger acid than B_2O_3, while in certain composition ranges, like binary lithium-silicate, it obviously acts as a base. Paul and Douglas (9) have defined acids and bases in borate and silicate glasses in a non-protonic solvent. As the bond strength between alkali and oxygen decreases with an increase in the size of the alkali ion, the extent of ionisation of the alkali silicate group increases with the increase in ionic radii of the alkali in the order, $Li_2O < Na_2O < K_2O < Rb_2O < Cs_2O$. Thus, the basic nature of the oxygen atoms is an important feature and has a profound bearing on the physics and chemistry of the glass. In terms of basicity, which refers to the state of the oxygen atoms, addition of a small concentration of a solute metal ion to a glass results in the oxygens of the glass donating their negative charge to the metal ion. In the Lewis sense, the oxygen behaves as a base and correspondingly the metal ions behave as Lewis acids. The ability of oxygen to donate negative charge is at a maximum when it exists as the free O^{2-} ion uninfluenced by surrounding cations. The polarisation of O^{2-} results in negative charge being drawn off and therefore the oxygen is less able to donate charge to a solute metal ion, i.e. it is less able to function as a Lewis base. The overall basicity of a glass containing both bridging and non-bridging oxygen will depend upon the relative proportion of these two types of oxygen, and this will also determine the total electron donation to the solute metal ion (1).

VII.1.2 Definition of optical basicity

Optical basicity concepts arose from studies on how the nature of the metal ion and its surrounding ligands affect optical transition energy. Jørgensen (10) related absorption energies to the effect of ligands on the radius of the electron charge density about the central ions (Nephelauxetic effect). He found that a variety of transition metal complexes are described by the simple expression, $hk = 1 - (E/E_F)$, where h is a parameter characterising the ligands, k is a parameter characterising the central ion, and E is the absorption energy of the ion-ligand system. E_F is the absorption energy the ion would have if the free-ion wave functions were confined to the volume available to them in the solid. Such expressions have been applied to the absorption energies of post-transition metal ions, which have $d^{10}s^2$ atomic ground state configurations. Jørgensen's studies (10) were concerned essentially with transition metal ions but it has been shown this nephelauxetic effect for p-block metal ions is fundamentally linked to that for transition metal ions.

Duffy and Ingram recognised that the electron cloud expansion described above represent the degree to which surrounding ligands donate electrons to a central ion, that is, act as a Lewis base. Thus they defined the optical basicity parameter as $\Lambda_{exp} = h/h_{O2-} = (E_F - E)/(E_F - E_{min})$, where E_{min} is the absorption transition energy of an ion in an ideal basic medium, approximated by CaO and SrO. h_{O2-} is the value of h for a probe ion in that ideal basic medium. In such a medium, there is a maximum donation of electrons by the ligands, and the absorption energy is therefore a minimum.

In the interaction between a p-block metal ion of the probe and surrounding oxygens, the decrease in frequency of the $6s \Rightarrow 6p$ transition can be thought of as a consequence of the covalence effect in which the electrons received from the oxygen are accommodated in σ and π bonding molecular orbitals (11,12). Some of this electron density is located between the inner electron core of the metal ion and its 6s orbital. One of the factors affecting the energy of the

6s ⇒ 6p process is the force of attraction that the 6s electrons experience from nucleus. This is shown schematically for the Pb^{2+} ion in Fig. VII. 1 (1). Much of the positive pull of the nucleus is screened by the inner electron core, but the electron density donated by the oxygens serves to increase this screening further which in turn allows the 6s electron to escape more easily to the 6p level. Electron donation by the oxygens to the probe ion therefore brings about a reduction in the 6s ⇒ 6p energy difference, and therefore a reduction in frequency in the UV absorption band, compared with the free Pb^{2+} ion. An underlying assumption is that when the orbital expansion parameters of the ligands are extrapolated to zero, then the electron donating ability of the ligands is zero; in effect they are able to provide an unperturbing environment for free Pb^{2+} ions. The extrapolated values of the $^1S_0 \Rightarrow {}^3P_1$ transition (which represents the energy difference corresponding to the 6s ⇒ 6p process) for Pb^{2+} is found to be 60700 cm^{-1} (13), and this will be referred to subsequently as $\nu_{free\ ion}$.

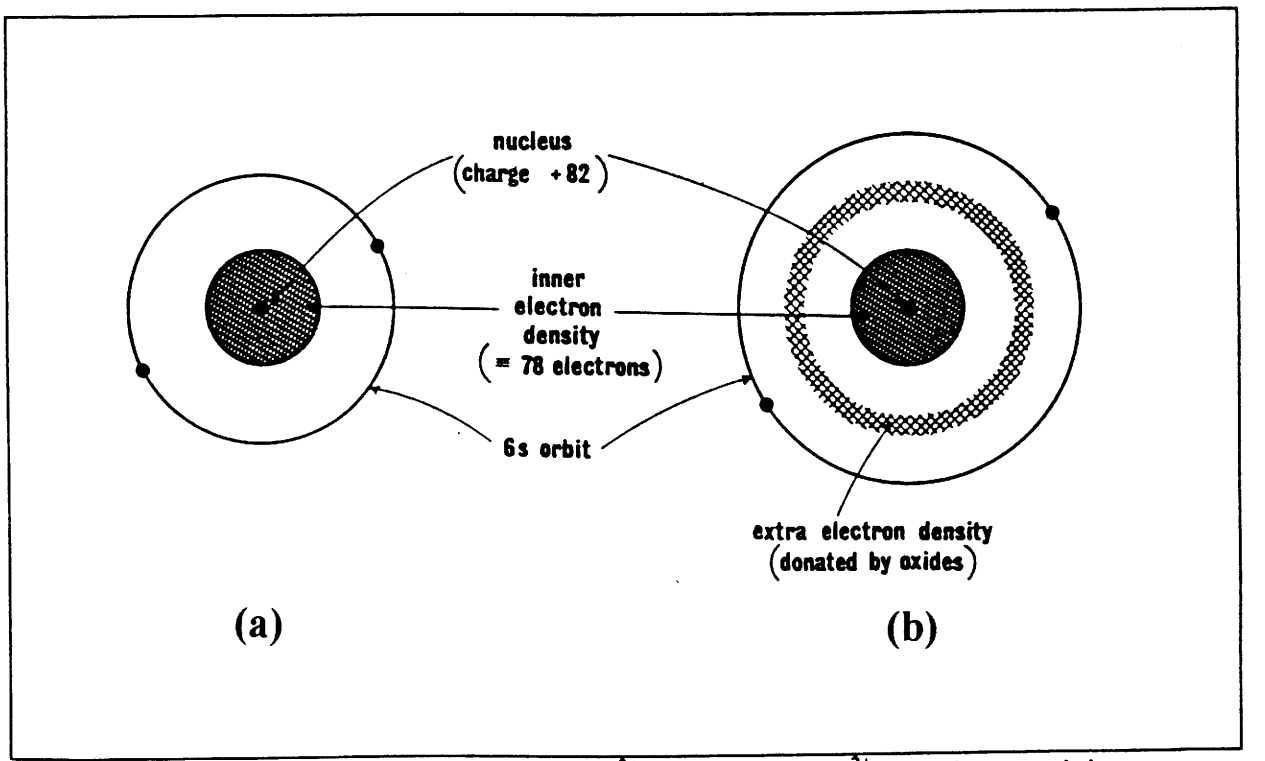

Fig. VII.1 Schematic diagram of (a) free Pb^{2+} ion, and (b) Pb^{2+} ion after receiving negative charge from neighbouring oxide ions (1).

The spectroscopic shifts observed in the $^1S_0 \Rightarrow {}^3P_1$ bands of Tl^+, Pb^{2+} and Bi^{3+} have been used for setting up scales of basicity (14). For Pb^{2+}, $\nu_{free\ ion}$ is 60700 cm^{-1} and ν_{O2-}, the frequency of Pb^{2+} in CaO is 29700 cm^{-1}. Thus on going from the unperturbed Pb^{2+} ion to the situation where the Pb^{2+} ion receives the electron density from free oxides, there is a spectroscopic shift of 31000 cm^{-1}. When the probe ion is influenced by the less basic oxides of a glass, the frequency shift is somewhat less. The spectroscopic shift represents the electron donating power of the oxides in the glass, and for comparing oxide glasses with each other, the ratio is derived from spectroscopic measurements and accordingly the glass basicity has been termed 'optical' basicity, Λ (15). Using Pb^{2+} as the probe ion

$$\Lambda_{Pb(II)} = (\nu_{free\ ion} - \nu_{glass})/(\nu_{free\ ion} - \nu_{O2-}) = \Delta\nu_{glass} / \Delta\nu_{O2-} = \Delta\nu_{glass} / 31000 \qquad \text{(Eq. VII.1)}$$

where ν_{glass} is the frequency of the Pb^{2+} ion in the glass. By definition, $\Lambda_{Pb(II)}$ (CaO) is unity.

Alexander et al. (15) suggested that the role of probe ions is different to that proposed by Ingram and Duffy. They have discriminated between the spectrum contributed to by Tl^+ ions acting as network modifiers (NM) and Tl^+ ions as charge compensating (CC) environments in alkali aluminosilicate glasses. Earlier studies by Easteal et al. (16) and Klein et al.(17) revealed discrepancies between experimental results and theoretical optical basicities for glasses containing significant fractions of NBO. Alexander et al. have revealed more seriously the theoretical flaw embedded in optical basicity theories such as the erroneous treatment of the absorption energy as a function of only one variable, as if absorption were occurring in an essentially free atom. Furthermore, optical basicity theory could be expected to work only when the structural environment of the probe ion varies little with composition, in which Frank-Condon offsets (18-20) vary weakly with composition. Following their interpretation, CC spectra shift but NM spectra do not change with composition. Later investigations for thallium spectra indicates that the conversion of Tl^+ into Tl^{3+} in molten borate glass is favoured by increasing basicity (21). This fact could explain the discrepancies of experimental results

measured by Tl probe ion and theoretical optical basicity. Alexander et al. noticed that the use of thallium for the measurement of optical basicity must be made with caution to ensure that the spectral band observed are those of Tl^{+}.

VII.1.3 Calculation of optical basicity

Probe ion spectroscopic studies of many glass systems have shown that optical basicity values can be assigned to individual oxides so that a theoretical optical basicity Λ_{th} can be calculated from the composition of a glass. The optical basicity of any oxidic medium is given by (1,22),

$$\Lambda_{th} = X_{AOa/2}\Lambda(AOa/2) + X_{BOb/2}\Lambda(BOa/2) + \ldots \qquad \text{(Eq. VII.2)}$$

where $\Lambda(AOa/2)$, $\Lambda(BOa/2)$, ... are the optical basicity values of the oxide and $X_{AOa/2}$, $X_{BOb/2}$, ... are their equivalent fraction, that is, the proportion of oxygens they provide. In effect, calculation of optical basicity by means of such a relation provides an easy and convenient method for obtaining a measure of the average electron density of the oxide(-II) atoms in an oxide medium. The optical basicities obtained from these relationships have been described as theoretical basicities and denoted as Λ_{th} to distinguish them from experimental values $\Lambda_{Pb(II)}$. In $CaO\text{-}P_2O_5$ glass, the oxygens are oxide ions influenced very strongly by the P^{5+} cations and less strongly by the Ca^{2+} cations in the glass. In this case, the Ca^{2+} ions neutralise one-sixth of the negative charge of the oxide while the P^{5+} ions neutralise five-sixths. The lowering of the electron donor power of the oxides by Ca^{2+} and P^{5+} ions might be expected to be due to,

i) the proportion of negative charge each cation neutralises,

ii) some polarising or electron-attraction property of each cation.

This latter property is known as the 'basicity moderating power' γ (23,24). The larger the value of γ, the more the electron charge clouds of the oxygen atoms would be contracted, thereby reducing their basicity. By using this value, the following general expression could be used to predict optical basicity;

$\Lambda_{th} = X_{Aa+}/\gamma_A + X_{Bb+}/\gamma_B + \ldots$ (Eq. VII.3)

where X_{Aa+}, X_{Bb+},... are the equivalent fractions of A^{a+}, B^{b+}, ... and γ_A, γ_B ... are the corresponding moderating parameters. For a simple oxide $1/\gamma = \Lambda_{th}$, the above relation could be expressed as (Eq. VII. 2) again. The γ value for representative elements are listed in Table VII. 1.

Element	γ (= $1/\Lambda_{th}$)
chlorine	3.73
nitrogen	3.73
sulphur	3.04
carbon	3.04
phosphorus	2.50
hydrogen	2.50
boron	2.36
silicon	2.09
zinc	1.82
aluminium	1.65
magnesium	1.28
calcium	1.00
lithium	1.00
sodium	0.87
potassium	0.73
rubidium	0.73
caesium	0.60

Table VII.1 Basicity moderating parameters γ (1).

VII.1.4 Basicity and Electronegativity

For the oxide(-II) species, the polarisation suffered by oxide(-II) in oxyanions and also in the oxides of non-metals, is much greater than in the more ionic oxides such as CaO or Na_2O. The amount of negative charge it donates to cations with which it coordinates depends markedly upon the other atoms attached to it and which polarise it. The extent of electron donation can be estimated from frequency shifts of optical absorption bands and is expressed as the optical basicity, Λ. From the experimental data on several oxides, Duffy and Ingram (23) have set up an empirical relationship between optical basicity and Pauling electronegativity χ_M, of the element (M) as $\Lambda = 0.75/(\chi_M - 0.25)$. This relationship conforms with the idea of diminishing electron-donor power as oxide(-II) is increasingly polarised and the increase in Λ correlates well with the increasing polarizability of the oxide ion. An important implication of this polarisation-optical basicity relationship is that the electronegativity of the oxide(-II) species is not a fixed quantity, but depends upon the state of polarisation and, in turn, upon the electronegativity of the other component element, M.

VII.1.5 Refractivity and optical basicity

The optical basicity of an oxidic medium can be thought of as representing the state of the oxide(-II) species after tightening of their electron charge clouds by the constituent cations. Wely and Marboe (25) suggested that the state of the oxide(-II) species could be regarded in terms of the oxide(-II) refractivity, R_{O2-}, and subsequent works (26-28) supported the existence of such a relationship. At last, it was proposed that refractivity could be used directly as a means for quantitatively expressing basicity (29,30). The molar refractivity, R_m, of a glass is obtained from the refractive index, n, using the Lorentz-Lorentz relation,

$$R_m = V_m(n^2-1)/(n^2+2) \qquad \text{(Eq. VII.4)}$$

where V_m is the molar volume.

The relation between refractive index and Λ_{th} has been obtained from the alkali or alkaline earth silicate experimental data given by Duffy (31) such that:

$$\Lambda_{th} = 0.35R_{O2-} - 0.81 \qquad \text{(Eq. VII.5)}$$

This relation diverges at high concentrations of alkali or alkaline earth metal oxides. In other words, this condition is fulfilled in glasses containing

i) cations with small refractivities or

ii) low concentrations of cations if they have large refractivities.

The optical basicity Λ_{th} can be also calculated starting from the polarizability α_m. If α_{O2-} is the average oxide polarizability, then the optical basicity of an oxidic system can be expresses in terms of α_{O2-} by (32),

$$\Lambda_{th} = 1.67\{1-(1/\alpha_{O2-})\} \qquad \text{(Eq. VII.6)}$$

The molar electronic polarizability, α_m, is given by

$$\alpha_m = (3V_m/4\pi N)(n^2-1/n^2+2) \qquad \text{(Eq. VII.7)}$$

where N is the Avogadro number.

Since, for oxidic systems, Λ represents the electron density residing on the oxide(-II) species, it is expected that Λ is related simply to the electronic polarizability of the oxide(-II), α_{O2-} . Thus for a single oxide, $MO_{z/2}$, it is the nature of the cation, M_{z+}, which affects both Λ and α_{O2-}; it is this property of M_{z+} which is reflected in the basicity-moderating parameter. If the basicity moderating parameter acts on other anions in the same way as it does on oxide(-II), then this relationship is anticipated to extend to the binary compounds of these other anions. In the case of sulphide materials, an analytical treatment of $^1S_0 \Rightarrow {}^3P_1$ and $^1S_0 \Rightarrow {}^1P_1$ absorption bands indicates reliable values for ν of 20400 cm^{-1} in zinc blende and 19700 cm^{-1} in wurtzite, which yield values for Λ of 1.30 and 1.32, respectively. A value of Λ for some fluorides, oxides and sulphide systems show a trend in α_{O2-} (Fig. VII.2). This implies that the

polarising power of the cations in sulphides operates in an analogeous fashion to that in oxide glasses.

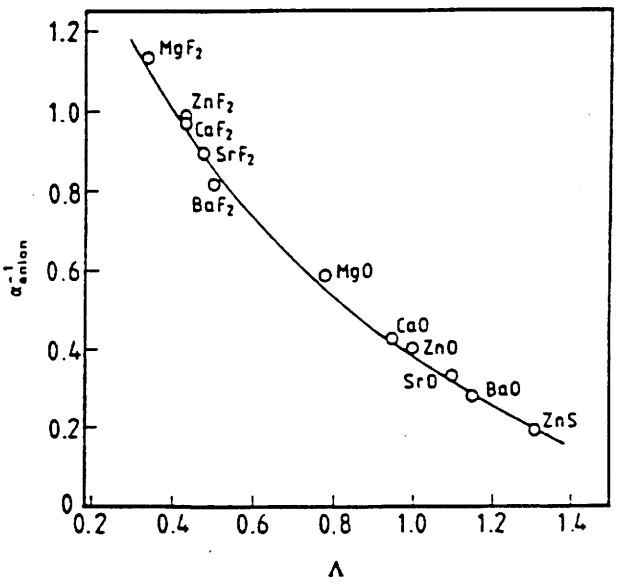

Fig. VII.2 Reciprocal of anion polarizability vs. optical basicity for binary fluorides and oxides (2).

VII.2 Optical basicity of Li_2S-B_2S_3 and Li_2S-As_2S_3 based glasses

VII.2.1 Evaluation of polarizability (α_{S2-})

We prepared Pb^{2+} doped Li_2S-B_2S_3 and Li_2S-As_2S_3 glasses and tried to obtain absorption spectra using a UV-VIS spectrometer with the help of J. A. Duffy and M. D. Ingram at the University of Aberdeen. These samples showed only optical band-edge shift but an absorption spectra for Pb^{2+} was not obtained; however, a qualitative trend suggested the possibility of a higher basicity than in oxide mediums.

The measurement of refractive index, n, was done with the help of Dr. G. LeFlem and F. Adamier. The refractive index was measured with a Mach-Zender interferometer with pulse laser with a wavelength of 790 nm.

By using the relation for refractive index concerning α_{O2-}, we calculated α_{S2-} and Λ (Table VII.2). The polarizability (α_{S2-}) increases with increasing Li_2S content, and the distribution of calculated optical basicities are located on the more basic side in Fig. VII.2. These results are similar to those found for alkali modified oxide glasses (33), which present the possibility that the optical basicity theories developed for oxide glasses can be applied to highly modified sulphide glasses.

Composition	**Refractive index (n)**	**Anion polarizability (α_{S2-})**	**Calculated optical basicity (Λ_{th})**
$0.67Li_2S$-$0.33B_2S_3$	1.954	4.40	1.29
$0.70Li_2S$-$0.30B_2S_3$	2.062	4.78	1.32
$0.75Li_2S$-$0.25B_2S_3$	2.115	5.15	1.35
$0.67Li_2S$-$0.33As_2S_3$	1.75	4.37	1.29
$0.75Li_2S$-$0.25As_2S_3$	1.85	4.87	1.33

Table VII.2 Measured refractive index (n), calculated polarizability (α_{S2-}) and optical basicity (Λ_{th}) with formula in (31).

VII.2.2 Compatibility of XPS and polarizability α_{S2-}

In IV.2, the XPS study for Li_2S-As_2S_3 glass showed two sulphide 2p peaks in glasses that contain bridging (BS) and non-bridging sulphur (NBS) atoms. The peak having the lower binding energy has been assigned to NBS, while the peak having the higher binding energy has been assigned to BS atoms. It was interpreted that the electron charge density on the NBS atom lowers the binding energy when compared to BS. The polarizability of the sulphur(-II) anion increases upon increasing the Li cation concentration, and this normally results in increasing the ionicity between the Li and S anions, i.e. increasing the covalency between glass former cation and the S anion.

Similar descriptions can be made in respect of an inductive effect. The concept of the inductive effect was first extended to inorganic solids by Noll in order to explain small differences in average Si-O bond lengths in silicates (34). As reviewed by Etourneau et al.(35), a situation exists in ternary compounds $T_u^{z+}M_v^{m+}X_x^{q-}$, in which the anion X^{q-} is coordinated between T^{z+} on one side and M^{m+} on the other. If T^{z+} is more electronegative then M^{m+} the anion X^{q-} will tend to share its electron preferentially with T^{z+} and therefore less electron density will be available for covalency in the M-X bond and vice versa. If we compare the electronegativity of the alkali cation Li^+ in the presence of (B or As) cations, both boron and arsenic have a higher electronegativity than Li^+. We might, therefore, expect a higher covalency for the glass former cation to sulphur bond, because of the higher electron density. This is consistent with previous XPS results.

VII.2.3 Optical basicity and ionic conductivity

In 1984, Hunter and Ingram (33) showed the possibility of a relationship between optical basicity and ionic conductivity in Na^+-ion conducting glasses. Recently, Shastry et al. (36) calculated similar results for fast ion conducting glasses and reported relationships between electronegativity, polarizability, basicity and conductivity. It appears that ion mobility depends on glass basicity which can be understood as a part of a general phenomenon in solids where cationic conductivity increases with increasing polarizability of the immobile network. The variations of ionic conductivity versus optical basicity for some glasses are presented in Fig. VII.3 (36). Considering binary glasses, the ionic conductivity in Li_2S-As_2S_3 and Li_2S-B_2S_3 increases upon increasing the Li_2S content as previously mentioned in Chapter V; the calculated basicity also increases in these glasses. From this, the conductivity/polarizability and conductivity/ basicity relationships in sulphide glasses may have similarities to those of oxide glasses.

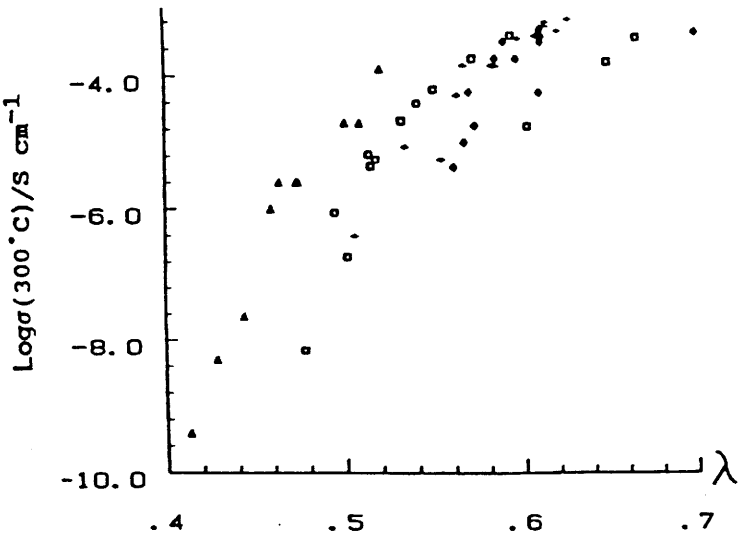

Fig. VII.3 The variation of ionic conductivity (at 300 °C) with the calculated optical basicity in oxide glass (36). **(+ ; Na_2O-SiO_2, Δ ; Na_2O-B_2O_3, O ; Na_2O-B_2O_3-$Si0_2$, □ ; Na_2O-Al_2O_3-B_2O_3, ◊ ; Na_2O-Al_2O_3-SiO_2)**

Conclusion

At the starting point of this work, we considered some of the issues concerned with the application of the optical basicity concept in glass chemistry as follows:

1) Optical basicity values are simply not known for sulphide glasses.

2) In highly modified (high Li content) glasses we do not know if or how Λ will vary with Li_2S content (when Li_2S becomes the major component).

3) Λ_{th} values are not equal to the Λ_{exp} values in borate glass ($\Lambda_{exp} > \Lambda_{th}$).

4) Should ΔΛ be large or small ?

5) How is the optical basicity related to ionic conductivity etc.

The Pb^{2+}-ion probe spectra were not obtained, however, the polarizability α_{S2-} versus Li content relation reasonably explains the glass network variation as an increase in basicity upon increasing the cation content, and this tendency correlated well with other spectroscopic observations. As in oxide glass, the possibility of utilising the similar empirical rules concerning basicity-polarizability, basicity-electronegativity in sulphide glass is expected. In addition, the basicity of the sulphide glass is higher than that for the same metal ions in oxide glasses as may be expected.

Globally, the optical basicity or polarizability of the anion could be used as an estimating tool to design the highest ionic conductivity composition. Principally, the observed results show that, even though there are some gaps in the theoretical consideration, the optical basicity is an useful indication on the change of local structure of glass.

References

1) J. A. Duffy and M. D. Ingram, J. Non-Cryst. Solids, **21** (1976) 373

2) J. A. Duffy, J. Chem. Soc. Faraday Trans., **88** (1992) 2397

3) J. Brönsted, Rec. Tran. Chim., **42** (1923) 718

4) T. Lowry, Chem. Ind. (London), **42** (1923) 43

5) A. Paul, *Chemistry of glasses*, 2nd Ed,(Chapman and Hall Co., 1990)

6)G. N. Lewis, *Valence and structure of atoms and molecules*
(Chemical Catalog. Co., New York, 1923)

7) W. A. Weyl and E. Thümen, Sprechsaal, **66** (1933) 197

8) H. Lüx and E. Rogler, Z. Anogan. Allegem. Chem., **250** (1942) 159

9) A. Paul and R. W. Douglas, Phys. Chem. Glasses, **8** (1967) 151

10) C. K. Jørgensen, *Absorption Spectra and Chemical Bonding in Complexes*
(Pergamon Press, New York, 1962)

11) J. A. Duffy and M. D. Ingram, Phys. Chem. Glases, **15** (1974) 34

12) H. Kawazoe, H. Hosono and T. Kanazawa, J. Non-Cryst. Solids, **29** (1978) 159

13) J. A. Duffy and M. D. Ingram, J. Chem Phys., **54** (1971) 443

14) J. A. Duffy and M. D. Ingram, J. Am. Chem. Soc., **93** (1971) 6448

15) M. N. Alexander, P. I. K. Onorato, C. W. Struck, G. W. Tasker and D. R. Uhlmann,
J. Non-Cryst. Solids, **91** (1987) 63

16) A. J. Easteal and D. J. Udy, Phys. Chem. Glasses, 14 (1973) 107

17) R. M. Klein and P. I. K. Onorato, Phys. Chem. Glasses, **21** (1980) 199

18) F. Seitz, J. Chem. Phys. **6** (1938) 150

19) C. W. Struck and W. H. Fonger, J. Luminescence, **10** (1975) 1

20) D. Curie, *Optical Properties of Ions in Solids*,
Ed B. di Bartolo, (Plenum, New York, 1975)

21) J. A. Duffy, Phys. Chem. Glasses, **32** (1991) 55

22) J. A. Duffy and M. D. Ingram, J. Non-Cryst. Solids, **76** (1992) 144

23) J. A. Duffy and M. D. Ingram, J. Chem. Soc. Chem. Commun., (1973) 635

24) J. A. Duffy and M. D. Ingram, J. Inorg. Nucl. Chem., **37** (1975) 1203

25) W. A. Weyl and E. A. Marboe, *The Constitution of Glasses*
(Interscience, New York, 1962)

26) A. Klonkowski, Phys. Chem. Glasses, **24** (1983) 166

27) A. Klonkowski, Phys. Chem. Glasses, **26** (1985) 11

28) A. Klonkowski, J. Non-Cryst. Solids, **72** (1985) 117

29) N. Iwamoto, Y. Makino and S. Kasahara, J. Non-Cryst. Solids, **68** (1984) 379

30) N. Iwamoto, Y. Makino and S. Kasahara, J. Non-Cryst. Solids, **68** (1984) 389

31) J. A. Duffy, J. Non-Cryst. Solids, **86** (1986) 149

32) J. A. Duffy, Phys. Chem. Glasses, **30** (1989) 1

33) C. C. Hunter and M. D. Ingram, Solid State Ionics, **14** (1984) 31

34) W. Noll, Angew. Chem. Int. Ed. Engl., **2** (1963) 73

35) J. Etourneau, J. Portier and F. Ménil, J. Alloys Comp., **188** (1992) 1

36) M. C. R. Shastry, K. J. Rao, A. Levasseur and M. Ménétrier,
J. de Phys. IV, **C2** (1992) C2-171

CONCLUSIONS

Le travail présenté dans ce mémoire avait un double but. Le premier était de développer l'étude d'une nouvelle famille de verres à base d'arsenites de lithium et le deuxième était d'étudier l'effet de formateur mixte associant certains de ces arsenites à des thioborates de lithium étudiés depuis quelques années dans notre groupe de recherche.

L'étude des verres à base d'arsenites de lithium avait été initiée par M.C.R. CHASTRY lors d'un stage post-doctoral ; beaucoup d'éléments restaient cependant à préciser.

Une étude détaillée du système As_2S_3-Li_2S-LiI fut donc entreprise.

L'orpiment, forme cristallisée de As_2S_3 est bien connu. Sa structure est constituée de pyramides AsS_3 ; chaque atome de soufre est pontant et l'atome d'arsenic est au sommet de la pyramide. Des plans faiblement liés les uns aux autres sont ainsi formés.

Les choses sont beaucoup moins claires quant à la forme non cristalline de As_2S_3. Si l'ordre à courte distance semble faire l'unanimité -pyramide AsS_3 semblable à celle présente dans l'orpiment- l'enchaînement de ces pyramides est très controversé. Les différentes hypothèses émises proviennent de l'interprétation différente d'études spectroscopiques. Certains auteurs présentent la phase amorphe comme étant un enchaînement désordonné de ces pyramides, d'autres comme étant une structure moléculaire avec des pyramides AsS_3 en faible interaction les unes avec les autres, d'autres encore comme des chaînes liées entre elles par des cycles à 12 chaînons. Ces études illustrent parfaitement la difficulté d'établir une structure d'un matériau amorphe. Les études spectroscopiques faites au laboratoire sur As_2S_3 permettent de penser qu'une structure de type moléculaire serait tout-à-fait possible.

L'étude du système As_2S_3-Li_2S-LiI a permis de mettre en évidence non seulement un domaine vitreux de faible envergure mais aussi deux phases cristallisées inédites Li_3AsS_3 et $LiAsS_2$.

Pour la première de ces phases cristallisées, la détermination structurale a pu être menée à bien sans problème. Li_3AsS_3 est formée de pyramides AsS_3^{3-} liées entre elles par des atomes de lithium. Ces derniers se trouvent dans deux sites différents. Le premier est tétraédrique ; le second atome de lithium est au sommet d'une pyramide ayant pour base 3 atomes de soufre.

Pour $LiAsS_2$, les choses sont beaucoup moins claires. Cette phase serait constituée de pyramides AsS_3 ayant deux atomes de soufre pontant, le troisième, non pontant, serait lié à un atome de lithium. Tous les atomes de lithium seraient au sommet d'une pyramide ayant 3 atomes de soufre pour base. Les chaînes ainsi formées seraient faiblement liées entre elles. Malheureusement, le facteur de reliabilité final voisin de 10 %, ainsi qu'une densité électronique anormalement élevée dans un site du lithium laisse planer un doute quant à la réalité de cet enchaînement. Plusieurs tentatives de préparation de cristaux suivies de déterminations structurales n'ont pas permis de trouver une solution satisfaisante. L'analyse chimique a été effectuée sur des cristaux triés après broyage d'un bloc polycristallin manifestement biphasé. (présence systématique de cristaux de Li_3AsS_3 et de ceux supposés être $LiAsS_2$). Cette analyse pourrait donc ne pas représenter la composition exacte des cristaux utilisés pour la détermination structurale.

L'analyse par XPS de Li_3AsS_3 montre très clairement un seul type d'atome de soufre dont "l'énergie" est proche de celle trouvée pour Li_2S, montrant ainsi son caractère très "négatif". Ce dernier point pourrait s'expliquer par la présence du doublet libre sur l'arsenic qui

provoquerait non seulement la forme pyramidale de l'unité élémentaire AsS_3 mais augmenterait l'ionicité de la liaison As-S. A titre de comparaison, l'étude du système B_2S_3-Li_2S-LiI avait, elle aussi, permis de comparer une phase cristallisée Li_3BS_3 à un verre de même composition. L'analyse XPS avait révélé une "énergie" pour les atomes de soufre non pontants supérieure de 0.7 eV à celle trouvée par les arsenites montrant ainsi un caractère beaucoup moins négatif. (Les électronégativités des atomes de bore et d'arsenic ont des valeurs identiques).

Pour $LiAsS_2$, deux types d'atome de soufre ont pu être identifiés ; l'un non pontant, tout-à-fait semblable à celui trouvé pour Li_3AsS_3, l'autre, beaucoup moins négatif, serait l'atome de soufre pontant. Leur pourcentage relatif déduit de l'étude XPS correspond parfaitement à celui trouvé lors de l'étude structurale.

Les études spectroscopiques infrarouge et Raman n'ont pas permis une attribution précise de tous les pics présents, très peu de références étant disponibles. Seuls les groupes de pics ont été attribués.

Comme nous l'avons mentionné antérieurement, l'étude du système As_2S_3-Li_2S-LiI a permis de mettre en évidence un domaine vitreux relativement modeste. Dans le système binaire, As_2S_3-Li_2S tout d'abord, la température de transition vitreuse augmente lorsque le taux de modificateur Li_2S augmente. Ce comportement paradoxal pourrait s'expliquer par l'évolution de la coordinence des atomes de lithium qui passe de 3 à 4 quand le taux de Li_2S augmente, comme l'ont montré les études structurales de $LiAsS_2$ et Li_3AsS_3. Ceci n'est vrai que si l'on suppose une évolution de comportement identique entre les phases cristallisées et les matériaux vitreux (ce qui est très vraisemblable). Le réseau serait donc réticulé par les atomes de lithium provoquant ainsi l'augmentation de Tg qui est observée. L'évolution de Tg dans le cas des verres ternaires est, par contre, tout à fait classique ; l'augmentation du taux de LiI

provoque une diminution importante de Tg. L'introduction dans le réseau vitreux de gros ions polarisables est, bien entendu, à l'origine de ce phénomène.

L'étude menée par absorption des rayons X fait apparaître un taux d'oxygène supérieur à ce qu'indiquait l'analyse chimique ; la manipulation à l'air des échantillons, provoquant une hydrolyse partielle du matériau est très certainement cause de ce phénomène. Les distances As-S sont trouvées plus courtes de 0.2 Å que celles déterminées dans les composés cristallisés. La difficile décomposition des pics communs aux distances As-O et As-S est probablement à l'origine de ce décalage.

L'étude XPS montre, dans les verres binaires, le caractère très négatif des atomes de soufre non pontants qui ont une "énergie" identique à ce qu'elle est dans Li_3AsS_3.

L'étude par spectroscopies infrarouge et Raman montre, là aussi, une similitude tout à fait frappante entre verre et cristal de même composition. Pour les autres compositions des matériaux amorphes, les pics présents ont pu être attribués aux différentes vibrations possibles dans les éléments structuraux présents.

L'étude de la conduction ionique des matériaux vitreux montre un comportement assez voisin de celui trouvé dans le système B_2S_3-Li_2S-LiI.

Dans le système binaire As_2S_3-Li_2S, l'énergie d'activation, le facteur préexponentiel et la conductivité, augmentent avec le taux en Li_2S. Une explication simple pourrait être que la présence de plus en plus importante d'atomes de soufre non pontants porteurs de fortes charges négatives piègent les atomes de lithium. L'XPS a, en effet, montré clairement l'aspect fortement négatif de ces atomes de soufre.

Dans le système ternaire, la variation de l'énergie d'activation, du facteur préexponentiel et de la conductivité à 25 °C est semblable, là aussi, à ce qui était observé dans le système B_2S_3-Li_2S-LiI. La diminution des deux premiers facteurs et l'augmentation de la conductivité,

jusqu'à un taux de LiI égal à 0.3, peut s'expliquer par la dispersion de LiI dans la matrice vitreuse ; Tg diminue, les gros ions I^- favorisent la conduction. Lorsque le taux en LiI augmente, il pourrait se former des agrégats de LiI comme dans les thioborates de lithium, qui auraient pour effet de diminuer considérablement la quantité d'ions lithium disponible pour le phénomène de conduction. Ces agrégats sont, bien sûr, de taille trop modeste pour être détectés par diffraction X. La conductivité ionique de ces verres est légèrement inférieure à celle des thioborates de lithium mais suffisamment attrayante cependant pour étudier le phénomène de formateur mixte en les associant ensemble. As_2S_3 et B_2S_3 présentent non seulement une identité formulaire mais les parties précédentes ont montré qu'associés séparément au modificateur Li_2S, leurs comportements étaient assez semblables (exception faite du changement de coordinence de l'atome de bore dans les verres modifiés).

Le système Li_2S-As_2S_3-B_2S_3 a ainsi été étudié. L'interprétation des phénomènes de conduction dépend essentiellement de la nature du matériau formé -homogène ou hétérogène- déterminée par la présence de un ou deux Tg. Une attention toute particulière a donc été portée à l'analyse thermique des échantillons. C'est ainsi qu'un domaine homogène a été mis en évidence pour de faibles teneurs en As_2S_3 suivi d'un domaine hétérogène pour des teneurs plus élevées avant de voir apparaître la cristallisation de $LiAsS_2$.

Une approche structurale des verres obtenus dans le petit domaine d'existence a été effectuée. Des résultats de ces études, quatre hypothèses se dégagent suivant la nature du réseau vitreux :

* Pour la partie homogène (présence d'un seul Tg) :

1. Une réelle solubilité existe entre As_2S_3 et B_2S_3 avec possibilité pour l'arsenic d'occuper un site tétraédrique comme le bore. Cette hypothèse évoquée à l'examen des résultats obtenus par XAS est bien improbable étant donné le caractère particulier des atomes d'arsenic.

2. Un seul réseau vitreux existe avec alternance de tétraèdres "BS_4" de triangles "BS_3" et de pyramides "AsS_3" liés, bien entendu, par des atomes de soufre pontants (et pour certaines compositions par des ions Li^+). Cette hypothèse laisse les atomes de bore et surtout d'arsenic dans leur site "naturel" respectif.
3. Aucune solubilité n'existe. Il y a alors juxtaposition de deux réseaux vitreux. Li_2S-B_2S_3 d'une part et Li_2S-As_2S_3 d'autre part. La composition exacte de chacun d'eux est très difficile à déterminer, Li_2S étant un facteur commun. L'analyse thermique, qui ne présente apparemment qu'un seul Tg, n'aurait pas une sensibilité suffisante pour détecter 2 Tg. Ces derniers sont en effet très proches, 173-185 °C dans le domaine d'existence des verres Li_2S-As_2S_3 ; 220-163 °C pour le même domaine des verres Li_2S-B_2S_3.

* Pour la partie hétérogène (présence de 2 Tg) :

4. Deux Tg ont été mis en évidence sans ambiguité, montrant la présence de deux réseaux vitreux (au moins), dont il n'est pas possible de préciser la composition.

Malgré les efforts déployés, il n'est pas possible de privilégier l'une ou l'autre de ces hypothèses. Seule la première semble très improbable.

Le phénomène de formateur mixte qui devait permettre, comme nous l'avons vu dans l'introduction, d'augmenter la conductivité ionique n'est manifestement pas observé, la conductivité ionique du verre contenant deux formateurs diminue même lorsque le taux de As_2S_3 augmente. Le petit domaine d'existence de ces verres ne permet pas de tirer de conclusion quant à la nature du phénomène.

La dernière partie est consacrée à l'étude de la basicité optique des verres binaires Li_2S-B_2S_3 et Li_2S-As_2S_3. Cette théorie, dérivée de celle de Lewis, permet d'expliquer simplement un certain nombre de propriétés ou de comportements. Elle peut avoir un caractère prédictif si

suffisamment de données sont accessibles. C'est le cas pour les verres à base d'oxydes, étudiés depuis plus de 20 ans. Pour les verres à base de sulfures, tout reste à faire.

Ce travail se voulait une modeste contribution à l'édifice en construction concernant les matériaux soufrés. Le but n'a été que partiellement atteint par manque de temps, mais a ouvert une voie de collaboration très fructueuse avec un groupe du département de Chimie de l'Université d'Aberdeen.

Appendix

A.1 Figure captions

Chapter I

Fig. I.1 Schematic representation of the parameters describing SRO in covalent amorphous solid (8).

Fig. I.2 Schematic two-dimensional representation of an A_2X_3 random network.

Fig. I.3 A modified random network (MRN) for a 2 dimensional oxide glass. The nominal composition is M_2O_3-G_2O_3, where M's are modifying cations and G's are network forming cations. Covalent bonds are shown by the solid lines and ionic bonds by the dotted lines. The unshaded regions are defined by the boundary which runs through the G-O (non-bridging) bonds. These highlight the percolation channels of M_2O_3 that run through the network (13).

Fig. I.4 Forms of holes in ideal equidistant molecule model of a liquid; a: tetrahedron, b: octahedron, c: trigonal prism capped with three half octahedra, d: archimedean antiprism capped with half octahedra, e: tetragonal dodecahedron (15).

Fig. I.5 Determination of the onset point of Tg, where T_1 is the maximum temperature of the peak, and T_2 is the minimum temperature of the valley.

Fig. I.6 Glass forming region of $yLiI$-$(1-y)[xLi_2S$ - $(1-x)As_2S_3]$ ternary glass system.

Fig. I.7 Glass forming region of xLi_2S-$(1-x)[(1-y)B_2S_3$ - $yAs_2S_3]$ ternary glass system.

Fig. I.8 Example of DSC trace in which more than one Tg is observed.

Chapter II

Chapter III

Chapter IV

Chapter V

Chapter VI

Fig. VI.11 Experimental As K-edge EXAFS spectra, $k^3\chi(k)$, of (a) v-As_2S_3, and (b) y = 0.1, (c) y = 0.2, (d) y = 0.3 with x = 0.67, and (e) y = 0.1, (f) y = 0.2, (g) y = 0.3 with x = 0.70 for the xLi_2S-(1-x)[(1-y)B_2S_3-yAs_2S_3] ternary glass system.

Fig. VI. 12 Magnitude of FTs in the range ~2.5 $Å^{-1}$ < k < 13 $Å^{-1}$ of $k^3\chi(k)$,of (a) v-As_2S_3, and (b) y = 0.1, (c) y = 0.2, (d) y = 0.3 with x = 0.67, and (e) y = 0.1, (f) y = 0.2, (g) y = 0.3 with x = 0.70 for xLi_2S-(1-x)[(1-y)B_2S_3-yAs_2S_3] glasses.

Fig. VI.13 Best-fitted (dotted curve) and experimental (solid curve) inverse Fourier transformed $k^3\chi(k)$, for the first shell in the FTs of Fig. VI.12 for (a) v-As_2S_3, and (b) y = 0.1, (c) y = 0.2, (d) y = 0.3 with x = 0.67, and (e) y = 0.1, (f) y = 0.2, (g) y = 0.3 with x = 0.70 for the xLi_2S-(1-x)[(1-y)B_2S_3-yAs_2S_3] ternary glass system.

Fig. VI.14 Experimental (solid curve) and fitted results (dotted curve) on the main peaks (a) y = 0.1, (b) 0.2 with x = 0.67.

Fig. VI.14' Continue over Fig. VI.14 (c) 0.3 with x = 0.67 and (d) 0.1 with x = 0.70.

Fig. VI.14'' Continue over Fig. VI.14 (e) 0.2, (f) 0.3 with x = 0.70.

Fig. VI.15 Normalised As K-edge XANES spectra for (a) v-As_2S_3, and (b) y = 0.1, (c) y = 0.2, (d) y = 0.3 with x = 0.67, and (e) y = 0.1, (f) y = 0.2, (g) y = 0.3 with x = 0.70 for the xLi_2S-(1-x)[(1-y)B_2S_3-yAs_2S_3] ternary glass system.

Fig. VI.16 Variation of main peak position with respect to x- and y-value in the As K-edge XANES spectra for the ternary glass system, xLi_2S-(1-x)[(1-y)B_2S_3-yAs_2S_3], (a) x = 0.67 and (b) x = 0.70.

Fig. VI.17 (a) Variation of free enthalpy of mixing versus the substitution ratio, (b) variation of the activity of two limit compositions versus the ratio of substitution (30).

Fig. VI.18 Simulated variation of the ratio of ionic conductivity σ_i to interface conductivity σ_c versus the amount of insulator substitution into the conductor material (33).

Chapter VII

A.2 Table captions

Chapter I

Table I.1 Ionic field strength of cations present in glass (4).

Table I.2 Classification of copositions according to the glass forming ability (7).

Table I.3 Chemical analysis obtained using Inductive Coupled Plasma spectrometry (ICP).

Chapter II

Table II.1 Structural data for As_2S_3 single crystal (2,3).

Table II.2 Comparison between planar random network model and molecular model (12).

Table II.3 Reported and calculated vibrational frequencies for As_2S_3 glass (IR & Raman).

Table II.4 Measured average radial distance As-S using several experimental methods.

Chapter III

Table III.1 Li_3AsS_3 crystal data and detailed measurements and structure solution.

Table III.1' Continued over Table III.1

Table III.2-a) Fractional atomic coordinates and equivalent isotropic displacement parameters (Å) in $Pna2_1$, $B_{eq} = (8\pi^2/3)\Sigma_i\Sigma_j U_{ij} a_i^* a_j^* \mathbf{a}_i \mathbf{a}_j$.

Table III.2-b) Anisotropic thermal parameters of Li_3AsS_3 relative to the thermal factor, $T = \exp[-2\pi^2(h^2a^{*2}U_{11}+k^2b^{*2}U_{22}+l^2c^{*2}U_{33}+2hka^*b^*U_{12}+2klb^*c^*U_{23}+2lkc^*a^*U_{13})]$.

Table III.3 Main interatomic distances (Å) and bond angles (°) in Li_3AsS_3.

Table III.4 $LiAsS_2$ crystal data and detailed measurements and structure solution.

Table III.4' Continued over Table III.4.

Table III.5-a) Fractional atomic coordinates and equivalent isotropic displacement parameters (Å) in Cc, $B_{eq} = (8\pi^2/3)\Sigma_i\Sigma_j U_{ij} a_i^* a_j^* \mathbf{a}_i \mathbf{a}_j$.

Table III.5-b) Anisotropic thermal parameters of $LiAsS_2$ relative to the thermal factor, $T = \exp[-2\pi^2(h^2a^{*2}U_{11}+k^2b^{*2}U_{22}+l^2c^{*2}U_{33}+2hka^*b^*U_{12}+2klb^*c^*U_{23}+2lkc^*a^*U_{13})]$.

Table III.6 Main interatomic distances (Å) and bond angles (°) in crystalline $LiAsS_2$.

Chapter IV

Chapter V

Chapter VI

Chapter VII